



**MONASH** University

***Development of one-step fluorescent biosensors  
by exploiting engineered antibodies***

***Jiaul Islam***

*BSc. (Honours) in Biochemistry and Molecular Biology*

A thesis submitted for the degree of *Doctor of Philosophy* at

Monash University in 2019

*Dept. of Chemical Engineering, Faculty of Engineering*

---

---

## Copyright notice

© *Jiaul Islam, 2019*

*I certify that I have made all reasonable efforts to secure copyright permissions for third-party content included in this thesis and have not knowingly added copyright content to my work without the owner's permission.*

## Abstract

Fluorescence-based biosensors are emerging as an alternative to the traditional bioassays. Most of the biomarkers are currently detected by multi-step assays including washing, blocking and secondary reagents. Unfortunately, only a few one-step fluorescent biosensors are reported despite their immense potential; hence, there is an extreme demand for these types of biosensors that can quantify target molecules without the need of further reagents and sample processing. There are a few reports of engineered antibody based fluorescent biosensors that utilise fluorescence intensity as the basis of analyte detection, however, these can be limited by the intrinsic background fluorescence of the sample matrix. An alternative approach is proposed in this PhD project where fluorescence emission wavelength shift of engineered, fluorescent antibody fragments is used as the basis of detection. Thus, the project aims to explore this exciting avenue of research for developing a fluorescent biosensor by exploiting engineered antibodies for single-step protein quantification that rely on fluorescence emission spectral alteration due to antigen binding.

In this PhD research project, a polarity sensitive fluorescent unnatural amino acid (Anap) was incorporated within the topological neighbourhood of antigen binding sites of a well-characterised single chain antibody (scFv) to develop a proof-of-concept. Herein, a rational design approach was employed to determine the optimal Anap incorporation sites based on an anti-EGFR scFv antibody homology model structure. The exposure of EGFR target to an anti-EGFR mutant containing Anap in the CDR2 region of the scFv heavy chain (H53Y) showed up to 20 nm blue wavelength shift in a dose-dependent manner. The concept was further validated in a second scFv-antigen model, using anti-cTnI scFv antibody for the detection of human cardiac troponin I (cTnI) biomarker where binding of the cTnI protein to the L27c-Y anti-cTnI mutant exhibited up to 37 nm blue-shift. Fluorescence characterisation revealed that the resultant spectral shift was due to the change of surrounding polarity of the Anap microenvironment caused by antigen binding. The level of detection for these biosensors was found to be between 1-5 nM in the buffer and the spiked

human blood sample. These findings demonstrate the potential for the development of fluorescent biosensors based on the wavelength shift of fluorescently labelled engineered antibodies, which detect the target in one-step and do not rely on sample processing. This one-step sensing strategy may reduce the significant time for detection of the target molecules and could potentially be applied to other antibody/antigen combinations for integration into a wide range of assay platforms (including homogenous, solid-phase assays, or multiplex assays) for one-step protein quantification.

---

## Declaration

This thesis contains no material which has been accepted for the award of any other degree or diploma at any university or equivalent institution and that, to the best of my knowledge and belief, this thesis contains no material previously published or written by another person, except where due reference is made in the text of the thesis.

Signature: .....

Print Name: .....

Date: .....

---

## Publications during enrolment

- Bobo D, Robinson KJ, **Islam, J.** Thurecht K, Corrie SR, “Nanoparticle-Based Medicines: A Review of FDA-Approved Materials and Clinical Trials to Date”, *Pharmaceutical Research* (2016) 33: 2373.
- Corrie SR, Coffey JW, **Islam J**, Markey KA, Kendall MAF, “Blood, sweat and tears: developing clinically relevant protein biosensors for integrated body fluid analysis”, *Analyst*, 2015, 140, 4350 – 4364
- **Islam J**, Riley B, Fercher C, Jones M, Buckle A, Howard C, Bell, TDM. Mahler, S., Corrie SR, “Wavelength-dependent fluorescent immunosensors via incorporation of polarity indicators near the binding interface of antibody fragments”, *in press, Analytical Chemistry*, available as “Just Accepted” online.

---

## Thesis including published works declaration

I hereby declare that this thesis contains no material which has been accepted for the award of any other degree or diploma at any university or equivalent institution and that, to the best of my knowledge and belief, this thesis contains no material previously published or written by another person, except where due reference is made in the text of the thesis.

This thesis includes one original paper published in peer reviewed journals. The core theme of the thesis is the development of a one-step fluorescent biosensor for detection of target ligand based on engineered antibodies. The ideas, development and writing up of all the papers in the thesis were the principal responsibility of myself, the student, working within the Dept. of Chemical Engineering under the supervision of Dr Simon Corrie.

(The inclusion of co-authors reflects the fact that the work came from active collaboration between researchers and acknowledges input into team-based research.)

In the case of *Chapter four* my contribution to the work involved the following:

<b>Thesis Chapter</b>	<b>Publication Title</b>	<b>Status</b> <i>(published, in press, accepted or returned for revision, submitted)</i>	<b>Nature and % of student contribution</b>	<b>Co-author name(s) Nature and % of Co-author's contribution*</b>	<b>Co-author(s), Monash student Y/N*</b>
<i>Chapter 4</i>	<i>Wavelength-dependent fluorescent immuno-sensors via incorporation of polarity</i>	<i>Published</i>	<i>82%. Concept design, collecting data and writing first draft</i>	<i>Blake Riley, input into one experiment and manuscript, 2.5%  Christian Fercher, input into one experiment and manuscript, 2%</i>	<i>Yes</i>

	<i>indicators near the binding interface of antibody fragments</i>			<i>Martina Jones, input into supervision and manuscript, 2%</i>  <i>Ashley Buckle, input into manuscript, 0.5%</i>  <i>Christopher Howard, input into manuscript, 0.5%</i>  <i>Rosalind Cox, input into one experiment, 2%</i>  <i>Toby Bell, input into one experiment and manuscript, 2%</i>  <i>Stephen Mahler, input into supervision and manuscript, 1.5%</i>  <i>Simon Corrie, input into supervision and manuscript, 5%</i>	
--	--	--	--	--	--

I have not renumbered sections of submitted or published papers in order to generate a consistent presentation within the thesis.

**Student signature:** \_\_\_\_\_ **Date:** 24 05 2019

The undersigned hereby certify that the above declaration correctly reflects the nature and extent of the student's and co-authors' contributions to this work. In instances where I am not the responsible author, I have consulted with the responsible author to agree on the respective contributions of the authors.

**Main Supervisor signature:** \_\_\_\_\_ **Date:** 24 05 2019

# Acknowledgements

When I started writing this acknowledgement section, it took me several minutes to think about the start and end of acknowledgements because the list of people and organisations involved in the project are quite long. I went back to the memory of a meeting with Dr Simon Corrie in an unrecalled day and month of 2013 at Café Nano of Australian Institute for Bioengineering and Nanotechnology (AIBN), The University of Queensland (UQ), Australia. I believe this Café has a contribution to a lot of great PhDs and excellent science! The purpose of the meeting was to get some work experiences under Dr Corrie for potential publications that could be helpful for possible PhD opportunity in the future. Luckily enough he had some intuitive ideas that fit my experience and career goal. After working about a year and a half, I possibly passed the initial testing (because Simon believes try before you buy!) and obtained support from Dr Corrie for the PhD application, and my journey started right there. Though Dr Corrie had created the path for me, it could be an uneven surface to reach my destination if I was not lucky enough to get Professor Stephen Mahler and Dr Martina Jones in the advisory panel. I cannot describe in words about the efforts, time and supervision I have received from my PhD advisors in the last 4 years. I have learned not only the scientific and research skills from my supervisors but also found them as my role model to follow every aspects of my life. As a principal advisor, Dr Corrie had facilitated me with the all necessary resources to conduct the experiments. He guided me in the right direction of the project that was built from sceptical ideas but resulted in the valuable outcomes for the biosensing field. Dr Corrie also ensured financial support throughout this project.

Professor Mahler had provided me with excellent supports as necessary, most notably providing me with the opportunity to work in his laboratory and provided critical advice on the direction of the project. The tips and suggestions I have received from Professor Mahler have significantly improved my in-depth knowledge and presentation skills, specifically public speaking abilities. I have implemented these skills for all the presentations including milestones or

conference seminars and most notably that earned me a best oral presenter award in the prestigious Bioprocessing Network Conference (Melbourne, Australia 2018) where Professor Mahler was a moderator.

Dr Martina Jones has been my experimental guru for the antibody engineering. I significantly acknowledge her great supports in developing this project from indecisive ideas. The direction of Dr Jones was outstanding in achieving the end goal of this project. As an example, getting the Anap UAA paper from Dr Jones was a kind of Eureka in this project! Likewise, her terrific guidance on the presentation slides on the milestone seminars helped me to overcome the hurdles of this journey. Dr Jones also assisted me in cloning of terminal mutants for anti-EGFR scFv and always provided with essential recommendations for experiments. The above stories are just a glimpse of the whole journey that is impossible to mention entirely here. I want to express my deepest gratitude to all of my supervisors for their immeasurable directions, suggestions and guidance in the completion of this PhD project.

My special thanks go to Professor Ross Barnard and Dr Simon Puttick of The University of Queensland for being examiners to all the milestones. I acknowledge their valuable feedback, insightful comments and suggestions that enhanced the strength of this project. I also thank them for the critical questions that have encouraged me to think in-depth and widen my knowledge in the respective scientific fields.

I would like to hugely thank member of Nanosensors Engineering Laboratory (NEL), Dept. of Chemical Engineering, Monash University, who treated me like a member of a family. Without the help of them, it was impossible to finish this journey smoothly. I particularly would like to mention the key members of the group, namely Kye Robinson, Gabriel Hyun, Vidhishri Kesarwani, Julia Walker, Edward Henderson and of course the head of the group Dr Simon Corrie. They just not only have aided for experimental needs or everyday laboratory matters but also provided moral support, encouragement and inspiration. The group's feedback on my work was immensely useful. Thank you so much for being supportive all the way.

My sincere thanks go to members of the Mahler group in AIBN, The University of Queensland. Especially, Dr Christopher Howard has provided the plasmids for bacterial expression of anti-EGFR scFv mutants. I also would like to thank Dr Howard for technical advice that was instrumental for executing many experiments. My special thanks go to Christopher J. de Bakker (former Researcher at AIBN) for the training on AKTA chromatography systems for protein purification. Apart from them, various other members helped me in many ways during my 1st year of PhD at AIBN particularly Michael Yeh for cloning assistance, Dr Mohamed Al Falah and Dr Sumukh Kumble for mammalian cell culture training. I also would like to thank Dr Christian Fercher for contributing in the chapter 4 manuscript as well as labelling anti-cTnI scFv with Cy5 dye via clickable UAA. Dr Amanda Nouwens from the School of Chemistry and Molecular Bioscience (SCMB), UQ kindly performed initial mass spectroscopy experiments. I wish to acknowledge the contribution of these great people by thanking them. I am also indebted to members of the ex-Kendall group at AIBN for the incredible help at all the time.

My special thanks go to Dr Noelene Quinsy at the Monash Protein Production Unit, Dept. of Biochemistry, Monash University. She demonstrated me expressing proteins in Expi293F™ cells. Since my relocation to Monash University, Dr Quinsy has provided me terrific supports by providing access to resources, equipment and the opportunity to work in her laboratory for protein expression. Without her technical and resource supports, I could not perform my experiments in an efficient way and on time. I am incredibly thankful to Dr Quinsy and her team.

During the early stage, while I was reviewing the literature to develop this project, I found a publication describing the applications of engineered antibodies in biosensors development. I remembered the name of the first author whom I coincidentally met in a lazy afternoon while working at Monash Protein Production Unit, and that was Dr Paul Conroy, a former Research Fellow at Monash University. Meeting with Dr Conroy was an exciting moment to me that eventually led to a productive collaboration resulting in biosensor development

for human cardiac troponin detection (chapter 5 of this thesis). Dr Conroy helped me in designing the constructs for unnatural amino acid incorporation into anti-cTnI scFv antibody. He also kindly provided the cTnI peptide as a gift and shared unpublished peptide-bound anti-cTnI scFv structure. I wish to express my deepest gratitude by thanking Paul for exceptional supports.

I am also indebted to members of Protein Engineering and Design Lab led by A/Prof Ashley Buckle, Dept. of Biochemistry and Molecular Biology, Monash University. The group provided technical help, particularly I acknowledge the contribution of Blake Riley who developed the model anti-EGFR structure. I also thank Irene Hatzinisiriou (Dept. of Biochemistry, Monash University) for providing me access to use BioRad ChemiDoc imaging equipment.

Similarly, Dr Toby Bell and his colleagues (School of Chemistry, Monash University) have provided outstanding assistance in fluorescence characterisation of the Anap incorporated scFv antibodies. The technical advice from Dr Bell was extraordinary that helped me to understand the underlying mechanism of the polarity dependent mechanism for fluorescent biosensing. I acknowledge the assistance of Dr Rosalind Cox and Dr Trent Ashton from Bell's group for fluorescence lifetime measurement and data analysis.

I acknowledge the services from different organisations such as Micromon Genomics (Monash University) and Australian Genome Research Facility (UQ) for DNA sequencing as well as Monash Proteomics Facility for mass spectroscopy experiments. I especially thank Dr David Steer for carrying out mass spectroscopy analysis in a brief period and many fruitful discussions. I also acknowledge the gift of plasmids from National Biologics Facility (UQ) and Professor Peter Schultz (The Scripps Research Institute, US). I would like to thank Prof George Lovrecz and his group at CSIRO (Parkville/Clayton, Victoria, Australia) for an initial optimisation experiment.

I express my sincere gratitude to Dr Daniel Heller of Cancer Nanomedicine Laboratory (Heller Lab), Memorial Sloan Kettering Cancer Centre for providing me with the opportunity to work in his laboratory. Dr

Heller provided me with the necessary resources and ensured my tenure in his lab was smooth. Dr Ryan William and Dr Zvi Yarri provided me with technical advice, helped in designing experiments and trained various instruments.

Apart from the assistance of numerous people for scientific matters, I also received assistance in preparing this thesis. My thanks go to Jane Moodie, Graduate Research Student Academic Support, Faculty of Engineering, Monash University who kindly reviewed grammatical errors in chapter 1-2 of this thesis. Members of NEL group, particularly Gabriel Hyun, also provided constructive feedback on grammatical issues.

I cannot complete this acknowledgement section without mentioning the contribution of my family. My parent's inspiration was always extraordinary. While I started this PhD, I also got a precious gift that was the birth of my daughter Nairah Islam in 2015. This PhD has grown up in parallel with the growth of my daughter over the last 4 years! While I was highly occupied with this PhD project, my wife (Tanjila Azad) had provided tremendous moral and family support. Probably a thank you is not enough to recognise her contributions, yet I still say thank you so much. Without the contribution of my family members, I could not reach to this stage.

Last not but least, I would like to acknowledge and thank for the financial support from the different organisations. Firstly, I acknowledge the contribution of the Australian Research Council, Australian Government for the scholarships which was provided via the different funding schemes (AIBN Group Leader Living Allowance and Monash Departmental Scholarship). This PhD program was supported by an Australian Government Research Training Program (RTP) Scholarship. I also thank other funding bodies such as Faculty of Engineering, Monash University for awarding the Graduate Research International Travel Award (AUD \$6666) and ARC Centre of Excellence in Convergent Bionano Science and Technology (CBNS) for the Student Travel Award (AUD \$1000). I also thank the BioProcessing Network Conference for awarding the best oral presenter by an early career researcher (AUD \$500). I am thankful for financial support from the NEL Group throughout my candidature.

## Lists of abbreviations

AMI	Acute myocardial infarction
Anap	(3-(6-acetylnaphthalen-2-ylamino)-2-aminopropanoic acid)
BGH	Bovine growth hormone
bp	Base-pairs (Nucleotide)
Cat#	Catalogue number
CD-CHO	Chemically-defined Chinese hamster ovary
CDR	Complementarity determining regions
CHO	Chinese hamster ovary
CNT	Carbon nanotube
C-term	Mutant containing Anap in the C-terminal site
cTnI	Cardiac Troponin I
DanAla	Dansylalanine
DARPin	Designed ankyrin repeat proteins
DBCO	Dibenzocyclooctyne
DLS	Dynamic light scattering
DPBS	Dulbecco's phosphate-buffered saline
DTT	Dithiothreitol
EDC	1-Ethyl-3-(3-dimethylaminopropyl)carbodiimide
EGFP	Enhanced green fluorescent protein
EGFR	Epidermal growth factor receptor
ELISA	Enzyme-linked immunosorbent assay
ESI-MS	Electrospray ionisation mass spectrometry
Fab	Fragment antigen binding
FRET	Foster resonance energy transfer
fUAA	Fluorescent unnatural Amino Acid
GBP	Glutamine (Gln) binding protein
GdnHCl	Guanidium hydrochloride
GFP	Green fluorescent protein
GSSG	Glutathione disulfide

H53Y	Tyrosine (Y) residue of heavy chain (H) at 53 position replaced with Anap
HA-tag	Hemagglutinin tag
HEK	Human embryonic kidney
HeLa	Henrietta Lacks
HER2	Human epidermal growth factor receptor 2
His-tag	Poly-histidine tag
HRP	Horseradish peroxidase
IMAC	Immobilized metal affinity chromatography
L27c-Y	Tyrosine (Y) residue of light chain (L) at 27c position replaced with Anap
LB	Luria-Bertani media or Lysogeny Broth
LOD	Level of detection
mAbs	Monoclonal antibodies
MW	Molecular weight
MWCO	Molecular weight cut off
NHS	<i>N</i> -Hydroxysuccinimide
Ni-NTA	Nickel-nitrilotriacetic acid
N-term	Mutant containing Anap in the N-terminal site
OD	Optical density
pAcF	<i>para</i> -acetylphenylalanine
pAzF	<i>para</i> -azidophenylalanine
PBS	Phosphate buffer saline
PCR	Polymerase chain reaction
PDB	Protein data bank
PEG	Polyethylene glycol
PET	Photoinduced electron transfer
POC	Point-of-care
POCT	Point-of-care technology
Q-body	Queenchbody
QD	Quantum dot

RNA	Ribonucleic acid
rpm	Revolutions per minute
sAbs	Single antibodies
scFv	single-chain variable fragment antibody
SD	Standard deviation
SDS-PAGE	Sodium dodecyl sulfate polyacrylamide gel electrophoresis
SEM	Standard error of the mean
SERS	Surface Enhanced Raman Scattering
smFRET	Single-molecule FRET
SNAP tag	self-labelling protein tag
SPR	Surface Plasmon Resonance
ssDNA	Single-stranded DNA
SUMO	Small Ubiquitin-like Modifier
SWCNT	Single-walled carbon nanotube
TAMRA	Carboxytetramethylrhodamine
TCSPC	time-correlated single photon counting
TIRF	Total internal reflection fluorescence
TMB	3,3',5,5'-tetramethylbenzidine
tmFRET	transition metal ion FRET
UAA	Unnatural Amino Acid
Units of measurement used	Nanomolar (nM), micromolar ( $\mu$ M), millimolar (mM), molar (M), microlitre ( $\mu$ L), millilitre (mL), litre (L), microgram ( $\mu$ g), milligram (mg), gram (g), nanometre (nm), Dalton (Da), kilodaltons (kDa), minutes (min), seconds (s), hours (hrs), n=number of replicates
UV	Ultraviolet
VEGFR2	Vascular endothelial growth factor receptor 2
V <sub>H</sub>	Variable heavy chain
V <sub>L</sub>	Variable light chain
WHO	World health organisation
WT	Wild type

# Contents

<b>1. INTRODUCTION</b>	<b>1</b>
1.1 BIOSENSORS: PRINCIPLES, TYPES AND RESEARCH NEEDS	1
1.2 THESIS STRUCTURE	11
<b>2. LITERATURE REVIEW</b>	<b>13</b>
2.1 ENGINEERED ANTIBODIES AS A BIO-RECOGNITION ELEMENT	14
2.2 FLUORESCENCE LABELLING STRATEGIES OF ENGINEERED ANTIBODIES	18
2.2.1 GENERAL METHODS FOR FLUORESCENCE LABELLING	18
2.2.2 FLUORESCENCE LABELLING BY UNNATURAL AMINO ACID (UAA)	21
2.3 USE OF ENGINEERED ANTIBODIES IN FLUORESCENT BIOSENSORS	30
2.4 SURFACE IMMOBILISATION OF ENGINEERED ANTIBODIES	38
2.5 RATIONALE OF THE PROJECT	44
2.6 AIMS AND HYPOTHESES	45
2.7 CHAPTER 2 SUMMARY	48
<b>3. METHOD DEVELOPMENT FOR FLUORESCENCE LABELLING OF ENGINEERED ANTIBODIES</b>	<b>49</b>
3.1 INTRODUCTION	50
3.2 MATERIALS AND METHODS	55
3.2.1 CLONING OF scFv INTO THE EXPRESSION VECTOR	55
3.2.2 INCORPORATION OF UAA IN MAMMALIAN CELLS	57
3.2.3 EXPRESSION OF EGFR (EXTRACELLULAR DOMAINS) PROTEIN	60
3.2.4 CHARACTERIZATION OF PURIFIED scFv MUTANTS	61
3.2.5 INCORPORATION OF UAA IN THE BACTERIAL CELLS	63
3.3 RESULTS AND DISCUSSION	69
3.3.1 INCORPORATION OF ANAP INTO N- AND C-TERMINI OF ANTI-EGFR scFv	71
3.3.2 INCORPORATION OF CLICKABLE UAA IN THE N- AND C-TERMINI OF ANTI-EGFR scFv	83
3.4 CHAPTER 3 SUMMARY	88
<b>4. DETECTION OF EGFR BY FLUORESCENTLY LABELLED ENGINEERED ANTIBODIES</b>	<b>91</b>

<b>4.1</b>	<b>PUBLISHED CHAPTER</b>	<b>93</b>
<b>4.2</b>	<b>SUPPORTING DATA</b>	<b>118</b>
<b>4.3</b>	<b>CHAPTER 4 SUMMARY</b>	<b>131</b>
<b>5.</b>	<b><u>DETECTION OF HUMAN CARDIAC TROPONIN- I BY FLUORESCENTLY LABELLED ENGINEERED ANTIBODIES</u></b>	<b><u>132</u></b>
<hr/>		
<b>5.1</b>	<b>INTRODUCTION</b>	<b>133</b>
<b>5.2</b>	<b>MATERIALS AND METHODS</b>	<b>140</b>
5.2.1	EXPRESSION, PURIFICATION AND CHARACTERISATION OF ANTI-CTNI SCFV ANTIBODIES	140
5.2.2	FLUORESCENCE MEASUREMENT	142
5.2.3	AFFINITY AND STABILITY TESTING	145
5.2.4	SURFACE ATTACHMENT OF H53Y AND L27C-Y BIOSENSORS	146
<b>5.3</b>	<b>RESULTS AND DISCUSSIONS</b>	<b>149</b>
5.3.1	DETECTION OF CTNI PROTEIN	149
5.3.2	SURFACE IMMOBILISATION OF H53Y AND L27C-Y BIOSENSORS	171
<b>5.4</b>	<b>CHAPTER 5 SUMMARY</b>	<b>176</b>
<b>6.</b>	<b><u>CONCLUSIONS AND FUTURE STUDIES</u></b>	<b><u>178</u></b>
<hr/>		
<b>7.</b>	<b><u>APPENDICES</u></b>	<b><u>184</u></b>
<hr/>		
<b>7.1</b>	<b>DNA SEQUENCE OF ANTI-EGFR SCFV</b>	<b>185</b>
<b>7.2</b>	<b>COMMONLY USED tRNA-AARS FOR UAA INCORPORATION</b>	<b>186</b>
<b>7.3</b>	<b>EXTRACT OF DNA SEQUENCE ANALYSIS FOR ANTI-EGFR SCFV MUTANTS</b>	<b>187</b>
<b>7.4</b>	<b>CLEAVAGE OF ANTI-EGFR SCFV SEQUENCE BY TRYPSIN</b>	<b>190</b>
<b>7.5</b>	<b>CRYSTALLISATION EXPERIMENTS OF ANTI-CTNI SCFV</b>	<b>190</b>
<b>7.6</b>	<b>CLONED SEQUENCE OF ANTI-CTNT SCFV ANTIBODY</b>	<b>191</b>
<b>7.7</b>	<b>EXTRACT OF DNA SEQUENCING FOR ANTI-CTNI SCFV MUTANTS</b>	<b>192</b>
<b>7.8</b>	<b>PARAMETERS OF CTNI PROTEIN</b>	<b>194</b>
<b>7.9</b>	<b>INDIRECT ELISA TO COMPARE BINDING BETWEEN L27C-Y AND WT ANTI-CTNI SCFV</b>	<b>195</b>
<b>7.10</b>	<b>FLUORESCENCE MEASUREMENT OF DY640 AND DY641</b>	<b>196</b>
<b>7.11</b>	<b>SOLVENT ACCESSIBILITY DETERMINATION BY BIOINFORMATICS TOOLS</b>	<b>197</b>
<b>7.12</b>	<b>PRINCIPLES OF SOME METHODS USED IN THIS THESIS</b>	<b>199</b>
7.12.1	FLUORESCENCE LIFETIME	199

7.12.2	BIO-LAYER INTERFEROMETRY	201
7.12.3	DYNAMIC LIGHT SCATTERING	202
<b>7.13</b>	<b>FLUORESCENCE DETECTION BY MINIATURISED FLUORIMETER</b>	<b>203</b>
<b>8</b>	<b>REFERENCES</b>	<b>204</b>

---

## List of figures

FIGURE 1: ELEMENTS OF A TYPICAL BIOSENSOR PLATFORM.....	2
FIGURE 2: CLASSIFICATION OF BIOSENSORS BASED ON BIORECOGNITION ELEMENTS AND TRANSDUCERS.....	3
FIGURE 3: SCHEMATIC COMPARISON BETWEEN MULTISTEP IMMUNOASSAYS AND SINGLE STEP IMMUNOSENSORS..	10
FIGURE 4: REPRESENTATION OF VARIOUS ANTIBODY FORMATS ILLUSTRATING COMMONLY USED SINGLE CHAIN FV (SCFV), BISPECIFIC AND FAB RECOMBINANT ANTIBODIES.....	16
FIGURE 5: GENERAL ILLUSTRATION OF UAA INCORPORATION DURING PROTEIN BIOSYNTHESIS.....	22
FIGURE 6: FLUORESCENCE LABELLING VIA UAA. ....	23
FIGURE 7: EVOLUTION OF A TRNA/TRNA SYNTHETASE PAIR IN E. COLI.....	26
FIGURE 8: VARIOUS STRATEGIES FOR DEVELOPING FLUORESCENT BIOSENSOR. ....	31
FIGURE 9: SCHEMATIC OF A TYPICAL FLUORESCENT IMMUNOSENSOR BY TAKING ADVANTAGE OF AN SCFV ANTIBODY AS A BIORECOGNITION ELEMENT..	33
FIGURE 10: REPRESENTATION OF Q-BODY REAGENTLESS FLUORESCENT BIOSENSORS. ....	37
FIGURE 11: DIFFERENT DETECTION MECHANISMS BASED ON SURFACE IMMOBILISATION..	41
FIGURE 12: ANAP INCORPORATION INTO SCFV SEQUENCES IN MAMMALIAN CELLS..	53
FIGURE 13: NUCLEOTIDE AND AMINO ACID SEQUENCE OF ANTI-EGFR SCFV. ....	70
FIGURE 14: BINDING INTERFACE OF ANTI-EGFR FAB ANTIBODY.....	71
FIGURE 15: CONFIRMATION OF CONSTRUCT CLONING.....	72
FIGURE 16: OPTIMISATION OF SCFV EXPRESSION FOR ANAP INCORPORATION. ....	73
FIGURE 17: PURIFICATION OF N-TERM MUTANT USING PROTEIN L AFFINITY CHROMATOGRAPHY..	76
FIGURE 18: CONFIRMATION OF EXPRESSION, PURIFICATION AND SELECTIVE ANAP INCORPORATION.....	77
FIGURE 19: PEPTIDE MASS FINGERPRINTING OF WT ANTI-EGFR SCFV.....	79
FIGURE 20: TESTING FUNCTIONALITY OF SCFV MUTANTS..	80
FIGURE 21: EMISSION SPECTRA OF N- AND C- TERM MUTANTS. ....	81
FIGURE 22: DENATURATION OF N- AND C-TERM MUTANTS WITH 7M UREA.....	82
FIGURE 23: MONITORING EXPRESSION OF SCFV MUTANTS FOR PACF UAA INCORPORATION.....	85

FIGURE 24: EXPRESSION AND CHARACTERISATION OF PAZF INCORPORATED N-TERM ANTI-EGFR SCFV MUTANT.....	87
FIGURE 25: OPTIMISED ANTI-CTNI SCFV WT SEQUENCE FOR EXPRESSION IN MAMMALIAN CELLS. ....	141
FIGURE 26: PEPTIDE-BOUND (FIREBRICK RED) AND UNBOUND (DEEP-TEAL CYAN) CRYSTAL STRUCTURE OF ANTI-CTNI SCFV ANTIBODY.....	149
FIGURE 27: MUTATION SITES FOR FLUOROPHORE INCORPORATION.. ....	151
FIGURE 28: CHARACTERISATION OF ANAP LABELLED ANTI-CTNI SCFV MUTANTS. ....	153
FIGURE 29: RESPONSE OF ANTI-CTNI-ANAP SCFV MUTANTS TO THE CTNI PEPTIDE.. .....	156
FIGURE 30: DETECTION OF THE CTNI PEPTIDE IN PBS BUFFER.....	158
FIGURE 31: DETECTION OF FULL-LENGTH CTNI PROTEIN IN PBS BUFFER AND HUMAN PLASMA. ....	160
FIGURE 32: TIME-CORRELATED SINGLE PHOTON COUNTING (TCSPC) MEASUREMENT TO DETERMINE THE FLUORESCENCE LIFETIME OF ANAP LABELLED L27C-Y MUTANT.....	161
FIGURE 33: EMISSION WAVELENGTH SHIFT IMAGING IN UVP (BIOSPECTRUM) GEL IMAGER.....	164
FIGURE 34: BINDING KINETICS ANALYSIS BY BIOLAYER INTERFEROMETRY.. ....	165
FIGURE 35: SIZE DISTRIBUTION STUDY FOR WT AND L27C-Y MUTANT IN DLS.. ....	167
FIGURE 36: CY5 FLUORESCENCE LABELLING OF THE L27C-Y SITE VIA PAZF UAA.....	169
FIGURE 37: COMPARISON OF THE MOST OPTICALLY ACTIVE MUTANTS.....	170
FIGURE 38: SCHEME DEMONSTRATES SURFACE IMMOBILISATION OF ANTIBODY ON SWCNT THROUGH FUNCTIONALISED SHORT OLIGONUCLEOTIDES.....	172
FIGURE 39: IMMOBILISATION OF H53Y BIOSENSOR ONTO CARBON NANOTUBE.....	173
FIGURE 40: IMMOBILISATION OF L27C-Y SENSOR ONTO AGAROSE BEADS.....	175
FIGURE 41: DETERMINATION OF FLUORESCENCE INTENSITY (FI) CHANGE BY THE FLUORIMETER. ....	182
FIGURE 42: PREDICTION OF TRYPSIN CLEAVAGE SITES BY EXPASY: PEPTIDECUTTER PROGRAM. ....	190
FIGURE 43: HYDROPHOBICITY OF CTNI PROTEIN.....	195
FIGURE 44: COMPARISON OF BINDING SPECIFICITY BETWEEN WT AND L27C-Y MUTANT.....	196
FIGURE 45: FLUORESCENCE MEASUREMENT OF NEAR-INFRARED FLUOROPHORE IN DIFFERENT SOLVENTS, (A) DY640 AND (B) DY641 FLUOROPHORE. ....	197
FIGURE 46: THE JABLONSKI DIAGRAM DEPICTS THE LIFE HISTORY OF AN EXCITED STATE ELECTRON IN A LUMINESCENT PROBE.....	199

FIGURE 47: SCHEMATICALLY SHOWING THE (A) PRINCIPLES OF BLI AND (B) STEPS INVOLVED IN A REPRESENTATIVE BINDING KINETICS ANALYSIS IN BLI.....	202
FIGURE 48: EXAMPLES OF FLUORIMETERS.....	203

## List of tables

TABLE 1: ENGINEERED ANTIBODY-BASED IMMUNOSENSORS AND IMMUNOASSAYS..	17
TABLE 2: FLUORESCENCE LABELLING OF SCFV ANTIBODY THROUGH TAGGING SYSTEMS.....	19
TABLE 3: FLORESCENT UAAS REPORTED IN THE LITERATURE TO DATE. ....	30
TABLE 4: COMMON SURFACE AND STRATEGIES OF ANTIBODY FRAGMENT IMMOBILISATION ONTO VARIOUS SOLID SURFACES.....	43
TABLE 5: PRIMER DESIGN FOR THE ANTI-EGFR SCFV MUTANTS.....	55
TABLE 6: PERFORMANCE AND DETECTION METHODS OF DIFFERENT CTNI IMMUNOASSAYS REPORTED FOR COMMERCIAL USE.....	135
TABLE 7: LISTS OF POC DEVICES DEVELOPED BY DIFFERENT COMPANIES. ....	136
TABLE 8: SEQUENCE OF ANTI-CTNI SCFV (SCFV 180).....	150
TABLE 9: LIFETIME MEASUREMENT IN THE ABSENCE AND PRESENCE OF CTNI PEPTIDE AND PROTEIN.....	162
TABLE 10: AFFINITY OF CONSTRUCTS DETERMINED BY BINDING KINETICS ANALYSIS IN BLI. ....	166
TABLE 11: COMMONLY USED UAA AND THEIR RESPECTIVE TRNA/TRNA SYNTHETASE SEQUENCE CONTAINING PLASMID. ....	186
TABLE 12: THE AMINO ACID SEQUENCE OF ANTI-CTNI SCFV.....	191
TABLE 13: RECOMBINANT CTNI AMINO ACID SEQUENCE PRODUCED IN E. COLI.....	194
TABLE 14: GETAREA 1.0 BETA GENERATED SOLVENT ACCESSIBILITY PREDICTION OF ANTI-CTNI SCFV SEQUENCE.....	197
TABLE 15: NETSURFP ANALYSIS OF SOLVENT ACCESSIBILITY PREDICTION FOR THE ANTI-EFR SCFV SEQUENCE.....	198

# Chapter One

## 1. Introduction

---

## 1.1 Biosensors: principles, types and research needs

The market for biosensors has grown exponentially over the last two decades and is forecast to be over USD 27b by 2022.[1] This market growth has primarily been driven by the need for a biosensing mechanism in diverse applications in various fields including development of biopharmaceuticals, detection of biomolecules as a means of diagnostics including lab-based, point-of-care, home and wearable diagnostics. Biosensors are also widely used in biological research to study biomolecular interactions. Apart from the diagnostics and biological research, biosensors have also found applications in monitoring infectious and environmental agents in the biodefense, food and agriculture industries.[2]

The term “biosensor” refers to an analytical device that can selectively interact with target molecules in biological samples and translate the binding event into measurable signals.[3-6] By most definitions a biosensor consists of three major elements as shown in *Figure 1*: (i) a biorecognition element, also known as a bioreceptor or bio-element (*e.g.* antibodies, cells, enzymes and aptamers); (ii) a transducer which converts affinity or activity interactions into quantifiable signals (*e.g.* nanoparticles, electrodes and fluorophores); and (iii) a system which is capable of converting detected signals into a suitable format for analysis.[7] Clark and Lyons reported the first biosensor in 1962, an enzyme electrode for blood gas content analysis.[8] The term was first coined by Cammann to describe ion-selective electrodes in 1977.[9] Despite significant research in this area; the key challenge remains to develop a universal biosensor platform for sensing disease-related proteins in real-time from complex biological solutions in a single-step.[10, 11]

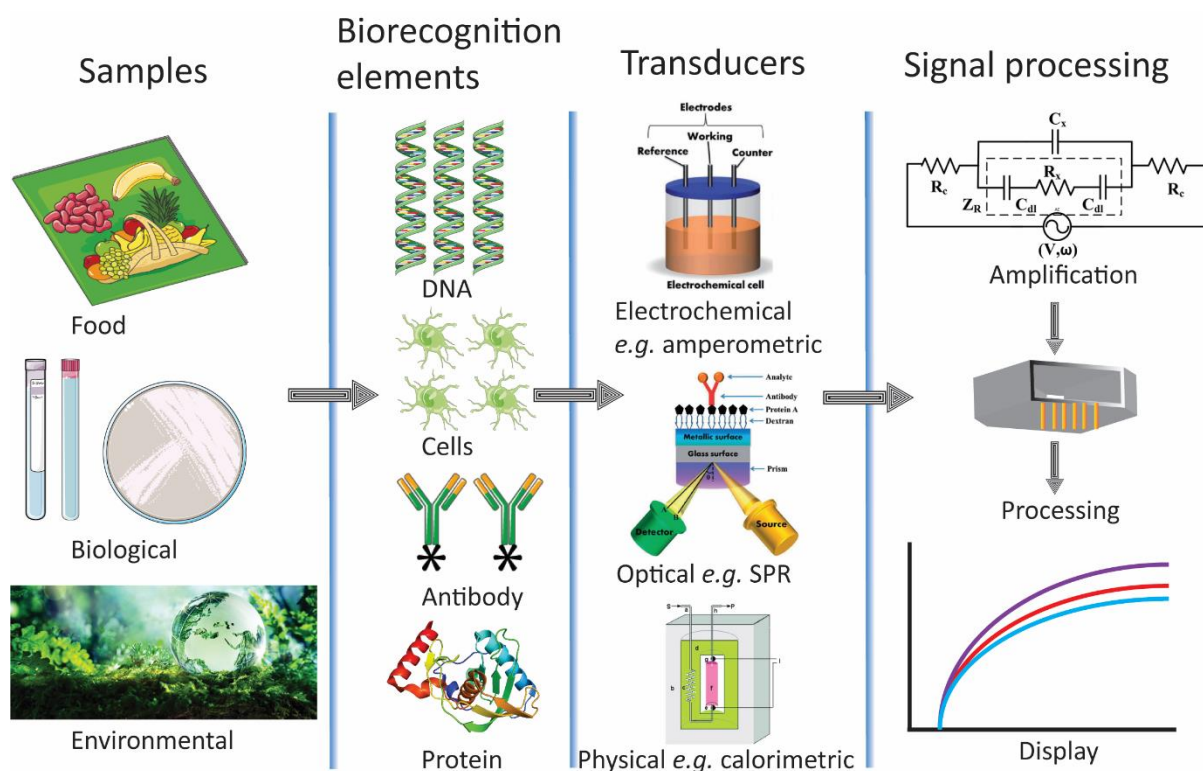


Figure 1: Elements of a typical biosensor platform.[7, 12] The diagram depicts different phase of a typical biosensing process and different component of a biosensor such as sample is added to the biorecognition element which is connected to a signal transducer. Once a binding event occurs, the signal is transduced either in the form of electrochemical, optical or physical properties for analysis.

Biosensors can be classified as “activity” or “affinity” types according to the biorecognition element used for interactions with a ligand (Figure 2). Activity-based biosensors mostly rely on the catalytic activity of enzymes by activation, inhibition or modification of analytes for signal generation.[13] The glucose biosensor is a classic example of an activity biosensor.[14] By contrast, affinity biosensors rely on the affinity between the surface-bound probes and target analytes (e.g. antibody-antigen interaction and DNA-RNA hybridisation to complementary sequences).[15] These affinity-based biosensors can be classified based on their recognition elements such as antibodies, proteins, aptamers, phage and small synthetic reporter molecules. Immunosensors are one of the commonly used affinity biosensors where antibodies are used as a biorecognition

element. Affinity biosensors are capable of being generic (e.g. for pregnancy tests and water quality monitoring) for different target molecules using single platforms and are able to generate signals from complex solutions.[10, 16] However, achieving lower limits of detection for proteins in human body fluids such as blood is still challenging.[17]

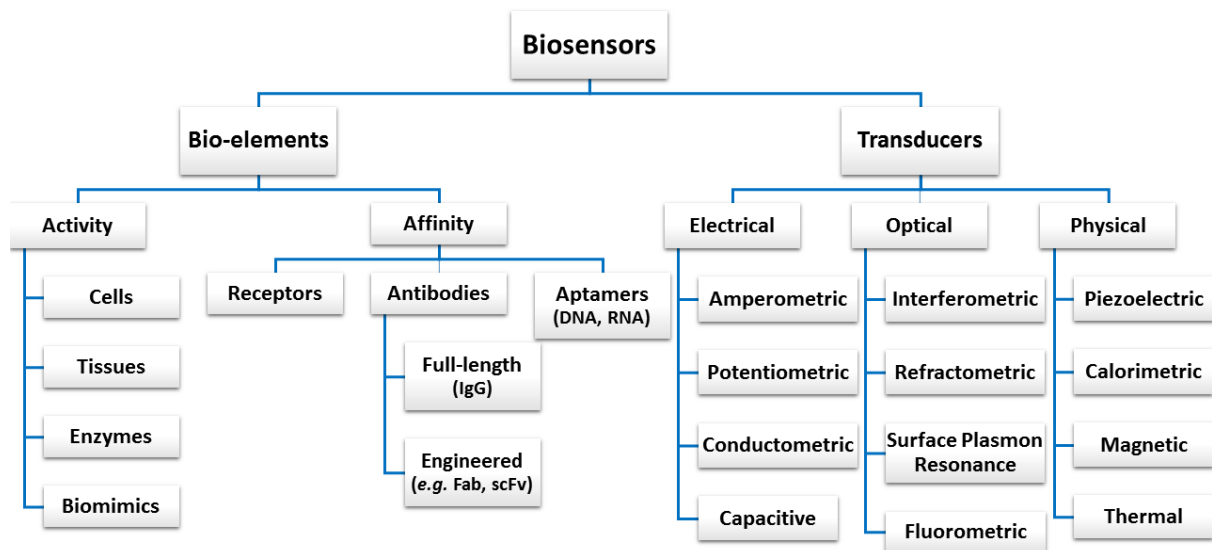


Figure 2: Classification of biosensors based on biorecognition elements and transducers. Two major forms of biosensors are based on the use of different types of biorecognition elements (e.g. antibodies) and transducers (e.g. fluorescence).[18, 19]

In affinity biosensor development, antibodies are considered as the prime class of biorecognition element utilised (hence these biosensors are referred to throughout this thesis as “immunosensors”).[20] Monoclonal antibodies (mAbs), an identical immunoglobulin produced by single B-cells as a part of body’s defence mechanisms, have been routinely used in immunoassays since the 1960s and are the most commonly employed antibody-based affinity probes.[21] Even though mAbs have been successful in the development of immunoassays, these antibodies have several disadvantages. In order to be integrated into a

biosensing platform, mAbs need to retain their specificity in complex biological fluids and need to be stable on the surface since the majority of biosensors involve surface immobilisation for signal transduction. Additionally, the large size of the antibody molecule can result in disoriented immobilisation, poor stability, and steric hindrance due to their structural similarity with other proteins in the complex human body fluid.[22] The constant regions (known as the Fc portion) of mAbs may interfere in surface immobilisation by contributing random conformational change or taking part in unwanted reactivity.[23] Despite the popularity of the use of mAbs in immunoassays, only a small fraction of these have found application in immunosensor development. The field becomes even narrower in terms of using engineered antibodies as an alternative to full-length antibodies. *Thus, there is an urgent demand for creating novel affinity biosensors based on engineered antibodies as a biorecognition element.*

A key element of biosensors is a transducer that converts the binding of target ligands to quantifiable signals. Depending on the detection principle employed, transducers can be classified into many types (*Figure 3*). The most commonly used transducers fall into three major groups: electrochemical, optical and physical transducers. Electrochemical biosensors rely on the catalytic activity of redox enzymes that produce electrical signals correlated with analytes. Though this type of biosensors exhibits a low level of detection (LOD), a significant drawback is poor stability of the sensors and the need for passivation of the sensor surface. Another key problem is the generation of false positive signals by every nonspecific protein attracted to the sensor surface leading to difficulties in the interpretation of measurements in complex biological solutions.[24] Additionally, the detection of large biomolecules (*e.g.* proteins) is difficult as electrochemical assays often rely on the molecular weight

cut-off (MWC0) layers on the transducers to reduce the transit of large nonspecific molecules to the surface.[17, 25]

Despite the dominance of electrochemical systems, many optical biosensors have emerged during the last few decades due to the fact that they not only offer comparable features (*e.g.* specificity, sensitivity and real-time monitoring) to traditional detection systems but also add the advantage of detection without a surface, or the need for a physical connection between the bioreceptor and transducer. Optical biosensors combine the biorecognition element with the optical transducer (*e.g.* fluorescent dye) and generally measure changes in the optical properties of a surface or of the bioreceptor following interaction with a target binder, mostly in the form of a refractive index, absorbance, fluorescence, luminescence, reflectance and Raman scattering.[26] Physical biosensors use transducers that convert physical changes (*e.g.* acoustic wave and light) upon binding to the target molecule. Some typical examples of physical biosensors include piezoelectric, calorimetric and magnetic biosensors.

Optical biosensors can be categorised into two types based on the detection mechanism used: label-free and label-based systems.[27] Label-free biosensors detect interactions directly based on the intrinsic properties of the analytes such as conformational change, or electrical property change in the surface probe.[28] Surface Plasmon Resonance (SPR) and Biolayer Interferometry (BLI) are among the most common examples of label-free biosensors. Whereas these types of biosensors enable real-time detection, they are mostly limited to use in a research laboratory due to the need for sophisticated laboratory infrastructure and highly skilled operators. Label-based biosensors detect changes occurring in the labelled molecules when they bind to the target. Some of the commonly used labels in these types of biosensors are nanoparticles,[29] enzyme reporters[26] and fluorescent tags.[30, 31] Fluorescence-based biosensors have emerged as an

alternative to the label-free detection systems because of the detection based on a simple change in fluorescence properties (*e.g.* intensity or wavelength) upon target binding. One of the main advantages of these sensors is the generation of a low signal-to-noise ratio during the detection of molecules as these sensors separate molecular recognition events from surfaces, therefore reducing interference from nonspecific adsorption.[32] Whereas label-free detections are limited to SPR, BLI and total internal reflection fluorescence (TIRF) technology, fluorescent biosensors can use a wide range of simple detection options such as spectroscopy, microscopy and flow cytometry.

Biosensing principles can be further classified into heterogeneous and homogeneous biosensing techniques.[33] Heterogeneous biosensing techniques often involve multiple steps (*e.g.* ELISA) including a washing step to remove unbound antigens and contaminants. They also require immobilisation of the bioreceptor onto the sensor surface, and the detection relies on diffusion of the sample to the sensor surface. Therefore, these techniques are systematically time consuming and laborious process which limits their applicability in point-of-care (POC) diagnostics. Homogeneous biosensing techniques produce signals without the necessity of sample processing such as washing steps (*i.e.* signal generation within the given samples), therefore reducing time and labour.[34] Several types of transducer can be employed to develop wash-free homogeneous bioassays including calorimetric, fluorescence, electrochemical and magnetic transducers. An example of a homogeneous assay is the Forster resonance electron transfer (FRET) mechanism where no additional step is required for signal generation.[35, 36] Although examples of homogeneous assays are regularly reported, there are fewer homogeneous biosensors that rely on a single assay component. *Hence, there is a compelling need to develop a homogeneous biosensor*

*using a single assay component for detection of the target protein in one step without the need for a separation step or additional reagents.*

The homo- or heterogeneous nature of biosensors mentioned above can also be alternatively termed as a solution or a solid-phase detection system respectively.[[37](#), [38](#)] Solution-phase biosensing can be carried out in a single step without the need for an immobilisation step, and hence it does not suffer the mass transfer limitations between the surface and bio-component. In some instances, recombinant proteins tend to denature upon attaching on the solid surface, and therefore solution-based detections are preferred.[[22](#), [39](#)] Conversely, solid- phase detection systems provide a number of extra benefits such as facilitating the immobilisation on the sensor surface, thus allowing detection on a flow channel such as microfluidic devices and lateral flow systems.[[40](#), [41](#)] Additionally, solid-phase methods enable exploitation of unique properties of sensor surfaces to improve the sensitivity of a biosensor. The majority of the currently available immunoassays are based on solid-phase detection methods which is also crucial for developing POC biosensors. In the past few decades, there has been a growing interest in the attachment of antibodies to the nanoparticle surfaces where the physicochemical properties of nanoparticles are utilised widely. These properties have been explored both in the therapeutics and diagnostics fields. For example, the optical properties of nanoparticles have found application in SPR based label-free detection. immobilisation of antibodies or their engineered fragments onto the nanoparticle surfaces may be useful for the fabrication of ratiometric biosensors.[[42](#)]

An emerging class of homogenous biosensor is a “reagentless” protein biosensor that depicts sensing in a single step (wash-free) without the need for secondary reagents (hence reagentless) to develop detectable signals.[[43](#)] A key feature of this approach is the use of a single sensor component in assay systems

which is vital for the development of POC diagnostics. Even though this technology offers the likelihood of laboratory-free diagnostics, only minor research has reported the development of reagentless fluorescent biosensors that exploit the advantages of antibody fragments as the bio-element. This type of biosensor has an exceptional capability to replace traditional bioassays. Conventionally, most disease-related proteins are detected using bioassays (*e.g.* ELISA) to diagnose the disease, a process which is a time consuming, multi-step process involving washing, blocking, labelling and a long incubation period, and that requires highly trained personnel and sophisticated laboratory infrastructure (*Figure 3A*). Alternatives to these traditional methods, such as a point-of-care testing system for disease diagnosis, are highly desirable to minimise long delays and monitor the progression of diseases in real time (*Figure 3B*).[\[44\]](#)

This project aims to develop a proof-of-concept for a one-step reagentless fluorescent biosensor by generating fluorescently labelled engineered antibodies that undergo spectral shifts upon analyte binding. While a range of biosensor platforms has been reported, reagentless biosensors that use affinity-based interactions to detect proteins using a variety of simple fluorescent methods have not been extensively explored. To date, only a few researchers have reported reagentless fluorescent biosensors.[\[45\]](#) Though detection methods in these reported biosensors depend on simple fluorescence modulation, the biorecognition element (such as single chain antibody or artificial families of antigen binding proteins known as DARPins) and the type of fluorophores (*e.g.* solvatochromic or TAMRA) may vary.[\[43, 46, 47\]](#)

The major challenge in developing this type of sensor is to identify a suitable fluorophore and incorporate it precisely into the targeted site and then screen these labelled sites to quantify the target analytes.[\[48\]](#) This project seeks

to address these challenges, and the literature review in the next chapter summarises progress to date in this field. Site-specific fluorescence labelling is a prerequisite for developing reagentless biosensors. Using traditional fluorescence labelling, it can be challenging to incorporate a desired fluorophore at specific site in a protein.[49] Unnatural amino acid technology for site-specific fluorophore incorporation has recently emerged as alternative to conventional dye labelling strategies.[50] The proposed biosensing method will significantly reduce assay time compared to traditional methods. Such a biosensor has the potential to be integrated into a range of existing and emerging diagnostic devices including microfluidic platforms and rapid test strips for routine diagnosis of diseases in pathology laboratories, clinics or in a home setting without the need for professionals. Apart from diagnostic applications, the proposed strategies for labelling recombinant antibodies could also be used in other applications such as reporter proteins for labelling cells, *in vivo* imaging and theranostics.[51, 52]

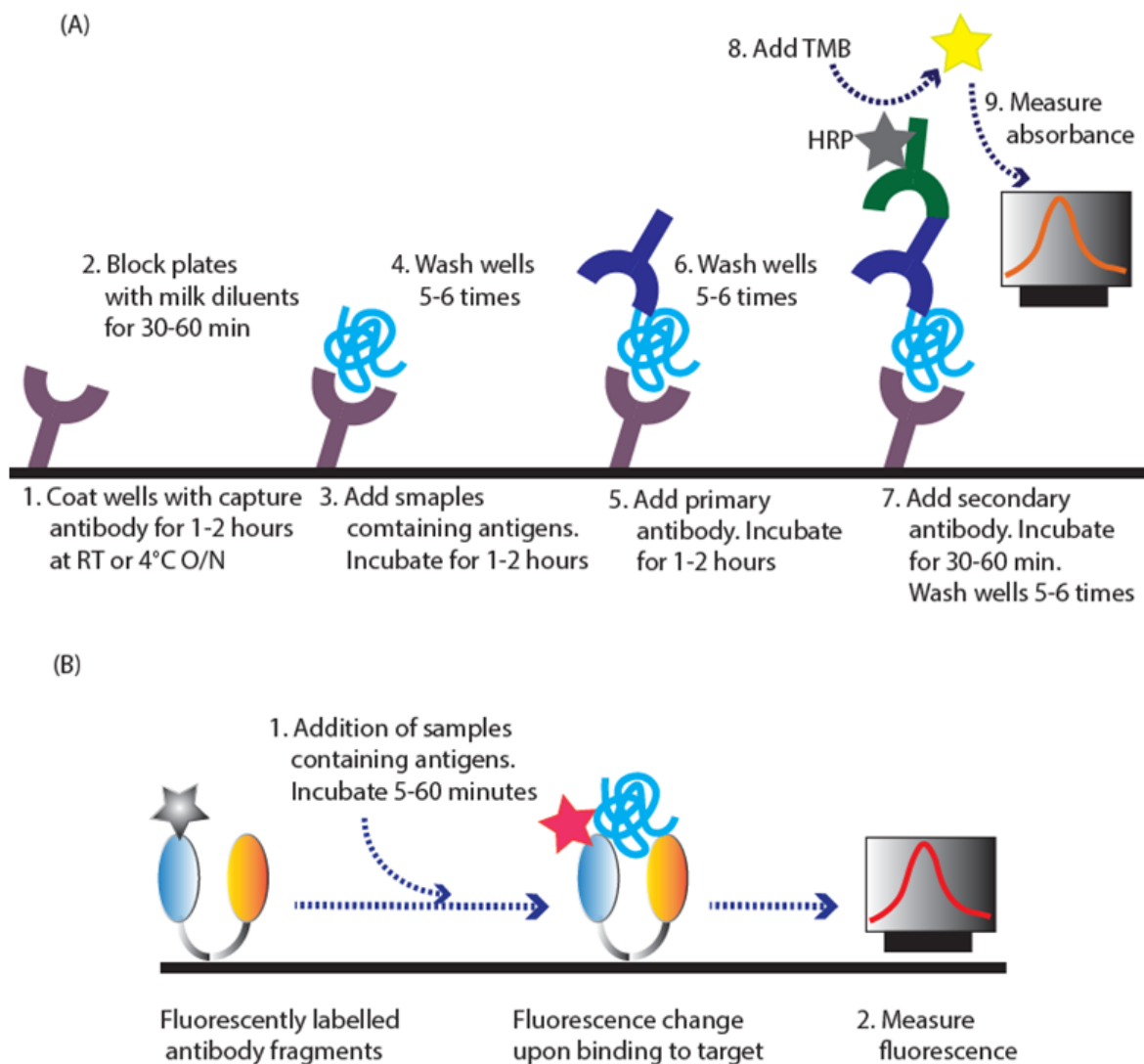


Figure 3: Schematic comparison between multistep immunoassays and single step immunosensors. (A) Traditional bioassays such as ELISA based on several steps (e.g. blocking, washing and incubation) and reagents (e.g. secondary antibody and TMB). (B) A one-step fluorescence-based immunodiagnostic technique based on engineered antibodies where sample is mixed with the modified antibodies and fluorescence is measured readily.

The preceding discussion identifies a significant gap for the development of a one-step biosensor for the detection of the target protein. Although different types of biosensors were reported, only a few biosensors had utilised engineered antibodies as bioreceptors and fluorescent dyes incorporated within the internal position of a protein for signal generation. Despite the fact that a class of reagentless biosensors had shown fluorescence intensity modulation (e.g. FRET, Quenchbody) upon binding to a target ligand, none of them utilised fluorescence

*emission spectra (a unique feature of specific fluorophores) as the basis of quantification. This thesis aims to address the above issues.*

## **1.2 Thesis structure**

In this thesis, Chapter 2 presents a comprehensive literature review focusing on antibody engineering for biosensing applications, site-specific fluorescence labelling of engineered antibodies via unnatural amino acids (UAA) and recent works on engineered antibody-based fluorescent biosensors. Chapter 3 describes the development of a method for site-specific genetic incorporation of UAAs to facilitate fluorophore labelling of antibody fragments. Briefly, this chapter outlines the expression of engineered antibodies in mammalian and bacterial systems for UAA incorporation followed by purification of these antibodies using a variety of chromatography methods. The purified antibodies were then thoroughly characterised using different bioanalytical methods. In the work reported in Chapter 4, the position of the UAA was varied in the internal sites of the engineered antibody using the methods developed in Chapter 3. A proof-of-concept was established for the rational design of polarity dependent fluorescent biosensors that showed dose-dependent response when binding to target analytes. The concept used anti-EGFR scFv as a model system for the detection of EGFR protein. The results of this work have been published in a peer-reviewed journal (Analytical Chemistry).

Chapter 5 describes the application of the -proposed method for the detection of human cardiac troponin I (cTnI) protein. The selection of fluorophore labelling sites was determined based on a structure-guided design instead of a homology model structure. The chapter also discusses the effects of surface immobilisation of anti-EGFR and anti-cTnI fluorescent biosensors on solid surfaces. Finally, Chapter 6 provides the conclusion of the research and outlines

some recommendations for the future research direction of the proposed biosensing method. The principles of some key methods, used throughout this research project, have also been described in the appendices of this thesis. Each of the chapters is structured as introduction, materials and methods, results and discussion, followed by a chapter summary.

# Chapter Two

## 2. Literature Review

---

The literature review focuses on a wide range of multi-disciplinary research areas which contribute to the development of a successful biosensor including the field of recombinant antibody technology, site-specific fluorescence labelling and surface immobilisation strategy. This review first presents a review of the potential of engineered antibodies in the biosensing field, fluorescence labelling methodologies of proteins, an update in the field of the engineered antibody-based fluorescent biosensors and possible future application of the proposed biosensors. The rationale of the proposed PhD research project and the specific aims of the project with the hypotheses and outcomes are described at the end of this chapter.

## **2.1 Engineered antibodies as a bio-recognition element**

The emergence of recombinant antibody technology has paved the way for the creation of miniaturised antibodies while retaining the specificity and functionality similar to their parent full-length antibody molecules. Current research is focusing on engineered antibodies for biosensing applications instead of full-length mAbs due to the greatly customised unique features such as minimised size, enhanced stability, improved specificity and affinity.[\[53\]](#) Additionally, these mAbs can be inexpensively produced using recombinant DNA technology in various expression systems. Genetic modification of the engineered antibodies allows introducing a functional group of choice at a specific location to simplify fluorescence labelling or surface immobilisation with high densities.[\[54\]](#) Evolution of engineered antibodies through genetic modification via recombinant DNA technology has opened up new opportunities in the *de novo* design of purpose-built antibodies that have profound possibilities in clinical diagnostic applications.[\[55\]](#) Antibodies are engineered mainly to alter immunogenic properties (*e.g.* humanisation) or structural modifications (*e.g.* size minimisation, affinity or stability engineering). Past reports indicated that the Fc region of full-

length mAbs does not play notable contributions in biosensor development but creates problems during immobilisation leading to reduced stability and nonspecific binding.[23] Engineered antibodies, on the other hand, can be more controllable due to their smaller size. Hence, this project focuses on the utility of antibody fragments over traditional mAbs for biosensing applications.

Typically, a full-length antibody is a “Y” shaped protein with a 150 kDa MW produced by B cells as a part of the mammalian immune response mechanism. Antibodies structurally consist of 2 distinct fragments: an antigen binding block (Fab) and a constant fragment (Fc). The Fab fragment is composed of both variable and constant domains of heavy and light chains that contain the antigen binding sites (paratopes). In the past, antibody size could be reduced by fragmenting it with proteolytic enzymes to yield Fab and F(ab)<sub>2</sub>' fragments without the Fc region. Genetic engineering led to the emergence of next-generation antibody formats to produce mono- and multivalent fragments. Antibodies can be formatted into many types depending on the polypeptide chains used. The most popular formats are made by fusing the variable light (V<sub>L</sub>) and heavy chains (V<sub>H</sub>) through Serine-Glycine polypeptide linker (*e.g.* single chain variable fragment (scFv)) or combining variable and constant heavy and light chain to form Fab fragments. These can be further engineered to create multivalent antibody fragments such as a bispecific antibody and a diabody.[23] Antibody fragments can be selected virtually for any specific antigen using the phage display or ribosomal display method followed by expressions in large quantities in different expression systems. Plukthun *et al.* first described the expression of antibody fragments in bacterial systems.[56] Since then the field has rapidly expanded, and now antibody fragments can be inexpensively produced in high yields in various expression systems including bacterial,

mammalian, yeast, plant and cell-free translation systems with novel modifications as required.[57, 58]

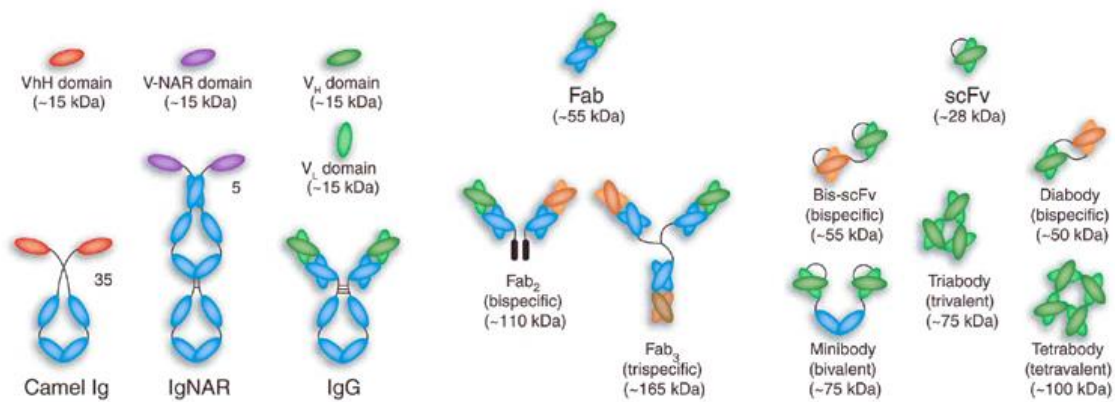


Figure 4: Representation of various antibody formats illustrating commonly used single chain Fv (scFv), bispecific and Fab recombinant antibodies. Figure adapted from Hudson et al., 2005, Nature Biotechnology.[23]

Past reports have indicated the profound growth of the engineered antibodies in the therapeutics and diagnostics field. As of Dec 2018, about 80 antibody-based novel therapeutics were approved by regulatory bodies including three antibody fragments, while 570 candidates were in either phase II or III clinical trials. Reports also indicated the abundance of antibody fragments in different phases of clinical trials such as 71 bispecific antibodies and 13 antibody fragments in various stages of trails including three scFvs, one bi-specific and a nanobody in phase III clinical trials.[59, 60] Engineered antibody-dependent immunoassays have also found many applications for the detection of target antigens. These may include but are not limited to the detection of disease-related proteins, antigens (e.g. prostate-specific antigens), viruses, bacteria, small molecules, toxins, and *in vivo* imaging.[35] Table 1 shows some of the examples of antibody-fragments used for the detection of target analytes. Engineered antibodies have certain beneficial features for biosensing applications.[30] For instances, they can be immobilised on the sensor surface

with a proper orientation at high densities. In addition, engineered antibodies show superior specificity due to lack of Fc region. Importantly, the small size, ease of recombinant production and suitability of genetic modification to introduce new functionality have made them an ideal candidate for biosensor development.[35] Despite the immense potential, the field of fluorescent biosensors that utilise engineered antibody fragments as the bioreceptors is still in its infancy. *This project intends to use a single chain antibody fragment for the development of a novel diagnostic tool.*

*Table 1: Engineered antibody-based immunosensors and immunoassays. Applications of (A) immunosensors were adapted from Sharma et al.[61] and immunoassays were adapted from Zeng et al.[35]; however, the table was updated with some of the recently reported immunosensors and immunoassays.*

Application	Analyte	Antibody format	Transducer
<b>(A) Application in immunosensors</b>			
Nitroaromatic explosives detection [62]	2,4,6-trinitrotoluene (TNT)	scFv	Chemoresistive
Deep vein thrombosis (DVT) disorders [63]	D-dimer	scFv	Electrochemical
Human immunodeficiency virus (HIV) [64]	HIV-1 virion infectivity factor	scFv	Piezoelectric
Toxic metabolite detection [65]	Aflatoxin B1	scFv	SPR
S. aureus detection [66]	Fc receptors	scFv	Piezoelectric
Listeriosis diagnosis [67]	<i>Listeria monocytogenes</i>	scFv	Electrochemical
Pesticide concentration detection [68]	Atrazine	scAb	Electrochemical
Encephalomyelitis diagnosis [69]	Venezuelan equine encephalitis virus	scFv	Resonant mirror
<i>Entamoeba histolytica</i> diagnosis [70]	<i>Entamoeba histolytica</i> antigens	scFv	Amperometric
Detection of doping [71]	Somatotropin	Half-sized Ab fragment	Surface Plasmon Resonance (SPR)
Detection of inflammation/ infection [72]	C-reactive protein (CRP)	Engineered antibody fragment, scFv	SPR
Detection of peptide [73]	GCN4	scFv	SPR
Biomolecular interaction study (Q-body) [47, 74]	Bone gala peptide, Claudine, toxins	scFv, Fab	Fluorescence
<b>(B) Application in immunoassay:</b>			

Study of cancer and infections [75-79]	Human epidermal growth factor receptor 2(HER2)/neu, c-Met protein Salmonella O-polysaccharide <i>B. anthracis spore</i>	scFv	Fluorescence
Detection of cancer [80, 81]	MUC1 (on breast cancer cells), HER2	scFv	chemiluminescence
Detection of bacterial antigen [82]	Salmonella antigen	scFv	Luminescence
Venezuelan equine encephalitis virus detection [83, 84]	<i>L. monocytogenes</i>	scFv	Electrochemical
Detection of clinically relevant molecule [85-87]	Parathion, HIV-1 virin infectivity factor, cytochrome P4501B1, rabbit IgG	scFv	QCM
Virus detection [88]	Rabies virus	Fab	ELISA
Detection of clinically relevant molecule [89-92]	Deoxynivalenol (DON), atrazine, testosterone	Fab	Label-free
Prostate specific antigen detection [93, 94]	Prostate specific antigen	scFv	Electrochemical
Detection of Ricin at high temperatures <sup>63</sup>	Ricin	scFv	Electrochemical
Explosive detection [95]	TNT	scFv	Electrochemical

## 2.2 Fluorescence labelling strategies of engineered antibodies

### 2.2.1 General methods for fluorescence labelling

Fluorescence labelling is one of the most critical steps in fluorescent biosensor development. Homogeneous protein-fluorophore conjugates and highly site-specific labelled proteins are a prerequisite to developing an efficient fluorescent probe. [96] Unfortunately, site-specific labelling of proteins is often challenging due to: (a) the structure can be compromised during the labelling reaction leading to disruption of function; (b) most of the commonly used fluorescence labelling chemistries operate in a random manner resulting in heterogeneous conjugates ; (c) fluorescence labelling via fusion tag limits the flexibility to label an internal site of a protein; (d) the labour intensive process requires optimisation; and (e) the poor labelling efficiency at the specific site.

Many strategies were developed for fluorescent labelling of proteins in the past; however, they were mostly used for random incorporation of fluorescent dyes (*e.g.* carbodiimide chemistry), or genetic fusion of a terminal tag to label them via fluorescent proteins (*e.g.* GFP) or short peptide tags (*e.g.* SNAP-tag).[97] Some of the fluorescently labelled antibody fragments via genetically fused tags are listed in *Table 2*. Though the above mentioned enzymatic and chemical labelling techniques are quite useful in specific scenarios, they suffer several limitations. Random fluorescence labelling is not ideal for biosensing purpose because the fluorescence labelling site plays a critical role in the modulation of fluorescence properties. The genetically fused tags used for fluorescence labelling are not flexible in different incorporation sites in a protein, are particularly impossible to insert in the internal site of a protein and are thus generally limited to the N- or C- terminus of the proteins. Furthermore, the large size of these tags often increases the size of the final construct, leading to structural changes, or reduced functionalities.[49]

*Table 2: Fluorescence labelling of scFv antibody through tagging systems. The table also demonstrates the type of conjugation and detection strategies.*

<b>Types of Tag</b>	<b>Size (approx.)</b>	<b>Antibody format</b>	<b>Detection strategy/coupling</b>
GFP	27kDa	scFv	Fluorescence anisotropy detection[98]
Split-GFP	11 amino acids	scFv	Fluorescence linked immunosorbent assay (FLISA)[99]
SNAP tag	19kDa	scFv	Coupling with O(6)benzylguanine derivative dyes[100]
Affinity tag	? <sup>a</sup>	scFv	Protein based microarrays[101]
FITC-E2	? <sup>a</sup>	scFv	Fluorescein Quenching[102]
Tryptophan (W) tag	? <sup>a</sup>	scFv	On-line detection-based fluorescence of W molecule[103]
Threonine (Thr) tag	1-17 amino acids	scFv	enzyme mediated Alexa488 dye incorporation[104]
Thr-Ser-Cys-Pro-His tag	? <sup>a</sup>	Fab	Chelates mediated labelling[105]

?<sup>a</sup> =unknown

LPETGG tag	6 amino acids	scFv	Sortase mediated coupling to oligoglycine containing dyes[ <a href="#">106</a> , <a href="#">107</a> ]
Holiday Junction	? <sup>a</sup>	Nanobody	ssDNA reacted with NHS activated TAMRA & DBCO dye followed by Sortase mediated ligation[ <a href="#">108</a> ]
Intein	? <sup>a</sup>	scFv	Intein mediated C terminal labelling via Cys containing peptide[ <a href="#">109</a> ]
BODIPY-TMR-Lysine	? <sup>a</sup>	scFv	Cell free translation system[ <a href="#">110</a> ]
ProX-Tag	12 amino acids	scFv, Fab	Cell free translation systems for TAMRA labelling[ <a href="#">47</a> ]

Maleimide chemistry is an attractive fluorophore labelling strategy introduced in the 1980s, and significant effort has been made for site-specific labelling of proteins by targeting of Cysteine (Cys) residues on the surface of recombinant antibodies.[[111](#), [112](#)] Renard and colleagues performed site-specific mutagenesis to introduce a Cys residue into the scFv antibody for coupling with IANBD ester [(N-((2-(iodoacetoxy)ethyl)-Nmethyl) amino-7-nitrobenz-2-oxa-1,3-diazole)] by mild reduction with 2-mercaptoethanol (10 mM) to obtain a partial reduction of disulphide bonds for efficient coupling. [[112](#)] This approach has also been applied to Fab fragments and mAbs by the same group.[[113](#)] Another report demonstrated Cys-modified diabodies with readily reducible disulphide bonds on the C-terminus for labelling with Alexa Fluor 488-Cy5 maleimide dyes.[[114](#)] Jeong *et al.* have also used thiol-mediated maleimide chemistry for scFv molecule labelling to develop fluorescent biosensors.[[115](#)] The Cysteine residue has been attractive because its thiol group can readily react with maleimide-functionalised dyes and also has applicability in surface immobilisation. However, a primary disadvantage of this technique is to maintain Cys molecules in a reduced state for an efficient bioconjugation. The disulphide bonds of native cysteine residues (common in antibodies) are also reduced during the reduction step expediting significant structural damage of the proteins. While this task is extremely tedious, some authors argued that the use of an optimum (*e.g.* mild)

level of reducing agents might overcome this issue by site-specific reduction, yet optimisation is required for each protein.[116]

### 2.2.2 Fluorescence labelling by unnatural amino acid (UAA)

Schultz and co-workers developed a novel strategy for efficient *in vivo* and *in vitro* fluorescence labelling by genetic incorporation of unnatural amino acids (UAA) with desired functional side chains. The UAAs, also called non-proteinogenic or non-standard amino acids, are modified or synthetic amino acids usually containing specific functional groups (*e.g.* azide) in their side chain, yet they retain the building block of the canonical amino acids to facilitate protein translation. In 2001, Wang *et al.* expanded the genetic code of *E. coli* to site-specifically incorporate UAA *in vivo* by suppressing amber stop codon (TAG). [117] In comparison to natural protein biosynthesis, the native tRNA and aminoacyl-tRNA synthetase (aaRS) pair does not recognise the UAA due to their astonishing specificity to one of the 21 canonical amino acids and its corresponding mRNA codons transcribed from the DNA sequence. Apart from the sense codons, nature is also privileged with three nonsense (also termed as stop or termination codon) codons, *e.g.* TAA (Ochre), TAG (Amber) and TGA (Opal). These codons usually do not encode any amino acids since no native tRNA-aaRS can charge them; hence, the protein synthesis terminates at this point. By reprogramming the protein translation mechanism by suppressing one of these termination codons, it is possible to create a paradigm of proteins bearing a unique functional group. In order to incorporate UAA, it is required to develop a modified tRNA-aaRS pair that can recognise its cognate UAA and a corresponding stop codon but does not cross-react with the canonical amino acids or codons (*Figure 5*). Usually, a suitable vector containing the gene for modified tRNA-aaRS is co-transfected with the plasmid containing the gene of interest and UAA is supplemented into the expression media.[118]

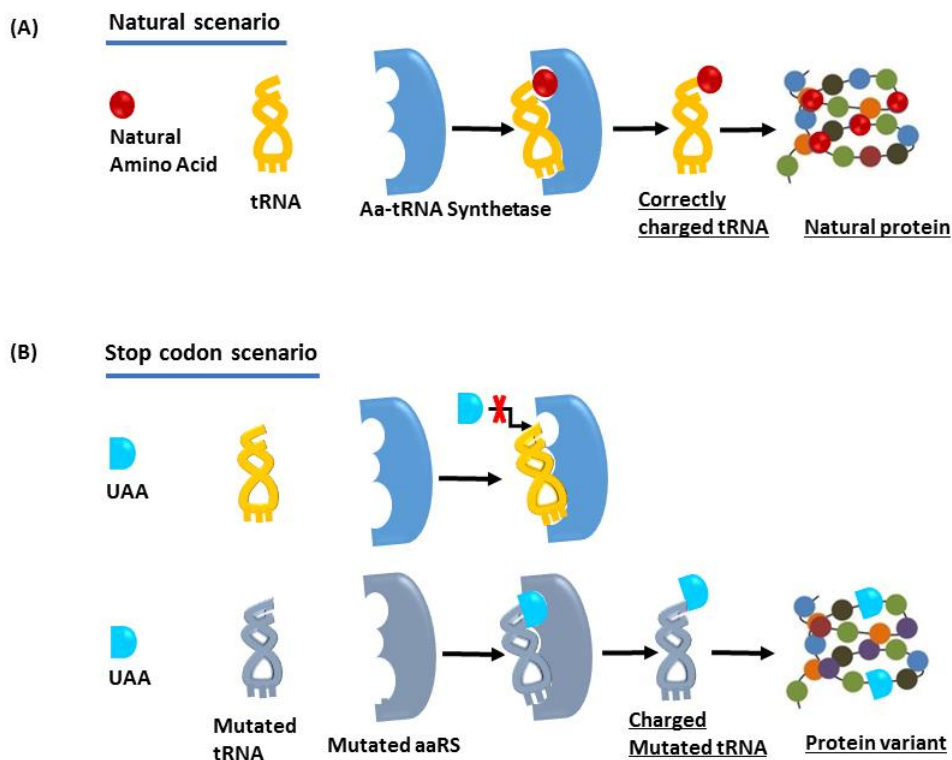


Figure 5: General illustration of UAA incorporation during protein biosynthesis. (A) Protein expression in a native system using natural amino acid and (B) UAA incorporation by suppressing stop codon.<sup>[119]</sup> In comparison to natural protein biosynthesis, UAA is not recognised by native tRNA-aaRS pair, hence a modified tRNA-aaRS pair is required to suppress the desired stop codon. The natural amino acid is presented in red, native tRNA is in yellow, native tRNA synthetase is in light blue, UAA is in blue and mutated tRNA, and tRNA synthetase is in grey.

Research has shown the diverse applications of unnatural amino acids. Since the genetic code expansion of about two decades, over 100 UAAs have been incorporated into proteins using a variety of expression systems including bacterial, yeast, and mammalian cells for diverse applications such as gene and drug delivery (e.g. antibody-drug conjugation), bispecific antibody development and studying biomolecular interactions.<sup>[120]</sup> Phenylalanine (Phe or F) and Tyrosine (Tyr or Y) derivatives are the most commonly used UAA [e.g. *p*-acetylphenylalanine (pAcF), *p*-azidophenylalanine (pAzF) *Figure 6A*] that facilitates fluorescent labelling based on a suitable click reaction chemistry. As an example, *Figure 6C* schematically displays amber codon suppression by pAcF

followed by coupling with Alexa 488 fluorophore. The ketone functionalised pAcF UAA undergoes oxime ligation with aminoxy- derivatives such as Alexa 488 dye through the formation of a stable oxime bond. Practical application of this approach was reported for the development of single-molecule FRET (smFRET, a biophysical method that measures FRET within a single molecule) detection systems wherein Alexa488 (donor) was incorporated via pAcF UAA to develop a FRET pair with Alexa594 fluorophore (acceptor) to study the folding and biophysical properties of bacteriophage T4 lysozyme.[121] Apart from the labelling with a dye molecule, several reports exemplified other applications of UAA such as bispecific Fab generation by linking pAcF UAA with the bifunctional ethylene linkers [122]; antibody-polymer conjugates for siRNA delivery;[123] and antibody-drug conjugate (e.g. auristatin agents to the anti-Her2 Fab and IgG antibody).[124]

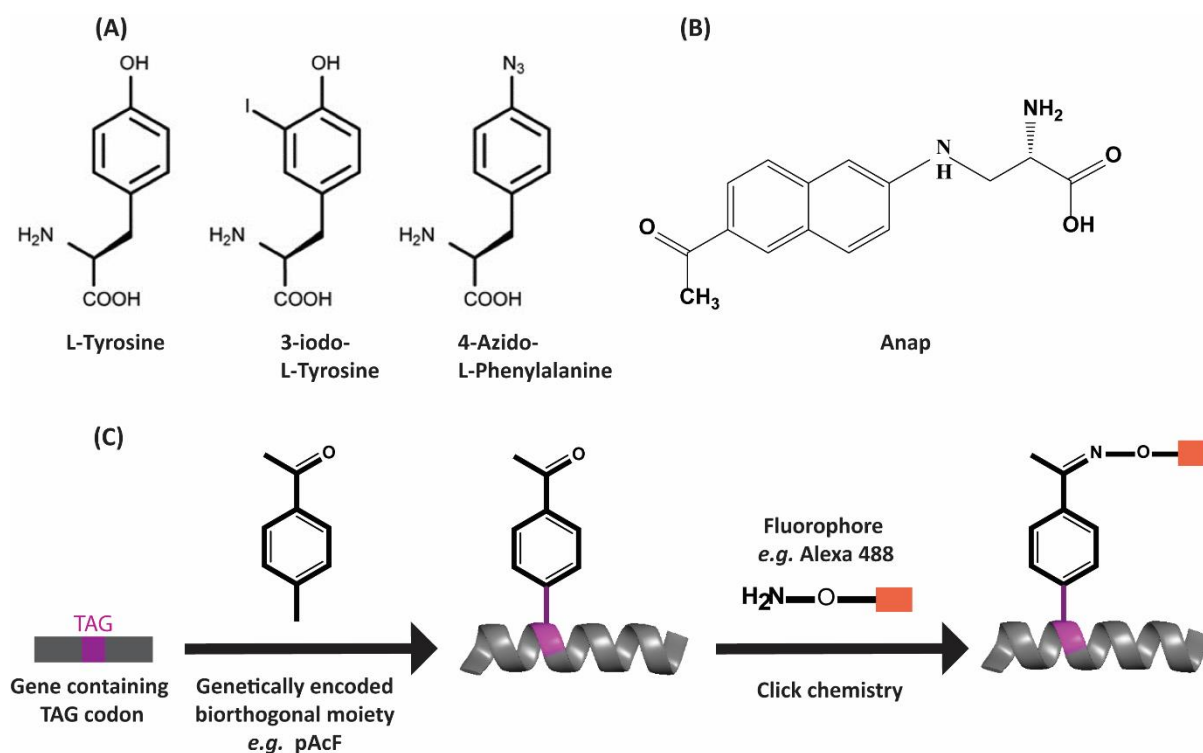


Figure 6: Fluorescence labelling via UAA. (A) Examples of standard and non-standard amino acids with the clickable functional group, and (B) structure of Anap fluorescent

amino acid. (C) Schematic diagram outlining the concept of efficient fluorescence labelling by suppressing amber codon. TAG stands for stop codon, and highlighted in purple, aminooxy functionalised fluorophore is presented as orange orange rectangle shape.

The key challenge of UAA technology is to develop an orthogonal tRNA and synthetase (aaRS) pair. The complexity is associated with the codon assignment for mammalian, bacterial or yeast expression system due to the genetic variability of these species, which has made it a tedious task to develop this orthogonal pair.[125] The orthogonality of either tRNA or synthetase is dependent on the complementarity of synthetases and tRNAs in a host organism as they vary between organisms (*i.e.* a synthetase or tRNA may be orthogonal in one host but not in another). The first orthogonal tRNA and its specific aaRS was evolved from *Methanococcus archaea* where it usually codes for a tyrosine amino acid. Jason W Chin *et al.* reported four orthogonal tRNA-aaRS pairs that form the basis of orthogonality for varieties of tRNA-aaRS plasmids generation in different expression systems.[126] The *Methanococcus janaschii* derived tyrosyl-tRNA synthetase (MjTyrRS)/tRNACUA pair is orthogonal in *E. coli* but incompetent in eukaryotic cells. Conversely, the tyrosyl-tRNA synthetase (EcTyrRS)/tRNACUA and leucyl-tRNA synthetase (EcLeuRS)/tRNACUA pairs are orthogonal to eukaryotic cells. In contrast, Pyrrolysyl-tRNA synthetase (PylRS)/tRNACUA pairs from certain *Methanosarcina archaea* are orthogonal across the bacteria, eukaryotic and animal cells.

Despite a lengthy process, past research has established a standard method for the generation of orthogonal tRNA-aaRS pairs.[127] The evolution process requires the creation of a library of tRNACUA and aaRS mutants by mutating amino acid residues on the active sites based on the crystal structures of tRNA and aaRS followed by screening in *E. coli* through multiple rounds of

positive and negative selections.[[118](#), [128](#)] *Figure 7* shows the methodology for developing an orthogonal tRNA-aaRS pair. The evolution process of this pair needs to ensure that the synthetase distinctly recognises the UAA without cross-reacting with the native amino acids and that it can charge and transfer UAA to its cognate tRNA and amber codon respectively. In the case of cross-reactivity of the synthetase with the natural amino acids, steps must be taken to evolve this enzyme by removing binding sites that recognise natural amino acids; thus, the process needs the creation of a massive library of mutants. The sequence of these synthetase mutants and tRNA are cloned into bacterial plasmids. These plasmids are co-transformed in *E. coli* with the plasmid containing a sequence of chloramphenicol acetyltransferase resistance gene bearing a stop codon. The mutants are selected by growing the cells in the presence of chloramphenicol and respective UAA. Next, positive clones from this round are co-transformed with a barnase toxic gene containing the stop codon.[[126](#)] This negative selection round eliminates the nonspecific tRNA-aaRS pairs that express the toxic protein in the absence of UAA. Cells containing only the UAA specific tRNA-aaRS pair survive this process, as this pair does not allow barnase gene expression by integrating native amino acids. With the expansion of further extensive research in developing this orthogonal pair, several groups have reported enhancement of the functionality of the orthogonal tRNA-aaRS pairs that have shown improved UAA incorporation efficiency.[[129](#), [130](#)]

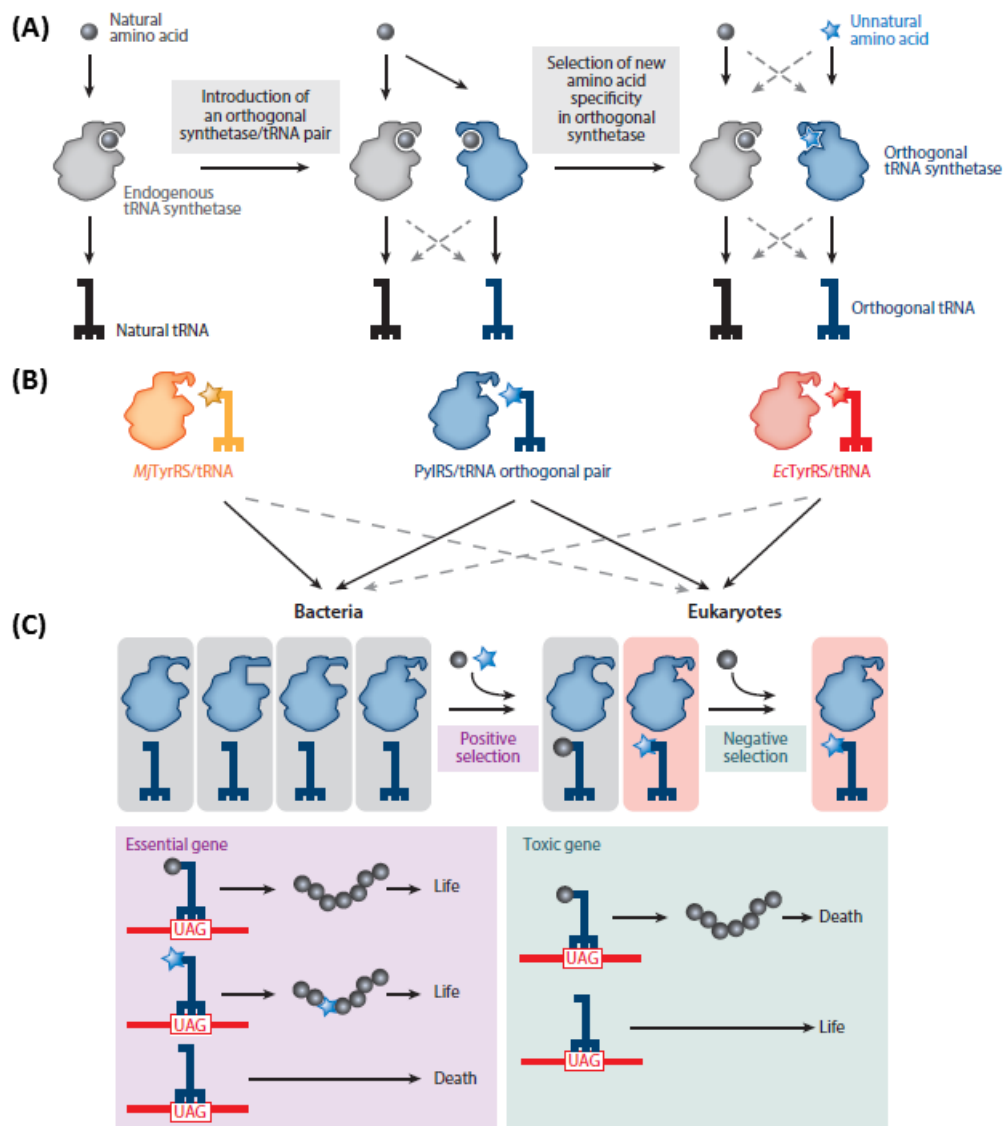


Figure 7: Evolution of a tRNA/tRNA synthetase pair in *E. coli*. Three major steps of the evolutionary process include (A) creation of a mutant library of tRNA and synthetase followed by testing them for cross-reactivity. If any of these orthogonal tRNA/synthetase pairs bind to common amino acids, the evolution process is required to destroy their natural amino acids binding sites so that it specifically recognises UAA. (B) Then the selected pairs are tested for orthogonality in different host systems. (C) Multiple rounds of positive and negative selection processes are conducted in the presence of a toxic gene to identify its host orthogonality. UAG (mRNA) shown in the figure is the transcribed form of TAG codon. Figure was adapted from Chin et al. with partial modification. [126]

A desirable feature of UAA technology is the *in vivo* fluorescence labelling of proteins as some of the UAAs are intrinsically fluorescent (fUAA), therefore eliminating the need for further labelling steps. [97, 131] The flexibility of UAA incorporation on any permissible site of a protein made this technique so unique

that it is ideal for fluorescence-based biosensing applications. Some of the fUAAs are sensitive to polarity of the local environment; therefore, their fluorescent properties are dependent on their immediate molecular environment, which can provide sufficient information during binding events leading to optical detection of target molecules. Despite the efficiency and versatility of this technique in site-specific fluorophore labelling, this promising technology has not been explored widely in recombinant antibody-based detection of the target molecule, at least not for immunosensors development.

Recent studies have demonstrated the convenience of fUAA use for biomolecular interaction studies. Lee *et al.* reported a unique approach by incorporating a polarity dependent fluorescent amino acid, Anap (3-(6-acetylnaphthalen-2-ylamino)-2-aminopropanoic acid), through genetic incorporation in response to an amber (TAG) suppression codon in yeast expression systems. Anap (*Figure 6B*) is a derivative of Prodan dye family which has variable emission spectra depending on the solvent polarity. The excitation and emission wavelength of Anap is 350 nm and 490 nm respectively in water. The group has selectively incorporated Anap by mutating Asparagine (Asn) at position 160 of the glutamine binding protein (GBP). When the Anap-labelled GBP was excited at 350 nm, a significant spectral shift of about 50 nm (from 480 nm to 430 nm) was observed in the presence of Gln in a dose-dependent manner with the gradual increase of Gln concentrations.[\[132\]](#)

Apart from yeast cells, Anap was also genetically encoded in mammalian cells. Chatterjee *et al.* described the development of a tRNA/tRNA synthetase pair for site-specific incorporation of this dye in mammalian expression systems (*e.g.* HEK293, HeLa, and CHO cells) with excellent fidelity and efficiency. Here, they have tested the system by introducing a TAG codon in enhanced green fluorescent protein (EGFP) for *in vivo* imaging.[\[131\]](#) In addition to these, several

investigations confirmed the utility of Anap as a FRET pair. A classic example may include genetically encoded FRET systems by introducing Anap within the proximity of terminally added GFP into a protein. This system removes the use of further labelling with an extrinsic fluorophore. Mitchell *et al.* showed this system by creating an amino-terminally SUMO\*-fused EGFP protein for expression in mammalian cells where they mutated two surface exposed amino acids into TAG codon for Anap incorporation.[133] During the native state, the fluorescence of Anap was quenched by EGFP, but proteolysis by SUMO protease cleaved EGFR resulting in the release of FRET interaction. Further validation of the systems carried out by monitoring Ca<sup>2+</sup>-dependent conformational change of calmodulin protein. A similar approach was executed for measuring Co<sup>2+</sup>-dependent transition metal ion FRET (tmFRET) to determine the distances between amino-terminal Ankyrin repeat domains of ion channel TRPV1 and the intracellular surface of the plasma membrane.[134]

Several investigations have described the utility of Anap in voltage-dependent sensing. Soh *et al.* deployed Anap for examining ligand-induced fluorescence change under voltage-clamp conditions in *Xenopus oocytes*. [135, 136] Few other groups have further studied the voltage sensing mechanism based on fluorescence modulation of Anap. [137] Besides the above diverse applications of Anap, Kramer *et al.* took advantage of this fluorophore for investigating protein misfolding by suppressing TAG codon in luciferase in the yeast cytoplasm. [97] The properties of Anap had not only been illustrated as modulation of fluorescence intensity or blue wavelength shift upon target binding but also demonstrated for ligand-mediated fluorescence diminution. For instance, Wen *et al.* reported decrement of Anap fluorescence intensity while studying the inhibition of human acid-sensing ion channels by the mambalgin-1 polypeptide. [138] They observed a pronounced fluorescence attenuation with the

concomitant increase of mambalgin-1 dose along with an approximate 7 nm redshift.

Apart from the Anap fUAA, several other fluorescent unnatural amino acids incorporated into different proteins. Summerer *et al.* reported the insertion of 2-amino-3-(5-(dimethylamino) naphthalene-1-sulfonamide) propanoic acid (dansylalanine, DanAla) into human copper/zinc superoxide dismutase (hSOD) in yeast expression systems.[139] The DanAla UAA has been identified as a polarity indicator that has a distinctive excitation and emission wavelength of 340 nm and 550 nm, respectively. The unfolding of hSOD protein containing DanAla UAA by GdnHCl showed notable fluorescence intensity change (3-11% increase) as well as a blue wavelength shift of about 14-27 nm. This amino acid was also incorporated in mammalian and insect cells for imaging and studying the functionality of neuronal protein by inactivation of a voltage-dependent K<sup>+</sup> channel.[140, 141] L-(7-hydroxycoumarin-4-yl) ethylglycine is another reported fUAA used for polarity-based probing. Wang *et al.* reported the incorporation of this molecule into the sperm whale myoglobin.[142] Denaturation of the myoglobin by urea showed fluorescence intensity modulation of up to 30%. Several other fUAAs incorporated into GFP for various fluorescence-based applications such as monitoring of pH by fluorinated Tyr and altering properties of GFP by 4-biphenyl-L-phenylalanine UAA.[143, 144] *Table 3* summarises the fluorescence properties and the host systems used for *in vivo* incorporation of the stated fUAAs. *Even though several fluorescent UAAs created and incorporated into proteins for studying various biomolecular interactions, none of them has been inserted into antibody fragments and tested in biological body fluids such as human blood for biosensing purposes.*

Table 3: Florescent UAAs reported in the literature to date. The table also shows the optical properties of the UAAs and the host system used for incorporation.

UAA	Excitation (nm)	Emission (nm)	Host	Environmental Sensitivity
Anap	350	495	Mammalian, Yeast	Yes, polarity
Dansylalanine	340	550	Yeast/insect/mammalian	Yes, polarity
Terphenyl-UAA	280	342	Bacterial	Yes, pH
Fluorotyrosine	470	500	Bacterial	No
p-Cyanophenylalanine	240	297	Bacterial	No
Hydroxycoumarin	340	480	Bacterial	Yes; polarity, pH

## 2.3 Use of engineered antibodies in fluorescent biosensors

Reagentless fluorescent biosensors are a distinct class of biosensors that are composed of the single sensor component, do not require further reagents for signal generation, and are capable of reporting the detection of target molecules based on simple fluorescence modulation.<sup>[145]</sup> These sensors are capable of integrating a range of biorecognition molecules such as antibodies, proteins, synthetic scaffolds and aptamers.<sup>[43]</sup> Recent advances have demonstrated a wide range of use of reagentless biosensors for detection of small molecules (*e.g.* ADP, ATP, and inorganic phosphates) as well as large molecules such as proteins.<sup>[146, 147]</sup> A key advantage of reagentless sensors is the use of a single sensor component which eliminates the necessity of secondary labelled products and subsequently eliminates the need for washing steps in the assays. Consequently, the sensitivity of this biosensor is not compromised by the secondary reagents (*e.g.* secondary detection antibodies).<sup>[148]</sup>

Several detection principles have been reported for developing reagentless fluorescent biosensors, for example, single fluorophore targeting conformational change detection [*e.g.* photo-induced electron transfer (PET) and polarity], dual labelling for creating FRET pairs or creating a modular design via peptide-

mediated fluorophore labelling (*Figure 8*).[\[149\]](#) FRET-based detection systems were widely reported in the development of the reagentless fluorescent biosensor; however, PET-based detection strategies have recently emerged.[\[45\]](#) One of the critical issues for developing a fluorescence-based method is the site-specific fluorescence labelling of an internal site of a protein which often leads to poor sensor functionality.[\[148\]](#) Although most of the above mentioned biosensors implemented fluorescence intensity as the basis of detection (*e.g.* intensity enhancement or quenching), only a few polarity dependent biosensors were designed. For example, the incorporation of the polarity-dependent ANAP dye into glutamine-binding protein, demonstrated by Lee *et al.*, produced a functional biosensor for glutamine but has not received further attention.[\[132\]](#)

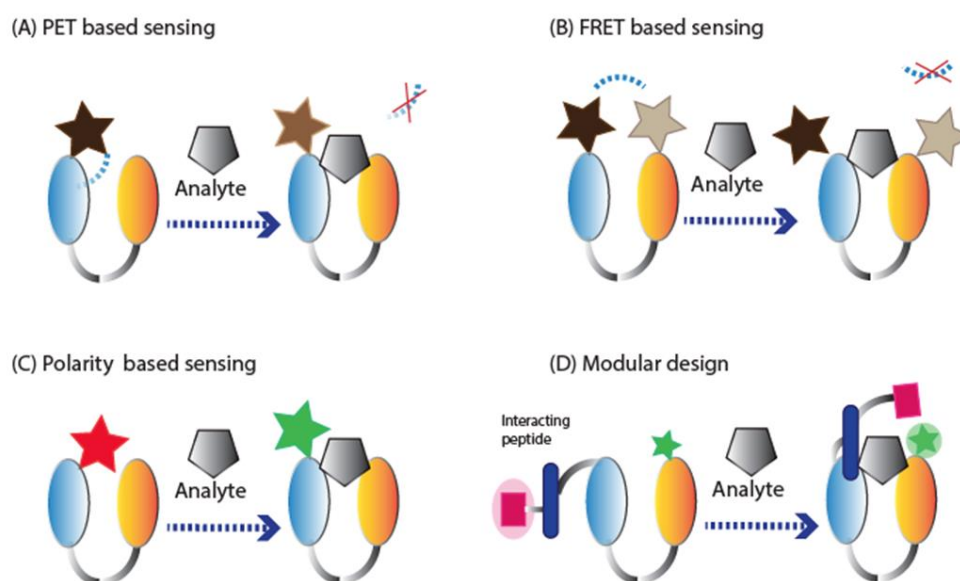


*Figure 8: Various strategies for developing fluorescent biosensor. (A) Photoinduced electron transfer (PET) based detection method by incorporation of a single fluorophore (B) FRET detection by incorporating acceptor and donor fluorophore. (C) Detection based on altering the local environment by polarity sensitive fluorophore. (D) Modular design where fusion tag is a part of the interaction with the analyte leading to bringing fluorophore within proximity for signal transduction. Fluorophores are presented as stars, analytes are presented as pentagon shape and fluorophores' interaction with native amino acids or adjacent acceptor or donor fluorophores are presented as dashed line with a red cross symbol.*[\[148\]](#)

The design of reagentless fluorescent biosensors comprises engineered antibodies combined with a detection system based on readily detectable changes in the fluorescence properties (*e.g.* fluorescence intensity, lifetime and wavelength) upon interaction with a target molecule.[\[43, 150\]](#)[\[151\]](#) In general, a fluorescent dye is incorporated into a specific location of engineered antibodies at which point its fluorescent properties are perturbed only when the specific target antigen is bound. Therefore, the selection of a fluorescent dye and incorporation site is critical for designing this type of biosensor. Depending on the types of fluorophore used to fabricate this type of biosensor, two types of fluorescence modulation can be achieved, *viz.* changes in the wavelength or the fluorescence intensity. Nonetheless, a wavelength shift is much more preferable over the intensity change because fluorescence intensity can be affected by various factors such as complex biological fluids and instruments.[\[152, 153\]](#) *Figure 9* represents a schematic of the scFv-based reagentless fluorescent biosensor where a solvatochromic fluorophore is integrated into a specific location of an scFv antibody. The microenvironment (polarity) of the fluorophore is altered upon binding to the target antigen resulting in the shift of emission spectra.

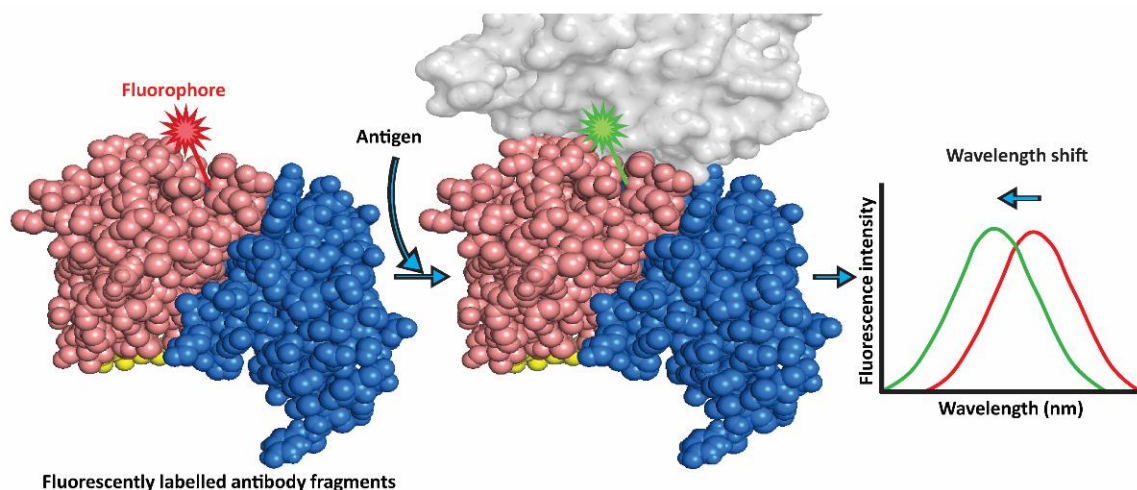


Figure 9: Schematic of a typical fluorescent immunosensor by taking advantage of an scFv antibody as a biorecognition element. This type of biosensor is designed by incorporating a polarity sensitive fluorophore (shown as red star) near the binding interface of an antibody. When the antigen binds to the fluorescently (red) labelled antibody, the surrounding local environment (e.g. polarity) of the fluorophore is changed leading to the shift of fluorescent properties (e.g. emission wavelength). The graph shows the concept of wavelength shift corresponds to the change of spectrum from red to green.

Only a few reagentless fluorescent biosensors have been reported to date. Renard *et al.* reported a reagentless fluorescent biosensor in the early 2000s by site-specific labelling of scFv antibody through a Cys residue.<sup>[112]</sup> The site of mutagenesis was determined based on the structure of the known antigen-antibody binding complex, targeting residues located in or near the complementarity-determining regions (CDRs) of hen egg lysozyme scFv molecule. They selected residues that are not crucial for interaction with the cognate antigen but accessible to solvents for efficient fluorophore incorporation. The Cysteine mutated scFv antibody was conjugated with IANBD ester under mild reduction with 2-mercaptoethanol (10 mM) that showed an antigen-mediated enhanced fluorescent intensity of up to 90% in the buffer and 40% in the serum. Further studies revealed similar results when the same concept was applied for the rational design of reagentless biosensors by using an scFv antibody against the dengue virus (DEN1).<sup>[113]</sup> While this strategy is

promising, constructing this type of sensor is difficult due to the optimisation of fluorophore coupling reaction under the reduced condition which is a time consuming and laborious multistep process.

Abe and colleagues reported a novel fluorescent probe based on an antigen-dependent PET quenching mechanism. The anti-BGP (bone gala protein) scFv antibody was modified with a ProX Tag (NH<sub>2</sub>-MSKQIEVNXSNE-COOH) in the N-terminus of V<sub>H</sub> domain to incorporate a rhodamine derivative fluorophore [TAMRA (Carboxytetramethylrhodamine) dye], using the amber suppression technique in cell-free translation systems.<sup>[47]</sup> The fluoro-labelled scFv antibody, termed as Quenchbody or Q-body, showed antigen-dependent fluorescence intensity variation. In the antigen-free state, the fluorescence of TAMRA was quenched due to the intramolecular interaction of TAMRA with the semi-conserved Tryptophan (Trp) located within the framework region. However, binding of target antigen resulted in a conformational change of the scFv antibody leading to the release of intramolecular Van der Waals interaction between Trp and TAMRA dye, resulting in an enhanced fluorescent signal. The authors suggested that the indole side chain of Trp acted as an electron donor in photo-induced electron transfer (PET) reaction and indicated that the addition of cognate antigen (BGP-C7 peptide or protein) showed a dose-dependent increase in intensity (5.2-5.6-fold). The quenching mechanism was validated by mutating Trp to Phenylalanine (Phe) residues where the intensity was reduced significantly compared to that of the wild-type scFv and varied based on the position of Trp mutation. The efficiency of this biosensor was also investigated in human plasma (50% plasma in PBST) revealing notable 7-fold intensity increase. The technique was further demonstrated by applying in a wide range of scFv antibodies and was implemented for detection of a wide range of small molecules such as 17 $\beta$ -estradiol, and drugs (*e.g.* morphine).<sup>[45]</sup> Further investigations were

carried out using a Fab format to improve affinity and stability. When comparing the fluorescence intensity of TAMRA-labelled scFv with TAMRA-labelled Fab antibody for BGP-C7 peptide capture, the intensity was increased markedly by 9.6-fold. However, the sensitivity was reduced because of the higher stability of the Fab molecule which restricted the access of TAMRA fluorophore to the  $V_H/V_L$  interface for quenching.[74] Interestingly, when they used dual labelled Q-body, the fluorescence response was significantly increased; nevertheless further research is required to improve the stability, affinity, and sensitivity of this type of probe.

The development of the Q-body is mostly restricted by protein production and the positioning of TAMRA or other suitable dyes within the proximate distance of native Trp residues. Since the emergence of the Q-body, it has mostly been synthesised in a cell-free translation system and recently in bacterial cells. In the cell-free translation systems, the researchers used commercially available tRNA labelled TAMRA dye that can readily be used for site-specific labelling in response to amber stop codon positioned in the Pro-X tag; however, no such tRNA-TAMRA conjugates can be used for *in vivo* production of this sensor. Hence, they relied on thiol-mediated fluorophore labelling to produce the Q-body in the bacterial cells. Other interesting strategies have also been reported to produce a Q-body such as the construction of Q-body by transamination reaction, photochemical crosslinking to antibody nucleotide-binding sites and one-pot construction by converting protein A and G domain to Fab based Q-bodies.[115, 154, 155] Jeong *et al.* described the expression of the Q-body in *E. coli* cytoplasm where they reported a higher yield of this sensor. They also systematically investigated the effect of spacer length in different rhodamine fluorophores and overserved a variable quenching behaviour.[115] Similarly, Ohashi *et al.* also investigated the effect of linkers between the dye and the scFv antibody. Here,

they also explored the insights of Q-body's fluorescence mechanism.[156] While varying the lengths of Gly-Ser linker, they found that maximal signal can be achieved based on the distance of the Trp which plays a critical role in fluorescence quenching during the native state. Nevertheless, this mechanism varies depending on the positions of Trp residues in distinct scFv antibodies.

To date, the Q-body biosensor has been applied to diverse applications including detection of small chemical compounds (*e.g.* drug, testosterone), peptides (*e.g.* BGP), and proteins (*e.g.* Claudin) and live imaging under the fluorescence microscopes. Jeong *et al.* showed the detection of Claudin, a 27 kDa transmembrane protein responsible for maintaining epithelial cell polarity and controlling cellular growth.[157] In this report, they expressed Fab-based Q-body in *E. coli* and then conducted a reasonable investigation of the utility of different dyes (*e.g.* TAMRA, R6G and ATTO520) for developing sensitive Q-bodies. Furthermore, they also showed detection of Claudin on the surface of living cells under the fluorescence microscopes which confirmed the applicability of this sensor for imaging applications. Some of the notable Q-body constructs and their potential applications are depicted in *Figure 10*.

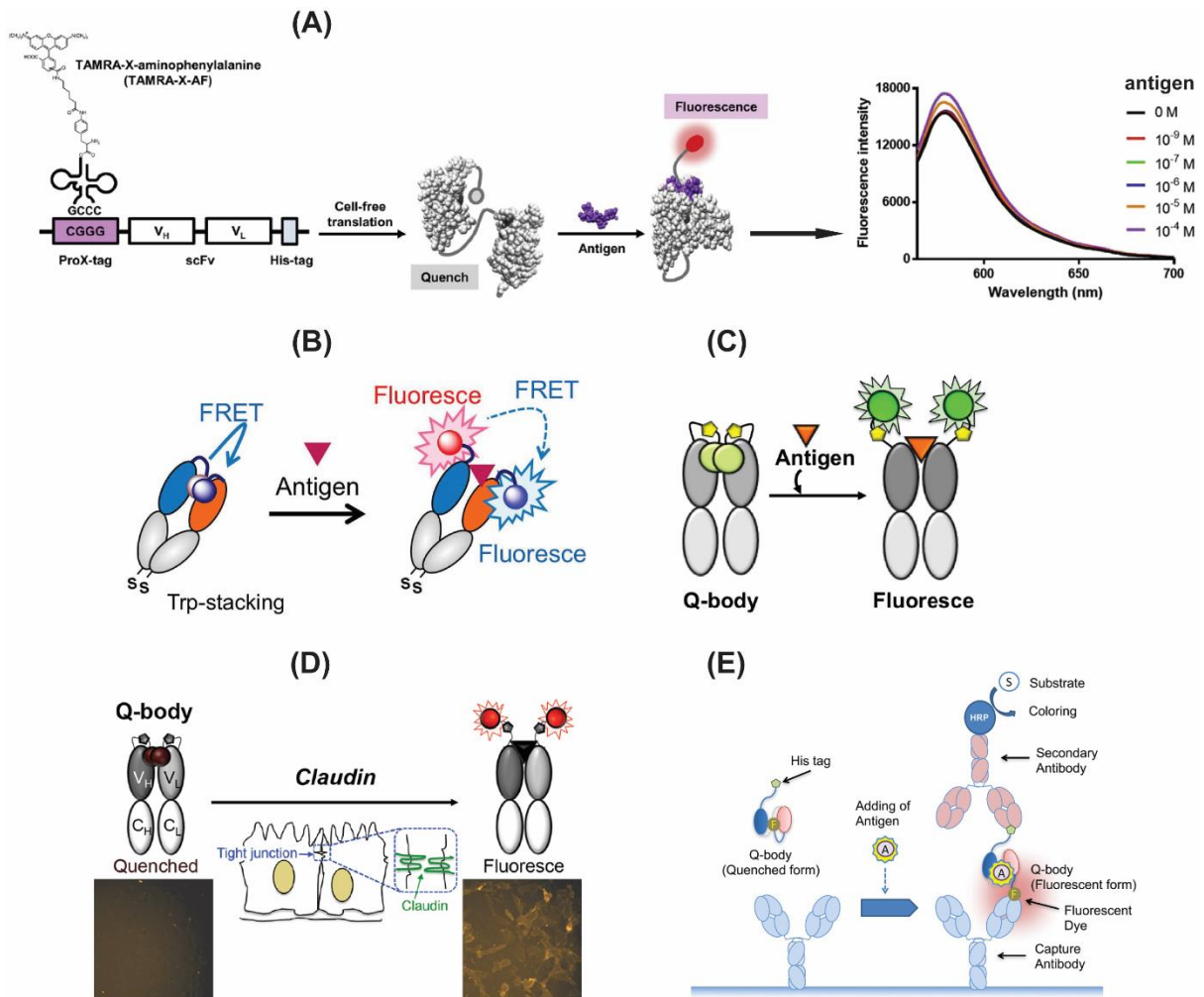


Figure 10: Representation of Q-body reagentless fluorescent biosensors. (A) Typical scFv based Q-body expression in cell-free translation which shows antigen mediated fluorescence intensity enhancement. [158] (B-C) Expansion of Q-body from scFv to Fab format where dual labelling of fluorophores used for developing a FRET pair or signal enhancement [74]. (D) Application of Q-body in cell-based fluorescence imaging, and (E) development of sandwich format ELISA. [156, 157]

While the novelty of the Q-body technology is apparent, it has some limitations as well. [159] This approach is most effective when TAMRA fluorophore is positioned in the termini of the scFv, which is highly dependent on the prevalence of native Trp residues. The precise position and number of Trp residues are critical factors in developing this type of sensor. Apart from that, this technique mostly utilises 12-amino acids long peptide tag (Pro-X) on the termini for the incorporation of fluorophores. Recently, Kurumida *et al.*

demonstrated Cy3 (Cyanine) dye labelling via UAA technology for Q-body production.[160] Recent reports also demonstrated increasing use of *in vivo* terminal Cys residue insertion into Q-bodies for dye labelling. One of the disadvantages of using the Pro-X tag is that it limits the flexibility of dye mobility within the internal sites of the scFv antibody except for the sites between the Ser/Gly linker. The detection of the target by Q-bodies is predominantly based on the change of arbitrary fluorescence intensity. The magnitude of intensity may vary among the fluorescence platform. Though in some instances a small blue wavelength shift of TAMRA dye (~5nm) was observed upon target binding, no systematic investigation has been carried out to validate the exact cause of this shift.[161] Fluorescence intensity enhancement has remained the only basis of detection for most Q-bodies. Nevertheless, these studies have only shown the use of fluorogenic dyes (*e.g.* TAMRA) which mostly rely on the change of fluorescence intensity. An emission wavelength guided method can be developed by using polarity dependent fluorophores (also termed as solvatochromic dyes) which rely on the shift of fluorescence emission spectra.[162, 163] To date, no report has described the implementation of such polarity sensitive fluorophore for scFv based biosensor development. *Hence, a research gap remains for developing a wavelength dependent biosensing mechanism by utilising a polarity dependent dye that responds to the polarity of the local microenvironment.*

## **2.4 Surface immobilisation of engineered antibodies**

Immobilisation of bio-component is a universal step in most of the commercially available biosensors. The success stories of true immunosensors are mostly dependent on a few critical factors. Firstly, the sensor needs to remain accessible for the analytes upon immobilisation on the sensor surface (*i.e.* functional); secondly, its ability to capture target analyte while maintaining its

sensory activity (*i.e.* sensitivity); and thirdly, no interference by the nonspecific binding or adsorption on the sensor surface (*i.e.* accuracy). All of these factors contribute to the stability of antibodies on the sensor surface. These problems can be resolved by either engineering the antibodies or the sensor surface. Apart from using engineering antibodies, the last decade has witnessed significant progress on using nanomaterials in biosensing as an alternative to the traditional surface due to the ease of controllability, added functionality, and advancement of knowledge in the field.[164]

Application of nanomaterials in the biosensing field has arisen intensely for various applications including as a transducer, recognition element and formation of sensor surface to integrate into the sensing instruments.[165] The potentiality of antibody-nanoparticle conjugates for targeted drug delivery has been reported extensively in the literature. At the same time, optical, physical, and electrochemical properties of nanomaterials have also been utilised widely for detection of disease biomarkers both *in vivo* and *in vitro* sensing. Most of the commonly used nanoparticles for biosensing application include, but are not limited to, carbon nanostructures, quantum dots, gold, and magnetic nanoparticles. As a key example, fluorescence emission spectra of carbon nanotube were observed to vary upon binding to the target antigen. Williams *et al.* have demonstrated a surface attachment of antibodies onto carbon nanotube that showed antigen-dependent emission spectral shift (~2 nm blue shift) of carbon nanotube upon target binding.[166] The spectral shift is attributed to the change of local environment on the surface of carbon nanotube upon binding of antigen, possibly caused by the removal of an H<sub>2</sub>O molecule from the surface of carbon nanotube pushing the local environment into a less-polar state (blue wavelength shift). Similarly, Neely *et al.* have conjugated antibodies on gold nanoparticles for the detection of a protein related to Alzheimer's disease based

on two-photon scattering assay (displacement of maximum absorbance wavelength of gold nanoparticle upon binding to target analyte).[167] This field is more prominent in the area of immunoassays where full-length antibodies are attached to nanoparticles with a distinct attribute for different types of assay development such as FRET, label-free detection (SPR) and electrochemical sensing.

Nevertheless, the field of antibody fragments conjugated nanoparticles for reagentless biosensing applications is in its infancy despite its endless possibilities. Recent research indicates that the use of antibody fragment conjugated onto nanoparticle surfaces can assist in improving the accuracy, signal amplification and sensitivity of the sensor (*Figure 11*).[168] Attachment of antibody fragments to nanoparticle surface for solid-phase measurements could be an alternative to immobilisation on traditional surfaces (*e.g.* polystyrene plate well) which may remove nonspecific adsorption onto the surface (*i.e.* improving accuracy). These ideas can also open possibilities for finding the application to develop POC diagnostic tools. By immobilising a single domain antibody fragment (sdAb) with quantum dot (QD) nanoparticle, Anderson *et al.* were able to detect ricin in an immunoassay.[169] They found that the fluorescence of the QD can be used as an alternative to traditional dyes used in conventional bioassays. They also found 10-fold improved sensitivity when detecting the same target using this QD-sdAb in SPR based label-free detection systems.

Nanoparticle-based sensing can also be employed in improving the detection limit in human serum, for example, Byun *et al.* used scFv immobilised on nanorod for detection of C-reactive protein with low concentrations (< 1ng/mL).[170] Here, they deliberately used scFv instead of full IgG to reduce the distance between antibody binding sites and sensor surface for improved signal in surface localised SPR measurement. Although many examples of

nanomaterials were reported for biosensing applications, they mostly relied on the physicochemical properties of the nanoparticles, and none of these sensors has solely relied on the modulation of properties of fluorophore incorporated into antibody fragments. Advancing on this aim may lead to a new form of solid-phase biosensor creation. *Due to the prospects of this emerging field, it may be possible to transform the proposed solution-based biosensors of this project to a solid phase biosensor by immobilising onto suitable nanoparticles to explore the potential benefits of solid phase detection methods.*

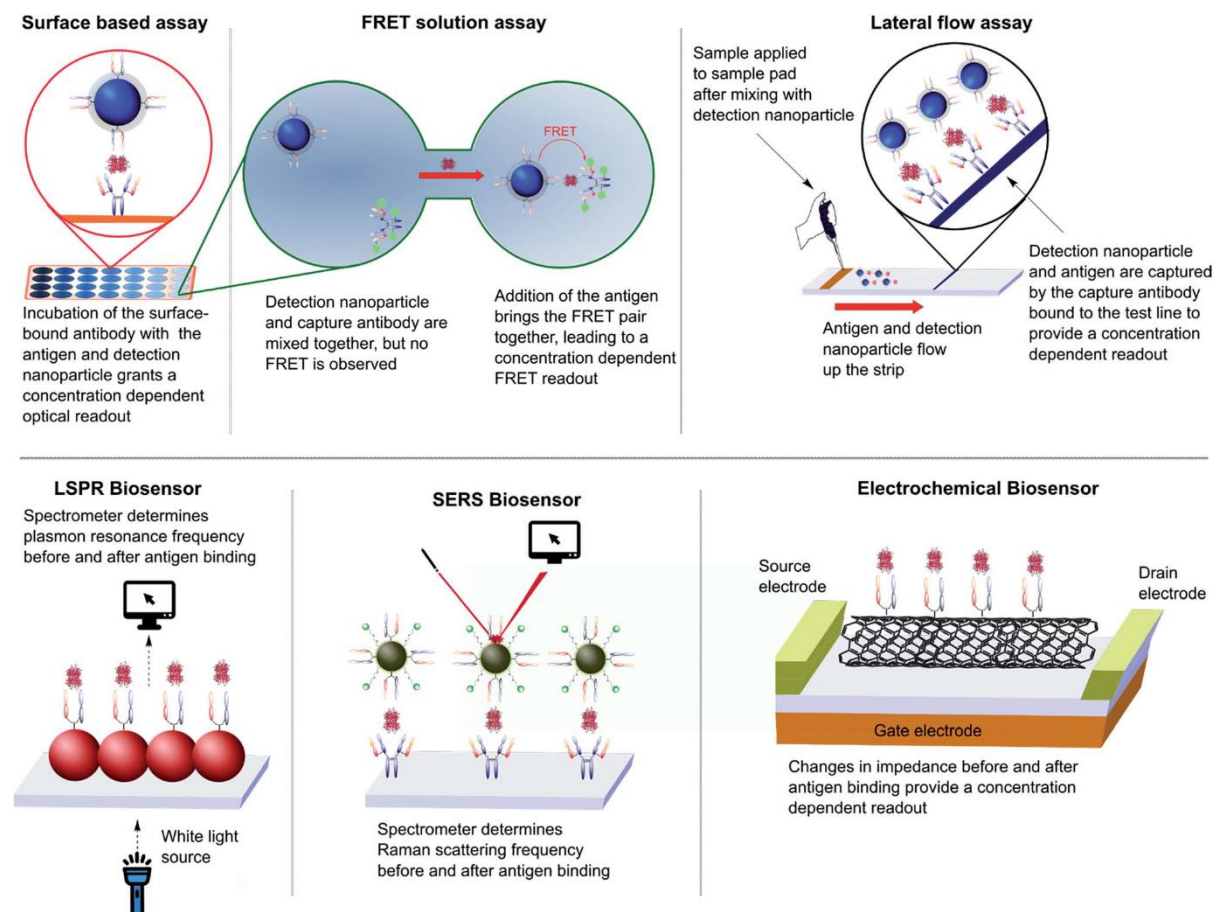


*Figure 11: Different detection mechanisms based on surface immobilisation. The figure is adapted from Daniel et al. without further modification. [168] The top left-hand figure shows nanomaterials as a FRET pair where binding of antigen-antibody on the nanoparticle surface leads to the transmission of energy between antibodies and nanoparticles. Nanoparticles have been used as a detection molecule in lateral flow assay where nanoparticle bound antigen is captured by immobilised antibody on the test strip.*

*In addition, nanoparticles have been implemented in SPR, surface-enhanced Raman scattering (SERS) and electrochemical biosensing (bottom figures).*

The chemistry for immobilising proteins onto surfaces plays a critical role. It has been found that sometimes proteins tend to denature upon immobilisation on the surface. This issue can be overcome by engineering the surface or the antibodies as well as screening suitable chemistry to retain the functionality of biocomponents of the sensors. There are many well-known protein immobilisation methods available such as covalent attachment of functional side chains of native amino acids (*e.g.* thiol, amine, and carboxyl functional group) through NHS-EDC chemistry. Several other immobilisation strategies such as affinity tags (*e.g.* His-tag), streptavidin-biotin interaction, fusion partner, protein A and protein G have also been reported for protein immobilisation.[\[39\]](#) Some of these strategies used for scFv antibody immobilisation are listed in *Table 4*. Though these approaches are used widely, many of them suffer several limitations, including nonspecific interactions and uncontrolled orientation.

In order to develop a sensitive sensor, the orientation of the antibody onto the surface is crucial. Because dis-oriented immobilisation of antibodies reduces the capabilities of binding to target antigen due to the restricted exposure of paratope to the antigen. The UAA technology can be used for well-controlled site-specific immobilisation by using a specific functional group that binds to a corresponding functional group on the surface.[\[171\]](#) For example, incorporation of pAzF in permissible site facilitates cycloaddition reaction with alkyne functionalised surfaces such as polystyrene and sepharose resin.[\[172\]](#) Azido group of pAzF can also be conjugated with DBCO functionalised surface. However, since the incorporation of multiple UAAs reduces the protein production yield significantly, it may not be feasible to implement the same

strategy both for fluorescence labelling as well as immobilisation purposes. A great deal of research demonstrated affinity tag (*e.g.* His-tag) as a prime choice due to their genetic fusion capability and reliable oriented scFv immobilisation.[\[22\]](#)

*Table 4: Common surface and strategies of antibody fragment immobilisation onto various solid surfaces.*

<b>Surface</b>	<b>Antibody formats</b>	<b>Immobilisation technique</b>
Gold surface	scFv/Fab	Chemical coupling through maleimide chemistry (-SH group on the gold surface) <a href="#">[22, 173]</a>
Gold surface	Fab	Covalent attachment on a gold surface by disulphide anchor <a href="#">[174]</a>
Gold/graphite surface	scFv	His (6X) tag <a href="#">[175]</a>
Gold surface	scFv	Gold binding fusion peptide <a href="#">[176]</a> <a href="#">[177]</a>
Gold coated sensor surface	scFv	Attachment through carboxy-terminal Cys molecule <a href="#">[73]</a>
Ultra-flat gold surface	scFv	Attachment through carboxy-terminal Cys molecule <a href="#">[178]</a>
Streptavidin monolayer	scFv	scFv fused with strep tag to immobilise on biotinylated surface <a href="#">[179]</a>
Glass slides	scFv	Direct printing of a thioredoxin-scFv fusion protein on glass slides <a href="#">[180]</a>
Carboxymethyl (CM) dextran	scFv	scFv was immobilised on CM dextran biosensor chip through NHS/EDC chemistry <a href="#">[181]</a>
Polyhydroxybutarate P(3HB) chip	scFv	scFv was immobilised on P(3HB) chip by polyhydroxyalkanoate depolymerase binding domain <a href="#">[182]</a>
Amine functionalised beads	scFv	scFv with carboxy -terminal glycan tag oxidised for covalent attachment to solid support <a href="#">[183]</a>
Hydrophilic polystyrene plates	scFv	scFv was genetically fused with polystyrene binding peptide (PS tags) for immobilisation on polystyrene surface <a href="#">[184]</a>
Streptavidin coated SPR chip	scFv	scFv was fused with Nano tag and SBP tag which has the affinity for streptavidin used for reversible immobilisation <a href="#">[185]</a>
Amine-terminated gels	scFv	Glutathione S-transferase fused scFv for enzymatic immobilisation on the matrix <a href="#">[186]</a>

Carbon Nano-tube	scFv	scFv with His-tag was immobilised on Ni-coated carbon nanotube[187]
poly(sodium 4-styrenesulfonate) surface	scFv	scFv with arginine linker was immobilised on self-assembled monolayer[188]
Gold surface	scFv	scFv was immobilised through native Cys residue on the gold surface of quartz crystal microbalance[189]

## 2.5 Rationale of the project

While the potential benefits of reagentless fluorescent biosensors are obvious, the review of the literature has revealed some knowledge gaps. Traditional mAbs failed to meet the expectation in biosensor construction due to large size and disoriented immobilisation. Engineered antibody fragments can be used as an alternative for improved sensitivity. Fluorescence labelling of proteins through the thiol-mediated coupling, fluorescent fusion proteins or peptide tags were successful in a particular scenario; however, these approaches did not produce a generic labelling technique, at least not for efficient site-specific and internal positioning of a protein.[190, 191] None of the recently reported scFv-based fluorescent probes was attached to a solid surface (*e.g.* nanoparticles) to explore the further application of fluorescent biosensors.

Although the reported biosensors showed detection of target proteins based on enhanced fluorescence intensity (*e.g.* Q-body), none of them demonstrated quantification of target proteins based on emission wavelength shift. Additionally, none of them reported a mechanism that relied on internally incorporated single fluorophore within an antibody that could produce signals without the need for any inter-molecular interactions. The rationale for this project is to employ the site-specific fluorophore labelling technique in internal positions of biorecognition elements (*e.g.* scFv antibody), so that they provide

systematic, robust and repeatable spectral responses upon specific analyte binding, and to investigate the potential for operation of this labelling in solid-phase assays, thus developing a new platform for one-step optical protein biosensors.

## 2.6 Aims and hypotheses

The broad aim of this project was to develop a one-step fluorescent biosensor by site-specific fluorescence labelling of scFv that shows changes in the fluorescence properties upon binding to the target antigen. This general objective was subdivided into three specific aims:

- ❑ Site-specific incorporation of UAA for fluorophore integration into scFv antibody
  - ❑ Optimisation of fluorophore incorporation sites for achieving antigen-dependent changes in fluorescent spectra
  - ❑ Detection of other biomarkers and immobilisation of the biosensors to develop a solid-phase detection strategy.
- ❑ **Site-specific incorporation of UAA for fluorescence labelling of the scFv antibody**

The first aim of this project was to incorporate a UAA for fluorescence labelling of single-chain antibody fragments.

*Hypothesis:* It was hypothesised that the anti-EGFR scFv gene sequence could be modified with a stop codon at a permissible site through molecular cloning which could be expressed in bacterial or mammalian expression systems. It was also hypothesised that UAA incorporation via the introduced stop codon could be used for the direct encoding of fluorescent UAA or one-step click conjugation reaction with a specific fluorescent dye.

*Approach:* The hypothesis was tested by cloning the scFv sequence into a suitable mammalian or bacterial expression vector [e.g. pcDNA3.1b (+) for mammalian expression, pET30(b)+ for bacterial expression]. During cloning, the amber suppression codon (TAG) was introduced into the amino- or carboxy-terminal sites (will be referred as N-term or C-term) in an scFv sequence for the incorporation of a fluorescent-UAA or clickable-UAA for fluorescence labelling. These mutants were expressed in respective expression systems and were purified using various chromatographic methods. The purified proteins were thoroughly characterised by standard bioanalytical techniques such as gel electrophoresis, mass spectroscopy, immunostaining and Western blotting. Clickable-UAA containing scFv mutants were labelled with suitable fluorophore by performing a bioconjugation reaction.

*Potential outcome:* Site-specific fluorescently (e.g. Anap, TAMRA) labelled scFv fragments.

#### **□ Optimisation of fluorophore incorporation sites for achieving analyte-dependent changes in fluorescent spectra**

The second aim of this project was to identify a suitable location within the scFv antibody for fluorophore incorporation for achieving dose-dependent fluorescence property change when binding to target analytes.

*Hypothesis:* It was hypothesised that the position of a fluorophore (e.g. Anap) could be varied within an internal permissible position of scFv antibody and the internal mutation sites could be screened based on a model structure of an scFv antibody. It was also hypothesised that any of the generated mutants could be used for the detection of target ligand based on fluorescence modulation.

*Approach:* The hypothesis was tested by selecting mutation sites based on a homology model structure or from the crystal structure. A model structure was developed using bioinformatics tools (e.g. iTASSER, SWISS-MODEL and

MODELLER). The antigen-bound and unbound model structures were used for the selection of possible fluorophore incorporation sites which might be affected by antigen binding resulting in the fluorescence change. Site-directed mutagenesis was carried out to incorporate TAG codon in targeted positions. The mutated sequences were cloned into suitable plasmid followed by the expression, purification, and characterisation using the methods developed in aim-1. Fluorescence spectroscopy was used to investigate the fluorescence of labelled mutants. The optically active mutants were further tested in biological fluids for clinical utilisation.

*Potential outcome:* Well characterised, optically active scFv mutant showing an antigen-mediated dose-dependent fluorescence response.

#### **❑ Detection of other biomarker and immobilisation of the biosensors for solid-phase detection strategy**

The final aim of this project was to apply the concept (developed in aim-2) for the detection of another clinically relevant biomarker. This was followed by testing the functionalities of these scFv antibody-based fluorescent biosensors on the surface of solid supports.

*Hypothesis:* It was hypothesised that the concept developed in aim-2 could be applied to other scFv antibodies for targeting a different biomarker. It was also hypothesised that the developed solution-phase biosensors could be immobilised on a solid surface without compromising functionality.

*Approach:* The hypothesis was tested by targeting a biomarker that has high clinical significance. The general applicability of this concept was justified by selecting the fluorophore incorporation sites based on a crystal structure-guided design. Following the selection of fluorophore incorporation sites, mutants were cloned, expressed, purified and characterised by using the methods optimised in aim 1 and 2. Application of these fluorescent biosensors was further extended to

solid-phase detection systems by immobilising on the solid surfaces such as nanoparticles.

*Potential outcome:* Development of a functional biosensor that shows activity in both solution and on the solid surface.

## **2.7 Chapter 2 summary**

The literature review clearly identified a knowledge gap in the area of polarity-dependent engineered antibody-based biosensors. It was found that traditional mAbs pose some limitations in biosensor fabrication; therefore, a shift to engineered antibody fragments is desirable. The literature search also revealed that only one type of engineered antibody-based fluorescent biosensor has been reported so far that could achieve the fluorescence intensity modulation upon binding to the target molecule. There is a clear research gap to exploit the benefits of unique fluorescence emission wavelength spectra that could be used for quantification of target proteins. Traditional fluorescence labelling strategies are not efficient enough to generate site-specific antibody-fluorophore conjugates; hence, UAA technology can be used as an alternative. Lastly, it has been found that it is possible to convert the solution-phase detection strategy to a solid-phase method by surface immobilisation.

In the next chapter, strategies for site-specific incorporation of UAA for fluorescence labelling of scFv antibodies (aim 1) are discussed. The chapter also includes bioinformatics analysis of scFv sequence confirming CDR regions, designing of scFv constructs, cloning of scFv sequence containing TAG stop codon via PCR based cloning methods, expression of scFv mutants in mammalian and bacterial expression systems, purification of scFv mutants, and lastly presents vigorous characterisation of these mutants to test the functionality in the presence of target analytes.

# Chapter Three

## 3. Method Development for Fluorescence Labelling of Engineered Antibodies

---

### 3.1 Introduction

The first aim of this project was to site-specifically incorporate fluorophores into antibody fragments, via the incorporation of UAA during protein expression. Previous research has shown UAA technology to be beneficial over the traditional strategies for site-specific fluorophore incorporation into proteins.[\[131-192\]](#) This novel strategy allows not only for adding unique functional groups (*e.g.* azides and alkynes) directly into the genetic repertoire of proteins during *in vivo* protein expression, but also allows one-step fluorescence labelling (*e.g.* fluorescent UAA) that can be used directly for the detection of target biomolecules.[\[132-193\]](#)

In the previous chapter, literature was reviewed to identify a suitable solvatochromic UAA fluorophore that exhibits polarity dependence upon its local environment. Such a fluorophore could conceptually be used for the detection of conformational change upon binding to a target analyte.[\[132\]](#) The availability of plasmids containing the corresponding tRNA-aaRS specific to its cognate UAA was also identified in the literature review. *Table 11* of the appendices presents a list of tRNA-aaRS examples used for incorporation of various UAA in different protein expression systems. The table also shows their envisioned purposes, particularly for labelling with different fluorescent dyes to develop strategies for detection of target ligands. Some of these tRNA-aaRS are commercially available, mainly through the Addgene plasmid depository, while others are available upon request from various research groups (*e.g.* Schultz Lab, Scripps Research Institute, La Jolla, USA).

The positioning of dye into a target location within an scFv antibody is critical for designing polarity-dependent fluorescent biosensors. Two feasible options can be used here: (a) integrate fluorophore *in vivo* using a solvatochromic fluorescent UAA (fUAA), or (b) use a UAA with a suitable functional group (*e.g.*

azide or ketone) for subsequent bio-orthogonal “click” reactions with DBCO-modified dyes. Among the available fUAA, Anap has excellent solvatochromic properties, and the associated resources (*e.g.* pAnap plasmids) are commercially available. Anap is a solvatochromic fUAA which is a polarity indicator and a derivative of the Prodan dye family, with emission peak varying by ~80 nm depending on the solvent polarity. Past studies have shown that it can be genetically incorporated into proteins using either mammalian or yeast expression systems. Lee *et al.* demonstrated incorporation of Anap in glutamine binding protein for the detection of glutamine based on the change of Anap polarity (~60 nm blue shift) in a dose-dependent manner.[132] Chatterjee *et al.* first demonstrated the evolution of tRNA-aaRS (pAnap) plasmid that can encode Anap in mammalian cells.[131] It was hypothesised that Anap could be incorporated into an scFv antibody for designing a wavelength-dependent biosensor.

Click chemistry is an extensively studied bio-conjugation reaction which can be performed under physiological conditions (a schematic presented in Chapter 2 in *Figure 6C*). This unique method allows bio-orthogonal attachment of two molecules through suitable one-pot chemistry in simple biological buffers. While over 100 UAAs genetically were encoded in different proteins, *p*-Acetylphenylalanine (pAcF) and *p*-Azidophenylalanine (pAzF) remain popular choices for the generation of antibody conjugates, particularly for the creation of antibody-drug conjugates for therapeutic application.[194] pAcF is a ketone-functionalised UAA that has been used widely for its ability to site-specifically label proteins. The ketone group of pAcF UAA readily undergoes click reaction with hydrazide or hydroxylamine or aminoxy-functionalised dyes. Ketone is one of the first functional groups to be added into proteins since the discovery of genetic code expansion.[195] Brustad *et al.* illustrated that the ketone group of

pAcF readily reacts with aminoxy-functionalised Alexa fluorophore via oxime ligation.[196] Another commonly used click reaction is the cycloaddition of azide-alkyne groups. Overwhelming research has reported the use of pAzF for the addition of alkyne functionalised reporters.[197, 198] The azide group of pAzF enables copper-free reaction with DBCO functionalised fluorophores.[199] The advantage of these functional groups is that they are not present in canonical amino acids; hence they can be used for site-specific labelling with a respective fluorophore, without any nonspecific labelling elsewhere in the protein. These chemical reactions have become an alternative to many traditional fluorescence-labelling strategies. This chapter aims to explore the suitability of fluorescent labelling of an scFv antibody by using either intrinsically fluorescent UAA or via UAA with click-chemistry reactive groups (*e.g.* azide and alkyne).

The overall aim of this chapter is to gain fundamental knowledge and skills for establishing and optimising UAA incorporation process in mammalian and bacterial expression systems. It is hypothesised that incorporation of a fluorophore (either Anap or any other potential fluorophore) into a suitable position of scFv could be useful for the detection of a target antigen. A graphical representation in *Figure 12* shows the general procedure followed for genetic incorporation of Anap in mammalian cells where plasmids for scFv antibody and pAnap are co-transfected, and Anap is supplemented during the post-transfection feed. The figure also highlights the *in vivo* mechanism that occurs within the cells in order to incorporate Anap UAA (the system was explained in detail in [Section 2.2.2](#)). Briefly, a pAnap plasmid expresses the aaRS-tRNA that charges Anap UAA and codes in response to the TAG codon (a transcribed form of TAG is GAU in mRNA, and the complementary codon in tRNA is CUA).

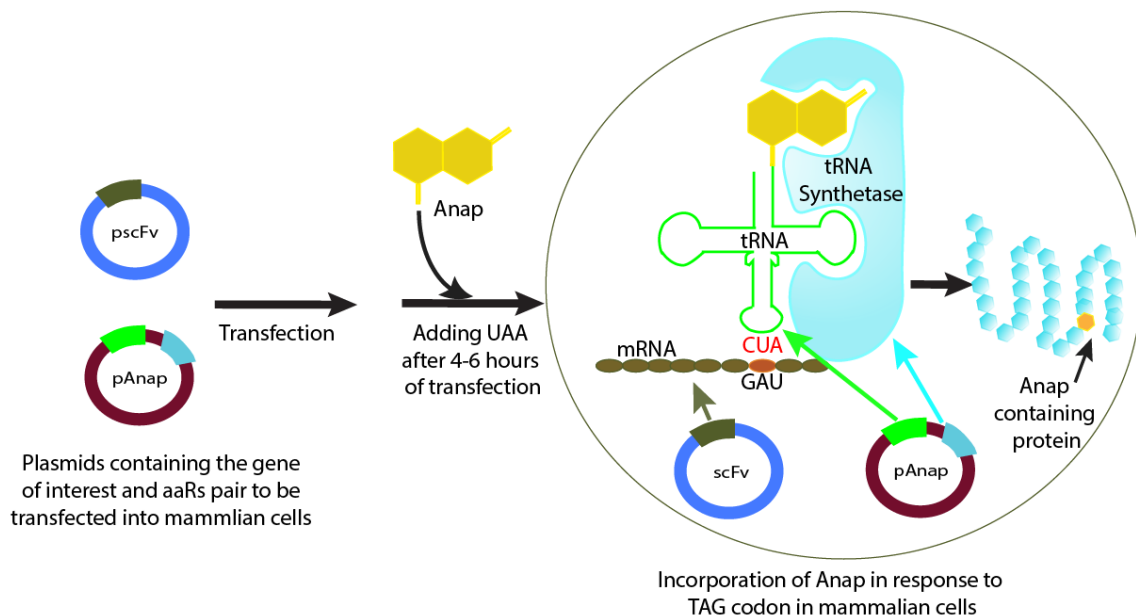


*Figure 12: Anap incorporation into scFv sequences in mammalian cells. Plasmids for the gene of interest (e.g. pscFv) and UAA plasmids (e.g. pAnap) are co-transfected into mammalian cells (e.g. HEK). UAA (e.g. Anap) is added to transfected culture medium after 4-6 hours and incubated for seven days for optimum expression of modified proteins. Protein expression is shown schematically in the circle. Structure of Anap in this figure is symbolic.*

In this chapter, an anti-EGFR scFv antibody is chosen as a model protein which was derived from panitumumab (Vectibix), a fully human monoclonal antibody approved by the FDA for the treatment of metastatic colorectal cancer.<sup>[200]</sup> This scFv antibody fragment is selected explicitly due to its relevance in biomedical research particularly for investigating biomolecular interactions, and because it has been highly characterised with respects to its sequence and binding properties previously.<sup>[106, 201, 202]</sup> Herein, the methodology for UAA incorporation into antibody fragments was optimised by targeting the terminus of the scFv antibody as the initial sites (will be called as N- or C- term mutant in the following sections) for fluorescence labelling. Specifically, it was aimed for:

- ❑ Incorporation of Anap UAA fluorophore in the N- and C-terminus of anti-EGFR scFv antibody in a mammalian cell expression system.
- ❑ Incorporation of pAcF and pAzF UAAs in the N- and C-terminus of anti-EGFR scFv antibody using bacterial expression systems, followed by post-purification labelling with DBCO-labelled fluorescent dyes.
- ❑ Characterisation of scFv mutants to test their functionality followed by investigation of fluorescence properties of these fluorescent-scFv mutants in the presence of ligand.

## 3.2 Materials and methods

### 3.2.1 Cloning of scFv into the expression vector

A bispecific antibody, containing the anti-EGFR scFv sequence, derived from panitumumab has previously been described. [203] The plasmid containing the sequence for this bispecific antibody was obtained from Dr Christopher Howard at The University of Queensland. The sequence for the panitumumab scFv portion was PCR (Polymerase Chain Reaction) amplified, digested by restriction enzymes, then cloned into pcDNA3.1 (+) vector for mammalian cell expression. Additionally, the anti-EGFR scFv sequence was also cloned into pET-30a (+) vector (Merck, Cat# 69909-3) for bacterial expression (Dr Howard performed cloning for bacterial plasmids). The DNA sequence of anti-EGFR scFv is shown in the appendices ([Section 7.1](#)).

**PCR amplification of scFv sequence:** In order to incorporate UAA, amber (TAG) stop codon is introduced in N-or C-term sites of scFv to develop a proof-of-principle for a fluorescent probe. The primers ([Table 5](#)) were synthesised from Integrated DNA Technologies (IDT) Technologies.

*Table 5: Primer design for the anti-EGFR scFv mutants, TAG codons are presented in bold and underlined; CTA is the reverse complement of TAG codon used in the reverse primer. Restriction sites are highlighted in green (AgeI) and blue (XbaI). Fw and Rv denote forward and a reverse primer.*

<b>TAG-EGFR-His (N-term).Fw</b>	AAATTT <b><u>ACCGGT</u></b> GTCCATTC <b><u>TAG</u></b> CAGCTCCAGCTGCA GGAATC
<b>TAG-EGFR-His (N-term).Rv</b>	TTTAAAT <b><u>TCTAG</u></b> ATTAATGATGATGATGGTGGTGCTTGATTTC CACCTTGGTGCC
<b>His-EGFR-TAG (C-term).Fw</b>	AAATTT <b><u>ACCGGT</u></b> GCCACCATGGGCTG
<b>His-EGFR-TAG (C-term).Rv</b>	TTTAAAT <b><u>TCTAG</u></b> ATTACT <b><u>ACT</u></b> CTTGATTTCACCTTGGTGCC

The PCR was performed according to the manufacturer's protocol (Phusion® high fidelity DNA polymerase, NEB Inc.). The amplified PCR products were purified by QIAquick PCR purification kit (QIAGEN). The concentration of amplicon was measured using a NanoDrop spectrophotometer (ThermoFisher Scientific).

A pcDNA3.1 (+) vector containing a mammalian leader sequence was obtained from the National Biologics Facility (The University of Queensland). The vector was digested by AgeI and XbaI restriction enzymes (NEB Inc.) to allow cloning downstream of the leader sequence. BamHI (NEB Inc.) restriction enzyme was also added during digestion to prevent reinsertion of the existing insert. The PCR products were digested with 0.5 µL DpnI (NEB Inc.) along with AgeI and XbaI restriction enzymes followed by incubation at 37°C for 2 hrs. The digested products were purified by using the QIAquick PCR purification kit (QIAGEN). About 5 µL of clean digested vectors and inserts were run through 1% (w/v) agarose DNA gel for confirmation of successful digestion. Following that, the ligation reaction (Quick Ligation™ Kit, NEB Inc.) was performed by following the manufacturer's protocol by mixing insert to vector ratio of 3:1 and 9:1. The reaction mixture was incubated for 20 min at room temperature, chilled on ice and transformed into bacterial cells.

***Transformation of ligation mixture:*** The ligation mixture was transformed into competent bacterial cells (Top10, ThermoFisher Scientific) by heat shock method. Cells were thawed on ice for approximately 10-15 min after removing from the -80°C freezer. About 2 µL of ligated products were added to 50 µL of cells and incubated on ice for 30 min. The mixture was heat-shocked at 42°C in a water bath for 45 s, cooled down immediately by placing on ice for two min. 500 µL of Lysogeny Broth (LB) media was added to the cells and incubated at 37°C in a shaker with 200 rpm for 1 hr. About 100-150 µL of cells were streaked on

ampicillin (Sigma, Cat# A0166-5G) containing LB agar plate. Plates were incubated overnight at 37°C.

**Colony PCR:** Emerging colonies were screened for the presence of the scFv insert by colony PCR. The PCR amplification was performed using universal T7-Forward, and BGH-Reverse primers and the reaction mixture was performed as per the manufacturer's protocol (Phusion® high fidelity DNA polymerase, NEB Inc.). Colonies were added to the reaction mixture as the source of DNA by single touch with a sterile tip followed by a quick dip in the reaction mixture. The reaction was carried out in Veriti 96 well thermocycler (Applied Bioscience), and samples were analysed by DNA gel electrophoresis.

**DNA sequencing:** Positive clones identified in the Colony PCR step was inoculated into 10 mL LB medium containing 100 µg/mL ampicillin and grown overnight for plasmid recovery. DNA isolation was performed as per the supplier's instruction (QIAamp DNA mini kit, QIAGEN). Plasmid DNA sample was sent for sequencing at the Australian Genome Research Facility (AGRF), Qld node, using T7-Forward and BGH-Reverse primers.

### **3.2.2 Incorporation of UAA in mammalian cells**

**Expression of anti-EGFR WT scFv and mutants in CHO cells:** CHO-S cells were seeded at about  $1 \times 10^6$  cells/mL in CD-CHO medium (Gibco, Invitrogen) supplemented with 8mM GlutaMAX (Gibco, Invitrogen), grown for two days to reach desired concentration of about  $3 \times 10^6$  cells/mL with expected viability of > 90%. Cells were aseptically transferred to a sterile tube, centrifuged at 200 g for 10 min at room temperature. Media was discarded, and cells were resuspended into fresh CD-CHO medium (supplemented with 8 mM GlutaMAX). Plasmid DNA (2-4 µg DNA/ml of cell suspension) was diluted with OptiPro (Gibco, Invitrogen) serum-free medium, and incubated for 30-60 s at room temperature.

Simultaneously, PEI-MAX (Polysciences) was also prepared as PEI: DNA of 4:1 (w/w) in OptiPro medium, incubated for 30-60 s at room temperature. Diluted DNA was mixed with PEI-MAX solution and incubated for 15 min to achieve complex formation. This complex was gently added to cells in culture flask followed by incubation at 37°C with humidified CO<sub>2</sub> of 7.5% for 5 to 6 hrs. Cultures were diluted 1:2 (v:v) with CD-CHO media supplemented with culture concentrations of 7.5% (v:v) Efficient Feed A (Gibco, Invitrogen), 7.5% (v:v) Efficient Feed B (Gibco, Invitrogen), 8 mM GlutaMax (based on the volume of CD-CHO added), and 0.4% (v/v) anti-clumping agent. Cultures were returned to the incubator at 32°C, 7.5% CO<sub>2</sub>, and incubated for 10-14 days.

***Expression of the anti-EGFR WT scFv in Expi293F cells:*** Approximately 24 hrs prior to transfection, Expi293F cells (Expi293F™, Cat# A14527, ThermoFisher Scientific) were grown to 1×10<sup>6</sup> cells/mL transfection (or to 0.5×10<sup>6</sup> 48 hrs prior to transfection). On the day of transfection, cells were adjusted to 2-3 × 10<sup>6</sup> cells/mL (> 95% viability) with the desired culture volume. Once the media was warmed at 37°C, and DNA and PEI were also thawed at 37°C in a water bath, the transfection mixture was prepared. The ratio of DNA: PEI were prepared as 1:4 (w/w) in DPBS. Approximately 1 µg of DNA per 1×10<sup>6</sup> cells/mL and 4 µg of PEI per 1 µg of DNA were used for transfection. The DNA/PEI mixture was incubated for 15-20 min at room temperature to achieve complex formation. The mixture was added directly to cells with constant swirling. The glucose concentration of the media was determined using the Accucheck glucose monitoring device (Roche) and adjusted to a final concentration of 33 mM in the media by adding glucose solution (1.67 M). Cells were incubated at 37°C, 5% CO<sub>2</sub> at 110-140 rpm in a shaking incubator (New Brunswick™ S41i - Eppendorf). After 5-6 hrs of post-transfection, 10-30 µM of unnatural amino acids (*e.g.* Anap) was directly added to the culture.

After 24 hrs of incubation, cells were fed with 5 g/L Lupin. The glucose concentration of the media was again determined after 72 hrs of post-transfection and adjusted to 33 mM by adding the glucose solution (1.67 M of stock concentrations). Additionally, 2 mM of GlutaMAX was added to the culture. Glucose concentration was further checked on day 5 and adjusted accordingly to 33 mM along with the addition of Lupin at 5 g/L final concentrations. Following incubation of 7 days after transfection, cells were harvested by centrifugation at 1500 g for 15 min at room temperature. The supernatant was decanted into a clean Falcon tube and filtered through a 0.22 µm filter (Millipore). The filtered supernatant was stored at 4°C or -80°C for further processing or long-term storage, respectively.

***Expression of the anti-EGFR scFv mutants in Expi293F cells:*** The N- and C-term anti-EGFR scFv plasmids were transfected following the protocol mentioned above with the exception of co-transfection with the pAnap plasmid. The scFv construct was co-transfected along with pAnap, a plasmid which codes for tRNA and tRNA synthetase pair specific to Anap described by Schultz group (Addgene.org, plasmid #48696). The transfection procedure was the same as described above except the anti-EGFR-scFv mutant plasmid: pAnap was 3:1 or 3:2 (w/w), and 20-50 µM Anap was supplied in the media during post transfection feed. The ratio was varied in the plasmid optimisation experiments.

***Purification of scFv mutants:*** The expressed proteins were purified by affinity chromatography. The immobilized metal (Ni-NTA) affinity chromatography (IMAC) column, HisTrap Excel 1×1 (GE Healthcare), was connected to AKTA Chromatography System (AKTA Explorer 100, GE Healthcare or AKTA Start), equilibrated with PBS buffer (pH 7.4). The filtered supernatant was loaded onto column followed by a wash with PBS (3 column volume). The column was washed with the PBS buffer containing 5-20 mM imidazole (pH 7.4) to remove

nonspecific proteins. Proteins were eluted by loading the PBS buffer containing 500 mM imidazole (pH 7.4). Proteins were buffer exchanged by HiPrep 26/10 Desalting column (GE Healthcare) to remove imidazole and subsequently further purified by using a Protein L affinity (GE Healthcare) column. The column was equilibrated with PBS buffer (pH 7.4). The protein sample from the desalting step was loaded into the column at a flow rate of 1 mL/min and subsequently eluted by using a buffer containing 0.1 M Glycine (pH 2.7-3.0). The eluted proteins were immediately buffer exchanged to PBS buffer (pH 7.4) by using a HiPrep 26/10 desalting column. Elution fractions were analysed by Sodium Dodecyl Sulphate Polyacrylamide Gel Electrophoresis (SDS-PAGE) method.

### **3.2.3 Expression of EGFR (extracellular domains) protein**

A pcDNA3.1(+) expression plasmid containing the DNA sequence (Met 1-Gly 645) of the extracellular domain of human EGFR with a carboxy-terminal human IgG1-derived Fc tag was obtained from the National Biologics Facility, The University of Queensland. The protein was expressed in Expi293F mammalian cells by following the standard mammalian cell culture procedure as described above. The expressed proteins were purified using Protein A affinity chromatography due to its strong affinity to Fc tag. This protein has been widely used as the target antigen throughout the experiments in this project. Details of expression, purification and characterisation are also discussed in chapter 4 materials and methods ([Section 4.2](#)).

EGFR (epidermal growth factor receptor) is a widely known biomarker for various malignancies such as lung, breast and colorectal cancer.[\[204\]](#) Full-length EGFR protein comprises of four extracellular domains, a single transmembrane domain, an intracellular juxta-transmembrane domain linked with a tyrosine kinase domain and a regulatory region.[\[205\]](#) Practically, it is challenging to express full-length EGFR protein due to the presence of transmembrane and

intracellular domain. Hence, only the extracellular domain of EGFR containing the panitumumab epitope tagged with human Fc domain was expressed. The Fc tag not only assists in the purification of the recombinant proteins but also improves solubility.[206] The EGFR-Fc protein was also previously reported as a target antigen for anti-EGFR scFv antibody.[207, 208]

### 3.2.4 Characterization of purified scFv mutants

**Gel electrophoresis (SDS-PAGE):** The expression and purity of proteins were confirmed by SDS-PAGE analysis. 5  $\mu$ L of LDS loading dye (NuPAGE, ThermoFisher Scientific) was added to 20  $\mu$ L of purified scFv, followed by heating at 98°C for 5 min before loading to 12% pre-cast Bis-Tris gel (NuPAGE, ThermoFisher Scientific). Gels were stained with GelCode blue staining reagent (ThermoFisher Scientific) overnight and destained vigorously in H<sub>2</sub>O for imaging. Gels were visualised in the BioRad or UVP gel imager for fluorescence detection at 300 nm (ProQ-emerald 300) or in the UVP gel imager (excitation at 365 nm).

**Indirect ELISA:** human EGFR protein (15  $\mu$ g/mL, expressed as per the protocol described in [Section 3.2.3](#)) was coated in triplicates to quadruplets in 96 well (Nunc flat bottom, Maxisorp) for overnight at 4°C. Additionally, VEGFR2 (R&D Systems, Cat#FAB357P) and fibrinogen (Sigma-Aldrich, Cat# F3879) nonspecific targets were coated at 10  $\mu$ g/mL as a control. The coating solution was decanted followed by the addition of 200  $\mu$ L of 2% (w/v) skim milk (Coles band, product# 7910660P) diluent (0.05% PBST) to each well and incubated for 1 hr at room temperature for blocking nonspecific proteins. Purified anti-EGFR WT scFv and mutants were added at a concentration of 10  $\mu$ g/mL. After 2 hrs of incubation, the wells were vigorously washed six times with PBST (PBS, 0.05% (v/v) Tween 20). The HRP-labelled anti-His antibody (MACS Miltenyi Biotech Cat#130-092-785) was diluted into a blocker solution (1:5000) and 100  $\mu$ L added to each well.

After 30-60 min incubation, the anti-His antibody was decanted, and the wells washed six times with PBST manually. About 100  $\mu$ L of 3,3',5,5'-tetramethylbenzidine (TMB, ThermoFisher Scientific) was added to each well followed by 10 min incubation for adequate colour development. The reaction was stopped by adding 2 M hydrochloric acid followed by recording absorbance at 450 nm in a Multiskan Microplate Spectrophotometer (ThermoFisher Scientific).

**Mass spectroscopy:** The purified proteins were further characterised by total mass and peptide mass fingerprinting analysis by mass spectroscopy. 10  $\mu$ M (10  $\mu$ L) samples were supplied without further treatment for total mass analysis to the Proteomics Facility at SCMB, UQ or Monash Proteomics & Metabolomics Facility, Monash University. The sample for peptide mass fingerprinting was carried out by treating with trypsin followed by ZipTip (Millipore) clean up.

Proteins were first injected onto a Dionex 3000 RSLC nanoUPLC system. Samples were desalted and concentrated online (5 min, 40  $\mu$ L / min) on a C4 pre-column (PepMan 300, 300 $\mu$ m  $\times$  5 mm, 5 $\mu$ m, 300 A) using buffer A, before transfer elution onto a C4 column (Acclaim PepMap 300, 75  $\mu$ m,  $\times$ 15 cm, 5  $\mu$ M, 300A). A gradient of 10 to 80% buffer B over 7 min was used for elution, where buffer A = 1% ACN/0.1% FA, buffer B = 80% ACN/0.1% FA using a flow rate of 500 nL/min. Eluted proteins were directly infused onto a TripleTof 5600 mass spectrometer. Data were acquired over 600 to 2000 m/z, with a 1 s accumulation time, and time bins to sum set to 4, GS1 = 7 psi, ISFV = 2300, TEM = 150 and the script Intact Protein Mode turned on. Data were deconvoluted using the Reconstruct Protein tool in the Bio Tool Kit (PeakView v2.1, Sciex). Mass range for deconvolution was adjusted as needed, using isotope spectrum resolution of 15000 and a limited mass range of 1000-2000 m/z. The experiment and data analysis were performed by Dr Amanda Nowen (SCMB), UQ and Dr David Steer, Monash Proteomics & Metabolomics Facility, Monash University.

**Fluorescent measurement:** The fluorescence spectra of anti-EGFR scFv mutants were collected in a 96 well plate (Costar®, Cat# 3915, Corning Inc.) using a Tecan Infinite 200 fluorescence spectrometer. About 200 µL of Anap labelled anti-EGFR scFv mutant was added to the well in replicates. Similarly, blank PBS of the same volume was added as a control for background spectra. Anap mutants were excited at 350 nm. The emission spectra were recorded between 390 nm to 550 nm.

Similarly, titrations experiments were carried out in 96 well plates. Wells were blocked in 2% (w/v) skim milk (Coles brand, product# 7910660P) in PBS buffer overnight at 4°C. Blocking solution was decanted followed by washing the plates 1-2 times with PBS buffer. About 200 µL of ~10 nM Anap mutants were added to each well in replicates (3-4 wells). A baseline measurement was carried out to ensure equal distribution of scFv mutants. Relevant controls such as denaturant (*e.g.* urea), nonspecific target (*e.g.* fibrinogen) and free Anap were also added in the respective wells. The ligand (EGFR) was added with variable concentrations ranging between 0 to 500 nM to the previously added 200 µL (10 nM) of anti-EGFR scFv mutants to investigate any shifts in emission spectra. Following incubation of approximately 60 min, fluorescence was measured. Data were analysed using the Excel software. Background emission was subtracted (Blank well with an equivalent volume of PBS buffer). Graphs were plotted in GraphPad Prism software. A similar approach was applied for the measurement of fluorescence in human plasma with the exception that EGFR was spiked in 5-10% of human plasma (diluted in PBS buffer).

### **3.2.5 Incorporation of UAA in the bacterial cells**

The N- and C-term anti-EGFR scFv sequences were cloned into pET30b (+) by Dr Christopher Howard at The University of Queensland. The pAcF specific pEVOL- pAcF plasmid was a gift from P.G Schultz, Scrips Research Institute

Scripps Research Institute, La Jolla, USA. The pEVOL-pAzF plasmid was sourced from Addgene plasmid depository (#31186).

### 3.2.5.1 Incorporation of pAcF UAA

**Mutant transformation:** BL21 (DE3) *E. coli* (NEB Inc.) cells were co-transformed with the plasmid of anti-EGFR scFv mutant and pEVOL-pAcPheRS plasmid that encodes the aminoacyl-tRNA synthetase/suppressor tRNA pair. About 0.5-1  $\mu$ L of DNA for each plasmid were added to 50  $\mu$ L of BL21 DE3 cells followed by incubation on ice for 30 min. Cells were heat-shocked at 42°C in a water bath for 45 s followed by incubation on ice for 2 min. 500  $\mu$ L of media (without antibiotics) was added to cells and incubated for 1 hr at 37°C at 200 rpm in shaking incubator (Ratek). 200  $\mu$ L of cells were streaked onto LB agar plate containing kanamycin (ThermoFisher Scientific) and chloramphenicol (Sigma-Aldrich) antibiotics. The plates were incubated at 37°C overnight. Only cells which have taken up both plasmids were expected to grow.

**Mutant expression:** A single colony was picked from the transformation plate and added to LB culture medium. Cells were grown overnight at 37°C in 20 mL LB medium supplemented with chloramphenicol (30  $\mu$ g/mL) and kanamycin (50  $\mu$ g/mL). Of the overnight culture, 5-10 mL was used to inoculate 500 mL of LB in a 2.5-L flask containing the same antibiotics. After incubation at 37°C and 250 rpm shaking for 1 hr, 5 mL of pAcF (500 mM) was added to the culture to a final concentration of 5 mM. When the optical density (OD) at 600 nm reached approximately 0.6, protein expression was induced by addition of arabinose (Sigma-Aldrich) and IPTG (Austral Scientific) to final concentrations of 0.1% (v/v) and 5 mM, respectively. After 4 hrs of induction at 37°C, cells were harvested by centrifugation at 6,000 g and 4°C for 15 min.

***Isolation of inclusion bodies:*** The bacterial pellet was suspended into 50 mM Tris, 20 mM EDTA, pH 8.0 by pipetting vigorously, and incubated for 1 hr at 20°C with 200 µg/mL lysozyme. Approximately 10-20 mL of the buffer was used for each gram of wet cell pellet. Triton 100 and NaCl were added to reach final concentrations of 2% (Triton), and 0.5 M (salt) and cells were disrupted by sonication (SoniPrep 150) at the 30 s on/off. The mixture was incubated for 30 min at 20°C [optional], then centrifuged (Sorvall RC 6) the viscous solution for 60 min at 25,000 g. The pellet was resuspended in the same volume of 50 mM Tris (VWR), 20 mM EDTA (Merck), pH 8.0 by pipetting vigorously, then centrifuged for 60 min at 25,000 g. This step was repeated twice. The resulting inclusion body pellet can be directly applied for refolding or can be frozen and stored (-80°C).

***Fluorescence labelling, solubilisation and refolding:*** Inclusion bodies were solubilised in alkoxyamine labelling buffer (50 mM sodium acetate, 150 mM NaCl, pH 4.0) and aminoxy-TAMRA (Biotium) was added in 50× in molar excess. Protein concentrations were adjusted to 5-10 mg/mL by concentrating down with Amicon Ultra-15 Centrifugal Filter Units (Millipore). Refolding of scFv mutants was achieved by rapid 1:100 dilution of the inclusion body solution in refolding buffer [0.1 M Tris, 0.5 M arginine (Sigma-Aldrich), 8 mM oxidised glutathione (GSSG; Sigma-Aldrich), 2 mM EDTA, pH 8]. The refolding step was carried out at 4°C and spun rapidly for the dilution process for at least 20 h. The solutions from the refolding step were concentrated down to ~20 mL followed by dialysis against PBS buffer (pH 7.4). Dialysed samples were purified using a HisTrap Hp (GE Healthcare) column by following a standard IMAC affinity chromatography method. Samples were analysed by SDS-PAGE technique.

**Fluorescence measurement:** As SDS-PAGE analysis did not show the presence of fluorescently labelled scFv mutant, further fluorescence characterisation was not carried out.

### 3.2.5.2 Incorporation of pAzF UAA

**Mutant expression:** The plasmids for scFv mutants [pET 30b (+), kanamycin resistant] and pEVOL-pAzF plasmid (chloramphenicol resistant, Addgene, Cat#31186) were co-transformed into BL21 *E. coli* cell as per supplier's instruction (New England BioLabs, NEB Inc.). A single colony was picked and added to the LB culture medium. Cells were grown overnight at 37°C in 20 mL LB medium supplemented with chloramphenicol (30 µg/mL) and kanamycin (50 µg/mL). Of the overnight culture, 2-3 mL was used to inoculate 500 mL of LB in a 2.5-L flask containing appropriate antibiotics. When OD reached approximately 0.6, protein expression was induced by adding 0.1% arabinose, 1 mM IPTG, and 3 mM pAzF (Irish Biotech) UAA. After induction, cells were transferred to 20°C for overnight expression. Cells were harvested by centrifuging at 10,000 g and pellets were stored at -80°C.

**Isolation of inclusion bodies:** The pellet was resuspended in 50 mM Tris, 20 mM EDTA (pH 8.0) then sonicated 3× (30 s on/off). 200 µg/mL of lysozyme was added to the sonicated samples. After incubation at 20°C for 1 hr, Triton 2% of 100× (final volume of the sample, v/v) and NaCl 0.5 M (final concentration) were added. Samples were centrifuged at 25000 g for 60 min. The supernatant was discarded, and the pellet was resuspended in fresh Tris/EDTA buffer (~20 ml). The solution was sonicated and centrifuged as previously. These steps were repeated twice. The pellet was either stored at -80°C or proceeded to the refolding step.

***Refolding and purification:*** The solubilised protein was resuspended by adding 2 mL of 0.1 M Tris, 6 M GdnHCl (Sigma-Aldrich), and 2 mM EDTA (Adjust pH 8.0). From this step, 1 mL of resuspended solution was added to 100 mL of refolding buffer (*i.e.* 1:100 dilution). The refolding buffer contains: 0.1 M Tris, 0.5 M Arginine, 8 mM oxidized glutathione (GSSG), 2 mM EDTA, pH 8.0. This step was carried out in the cold room with stirring. The buffer was added dropwise, 1 mL each time followed by incubation for at least 20 hrs at the cold room. The solution was concentrated down by Amicon concentrator (10 MWCO) to about 20 mL. Samples were dialysed (6-8 kDa, SnakeSkin dialysis kit) against 3 L PBS, pH 7.4 for 3× in fresh buffer. Dialysed solution was concentrated down to 1-2 mL volume (filter 0.22 µ). The scFv mutants were purified by Size Exclusion Chromatography (SEC, HiPrep Sephacryl S-100 HR, GE Healthcare) and eluted in PBS buffer. Elution fractions were analysed by SDS-PAGE method.

***Fluorescence labelling of pAzF containing scFv mutants:***

Dibenzocyclooctyne (DBCO) functional group efficiently binds to azido group. In this experiment, a DBCO functionalised Rhodamine fluorophore derivative (TAMRA) was attached via click reaction. The labelling reaction was performed by adding DBCO-TAMRA to N-term pAzF mutant in molar excess of ten times (10:1). First, 4.5 mM of DBCO-TAMRA (Dibenzocyclooctyne-PEG4-Fluor 545, Sigma-Aldrich, and Cat #760773) solution was prepared by dissolving the dye into the PBS buffer. About 7 µL of DBCO-TAMRA fluorophore was then added to 250 µL (12 µM) of N-term pAzF mutant. The mixture was incubated in room temperature for about 60 min. The excess unreacted dyes were removed by buffer exchanged using a PD10 desalting column (GE Healthcare). The TAMRA labelled N-term mutant was concentrated down by Amicon Ultra-15 Centrifugal Filter Units. Fluorescence labelling was confirmed by SDS-PAGE analysis.

***Fluorescence measurement of TAMRA labelled N-term mutant:*** 100  $\mu$ L (50 nM) of TAMRA labelled N-term scFv antibody was added into wells in triplicate in a black plate (Costar, all black). The baseline fluorescence was measured by exciting the mutant at 545 nm in a Tecan Infinite 200 fluorescence spectrometer. The emission was recorded between 560-700 nm. 100  $\mu$ L (500 nM) of EGFR ligand was added to the respective well and incubated for 45 min. Simultaneously, the same volume of PBS buffer was added to respective wells containing the TAMRA labelled N-term mutant to use as a control. Additionally, the effect of the unfolding of TAMRA labelled N-term mutant was investigated by adding 7 M of urea (Sigma-Aldrich). The samples were excited at 545 nm, and emission was recorded between 560-700 nm, as previously described.

### 3.3 Results and Discussion

Prior to experimental studies with a target protein of interest, it is useful to investigate the sequence/structure and how these relate to the intended function. The anti-EGFR scFv sequence was previously reported (US patent# US5844093A), and here it was further analysed to justify CDRs using bioinformatics tools.[203-209] Sequence search in the structural antibody database (sAbDb) identified the CDR regions, as shown in *Figure 13A* (highlighted in magenta colour).[210] The gene sequence and their corresponding amino acids (presented in as Kabat numbering scheme) for the heavy and light chains are also presented in the same figure. Cross-validation of CDRs using IMGT Collier-De-Perles CDR prediction tool revealed similar result with 1-2 amino acids having up- or downstream variations in CDRs in comparison to published data (*Figure 13B*).[211, 212]

(A)

Nucleotides	CAG CTC CAG CTG CAG GAA TCC GGC CCT GGC CTG CTC AAG CCC TCC GAG ACA CTG TCC CTG ACC TGC ACA GTG TCC GGC GGC TCT GTG TCC TCC GGC GAC TAC TAC
Amino acid	Q L Q L Q E S G P G L V K P S E T L S L T C T V S G G S V S S G D Y Y
VH Heavy Chain	H1 H2 H3 H4 H5 H6 H7 H8 H9 H10 H11 H12 H13 H14 H15 H16 H17 H18 H19 H20 H21 H22 H23 H24 H25 H26 H27 H28 H29 H30 H31 H32 H33 H34 H35
	HFR1 CDR-H1
Nucleotides	TGG ACC TGG ATC AGA CAG TCC CCC GGC AAG GGC CTG GAA TGG ATC GGC CAC ATC TAC TAC TCC GGC AAC ACC AAC TAC AAC CCC AGC CTG AAG TCC CGG CTG ACC
Amino acid	W T W I R Q S P G K G L E W I G H H I Y Y S G N T N Y N P S L K S R L T
VH Heavy Chain	H35A H35B H36 H37 H38 H39 H40 H41 H42 H43 H44 H45 H46 H47 H48 H49 H50 H51 H52 H53 H54 H55 H56 H57 H58 H59 H60 H61 H62 H63 H64 H65 H66 H67 H68
	HFR2 CDR-H2 HFR3
Nucleotides	ATC TCC ATC GAC ACC TCG AAG ACC CAG TTC TCC CTG AAG CTG TCC TCC GTG ACC GGC GCT GAC ACC GCT ATC TAC TAC TGG GTG GGC GAC AGA GTG
Amino acid	I S I D T S K T Q F S L K L S S V T A A D T A I Y Y C V R D R V
VH Heavy Chain	H69 H70 H71 H72 H73 H74 H75 H76 H77 H78 H79 H80 H81 H82 H82A H82B H83C H83 H84 H85 H86 H87 H88 H89 H90 H91 H92 H93 H94 H95 H96 H97
	HFR3 CDR-H3
Nucleotides	ACC GGC GCC TTC GAC ATC TGG GGC CAG GGC ACC ATG GTC ACC GTG TCC
Amino acid	T G A F D I W G Q G T M V T V S
VH Heavy Chain	H98 H99 H100 H100A H101 H102 H103 H104 H105 H106 H107 H108 H109 H110 H111 H112
	HFR4
Nucleotides	GAC ATC CAG ATG ACC CAG TCC CCC TCC ACC CTG TCC GGC TCC GTG GGC GAT AGA GTG ACC ATC ACC TGT CAG GGC TCC CAG GAC ATC TCC AAC TAC CTG AAC
VL Amino acid	D I Q M T Q S P S S L S A S V G D R V T I T C Q A S Q D I S N Y L N
VL Light Chain	L1 L2 L3 L4 L5 L6 L7 L8 L9 L10 L11 L12 L13 L14 L15 L16 L17 L18 L19 L20 L21 L22 L23 L24 L25 L26 L27 L28 L29 L30 L31 L32 L33 L34
	IFR1 CDR-I1 IFR3
Nucleotides	TGG TAT CAG CAG AAG CCC GGC AAG GCC CCC AAG CTG CTG ATC TAC GAC GCC TCC AAC CTG GAA ACC GGC GTG CCC TCT GGC TTC TCC GGC TCT GGC ACC GAC TTT ACC
VL Amino acid	W Y Q Q R P G K A P K L L I Y D A S N L E T S V P S R F S G S G S G T D F T
VL Light Chain	L35 L36 L37 L38 L39 L40 L41 L42 L43 L44 L45 L46 L47 L48 L49 L50 L51 L52 L53 L54 L55 L56 L57 L58 L59 L60 L61 L62 L63 L64 L65 L66 L67 L68 L69 L70 L71 L72
	IFR2 CDR-I2 IFR3
Nucleotides	TTC ACC ATC TCC AGC CTC CAG CCG GAG GAT ATC GCC ACC TAC TTT TGC CAG CAC TTC GAC CAT CTG CCG CTG GCC TTC GGC GGA GGC ACC AAG GTG GAA ATC AAG
VL Amino acid	F T I S S L Q P D I A T V F C Q R F D H L P L A F G G G T K V E I K
VL Light Chain	L73 L74 L75 L76 L77 L78 L79 L80 L81 L82 L83 L84 L85 L86 L87 L88 L89 L90 L91 L92 L93 L94 L95 L96 L97 L98 L99 L100 L101 L102 L103 L104 L105 L106 L107
	IFR3 CDR-I3 IFR4

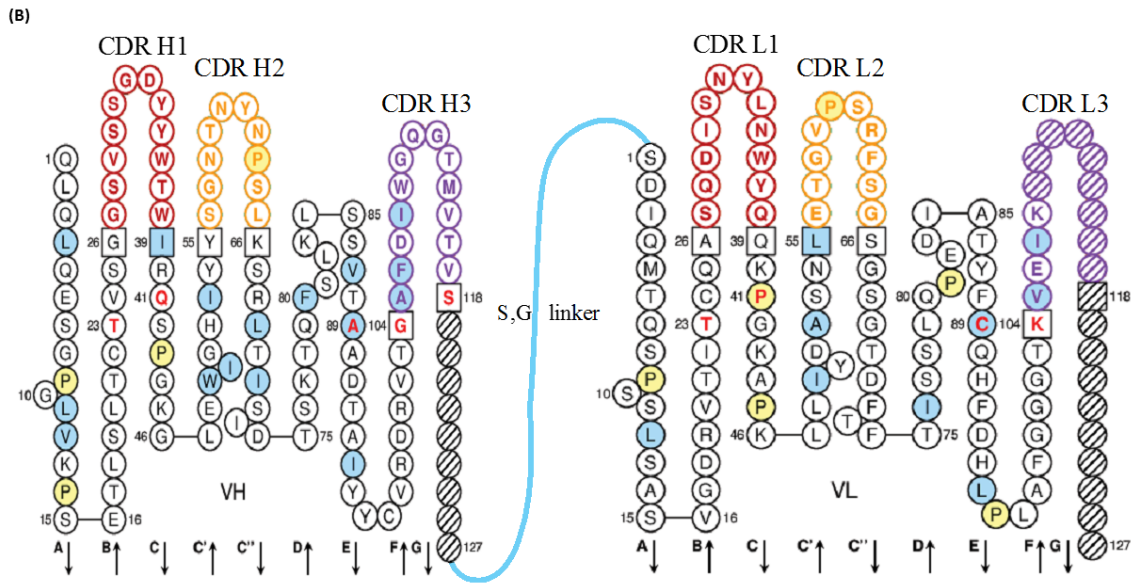


Figure 13: Nucleotide and amino acid sequence of anti-EGFR scFv. The Amino acid sequence is represented as Kabat numbering scheme (determined by the sAbDb tool; <http://opig.stats.ox.ac.uk/webapps/sabdab-sabpred/Welcome.php>). (B) Collier-De-Perles CDRs prediction of anti-EGFR scFv through IMGT bioinformatics tool [<http://www.imgt.org/3Dstructure-DB/cgi/Collier-de-Perles.cgi>].<sup>[212]</sup> The CDRs of heavy and light chains were determined separately using the template provided in Collier-De-Perles CDRs prediction tool which was joined by a serine-glycine (S, G linker, blue).

The binding interface and amino acid sequence of anti-EGFR scFv antibody were further compared against the published crystal structure of anti-EGFR Fab antibody in association with EGFR domain III.<sup>[213]</sup> The crystal structure of the anti-EGFR Fab: EGFR Domain III complex showed binding spheres covering a significant portion of the surface involving all the CDRs in the heavy and light chain (Figure 14). Interestingly, the Tyr residues in H1 (35Y) and H2 (54Y and 55Y; alternatively read as H52Y and H53Y as per Kabat numbering where H stands for heavy chain) were found to be involved in the interactions with the  $\beta$ -strand of EGFR Domain III. On the other hand, the light chain showed less interaction with the EGFR, mainly via Y32 residue of CDRL1, Y50 residue of CDRL2 and three residues of the CDRL3 (F91, D92 and L94).

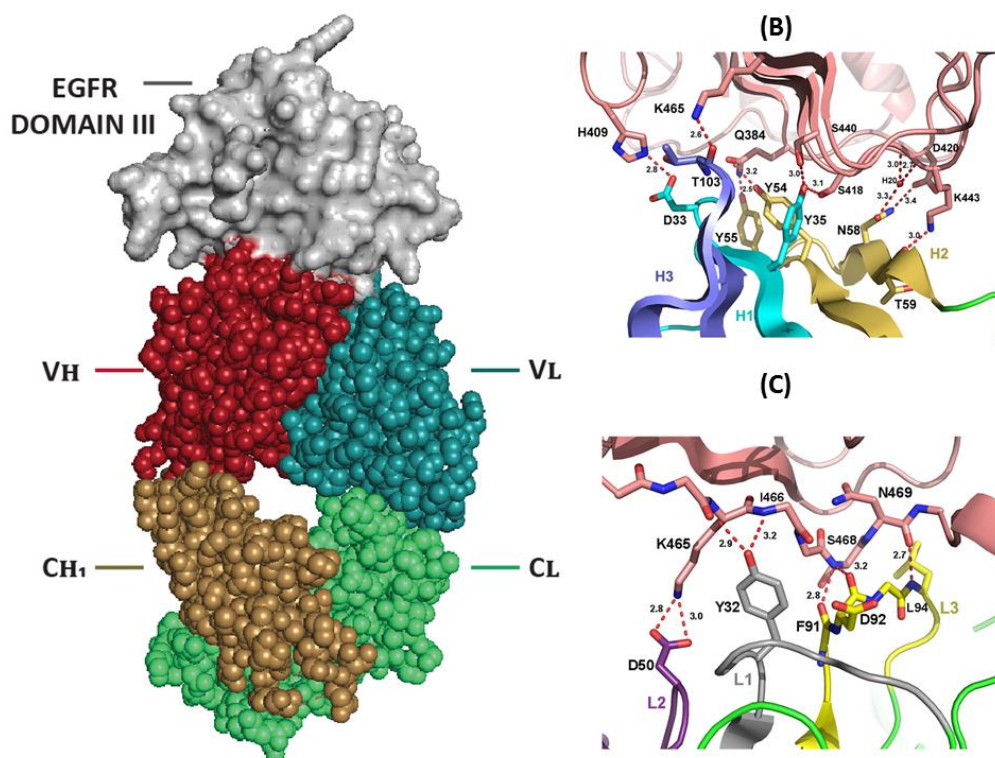
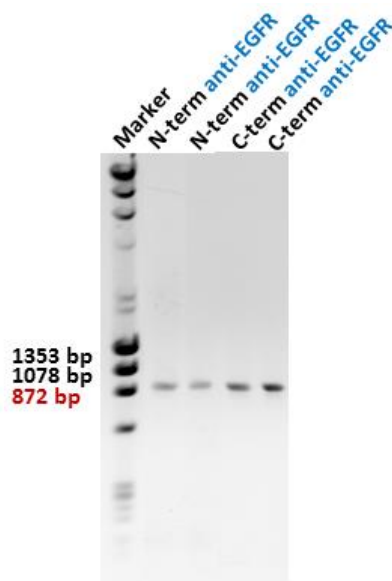


Figure 14: Binding interface of anti-EGFR Fab antibody. (A) Structure of anti-EGFR Fab antibody in complex with Domain III of EGFR protein. (B) EGFR interaction with the heavy chain as represented in cyan (H1), gold (H2) and blue (H3). (C) Epitope binding interfaces ( $\beta$ -sheet of EGFR) of the light chain. The CDRs of light chains (L1, L2 and L3) are represented in grey, purple, and yellow colour respectively. Whereas figure A was generated by using PyMOL molecular visualisation tool from the deposited structure in protein data bank (PDB: 5SX4), figure B-C was reproduced from Sickmier et al.<sup>[213]</sup>

### 3.3.1 Incorporation of Anap into N- and C-termini of anti-EGFR scFv

Molecular cloning was carried out to modify the anti-EGFR scFv wild-type (WT) sequence for the insertion of TAG codons into the N- and C- term of the scFv without adding any other amino acids. The modified sequences were cloned into the selected restriction sites of the mammalian vector. Vector constructions were confirmed by colony PCR method where inserts were identified by DNA gel electrophoresis. The gel showed expected ( $\sim 876$  bp, calculated based on the base pairs of the scFv sequence shown in [Section 7.1](#)) bands for each insert (*Figure 15*). Vector construction was further confirmed by DNA sequencing of positive

clones identified in colony PCR, and these clones were subsequently grown in DH5 $\alpha$  bacterial cells for plasmid isolation. DNA sequencing analysis showed nearly 100% sequence similarities (multiple sequence alignment presented in the appendices, [Section 7.3](#)). These plasmids were then amplified in large-scale culture and subsequently purified (DNA Midi and Maxi prep) for transfection into mammalian cells.



*Figure 15: Confirmation of construct cloning. Colony PCR confirms insertion of N-/C-terminal TAG containing anti-EGFR scFv gene in pcDNA3.1(+). Lane 2-3 confirms inserts of the N-term mutant. The PCR was performed using two different colonies from the transformation plate. Similarly, Lane 4-5 confirms inserts of C-term mutant and the PCR was performed using two different colonies from the transformation plate. The inserts are approximately 876 bp in size and appeared just above the 872 bp marker.*

Optimisation of Anap incorporation was primarily carried out in Human Embryonic Kidney (HEK) Expi293F cells or Chinese Hamster Ovary (CHO) cells to produce sufficient yields throughout the PhD project. This optimisation process was carried out over a two-month period and hence was not comprehensive, however, was sufficient for the purposes of the project. Previous studies have reported protocols for Anap incorporation into proteins;[191]

however, it may vary between laboratory settings, expression in different cell lines, transfection/expression strategies, e.g. the ratio of plasmids and Anap concentrations. Furthermore, to the best of our knowledge, no report has described a protocol for Anap incorporation in antibodies or antibody fragments. Firstly, the post-transfection incubation time for protein expressions was systematically investigated. Protein expressions in CHO-S cells generally take 10-14 days.[214] Past reports indicated a high yield of protein expressions in 7 days using the Expi293F HEK cells.[215] The Western blotting experiment was performed to monitor mutant expression in Expi293F HEK cells. As shown in *Figure 16A*, significant protein expression was evident within 3 days of transfection followed by a minor increase between days 5-7. Hence, cells were grown for 7 days from the day of transfection for protein expression throughout this project.

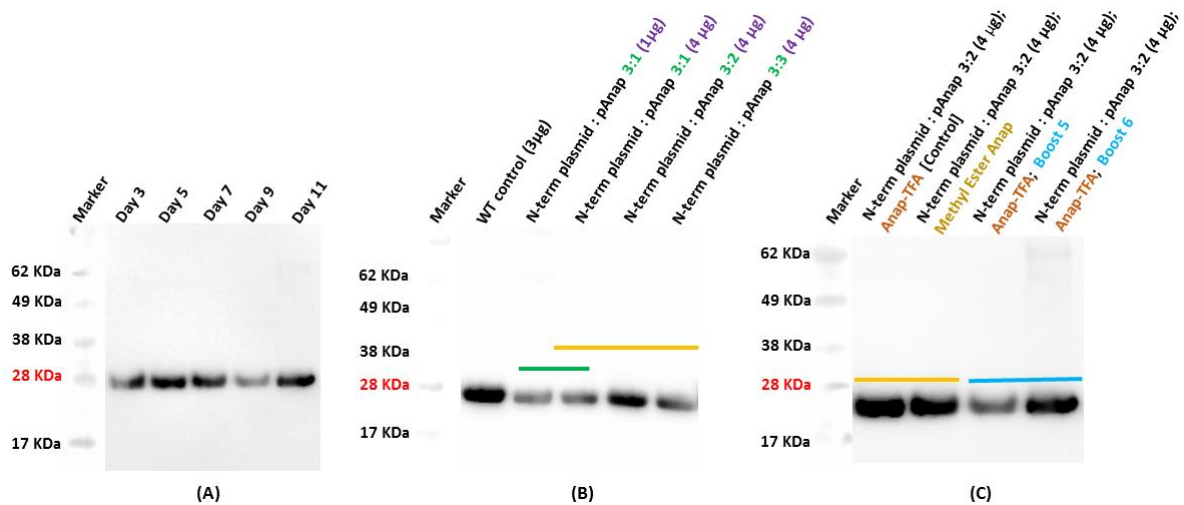


*Figure 16: Optimisation of scFv expression for Anap incorporation. Western blot analysis demonstrates optimisation of Anap incorporation into N-terminus of anti-EGFR scFv. Mutant was detected by HRP-labelled anti-His tag antibody. (A) Expression of N-term mutant increased over time in Expi293F HEK cells. (B) Investigation of plasmid ratio and the total amount of plasmid for transfection; (C) comparison between Anap-TFA and Anap-methyl ester (lane 1, 2); comparison of using commercially available protein expression boost kits (lane 3, 4). Bands appeared below 28 kDa corresponds to approximate MW (26 kDa) of mutants.*

The ratio of plasmids for co-transfection (plasmid for scFv: plasmid for tRNA-aaRs) is believed to be critical for efficient incorporation of Anap and expression of the mutants because incorporation of Anap is dependent on the expression of the tRNA-aaRS pair. However, excessive addition of DNA may be toxic to cells; therefore, an optimum ratio is desirable. Despite Chatterjee *et al.* have reported an optimal plasmid ratio of 3:1 (plasmid for protein: pAnap) as optimal for Anap incorporation in enhanced green fluorescent protein, an experiment was carried out to vary the scFv: pAnap plasmid ratio (*e.g.* 3:1, 3:2 or 3:3), along with the total amount of DNA added (1 vs 4 µg).<sup>[191]</sup> Western blot analysis on samples collected directly from the culture supernatant showed that a total of 4 µg of DNA in 3 million cells/mL at a plasmid ratio of 3:2 resulted in marginally improved expression yield (*Figure 16B*) in comparison to the control.

Apart from the optimisation of plasmid concentration, the incorporation efficiency of different Anap products was also tested, using the N-term variant. Currently, two forms of Anap are available commercially with minor structural differences (Anap-TFA and Anap-Methyl Ester, AsisChem, Cat# ASIS-0014 and ASIS-0146). While testing their incorporation efficiency using the same transfection and culture condition, Anap-TFA was observed to be more soluble in aqueous solutions although there was little difference in expression yield between the two derivatives (*Figure 16C*). Henceforth, Anap-TFA was used for incorporation into scFv mutants throughout the project. Moreover, the effect of supplementing commercially available protein expression boosts (HyClone Cell Boost 5 and 6 Supplement, GE Healthcare) on protein yield was also evaluated. According to the manufacturer, the supplements provide nutrients such as lipids, amino acids, vitamins, and growth factors to cell lines that lead to increased protein expression. Using the Anap-TFA and under same culture condition, as used in the above experiments, supplementation of these boosts did not indicate

any proof of such enhancement in protein yield as analysed by Western blot method (*Figure 16C*).

Using the optimised conditions, the expressed scFv mutants were purified from the culture supernatant by affinity chromatography such as Ni-NTA IMAC followed by Protein L affinity chromatography. The Ni-NTA complex has been used widely in affinity purification due to its ability to form a complex with the poly-Histidine tag of proteins through the transition metal ( $\text{Ni}^{2+}$ ) ion when complexed with NTA.[\[216\]](#) Protein L strongly binds to human Kappa light chain of the VL domain – while panitumumab contains this sequence, not all IgG sequences do, and so this process is not necessarily generally applicable. *Figure 17* shows a typical purification profile used for N-term mutant purification using Protein L column.

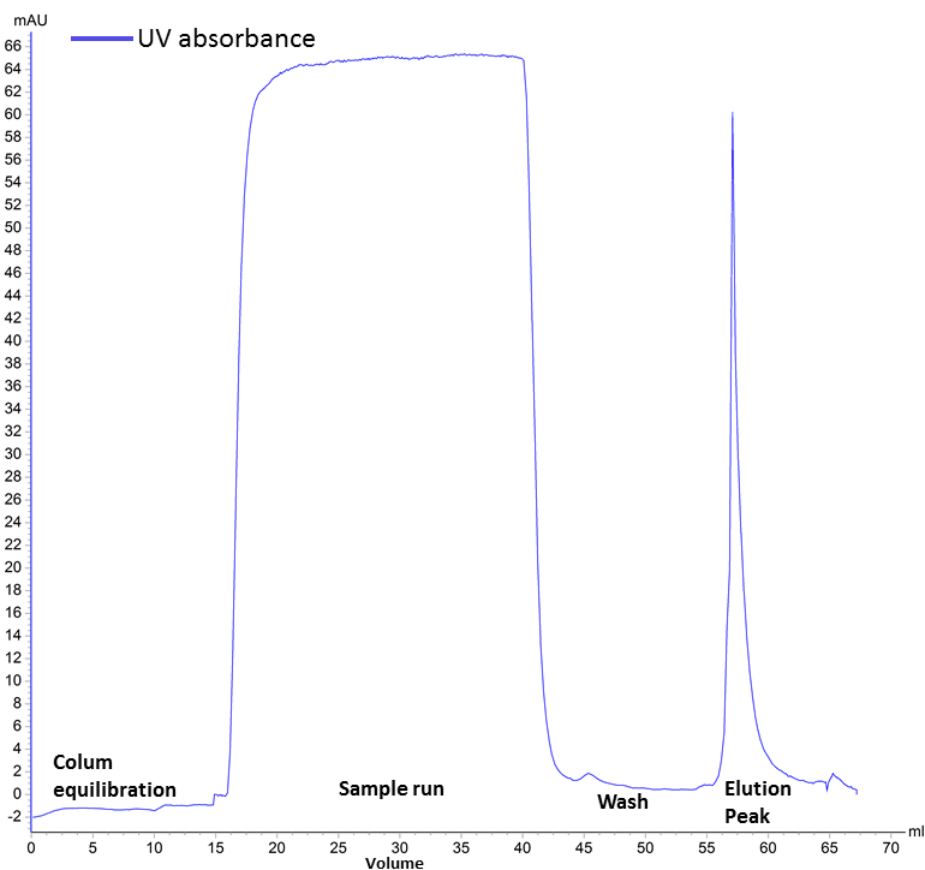


*Figure 17: Purification of N-term mutant using protein L affinity chromatography. The purification process involved various phases including column equilibration with equilibration buffer followed by sample application, wash out weakly bound contaminant proteins and elution of mutant with low pH buffer, typically 0.1M glycine buffer (pH 2.5-3.0). Proteins were immediately buffer exchanged to PBS buffer to avoid precipitation. The chromatogram was extracted from UNICORN 1.1 software.*

While purification via Ni-NTA column showed a reasonable amount of protein expression, the eluted fractions also contained contaminating proteins. Additional purification with Protein L column showed nearly 100% pure scFv mutant as illustrated by SDS-PAGE analysis in *Figure 18A (Lane 2 and 3)*. Analysis of protein yield discovered that a reasonable amount of protein expression per litre of culture was achieved, ranging from 0.1-0.8 mg/L for N- and C-term mutant and 1.5-3 mg/L of WT anti-EGFR-scFv antibodies. The resultant protein concentrations suggest a lower expression yield of scFv mutants due to position specific labelling with the Anap UAA. This is evident in

the gel image presented in *Figure 18B*, which clearly demonstrates decreased protein expression in UAA containing mutants comparing to WT scFv from a normalised culture volume of 300 mL.

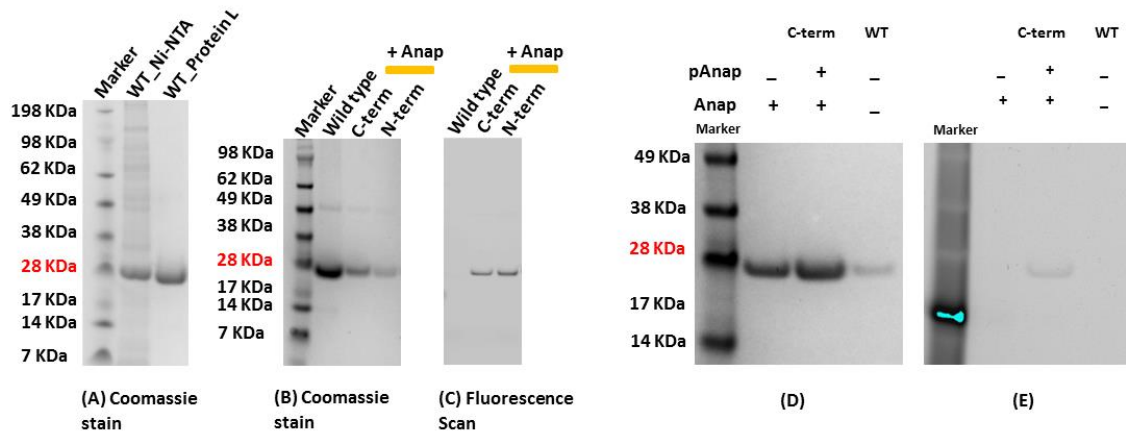


*Figure 18: Confirmation of expression, purification and selective Anap incorporation. (A) SDS-PAGE analysis demonstrated the purity of WT scFv after Ni-NTA and Protein L affinity chromatography. While lane 2 shows significant impurities following Ni-NTA purification, lane 3 illustrates purification with protein L column produces nearly 100% pure protein. (B) Coomassie-stained gel showing expected size band of the scFv mutants and (C) fluorescence scanning of the same gel shows respective fluorescence bands confirming Anap incorporation. While Coomassie staining shows band for all scFv mutants, fluorescence scanning of the same gel shows fluorescence band only for C-term and N-term mutant. (D) Coomassie staining under the white light shows bands for C-term and WT; however, (E) fluorescence scanning of the gel confirms fluorescence band only in the presence of Anap UAA and pAnap plasmid. The protein concentrations of samples were not normalised; hence the band intensities varied.*

The purified scFv mutants were thoroughly characterised to confirm the expression of correct scFv mutants containing Anap UAA. The SDS-PAGE analysis of purified WT, C- and N-term anti-EGFR scFv mutants showed a strong band below 28 kDa molecular weight (MW) mark, which corresponds well to the theoretical molecular weight of 26.3 kDa. The fluorescence of the Anap residue incorporated in C- and N-term mutants was detected by scanning the same gel under 300 nm light using Bio-Rad ChemiDoc gel imaging systems or UVP gel doc systems containing excitation wavelength of 350 nm. Lane 2 and 3 of *Figure 18B*

shows fluorescence band for Anap mutants. It was noticed that the N-term mutant was found brighter than the C-term mutant due to poor Anap incorporation efficiency at the C-term site.

The selectivity of Anap incorporation (by selective suppression of TAG codon) and the fidelity of the pAnap plasmid were verified by expression of C-term construct with and without co-transfection with the pAnap plasmid (*Figure 18D-E*). While expression of the C-term mutant is evident in both the absence and presence of pAnap in Coomassie staining of SDS-PAGE analysis, fluorescence scanning of the same gel showed fluorescence band only in the presence of Anap and its corresponding pAnap plasmid. This finding signifies the selective incorporation of Anap in response to TAG codon, and importantly, Anap did not cross-react with the endogenous protein synthesising machinery. It should be noted that the concentrations of scFv antibody samples were not normalised; hence, the intensities of bands varied based on the expression yield observed.

Electrospray ionisation mass spectroscopy (ESI-MS) analysis was executed to confirm the expression of the expected scFv antibody. Intact mass analysis of WT mutant exhibited an expected mass of 26309 Da. The theoretical mass of WT anti-EGFR scFv was determined as 26331 Da (calculated in ExPASy PortParam bioinformatics portal). Incorporation of Anap into the anti-EGFR scFv mutants was confirmed by the intact mass analysis, which is presented in chapter 4 (manuscript supporting data figure S3, [Section 4.2](#)). Apart from the intact mass analysis, peptide mass fingerprinting was also carried out to confirm the sequence of the WT scFv. Peptide mass analysis enables to determine the sequence of a protein of interest by analysing specific peptides which are generated by cleaving a protein (with a protease enzyme such as trypsin) into small peptide sequences. Then the masses of the peptides are compared and

ordered based on the known sequence in the database (PeakView). The cleavage sites of proteins can be theoretically predicted and used for comparison. The prediction of anti-EGFR scFv by ExPasy: PeptideCutter program is presented in [Section 6.4](#). The peptide fingerprinting displayed nearly 100% sequence coverages with high confidence that agrees well with the theoretical anti-EGFR scFv sequence; however, exhibited 4% mismatch mostly in the His-tag (*Figure 19*). It may be noted that the C-term mutant was not considered for mass spectroscopic analysis due to inefficient labelling with Anap that resulted in the mixture of labelled and unlabelled products.

HHHH**HH**QLQLQESGPGLVKPS**ETLS**LTCTVSGGSVSSGDY**Y**WTWIRQSPGK  
 GLEWIGHI**Y**SGNTN**YNP**SLK**S**RLTISIDTSKTQFSLKLS**S**VTAADTAI**Y**  
 CVRDRVTGAFDIWGQGTMTVSSGGGGSGGGGSDIQMTQSPSSLSA  
 SVGDRVTITCQASQDI**S**NYLNWYQ**Q**KPGKAPKLLIYDASNLETGVPSRFSG  
 SSGSGTDF**TFT**TISS**LQ**PE**DI**ATYFCQHFDH**L**PLAFGGG**T**KVEIK

Green = High confident, Red = Low confident, Grey = Unidentified.

Percentage of coverage: 96%

*Figure 19: Peptide mass fingerprinting of WT anti-EGFR scFv. Mass spectroscopy confirms nearly 100% sequence similarities. Green coloured amino acids are confirmed with high confidence, whereas amino acids are highlighted red detected with low confidence.*

The functionality of scFv mutants was tested by indirect ELISA immunoassay. A schematic presented in *Figure 20A* shows the strategy applied for the detection of the target molecule. Detection of bound purified WT and mutant anti-EGFR scFv using HRP-labelled anti-His antibodies showed significant binding to the EGFR target as depicted in *Figure 20B*. The C- and N-term mutants showed similar absorbance at 450 nm in comparison to WT confirming that Anap incorporation to mutants did not cause a substantial change in binding ability. Binding specificity was confirmed by exposing these mutants to control nonspecific proteins such as a structurally similar analogue of

EGFR (e.g. VEGFR) and fibrinogen. The controls did not produce significant absorbance signal confirming the specificity of scFv mutant antibodies.

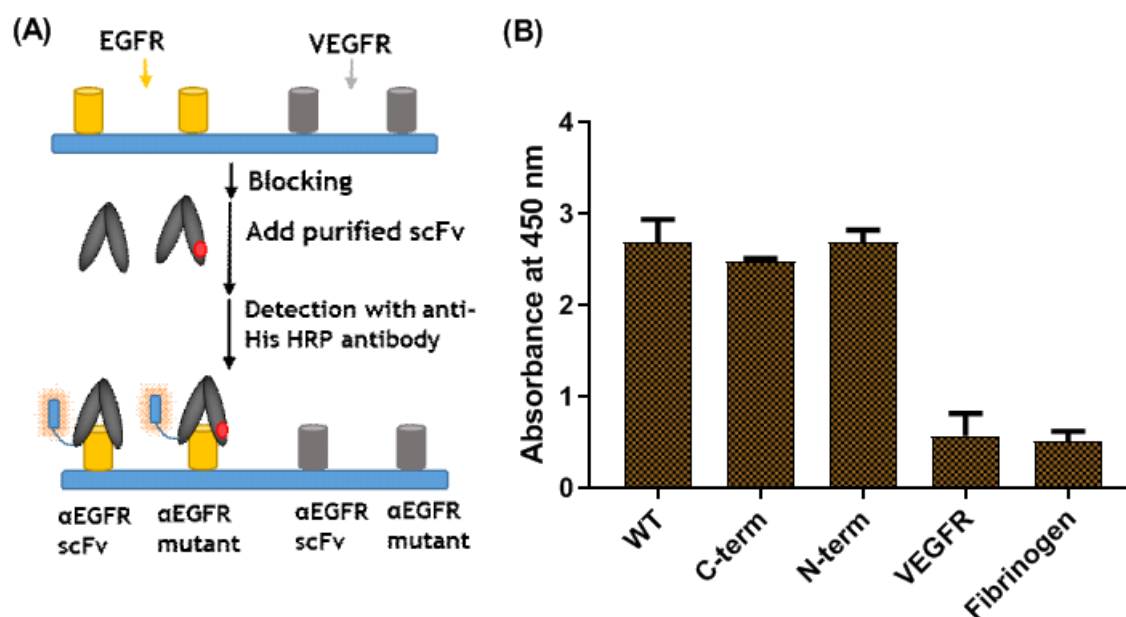


Figure 20: Testing functionality of scFv mutants. (A) Schematic illustrations of indirect ELISA methods used to test purified WT, C-term and N-term anti-EGFR scFv mutants. (B) Detection of mutants binding to EGFR protein. VEGFR and Fibrinogen were used as negative control ligands in this experiment. Error bars are presented in  $\pm$  SD, n=4.

Following the confirmation of functional scFv Anap mutants, the fluorescence spectra of each mutant were investigated (Figure 21A). Excitation of the N- and C-term mutants at 350 nm produced the maximum emission wavelength at 495 nm which is not significantly different to that of the free Anap in aqueous buffers (e.g. PBS). This suggests that the C- and N-term sites are highly exposed to solvents, and the microenvironment of Anap in these sites is of similar polarity to that of the free dye in PBS buffer.

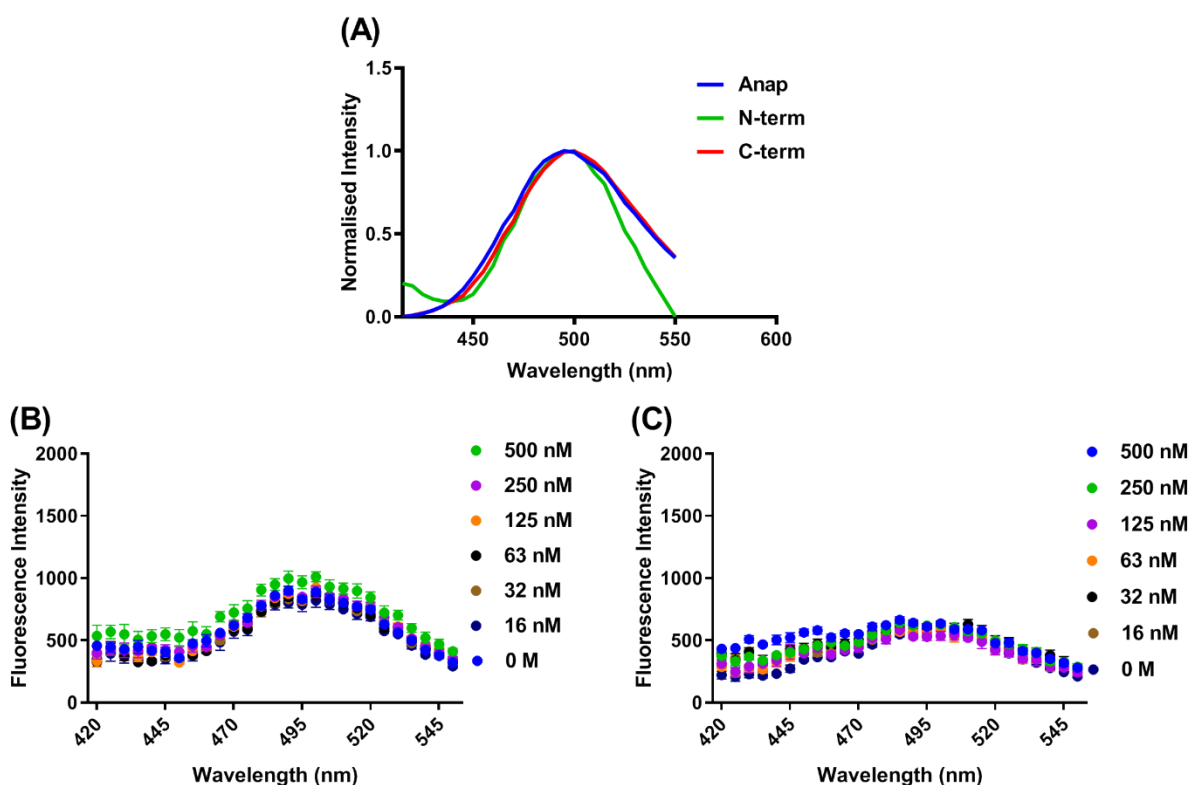
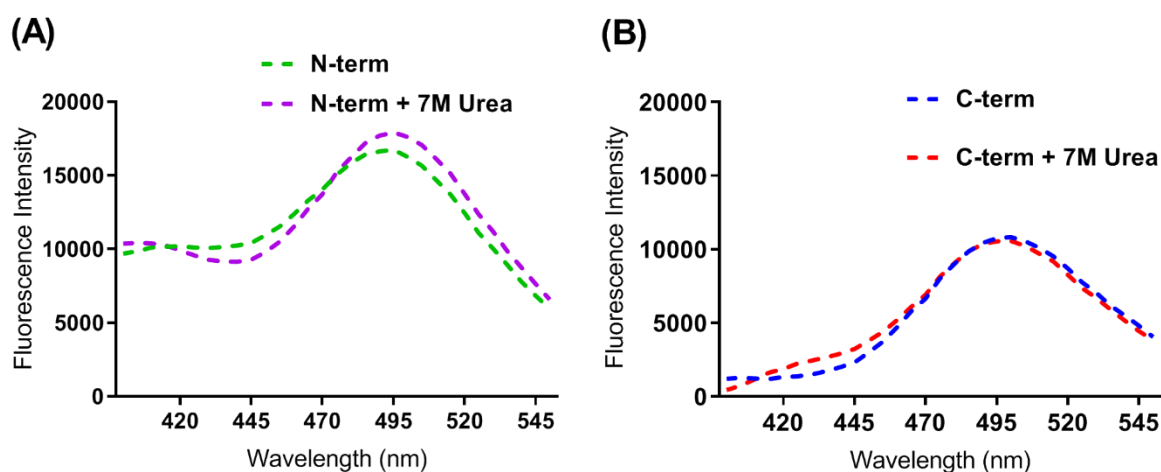


Figure 21: Emission spectra of N- and C-term mutants. (A) Normalised fluorescence intensity of free Anap and mutants in PBS buffer. Fluorescence measurement of (B) N-term and (C) C-term anti-EGFR scFv mutant did not show creditable fluorescence modulation in a dose-dependent titration (0-500 nM) of ligand (EGFR). Error bars are represented in  $\pm$  SEM,  $n=3$ .

Next, the optical properties of these mutants were investigated by fluorescence analysis in the presence of the EGFR target (Figure 21B-C). Exposure to various concentrations (0-500 nM) of EGFR antigen to the N- or C-term mutant exhibited no significant fluorescence modulation compared to the control. The emission maxima remained unchanged at 495 nm for both the N- and C-term mutants. This finding is consistent with the data presented in Figure 22; *i.e.* as the N- and C-termini are highly solvent-exposed sites and are located far from the binding interface, it is unlikely that antigen binding would affect the local polarity of incorporated Anap dye.

Further characterisation of these mutants was carried out to study possible quenching of fluorescence intensity. Hypothetically, denaturation of the

proteins leads to the unfolding of protein structure resulting in the release of interactions between dyes and amino acids involved in fluorescence quenching. [115] Hence, in the case of quenching of a fluorophore within a protein, a fluorescence intensity change is expected in the unfolded state. Herein, the scFv constructs were denatured by high concentrations of urea to investigate for a possible quenching effect (*Figure 22*). The resulting emission spectra of the mutants in the presence or absence of urea showed no indication of fluorescence quenching by adjacent native amino acids as the fluorescence intensities remain mostly unaffected.



*Figure 22: Denaturation of N- and C-term mutants with 7M Urea. (A) C-term mutant did not show any significant fluorescence intensity change. While N-term mutant (B) showed a slight increase in intensity, it was considered to be insignificant due to the increment of intensity being very low.*

It was found that several external factors affected the fluorescence measurement which were optimised in this chapter. Firstly, several types of microplates for fluorescence measurements were tested. Fluorescence of Anap-labelled mutants was detected mostly in 96 well plates in the Tecan fluorescence spectrometer. Two types of 96 well plates were tested (black walls with clear bottom vs. all black) and found a substantial difference in the background signal. Anap was excited from the bottom of the plate when a black plate with the clear

bottom was used. It was found the plate contributed significantly high fluorescence background in the Anap emission region. In contrast, switching to all black plates in which Anap was excited from the top of the plate reduced ~20% background fluorescence in the region of 400-500 nm compared to a transparent bottom plate. Secondly, as Anap is known to be sensitive to the local environment, the interaction of mutants on the plate wall was occasionally found to produce spectral changes. This issue was resolved by blocking the plate wells with a buffer containing skim milk.

Though TAMRA fluorophores incorporated into N- or C- term sites of Q-body biosensors had produced significant fluorescence intensity enhancement in response to antigens, labelling of anti-EGFR scFv mutants with Anap into these sites did not exhibit noteworthy fluorescence modulation. The mechanism of Q-body demonstrated that fluorescence of TAMRA was quenched by nearby Trp residues, however fluorescence of Anap was not quenched similarly despite the prevalence of Trp residues within close proximity. This was further supported by the denaturation experiment where Anap labelled mutants did not show significant fluorescence changes, whereas Q-body had shown substantial fluorescence enhancement.[\[47, 74\]](#) The comparison suggests that alternative sites need to be sought as site-specific labelling of the anti-EGFR scFv mutants at the termini did not show optical activities. Mutagenesis of internal residues must be undertaken to identify a specific site that undergoes a significant change in polarity upon selective analyte binding.

### **3.3.2 Incorporation of clickable UAA in the N- and C-termini of anti-EGFR scFv**

The N- and C-term mutants were modified with pAcF and pAzF UAA in bacterial expression systems and subsequently labelled with aminoxy- and DBCO-functionalised TAMRA fluorophores through click reaction. Instead of

using the mammalian expression for UAA incorporation, the bacterial protein expression system was employed mainly due to the limited availability of UAA specific plasmids. Though past reports indicated the generation of pAcF and pAzF specific tRNA-aaRS for the mammalian system, these plasmids were not compatible with the plasmids for anti-EGFR scFv expression in Expi293F HEK cells. These tRNA-aaRS plasmids were designed primarily for TReX-293 HEK cells where proteins expressed under the regulation of tetracycline repressor. [217]

### **3.3.2.1 Incorporation of pAcF into N- and C-term sites of anti-EGFR scFv**

The mutants were expressed as inclusion bodies in BL21 *E. coli* strain. Protein expression was monitored by collecting samples routinely and analysed by the SDS-PAGE method (*Figure 23*). While the pre-induction sample did not show any protein expression, induction with IPTG resulted in the appearance of proteins of the expected molecular weight (below 28 kDa) that consistently increased as time progressed. The gel image also indicates the superior expression of the C-term mutant compared to the N-term mutant (Lane 4, 5, 6 vs Lane 9, 10 and 11). The variability in the level of expression is due to the effect of low UAA incorporation efficiency, where the N-term mutant expression is terminated if the UAA is not incorporated, which is also consistent with the expression of N- and C-term mutants seen in mammalian cells (*Figure 18B*)

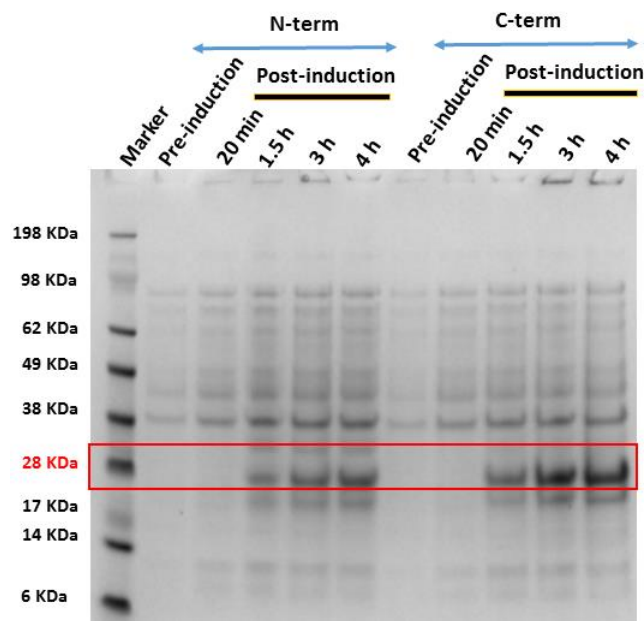


Figure 23: Monitoring expression of scFv mutants for pAcF UAA incorporation. Pre-induction samples were run in lane 2 and 7. A gradual increase in N-term pAcF anti-EGFR expression was observed in Lane 3-6. A similar expression was also observed for the C-term mutant as depicted in lane 8-11.

Isolation of inclusion bodies was performed from the harvested cells followed by solubilisation steps.[218] Conjugation of the fluorophore to the keto-functional UAA was carried out prior to refolding the scFv mutants to avoid further purification and to maximise labelling efficiency. This step also helped to avoid the presence of DTT (used during refolding), which interferes with the conjugation process.[219] One of the disadvantages of using the ketone functional group is that the reaction with aminoxy-dye needs to be conducted at low pH (<4.0). For effective conjugation, the reaction also requires elevated temperature (e.g. 37°C) and significantly high concentrations of proteins (e.g. millimolar). Though prior studies indicated that the use of catalysts such as aniline might improve the conjugation efficiency to some extent, maintaining a low pH is still required.[220] Following the conjugation reaction, the conjugated sample was refolded followed by purification with HisTrap HP column. The SDS-PAGE analysis of eluted samples did not show any expected band in the gel

(result not shown). One of the possible explanations for this outcome is that multiple complicated steps such as isolation of inclusion bodies, solubilisation, conjugation, refolding and subsequent purification steps significantly contributed to the loss of expressed proteins. It was also found that the protein concentration was significantly low ( $\sim 5 \mu\text{M}$ ) after solubilisation step and carrying out oxime linkage reaction at low pH also contributed to precipitation of scFvs. This finding suggests that perhaps bioconjugation of a dye through ketone bearing molecule could only be suitable to scFv antibodies that are stable at low pH for an extended period. Nevertheless, recent discovery indicates the development of an aniline variant that assists oxime ligation at nearly neutral pH.[\[221\]](#)

### **3.3.2.2 Incorporation of pAzF into N- and C-term sites of anti-EGFR scFv**

Incorporation of pAzF UAA into N- and C-term mutants was carried out in a similar fashion as described for pAcF UAA. However, the process was optimised to improve protein expression and subsequent processing for solubilisation, conjugation and refolding. For instance, the scFv mutant was expressed overnight at  $20^\circ\text{C}$  instead of  $37^\circ\text{C}$  for 4 hrs (details can be found in [Methods section 3.2.4.2](#)). The SDS-PAGE analysis of the purified refolded samples showed a distinct band in the expected region ( $\sim 28 \text{ kDa}$ ) with high purity (*Figure 24A*). Bioconjugation reaction of DBCO-functionalised TAMRA fluorophore with the purified N-term mutant showed a bright fluorescent band, as shown in *Figure 24B*. Fluorescence labelling of the C-term mutant was not attempted for a few reasons. Labelling of C-term mutant may produce a mixture of the labelled and unlabelled product as observed for Anap labelling which will not be beneficial for downstream fluorescence studies. Apart from that, most of the Q-bodies were produced by labelling TAMRA fluorophore with the amino-terminal site due to the abundance of Trp residues in the heavy chain (N\_VH-VL\_C orientation). This is also true for anti-EGFR scFv which has maximum Trp

residues (four) in the heavy chain compared to a single Trp residue in the light chain.

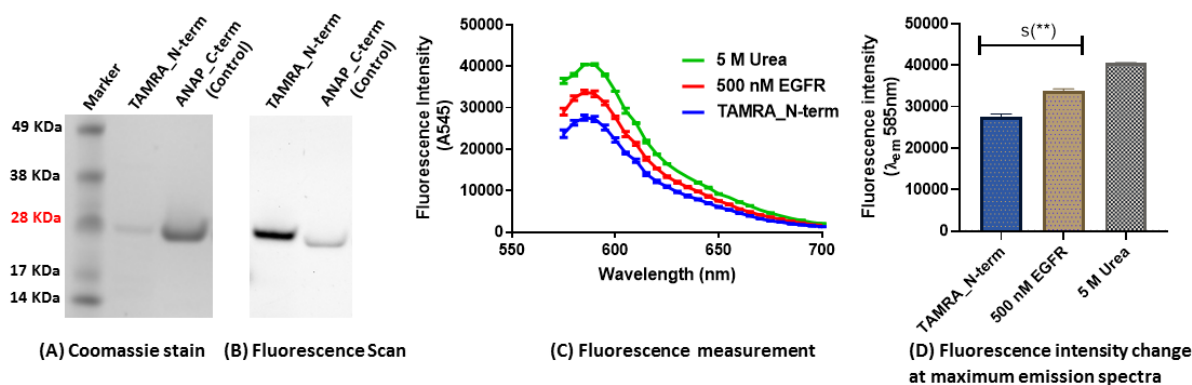


Figure 24: Expression and characterisation of pAzF incorporated N-term anti-EGFR scFv mutant. (A) SDS-PAGE analysis illustrates confirmation of DBCO-TAMRA labelling to the amino-terminal site of anti-EGFR scFv. Coomassie staining shows the presence of TAMRA labelled N-term mutant. C-term Anap anti-EGFR scFv used as a control. (B) Fluorescence scanning of the same gel shows bright fluorescence of TAMRA N-term mutant. (C) Emission spectra of the TAMRA labelled N-term mutant, in the presence and absence of EGFR, and after denaturation with 5M Urea. Addition of EGFR protein led to fluorescence enhancement. A similar effect was also observed when the mutant was denatured by 5 M urea. (D) Fluorescence intensity enhancement at maximum emission wavelength ( $\lambda_{em}$  585 nm). Statistical analysis with *t*-test showed a significant difference in (*s* \*\*) between TAMRA labelled N-term mutant (no EGFR ligand) and in the presence of 500 nM EGFR. Error bars are shown as  $\pm$ SEM, *n*=2-3.

After confirming efficient labelling with TAMRA dye, the fluorescence of the mutant was investigated in the presence of the target ligand. Excitation of TAMRA labelled N-term mutant at 545 nm displayed maximum emission spectra at 585 nm, in agreement with the previously published data (Figure 24C). [222] The result agrees well with the previous illustration on the utility of TAMRA fluorophore labelled in the N- and C-term sites in Quenchbody biosensor. [47] Addition of EGFR ligand (~500 nM) showed a fluorescence intensity enhancement of ~21% (1.2 fold). The increase is in accordance with the Q-body biosensors reported by Abe *et al.* where they observed a modest fluorescence intensity change of 1.3-1.7-fold for the detection of the bone gala peptide, lysozyme and morphine. [47, 74] Statistical analysis was performed with

a t-test on the maximum fluorescence intensity enhancement in the presence of EGFR ligand (*Figure 24D*). The unpaired t-test showed a significant ( $p = 0.0058$ ) difference between the means  $6202 \pm 877.6$  (relative fluorescence units). The mutant was denatured by treating with high concentrations of urea to investigate the potential fluorescence quenching of TAMRA dye. In theory, denaturation of protein leads to the unfolding of the native structure; therefore, remove the quenching effect of dye due to the release of interaction between the fluorophore and amino acids. Fluorescence measurement of denatured N-term TAMRA mutant discovered even a greater fluorescence enhancement (~42%) confirming possible quenching of TAMRA in the native state.

While the incorporation of Anap into N- and C-term of anti-EGFR scFv did not display significant fluorescence change, replacing Anap with TAMRA fluorophore, exhibited significant fluorescence intensity enhancement comparable to that observed with Q-Body biosensors. This result is in line with the expected behaviour of TAMRA, which is known to undergo photo-induced electron transfer with tryptophan residues.[\[47\]](#) The finding further suggested that the mechanism of detection may differ between the fluorophore selections. Nonetheless, a Q-body was produced by reacting DBCO-TAMRA with azide-functionalised unnatural amino acids for the detection of EGFR which was not reported previously.

### **3.4 Chapter 3 summary**

A principal aim of this chapter was to explore site-specific fluorescence labelling of scFv antibodies via genetically encoded intrinsically fluorescent UAA or clickable UAAs. Moreover, the methods for UAA incorporation into scFv antibody fragments were optimised to ensure sufficient yields of UAA-modified proteins throughout the thesis project. It was intended to incorporate Anap UAA into the terminal sites of the scFv to establish an optimum method for

fluorescence labelling of the scFv antibody. The constructs were extensively characterised to confirm the expression of correct scFv sequence mutants in both mammalian and bacterial cells by using various bioanalytical methods. Exposure of N- and C-term mutants to EGFR ligand did not produce noteworthy wavelength change or fluorescence intensity alteration. Presumably, these sites are not ideal for polarity dependent sensing due to the distance from the antigen binding sites. The binding of the target ligand did not cause a significant change of solvents accessibility into the N- or C-term sites. Hence, fluorescence properties remained unchanged. Denaturation of mutants also did not show strong fluorescence modulation; hence confirming no possible evidence of fluorescence quenching of Anap during the native state.

This chapter also investigated fluorescence labelling of scFv antibody via click chemistry to incorporate TAMRA fluorophore. Results showed that fluorescence labelling via ketone functionalised UAA (pAcF) was not successful as the conjugation reaction needed to be maintained at low pH. Apart from that, the expression of the scFv mutant for pAcF integration at 37°C for 4 hrs did not result in high protein yield. Simultaneously, the mutants were also expressed for pAzF incorporation. Optimisation of the expression protocol indicated a higher yield when proteins were expressed at 20°C overnight. Fluorescence labelling of TAMRA dye via click reaction with pAzF containing N-term mutant showed a superior fluorescence labelling efficiency as the conjugation reaction can be performed at neutral pH in room temperature. Exposure of TAMRA labelled N-term mutant to EGFR target revealed enhanced fluorescence intensity, which was further supported by denaturation with urea. Thus, a Q-body was produced for EGFR detection.

The outcome of the work described in this chapter is the optimisation of expression of scFv incorporating UAA for fluorophore labelling, and the

conclusion is that the N- and C-term sites are not suitable for use in an assay for measuring ligand-induced changes in fluorescence wavelength. Therefore, optimal sites for fluorophore incorporation at an internal site need to be investigated based on either a model or crystal structure. The following chapter describes the identification of possible internal sites for Anap incorporation into anti-EGFR scFv. As the crystal structure of anti-EGFR Fab was unpublished at the time these studies were performed, a homology model was developed to identify mutation sites for Anap labelling.

# Chapter Four

## 4. Detection of EGFR by Fluorescently Labelled Engineered Antibodies

---

*Chapter 4 is published in Analytical Chemistry*

*(<https://doi.org/10.1021/acs.analchem.9b00445>, date of publication 22 May 2019). The manuscript along with supplementary data is included here without modification.*

This chapter aims to identify an internal site of the scFv for fluorophore incorporation that corresponds to antigen binding. Renard *et al.* described three criteria for labelling of scFv antibody to develop a fluorescent biosensor. [112, 113] Firstly, the mutation site needs to be in the hypervariable region of scFv that could be affected by antigen binding. Secondly, the site needs to be accessible to the solvent for efficient conjugation with the fluorophore. Thirdly, the site is not crucial for folding or functionality of scFv antibody. They also suggested positioning the fluorophore within the proximity of Tyr, Trp or Phe residue along the sequence for possible fluorescence quenching of the dye. Nevertheless, the group used fluorescence intensity change as the basis of detection of the targets.

Due to the unavailability of anti-EGFR scFv crystal structure, a rational design approach was proposed to select internal sites for Anap incorporation. A homology model structure was created to identify sites of fluorophore incorporation by following the criteria mentioned above. However, importance was given to rely on emission wavelength difference instead of fluorescence intensity as a basis of detection. The following manuscript has described details of the methodology and outcome of the investigation. It may be noted that as this chapter is presented as standalone publication without any modification, [223] there are some overlaps in the description of materials and methods with section 3.4.

## 4.1 Published Chapter

### **Wavelength-dependent fluorescent immunosensors via incorporation of polarity indicators near the binding interface of antibody fragments**

**Jiaul Islam**<sup>1, 2</sup>, Blake T Riley<sup>3</sup>, Christian Fercher<sup>1,4</sup>, Martina L Jones<sup>2,4</sup>, Ashley M Buckle<sup>3</sup>, Christopher B Howard<sup>2,4</sup>, Rosalind P Cox<sup>5</sup>, Toby D M Bell<sup>5</sup>, Stephen Mahler<sup>2,4</sup>, Simon R Corrie<sup>1, 2\*</sup>

<sup>1</sup>*Department of Chemical Engineering, Monash University, Clayton, Australia, ARC Centre of Excellence in Convergent BioNano Science and Technology*

<sup>2</sup>*Australian Institute for Bioengineering and Nanotechnology (AIBN), The University of Queensland, St Lucia, Australia*

<sup>3</sup>*Dept. of Biochemistry and Molecular Biology, Biomedicine Discovery Institute, Monash University, Clayton, Australia*

<sup>4</sup>*ARC Training Centre for Biopharmaceutical Innovation, Australian Institute for Bioengineering and Nanotechnology (AIBN), The University of Queensland, St Lucia, Australia*

<sup>5</sup>*School of Chemistry, Monash University, Clayton, Victoria, Australia*

*\*Corresponding Author: Simon.Corrie@monash.edu, Phone: +61 03 9905 9621*

### **Abstract:**

Herein we describe a fluorescent immunosensor designed by incorporating an unnatural amino acid fluorophore into the binding site of an EGFR-specific antibody fragment, resulting in quantifiable EGFR-dependent changes in peak fluorescence emission wavelength. To date, immunosensor design strategies have relied on binding-induced changes in fluorescence intensity that are prone to excitation source fluctuations and sample-dependent noise. In this study, we used a rational design approach to incorporate a polarity indicator (Anap) into specific positions of an anti-EGFR single chain antibody to generate an emission wavelength-dependent immunosensor. We found that when incorporated within the topological neighbourhood of the antigen binding interface, the Anap emission wavelength is blue-shifted by EGFR-binding in a titratable manner, up to 20 nm, with nanomolar detection limits. This approach could be applicable to other antibody/antigen combinations for integration into a wide range of assay platforms (including homogenous, solid-phase assay, or microfluidic assays) for one-step protein quantification.

*Key words: Fluorescence, biosensor, Anap, antibody fragment, EGFR, unnatural amino acids, polarity indicator*

Measuring the concentration of disease-related proteins from body fluids is a cornerstone of biomedical research and clinical diagnostics. The Enzyme-Linked Immunosorbent Assay (ELISA) principle introduced in the 1970s forms the basis of nearly all commercial and research immunoassays.<sup>1</sup> It is a multi-step process in which a protein is captured onto a surface via a capture antibody, and subsequently quantified in a second step by indirectly measuring the concentration of a detection antibody labelled with a reporter molecule. Advances in detection strategies have improved detection limits dramatically,<sup>2</sup> however the need for two unique antibodies, additional reagents, and washing/blocking steps, is universal. Some ELISAs have made the transition from laboratory assay into hand-held, point-of-care systems that rely on microfluidics to handle the multi-step process,<sup>3</sup> yet they still need to perform a series of relatively complex tasks. An emerging alternative to ELISA is “immunosensors” (also referred to as “reagentless biosensors”) in which binding of a protein to a capture antibody (or related binder) generates an immediately detectable change in optical signal.

The critical design aspects when inserting fluorescent labels into antibody fragments for immunosensing include the need for highly efficient site-specific labelling, with minimal effects on affinity, and sufficient spectral changes upon target binding to provide a clear, unambiguous readout. Many fluorophore incorporation strategies have been developed for efficient labelling of protein, including fusion proteins (*e.g.* GFP); chemical conjugations (*e.g.* maleimide chemistry, amine labelling); various enzymatic methods (*e.g.* biotinylation of protein for avidin-functionalised fluorophore); and genetic incorporation of short peptide tags (*e.g.* SNAP-tag as self-labelling protein tag).<sup>4-6</sup> Although each technique has its merits, they present several limitations, including (a) limitation of labelling sites to

a specific side-chain or N/C terminus only); (b) increased size of the resultant protein conjugate, potentially leading to altered physicochemical behaviour; and (c) additional downstream purification steps to separate labelled antibody fragments from unlabelled reagents.<sup>7</sup>

In the early 2000s, the development of genetic code expansion and unnatural amino acid (UAA) technologies enabled the site-specific incorporation of unique functional groups into any permissible location of a protein.<sup>8</sup> In biosensor development, this technique facilitates the introduction of intrinsically fluorescent groups into a target location by introducing a re-purposed stop codon into the coding sequence and has been implemented in *E. coli*, yeast, and mammalian expression systems.<sup>9</sup> The process requires supplementation of a plasmid containing the sequence of a modified tRNA/tRNA synthetase (aaRs) pair which can recognise a specific UAA for incorporation in response to a specific stop codon.<sup>10</sup> Over 100 different UAAs have been incorporated into various proteins for diverse applications ranging from antibody-drug conjugates to bispecific antibody development.<sup>11-12</sup>

While the incorporation of environmentally sensitive dyes into proteins has been widely explored, the application of the concept to immunosensors has received limited attention. Renard *et al.* described the engineering of antibody fragments by a two-step process: mutating amino acids near the binding loops to cysteines, and subsequently labelling them with maleimide-functionalised dyes.<sup>13</sup> While this work helped to highlight some fundamental design criteria by identifying permissive sites for mutation, the problem of interference with critical disulphide bonds when attempting to label the introduced cysteines selectively is difficult to solve.<sup>14</sup> Abe and Ueda *et al.* have published a series of articles describing the development of a genetically controlled mutant antibody fragment which they call “Quenchbody” or

“Q-body”. The technique is based on the introduction of a ProX tag (12 amino acid sequence incorporating amber codon for enhanced expression and UAA incorporation) into the scFv (single chain variable fragment) sequence, allowing direct incorporation of carboxytetramethylrhodamine (TAMRA)-modified phenylalanine derivatives in cell-free translation systems.<sup>15, 16</sup> The changes in fluorescence spectra are attributed to the phenomenon of photoinduced electron transfer (PET), in which emission from TAMRA-labelled antibody fragments in the native state compete with electron transfer interactions with Trp residues in close proximity, leading to quenching of TAMRA emission intensity. Recently, these constructs have been improved by the incorporation of donor and acceptor dyes to produce ratiometric FRET sensors.<sup>17,18</sup> In some instances, a small ~5 nm blue-shift was also observed; however, the cause of this shift was not investigated. Wavelength-dependent or ratiometric sensors are preferable in the case of biological samples (*e.g.* blood, tissue), because they are significantly less affected by instrument and biological noise.<sup>19, 20</sup>

In this study, we have incorporated an environmentally sensitive fluorescent UAA 3-(6-acetylnaphthalen-2-ylamino)-2-aminopropanoic acid, Anap, a derivative of the established membrane probe, Prodan) into the CDRH2 region of an anti-EGFR scFv (variable heavy and light chains cloned from Panitumumab, Vectibix, see Supplementary Information for details) where it shows target-dependent changes in both fluorescence intensity and peak emission wavelength. By modelling an scFv based upon an X-ray crystal structure of an anti-EGFR Fab, six mutation sites were chosen for Anap incorporation. Mutation in close proximity to the EGFR binding site generated dose-dependent changes in fluorescence emission spectra in the presence of the specific antigen, with minimal effects on stability or binding

kinetics. Our results suggest that proteins in human plasma-containing solutions can be quantified in a single step, without washing, and at nanomolar detection limits.

## Experimental Section

**Materials:** Anap-TFA (AsisChem Inc); pAnap (Addgene); Culture flask (Corning); polyethylenimine (PEI 25000, Polysciences); D-glucose (Merck); 12% Tris gel (Invitrogen); Seeblue plus2 protein standard (ThermoFisher Scientific); GelCode blue stain reagent (ThermoFisher Scientific); Gel apparatus (Life Technology); ECL solution (ThermoFisher Scientific); acetone (Merck); acetonitrile (Sigma Aldrich); ethanol (ThermoFisher); methanol (Merck), DMSO (Merck); PBS (Gibco, Invitrogen); Expi293 cells (ThermoFisher Scientific); Expi293 expression media (ThermoFisher Scientific); GlutaMAX (ThermoFisher Scientific); filter (0.22  $\mu\text{m}$ –0.45  $\mu\text{m}$ , Pall Inc.); Protein L column (GE Healthcare); HisTrap Excel column (GE Healthcare); HiPrep 26/10 desalting column (GE Healthcare); HiTrap Protein A column (GE Healthcare); anti-His-IgG (MACS Miltenyi Biotech), Gel filtration standard (BioRad), TSKgel 3000SWXL HPLC-SEC column (Tosoh Bioscience), Prometheus NT.48 nanoDSF instrument (Nanotemper), Zetasizer Z (Malvern Panalytical).

**SDS-PAGE gel electrophoresis:** 5  $\mu\text{L}$  of LDS loading dye (NuPAGE, ThermoFisher Scientific) was added to 20  $\mu\text{L}$  of purified protein. Samples were heated at 98°C for 5 minutes before loading into 12% pre-cast gel. The gel was visualised in UVP Biospectrum gel imager for fluorescence detection at 365 nm. Gels were stained overnight with GelCode blue staining reagent and destained vigorously in MilliQ water for coomassie imaging.

**Western blot analysis:** 10  $\mu$ L of culture sample was loaded into SDS PAGE gel and run for 1 hour at 100 V followed by transfer to PVDF membrane using standard Western blotting procedure. The membrane was blocked in PBS containing 5% skim milk followed by incubation with 1:5000 anti-His-IgG-HRP antibody. ECL solution was added as per manufacturer protocol and visualised in UVTech chemiluminescence imager.

**Indirect ELISA for testing functionality of anti-EGFR scFv:** EGFR (15  $\mu$ g/mL) was coated in triplicates in 96 well plates (Nunc flat bottom, Maxisorp) and incubated overnight at 4°C. Additionally VEGFR and fibrinogen were coated at 10  $\mu$ g/mL as negative controls. Plates were blocked with 200  $\mu$ L of 2% skim milk diluent (1 $\times$  in PBST) for one hour at room temperature. Purified anti-EGFR WT scFv and Anap mutants were added at concentration of 10  $\mu$ g/mL. After 2 hours incubation, the wells were vigorously washed six times with PBST (1 $\times$  PBS, 0.05% Tween 20). HRP labelled anti-His antibody was diluted into blocker solution (1:5000) and added 100  $\mu$ L to each well. After 60 minutes incubation, the anti-His antibody was decanted and washed six times with PBST. 100  $\mu$ L of 3,3',5,5'-tetramethylbenzidine (TMB, Thermo Fisher Scientific) was added to each well followed by 10 minutes incubation for adequate colour development. The reaction was stopped by adding 2 M hydrochloric acid. The colorimetric reaction was analysed by recording absorbance at 450 nm in a Multiskan Microplate Spectrophotometer (ThermoFisher Scientific). Data were plotted and analysed in GraphPad Prism 7.05.

**Steady-state fluorescence measurements:** Emission spectra of Anap in polar solvents (acetone, acetonitrile, ethanol, methanol, and DMSO; spectroscopy or HPLC grade used as received) were collected on a Varian model Cary Eclipse

fluorescence spectrophotometer with intensity corrected for detector efficiency. Quantum yields were determined using the comparative method (Eqn 1) with quinine sulphate as a reference (QY = 0.55 in water and acid).<sup>21</sup> All solutions were degassed by bubbling with nitrogen for 15 minutes immediately prior to measurement.

$$\varphi_x = \varphi_{ref} \frac{A_x}{A_{ref}} \cdot \frac{n_x^2}{n_{ref}^2} \cdot \frac{(1-10^{-abs_{ref}})}{(1-10^{-abs_x})} \quad \text{Eqn 1}$$

Where  $A$  is the area under the emission spectrum,  $n$  is the refractive index,  $abs$  is the absorbance of the excitation wavelength,  $ref$  indicates the reference sample and  $x$  is the sample under investigation.

The fluorescence of anti-EGFR scFv mutants was measured in 96 well plate (Costar, black bottom) format using a Tecan Infinite 200Pro fluorescence plate reader. 150  $\mu$ L of 10 nM N-term, H53Y and 100 nM of C-term mutant in PBS buffer was added to each well and 100  $\mu$ L of target ligand, EGFR, was added to wells with concentration ranging from 0 nM to 200 nM. Emission spectra were recorded between 400 nm to 550 nm, using 365nm excitation. Experiments were run in triplicate for statistical analysis. Unless otherwise specified, all data were collected in triplicate, plotted in GraphPad Prism 7.05, with resultant plots displaying either representative spectra or means plus/minus standard deviations. Binding curves were generated by fitting Lorentzian functions to individual steady-state spectra, extracting the average peak emission wavelength and standard errors, then fitting a 4-parameter logistic (4PL) curve through the data points, ensuring that all resultant  $R^2$  values were greater than 98%.

## Results and Discussion:

### Expression and characterisation of UAA-mutated anti-EGFR scFv constructs

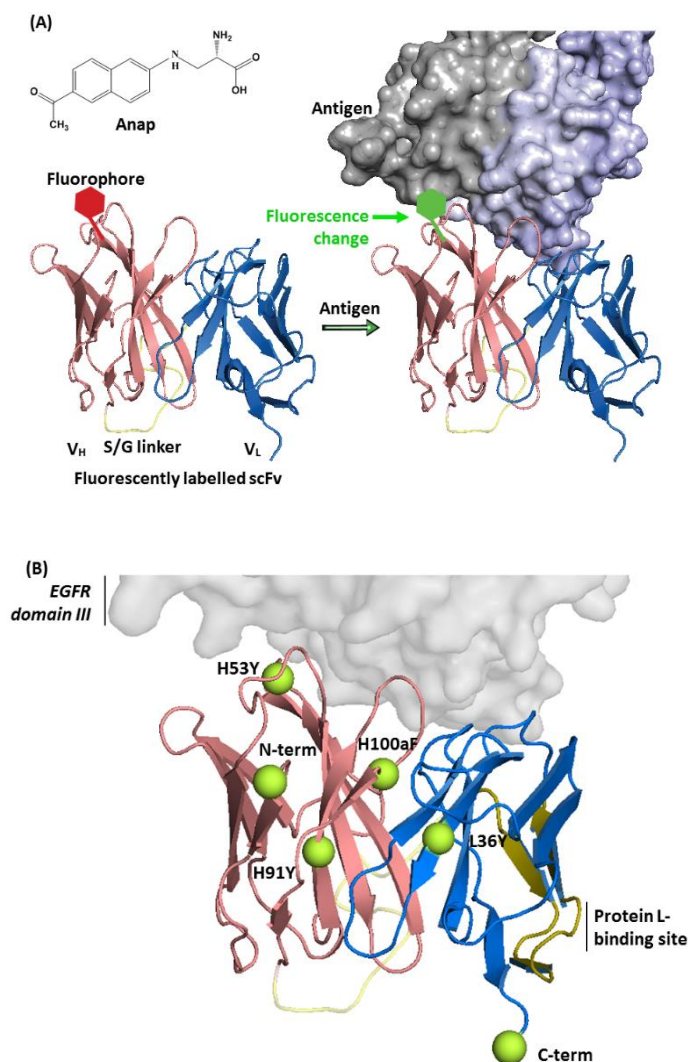


Figure 1: (A) Schematic diagram of an emission wavelength-dependent fluorescent immunosensor: an scFv antibody fragment (V<sub>H</sub> domain in pink, V<sub>L</sub> domain in blue, Serine-Glycine linker [S<sub>4</sub>(GGGG)<sub>3</sub> as transparent yellow) displays a polarity-dependent fluorophore (red hexagon). Selective binding to the target antigen (grey surface) changes the environment of the fluorophore (green hexagon; with chemical structure displayed in inset) resulting in a distinctly different emission spectrum. (B) Within the model anti-EGFR scFv structure (V<sub>H</sub> domain in pink, V<sub>L</sub> domain in blue, S/G linker as yellow transparent, Protein L binding site in gold), sites targeted for mutation to the polarity-dependent fluorophore Anap (lime-coloured spheres) are spread throughout the molecule, with the H53Y mutation close to the binding interface with EGFR domain III (grey transparent surface).

To design a fluorescent immunosensor, we incorporated the fluorescent polarity indicator, Anap, into anti-EGFR scFv by site-specific mutation (Figure 1A). The emission wavelength of Anap varies by >60 nm ( $\sim 3000\text{ cm}^{-1}$ ) across a range of polar solvents (Figure S1A) suggesting that binding events should generate a detectable change in Anap emissionwavelength. Six sites were selected for mutation including four internal (H53Y, H91Y, L36Y, and H100aF) and the N/C terminal sites (Figure 1B, Table S1; detail in SI Materials & Methods). Mutant and wild type (WT) sequences were successfully expressed in mammalian protein expression systems. Following purification with Ni-NTA metal affinity chromatography, these mutants were tested preliminarily for fluorescence modulation in the presence of EGFR ligand and H53Y mutant (Anap incorporated in the CDRH2 loop at Tyr53, Kabat Numbering Scheme) showed a significant wavelength shift in the fluorescence emission spectrum. Thus, H53Y mutant was thoroughly characterised along with the WT, N-term (Anap incorporated at N-terminus of scFv) and C-term (Anap incorporated at C-terminus of scFv) as controls. We observed variable expression level of each mutant; the yield of WT was approximately 3 mg/L, C-term mutant showed expression at about 1.5 mg/L, while N-term and H53Y were expressed at 0.1-0.8 mg/L.

Incorporation of Anap into anti-EGFR scFv mutants was confirmed by SDS-PAGE and Western blotting (WB; Figure 2). Coomassie staining of the SDS-PAGE gels confirmed successful expression of the WT, C-term, N-term and H53Y mutants (Figure 2A), while observation of the gel under UV light showed selective Anap incorporation into the mutants (Figure 2B). Anap incorporation was also confirmed with mass spectrometry (Figure S3), where we observed a difference of 272 Da

increase for the N-term mutant (equivalent to the molecular weight of Anap) and a 91 Da increase for the H53Y mutant (equivalent to the molecular weight difference between Anap and tyrosine). The high efficiency of Anap incorporation is consistent with Chatterjee *et al.*<sup>22</sup> In the case of the C-term mutant, the Anap incorporation was much lower than for the other mutants because the TAG codon was added after the purification tag, hence distinction between labelled and unlabelled protein was not possible by mass spectroscopy. To confirm selective incorporation, we expressed the C-term mutant both with and without Anap and pAnap, showing that fluorescent protein was only produced when both reagents were included (Figure S2). We consider C-term as a useful control, given that it is effectively the mutant with lowest direct Anap incorporation in comparison to the other constructs. Western blot analysis provided further confirmation of expression, with some indication of dimerization which was also visible in the Coomassie staining (Figure 2C). Indirect ELISA analysis of the mutants confirmed that target binding was selective and did not vary significantly across the mutant constructs (Figure 2D).

We observed that each mutant showed emission spectra with distinct peak emission wavelengths, which we attribute to the effects of the unique local environment associated with Anap at each mutated position (Figure 2E). Interestingly, we also observed fluorescence intensity difference among the mutants. Whilst this was expected for the C-term mutant due to low Anap incorporation efficiency, we found significant intensity differences between N-term and H53Y mutants as depicted in Figure 2B and in fluorescence emission spectra (Figure S4). This is consistent with the lower quantum yield of Anap in PBS buffer in comparison to that for Anap incorporated into the scFv construct (Table S2). The N-term site is presumably more

solvent exposed ( $\Phi_{\text{flu}}-0.4$ ) compared to the H53Y site ( $\Phi_{\text{flu}}-0.5$ ), so it is not surprising that N-term could be less bright than H53Y. Theoretically, it is possible that differences in fluorescence intensity could be due to spontaneous read-through of the amber codon, however, this is very unlikely given the thorough characterisation of the pAnap in mammalian cells in prior studies.<sup>22</sup> The peak wavelength for the N- and C-term species was consistent with that of free Anap in PBS buffer (~495 nm), whereas H53Y was blue-shifted to 475 nm, and the H91Y, L36Y, and H100aF mutants also showed distinct blue-shifts in comparison to free Anap, even though they could only be partially purified (Ni-affinity columns). This is likely due to the difference in the polarity the dye experiences in these positions; while the N- and C-termini are highly solvent-exposed sites, the other mutations are at partially buried, and hence more hydrophobic sites.

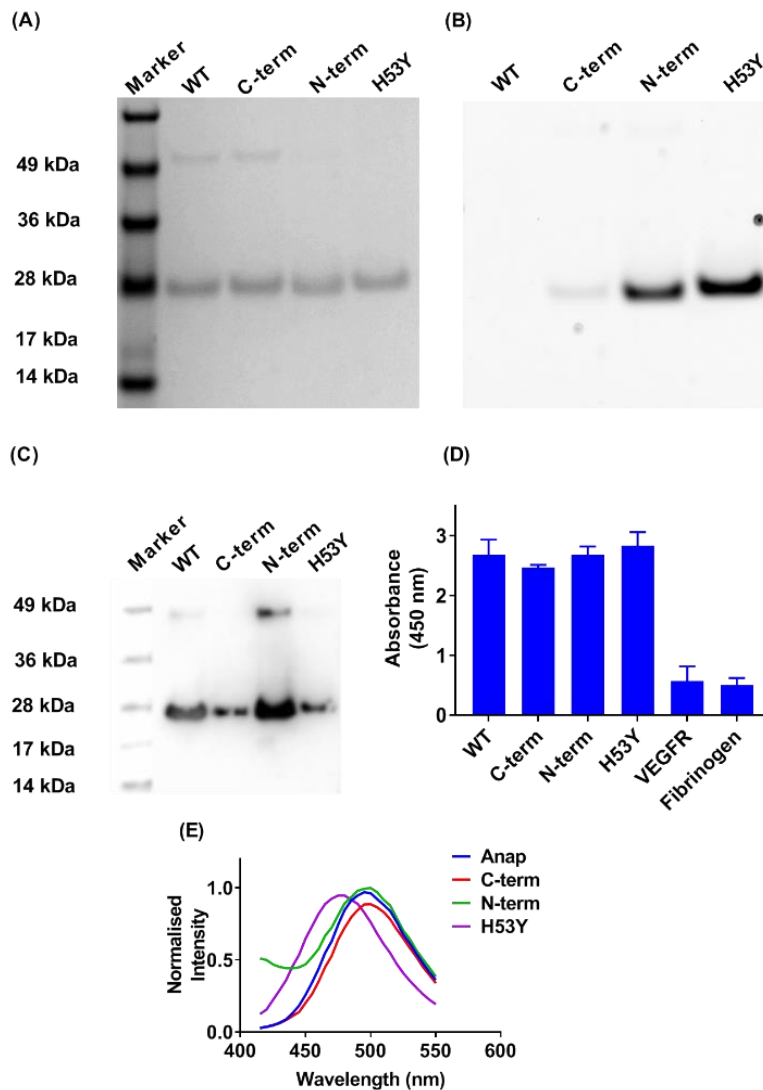


*Figure 2: Confirmation of Anap incorporation into functional anti-EGFR scFv mutants. (A) Coomassie staining shows protein expression and purity of samples, using 30  $\mu\text{g}/\text{mL}$  in each lane. Bands appeared below 28 kDa corresponds to the approximate theoretical molecular weight of Anap mutants (26.3 kDa). Minor dimerization of WT and C-term was also observed ( $> 49$  kDa marker). (B) Fluorescence image of the same gel confirming Anap incorporation. (C) Western blot in which the presence of His-tagged antibody fragments was confirmed using HRP-labelled anti-His-antibody. (D) ELISA showing comparable binding specificity for target antigens. Nonspecific binding was tested by coating wells with VEGFR or fibrinogen instead of EGFR. (E) Fluorescence emission spectra of Anap in different positions in the anti-EGFR scFv.*

We next investigated the effect of the UAA on the structural and functional properties of the fragments. To our knowledge, the effects of UAA mutations on antibody structure/function have not been systematically investigated. Each mutant was analysed by HPLC-SEC chromatography to determine if mutations affected protein aggregation (Figure 3A-D). A mixture of scFv monomers and dimers was observed for the WT, C-term and H53Y constructs, consistent with SDS-PAGE/WB analysis, yet no evidence of aggregation was observed. This was supported by dynamic light scattering (DLS) indications of fragment size, whereby each mutant showed a monodisperse population in the range 4–6 nm (Figure 3E and Figure S5). Interestingly, the N-term mutant non-specifically bound to the size-exclusion column matrix (Figure 3D), so we could not determine its aggregation potential using this approach. Indeed, gel analysis of the same samples suggested only the presence of single bands at the expected molecular weight (Figure 3D inset). Thermal stability tests shown in Figure 3F indicated that unfolding was initiated in a narrow temperature range across the four mutants, although the H53Y mutant appeared to unfold at a slightly lower temperature. Aggregation measurements based on backscatter analysis again indicated a narrow temperature range across the four mutants (Figure 3G), although H53Y and N-term started to aggregate at temperatures ~4–5°C lower than the others. Taken together, these data suggest that Anap mutation resulted in observable yet minor effects on thermal stability and aggregation.

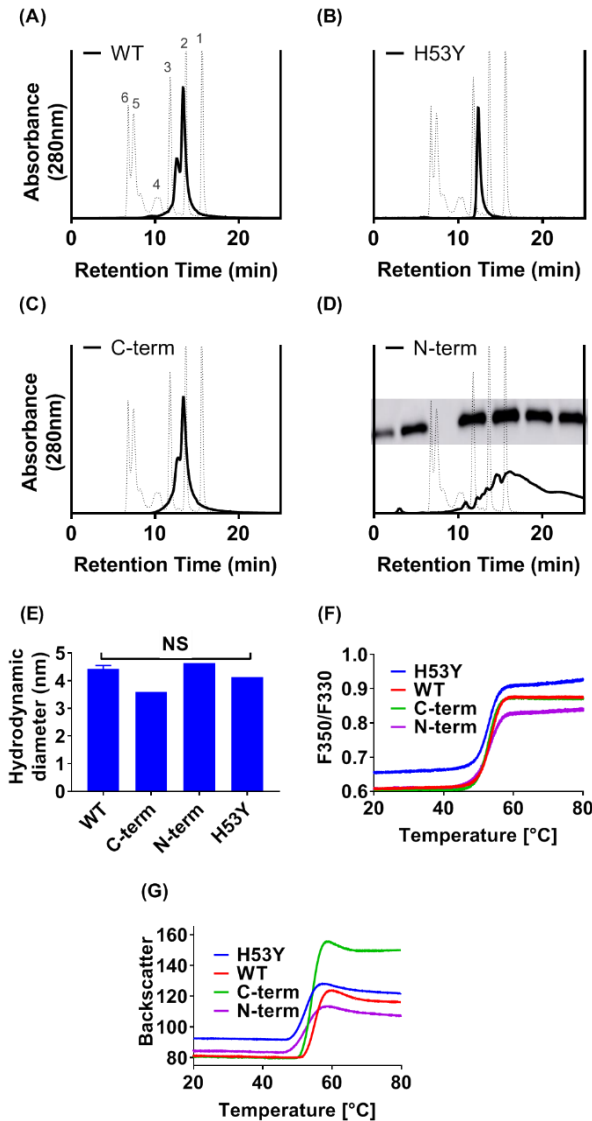


Figure 3: Effect of Anap mutation on structural properties of the anti-EGFR scFv mutants. (A-D) Analytical size exclusion chromatography shows consistent retention times (y-axis is normalised absorbance), however N-term mutant consistently eluted as a broad peak in the low molecular weight range. (D-inset) Presence of the N-terminal mutant was confirmed by immunoblotting indicating unspecific interactions of this mutant with the column matrix. The elution samples of the N-term mutant from the SEC column (collected as seven elution fractions over 20 minutes, bands correspond to each fraction) were analysed in Western blot experiment. Dashed lines represent the molecular weight standard which is described in figure A, 1 – 13.7 kDa, 2 – 17 kDa, 3 – 44 kDa, 5 – 670 kDa, 6 – aggregates. (E) Stability of Anap mutants was further investigated by analysing the size distribution of mutants using DLS and analysing (F) thermal unfolding and (G) aggregation analysis.

Beyond the stability and aggregation potential of the mutant scFvs, it is important to confirm that UAA mutation does not reduce the affinity of the fragment for the target analyte. Interaction analysis was performed to confirm target binding and to quantify the kinetic rate constants and equilibrium dissociation constants for the WT and three mutant constructs ( $k_a$ ,  $k_d$ ,  $K_D$ , respectively). Bio-Layer Interferometry (BLI) data suggest that Anap mutations had minimal effect on the binding and affinity of the scFvs for the target protein (Table 1, Figure S6), given that there is less than 10-fold difference in  $K_D$  values, which is within the error of the method. Furthermore, nanomolar affinities obtained for the mutants are in close agreement with those for WT anti-EGFR scFv and anti-EGFR Fab.<sup>23</sup>

*Table 1: Binding kinetics analysis for Anap mutants*

	$K_D$ (nM)	$k_a$ (M <sup>-1</sup> s <sup>-1</sup> ) × 10 <sup>4</sup>	$k_d$ (s <sup>-1</sup> ) × 10 <sup>-4</sup>
WT	1.6 ± 0.1	9.1 ± 0.1	1.5 ± 0.1
C-term	2.8 ± 0.5	4.8 ± 0.2	1.3 ± 0.2
N-term	1.7 ± 0.4	7.6 ± 0.3	1.3 ± 0.3
H53Y	4.5 ± 0.5	6.7 ± 0.1	3.0 ± 0.1

### **Fluorescence analysis in the presence of the specific antigen**

The fluorescence response of the Anap-labelled scFv mutants in the presence of various concentrations of EGFR was investigated with fibrinogen as a nonspecific protein control. The C-term and N-term mutants did not show any significant fluorescence change in the presence of EGFR target (Figure 4A, B), likely because Anap incorporation sites at the protein termini are highly exposed to the solvent in both bound and unbound states, and hence show minimal change in polarity upon

target binding. The addition of EGFR to H53Y saw blue-shifting of the Anap emission spectrum via the appearance of a new emission peak in the 430 – 470 nm range concomitant with the loss of some intensity at longer wavelengths. An isoemissive point at ~480 nm indicates that the spectral changes are due to two species: H53Y bound with EGFR with an emission maximum of ~460 nm and unbound H53Y at 475 nm. There is also a small increase in total fluorescence emission upon maximum binding of EGFR to H53Y (~1.2 fold) and a maximal intensity difference of ~1.4-fold (46%) at 460 nm (Figure 4C). This is consistent with the behaviour of Anap in polar solvents where a similar blue shift and increase in emission quantum yield is observed on moving from water (PBS) to methanol (Table S2). The blue-shifting of the emission peak observed upon binding to EGFR indicates there is a further decrease in the polarity experienced by Anap, likely due to EGFR reducing Anap's exposure to the solvent.<sup>24</sup> Non-specific proteins (fibrinogen in this case) showed negligible fluorescence modulation, even at very high concentration. A binding curve depicting the fluorescence at the maximum emission wavelength of Anap mutants is shown in Figure 4D, in comparison to that of the N- and C-terminal mutants. Using a typical 4-parameter logistic (4PL) equation, the apparent EC50 or  $K_D$  was ~1 nM, largely consistent with BLI analysis in Table 1. The limit of detection (LOD) was calculated to be ~0.6 nM in PBS buffer (Figure 4D), defined as the lowest concentration with signal higher than 1.65 standard deviations above baseline.<sup>25</sup> The same EGFR titration experiment was also performed in 5% human plasma in order to investigate the effect of blood proteins on the assay detection limit and sensitivity (Figure 4F). The presence of serum proteins did not affect the observed trends in the emission spectra, and the binding curve showed a detection limit of ~3 nM. We attribute the higher detection

limit to fluorescent noise from serum proteins in the spectral range of Anap, which also increased the background fluorescence intensity signals (Figure 4E).

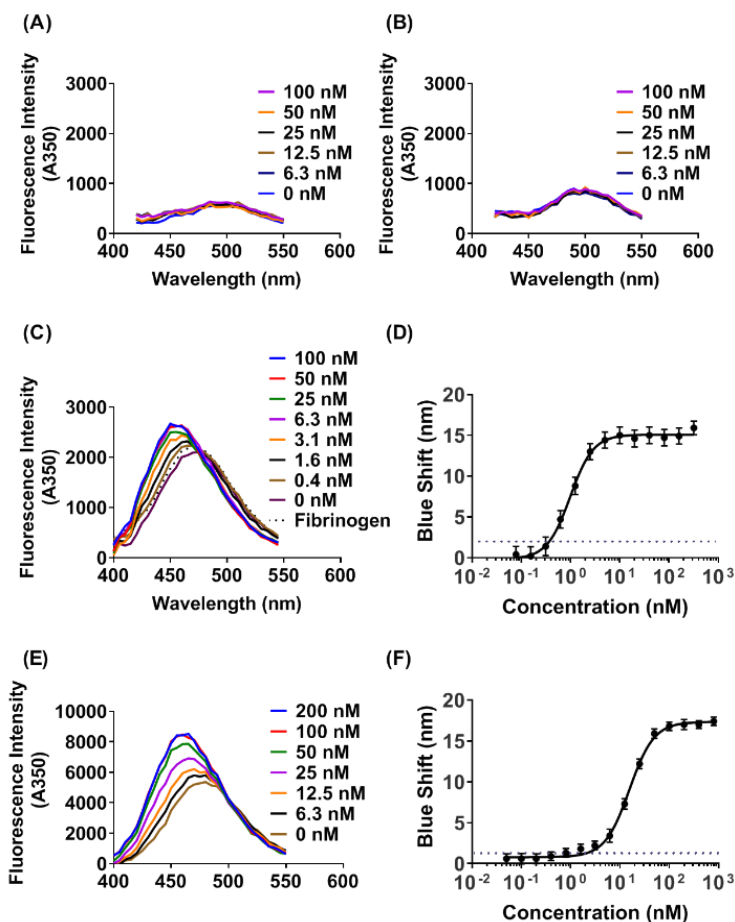


Figure 4: Fluorescence spectra for antibody fragments in PBS [(A) C-term, (B) N-term, (C) H53Y and (E) H53Y with 5% human plasma], in the presence of different EGFR concentrations. In the case of H53Y, binding curves for reactions performed in (D) PBS and (F) PBS + 5% human plasma were constructed based on the difference in peak wavelengths with respect to the negative control.

We undertook time-resolved fluorescence studies of Anap and H53Y to gain further understanding into the polarity and EGFR-dependent changes observed in the steady-state fluorescence spectra of Anap and H53Y. We collected fluorescence

decay histograms of free Anap dissolved in a range of polar solvents from acetone to PBS buffer (Figure S1C, D). Interestingly, Anap displayed bi-exponential lifetimes in all solvents trialled (Table S2), consistent with earlier studies on the related dye, Prodan and other Prodan derivatives.<sup>26, 27</sup> Polarity sensitivity of Prodan emission arises from the molecule exhibiting a significant excited state dipole formed by redistribution of electron density from the amine group to the carbonyl upon photoexcitation. Polar solvents stabilize this excited state leading to a red-shift in emission. Hydrogen bonding in protic solvents has also been shown to contribute to the observed red-shift by enhancing the intramolecular charge transfer.<sup>27, 28</sup> Compared to Prodan, Anap has an additional amino acid functionality (Figure 1A inset) which allows for incorporation into protein, however, this is structurally well-separated from the amine and carbonyl groups and the aromatic core, and thus is not expected to alter the underlying photophysics substantially compared to Prodan. The observed emission maximum wavelengths for Anap are consistent with this, red-shifting substantially with increasing solvent polarity ( $\epsilon_s$ ) and with the protic alcohols showing greater red-shifting than the aprotic, yet more polar solvent, DMSO.

To compare the time-resolved behaviour of Anap in the different solvents we calculated the average lifetime  $\langle\tau\rangle$  from the two decay components using Eqn S1. It can be seen that the average lifetime initially increases from buffer to the less polar solvents ethanol and methanol before decreasing with further reduction in solvent polarity. This is broadly in line with the trend in quantum yield which also peaks in the alcohols. Anap incorporated into H53Y also revealed a bi-exponential

fluorescence decay (Figure S1D) with a small increase in  $\langle\tau\rangle$  which, with the observed blue-shift in emission, confirms that Anap experiences a marginally less polar environment in H53Y than in buffer alone. Binding with EGFR leads to a further increase in  $\langle\tau\rangle$  with Anap now experiencing an environment with a decreased polarity similar to Anap in ethanol or DMSO. Interestingly, while H53Y contains a Trp residue in close proximity, there is no evidence of PET quenching to any meaningful extent. This suggests that the fluorescence changes observed in Anap incorporated into H53Y are based solely on polarity-dependent changes in the fluorescence spectra.

While a range of biosensing platforms have been developed, reagentless immunosensors that use affinity-based interactions to detect proteins using a variety of simple fluorescent methods have not yet been extensively investigated. We endeavoured to develop an immunosensor that would allow for rapid detection of proteins in biological environments, by generating fluorescently labelled engineered antibody fragments that undergo polarity/structural-dependent spectral shifts upon analyte binding. Incorporation of Anap at residue H53Y in anti-EGFR showed significant dose-dependent emission shift ( $\sim 15$  nm) and modest fluorescence intensity enhancement. We were able to detect low concentrations of target antigen in a range of 0.5–5 nM in buffer and diluted human plasma, which is comparable to secreted EGFR levels collected from the blood of lung, breast and ovarian cancer patients.<sup>29</sup> Beyond EGFR, other clinically relevant blood-based biomarkers in this range include C-reactive protein, haptoglobin, and a range of complement proteins.<sup>30</sup> Interestingly, the N- and C-terminal mutants showed no changes in

fluorescence emission spectra, which suggests that these locations might be useful for other applications, such as imaging, to create fluorescence antibody conjugates with stable emission profiles.<sup>22</sup> At this stage, screening of multiple constructs is required to identify optically-responsive mutants, however, in the future we suggest that it may be possible to identify specific residues based either on sequence or 3D structures that could be applied across a range of antibodies or antibody-like scaffolds, for detection of different targets.

Renard *et al.* previously reported “knowledge-based” design of fluorescent reagentless biosensors by introducing cysteine mutations and labelling resultant scFvs with maleimide-functionalised dyes.<sup>13, 31</sup> Even though they were able to optimise a mild reaction condition for efficient labelling, it required significant optimisation for each unique antibody fragment in order to achieve highly efficient labelling to the free cysteine while maintaining the critical intramolecular disulfides. Our results are largely consistent with Renard *et al.*'s findings in that the H53Y mutant, which showed the clearest target-dependent changes in emission spectra, was also within the CDR2 of the V<sub>H</sub> domain and likely interacting directly with the incoming target protein. This is in contrast to the solvent-exposed sites at the termini, which yielded negligible fluorescence changes upon binding of EGFR. A key advantage therefore of UAA mutation in this context is that as long as functional and stable mutants are produced, there is no post-labelling step required, and hence the requirement for the permissive site to be solvent exposed can be relaxed. This may open up a wider range of dyes that utilize different photophysical mechanisms. Furthermore, the labelling efficiency is 100% for intermolecular amber codons, in cases where truncated products can be easily distinguished from full-length products.

Ueda and colleagues have developed the “Qbody” platform in which scFv constructs are genetically modified with TAMRA dyes in cell-free translation systems, most commonly at the N-terminus, C-terminus, or within the serine/glycine linker. This group has applied Qbodies in a range of sensor applications including detection of antibiotics, drugs and recently in imaging<sup>32</sup> and have demonstrated variations based on different antibody fragments (*e.g.* Fab)<sup>15</sup> and incorporation of multiple dyes for ratiometric sensing.<sup>17,33</sup> Our approach has some unique differences based on the point mutation approach and the photophysical mechanisms involved. Firstly, by avoiding the 12-aa ProX tag (used to increase expression yield in cell-free systems), we can use point mutations at any internal permissive site, expanding the range of possible locations for fluorophore incorporation. Secondly, while the PET-quenching mechanism involving TAMRA relies on the presence of nearby tryptophan residues, we observed no evidence of PET quenching in H53Y (despite the close proximity of Trp residue), hence the spectral response is dependent solely on the Anap location and polarity changes. Thirdly, for biosensing in complex biological systems, it is likely that fluorescence intensity changes will not be sufficient for calibration between samples. In using polarity indicator dyes, it is possible to rely on the wavelength shift to construct calibration binding curves without the need for incorporation of multiple fluorophores, and others have shown that at least in the NIR spectrum, extremely small wavelength shifts (~1–2 nm) are reliably detected in pre-clinical animal studies *in vivo*.<sup>34</sup>

## **Conclusion:**

Reagentless immunosensors that can detect proteins via an affinity-based fluorescence change are a useful, yet underdeveloped diagnostic tool. We developed a sparse library of anti-EGFR scFv fluorescent immunosensors by incorporating the

UAA Anap at selected locations in the scaffold informed by rational, structure-based design principles. We found that incorporation of Anap in close proximity to the binding sites could generate dose-dependent emission wavelength shifts in the presence of the specific antigen down to nanomolar range concentrations in solution and in the presence of human plasma. We identified fluorophore incorporation sites, confirming the generality and applicability of this system to the antibody scaffold. As a proof of principle, incorporation of fluorescent UAAs in an scFv scaffold could potentially be applied to other antibody fragments for detecting a wide range of protein biomarkers and across a wide range of existing and emerging technology platforms.

### **Acknowledgements:**

The authors would like to acknowledge funding from the Australian Research Council's Centre of Excellence in BioNano Science (CE140100036) and Monash University's Interdisciplinary Research Fund. We also acknowledge technical support from Dr Trent Ashton at Monash University's School of Chemistry, Dr Noelene Quinsey at Monash University's Protein Production Unit and Dr David Steer from Monash University's Proteomics Platform.

### **Supporting Information:**

Supporting information is available free of charge via the Internet at <https://pubs.acs.org/journal/ancham>. Included is additional experimental methods along with supporting data - gel images, life-time analysis, ESI-MS analysis, BLI and DLS data.

## References:

1. Engvall, E.; Perlmann, P., enzyme-linked immunosorbent assay (ELISA) quantitative assay of immunoglobulin-g. *Immunochemistry* **1971**, 8 (9), 871- 874.
2. Corrie, S. R.; Plebanski, M., The emerging role of nanomaterials in immunological sensing - a brief review. *Mol. Immunol.* **2018**, 98, 28-35.
3. Han, X.; Li, S. H.; Peng, Z. L.; Othman, A. M.; Leblanc, R., Recent Development of Cardiac Troponin I Detection. *ACS Sens.* **2016**, 1 (2), 106-114.
4. Ferrara, F.; Listwan, P.; Waldo, G. S.; Bradbury, A. R. M., Fluorescent Labeling of Antibody Fragments Using Split GFP. *PLoS One* **2011**, 6 (10):e25727.
5. Ismail, N. F.; Lim, T. S., Site-specific scfv labelling with invertase via Sortase A mechanism as a platform for antibody-antigen detection using the personal glucose meter. *Sci. Rep.* **2016**, 6: 19338.
6. Toseland, C. P., Fluorescent labeling and modification of proteins. *J Chem Biol* **2013**, 6 (3), 85-95.
7. Liu, J. Q.; Hanne, J.; Britton, B. M.; Shoffner, M.; Albers, A. E.; Bennett, J.; Zatezalo, R.; Barfield, R.; Rabuka, D.; Lee, J. B.; Fishel, R., An Efficient Site-Specific Method for Irreversible Covalent Labeling of Proteins with a Fluorophore. *Sci Rep.* **2015**, 5: 16883.
8. Wang, L.; Brock, A.; Herberich, B.; Schultz, P. G., Expanding the genetic code of Escherichia coli. *Science* **2001**, 292 (5516), 498-500.
9. Lang, K.; Chin, J. W., Cellular Incorporation of Unnatural Amino Acids and Bioorthogonal Labeling of Proteins. *Chem. Rev.* **2014**, 114 (9), 4764-4806.
10. Kim, C. H.; Axup, J. Y.; Schultz, P. G., Protein conjugation with genetically encoded unnatural amino acids. *Curr. Opin. Chem. Biol.* **2013**, 17 (3), 412-419.
11. Kim, C. H.; Axup, J. Y.; Dubrovskaya, A.; Kazane, S. A.; Hutchins, B. A.; Wold, E. D.; Smider, V. V.; Schultz, P. G., Synthesis of Bispecific Antibodies using Genetically Encoded Unnatural Amino Acids. *J. Am. Chem. Soc.* **2012**, 134 (24), 9918-9921.
12. Axup, J. Y.; Bajjuri, K. M.; Ritland, M.; Hutchins, B. M.; Kim, C. H.; Kazane, S. A.; Halder, R.; Forsyth, J. S.; Santidrian, A. F.; Stafin, K.; Lu, Y. C.; Tran, H.; Seller, A. J.; Biroce, S. L.; Szydluk, A.; Pinkstaff, J. K.; Tian, F.; Sinha, S. C.; Felding-Habermann, B.; Smider, V. V.; Schultz, P. G., Synthesis of site-specific antibody-drug conjugates using unnatural amino acids. *Proc. Natl. Acad. Sci. U. S. A.* **2012**, 109 (40), 16101-16106.
13. Renard, M.; Belkadi, L.; Hugo, N.; England, P.; Altschuh, D.; Bedouelle, H., Knowledge-based design of reagentless fluorescent biosensors from recombinant antibodies. *J. Mol. Biol.* **2002**, 318 (2), 429-442.
14. Brient-Litzler, E.; Pluckthun, A.; Bedouelle, H., Knowledge-based design of reagentless fluorescent biosensors from a designed ankyrin repeat protein. *Protein Eng., Des. Sel.* **2010**, 23 (4), 229-241.
15. Abe, R.; Jeong, H. J.; Arakawa, D.; Dong, J. H.; Ohashi, H.; Kaigome, R.; Saiki, F.; Yamane, K.; Takagi, H.; Ueda, H., Ultra Q-bodies: quench-based antibody probes that utilize dye-dye interactions with enhanced antigen-dependent fluorescence. *Sci. Rep.* **2014**, 4: 4640.

16. Abe, R.; Ohashi, H.; Iijima, I.; Ihara, M.; Takagi, H.; Hohsaka, T.; Ueda, H., "Quenchbodies": Quench-Based Antibody Probes That Show Antigen-Dependent Fluorescence. *J. Am. Chem. Soc.* **2011**, 133 (43), 17386-17394.
17. Jeong, H. J.; Ohmuro-Matsuyama, Y.; Ohashi, H.; Ohsawa, F.; Tatsu, Y.; Inagaki, M.; Ueda, H., Detection of vimentin serine phosphorylation by multicolor Quenchbodies. *Biosens. Bioelectron.* **2013**, 40 (1), 17-23.
18. Chung, C. I.; Makino, R.; Dong, J. H.; Ueda, H., Open Flower Fluoroimmunoassay: A General Method To Make Fluorescent Protein-Based Immunosensor Probes. *Anal. Chem.* **2015**, 87 (6), 3513-3519.
19. Tsien, R. Y.; Poenie, M., fluorescence ratio imaging - a new window into intracellular ionic signaling. *Trends Biochem. Sci.* **1986**, 11 (11), 450-455.
20. Lakowicz, J. R., Principles of fluorescence spectroscopy. 3rd edition ed.; *Springer: New York* **2006**.
21. Melhuish, w. H., quantum efficiencies of fluorescence of organic substances - effect of solvent and concentration of fluorescent solute. *J. Phys. Chem.* **1961**, 65 (2), 229-235.
22. Chatterjee, A.; Guo, J. T.; Lee, H. S.; Schultz, P. G., A Genetically Encoded Fluorescent Probe in Mammalian Cells. *J. Am. Chem. Soc.* **2013**, 135 (34), 12540-12543.
23. Sickmier, E. A.; Kurzeja, R. J. M.; Michelsen, K.; Vazir, M.; Yang, E.; Tasker, A. S., The Panitumumab EGFR Complex Reveals a Binding Mechanism That Overcomes Cetuximab Induced Resistance. *PLoS One* **2016**, 11 (9): e0163366.
24. Lee, H. S.; Guo, J. T.; Lemke, E. A.; Dimla, R. D.; Schultz, P. G., Genetic Incorporation of a Small, Environmentally Sensitive, Fluorescent Probe into Proteins in *Saccharomyces cerevisiae*. *J. Am. Chem. Soc.* **2009**, 131 (36), 12921- 12923.
25. Allegrini, F.; Olivieri, A. C., IUPAC-Consistent Approach to the Limit of Detection in Partial Least-Squares Calibration. *Anal. Chem.* **2014**, 86 (15), 7858-7866.
26. Pospisil, P.; Luxem, K. E.; Ener, M.; Sykora, J.; Kocabova, J.; Gray, H. B.; Vlcek, A.; Hof, M., Fluorescence Quenching of (Dimethylamino)naphthalene Dyes Badan and Prodan by Tryptophan in Cytochromes P450 and Micelles. *J. Phys. Chem. B* **2014**, 118 (34), 10085-10091.
27. Gonzalez-Jimenez, J.; Cortijo, M., Resonance energy transfer between tryptophan-214 in human serum albumin and acrylodan, prodan, and promen. *Protein J.* **2004**, 23 (5), 351-355.
28. Yang, Y. G.; Li, D. L.; Li, C. Z.; Liu, Y. F.; Jiang, K., Hydrogen bond strengthening induces fluorescence quenching of PRODAN derivative by turning on twisted intramolecular charge transfer. *Spectrochim. Acta, Part A* **2017**, 187, 68-74.
29. Maramotti, S.; Paci, M.; Manzotti, G.; Rapticetta, C.; Gugnoni, M.; Galeone, C.; Cesario, A.; Lococo, F., Soluble Epidermal Growth Factor Receptors (segfrs) in Cancer: Biological Aspects and Clinical Relevance. *Int J Mol Sci.* **2016**, 17 (4), e593.
30. Anderson, N. L.; Anderson, N. G., The Human Plasma Proteome: History, Character, and Diagnostic Prospects. *Mol. Cell. Proteomics* **2002**, 1 (11), 845-867.
31. Renard, M.; Bedouelle, H., Improving the sensitivity and dynamic range of reagentless fluorescent immunosensors by knowledge-based design. *Biochemistry* **2004**, 43 (49), 15453-15462.

32. Nhat, K. P. H.; Watanabe, T.; Yoshikoshi, K.; Hoshaka, T., Antibody-based fluorescent and fluorescent ratiometric indicators for detection of phosphotyrosine. *J. Biosci. Bioeng.* **2016**, 122 (2), 146-154.
33. Ohashi, H.; Matsumoto, T.; Jeong, H. J.; Dong, J. H.; Abe, R.; Ueda, H., Insight into the Working Mechanism of Quenchbody: Transition of the Dye around Antibody Variable Region That Fluoresces upon Antigen Binding. *Bioconjugate Chem.* **2016**, 27 (10), 2248-2253.
34. Williams, R. M.; Lee, C.; Galassi, T. V.; Harvey, J. D.; Leicher, R.; Sirenko, M.; Dorso, M. A.; Shah, J.; Olvera, N.; Dao, F.; Levine, D. A.; Heller, D. A., Noninvasive ovarian cancer biomarker detection via an optical nanosensor implant. *Sci. Adv.* **2018**, 4 (4): eaaq1090.

## 4.2 Supporting data

### Supporting information for

#### **Wavelength-dependent fluorescent immunosensors via incorporation of polarity indicators near the binding interface of antibody fragments**

**Jiaul Islam**<sup>1, 2</sup>, Blake T Riley<sup>4</sup>, Christian Fercher<sup>1,3</sup>, Martina L Jones<sup>2,3</sup>, Ashley M Buckle<sup>4</sup>, Christopher B Howard<sup>2,3</sup>, Rosalind P Cox<sup>5</sup>, Toby D M Bell<sup>5</sup>, Stephen Mahler<sup>2,3</sup>, Simon R Corrie<sup>1, 2\*</sup>

<sup>1</sup>*Department of Chemical Engineering, Monash University, Clayton, Australia, ARC Centre of Excellence in Convergent BioNano Science and Technology*

<sup>2</sup>*Australian Institute for Bioengineering and Nanotechnology (AIBN), The University of Queensland, St Lucia, Australia*

<sup>3</sup>*ARC Training Centre for Biopharmaceutical Innovation, Australian Institute for Bioengineering and Nanotechnology (AIBN), The University of Queensland, St Lucia, Australia*

<sup>4</sup>*Dept. of Biochemistry and Molecular Biology, Biomedicine Discovery Institute, Monash University, Clayton, Australia*

<sup>5</sup>*School of Chemistry, Monash University, Clayton, Victoria, Australia*

*\*Corresponding Author: Simon.Corrie@monash.edu, Phone: +61 03 9905 9621*

#### **Table of contents:**

---

Supplemental Experimental Section	S-2
Table S1. Amino acid sequence of each mutant	S-4
Table S2: Summary of steady-state and time-resolved emission properties of Anap in a range of polar solvents	S-5
Figure S1. Steady state and time-resolved fluorescence analysis of Anap in a solvent series or incorporated into H53Y.	S-5
Figure S2. Confirmation of Anap incorporation selectively in response to TAG codon in the presence of Anap and panap plasmid.	S-6
Figure S3. ESI-MS analysis.	S-6
Figure S4. Fluorescence measurement of N-term and H53Y mutants from 50 nM concentrations	S-7
Figure S5. Correlation functions of Anap mutants	S-7
Figure S6. Binding kinetics of Anap mutants	S-8

## **Supplemental Experimental Section:**

***Cloning of anti-EGFR scFv:*** A bispecific antibody containing the sequence of anti-EGFR gene was previously cloned into mammalian expression vectors by Howard et al.<sup>1</sup> The sequence of anti-EGFR scFv gene was PCR amplified (Phusion® high fidelity DNA polymerase, NEB Inc.) and cloned into pCDNA3.1 (+) vector (Invitrogen) using AgeI and XbaI restriction sites. We have modified the gene by introducing TAG codon at the N- and C- terminus while designing the forward and reverse primer (N-term forward primer ACCGGTGTCCATTCTAGCAGCTCCAGCTGCAGGAATC; C-term reverse primer TCTAGATTACTACTTGATTTCCACCTTGGTGCC). The other mutants were synthesised and cloned into the same vector by GenScript. The sequences of all mutants were verified by DNA sequencing. The amino acid sequence of each mutant is shown in Table S1.

***Expression and purification of anti-EGFR scFv mutants and EGFR-Fc protein:*** TAG mutated anti-EGFR scFvs were expressed in Expi293F™ cells by co-transfecting with pAnap (3:1) by following a similar approach described previously.<sup>2</sup> About 30–50 µM of Anap-TFA were added after 4–6 hours to the post-transfection culture. The culture media was supplemented with 33 mM glucose and 2 mM GlutaMAX following 24 hours and 72 hours of post-transfection period. Cells were harvested after 7 days by centrifugation at 1200× g for 10 minutes. The supernatants were filtered through a 0.22 µm filter before loaded onto purification column. A HisTrap Excel column (GE Healthcare) was connected to AKTA Chromatography System (AKTA Start, GE Healthcare), equilibrated with 1× PBS buffer (pH 7.4). Filtered supernatant was loaded onto the column followed by washing with 1× PBS (3 column volume). Proteins were eluted by loading 500 mM imidazole (pH 7.4) and buffer exchanged to 1× PBS buffer (pH 7.4) by using a HiPrep 26/10 desalting column. Further purification

was carried out by using Protein L affinity (GE Healthcare) column to remove non-specifically bound contaminant protein from Ni-NTA affinity purification step. The column was equilibrated with 1× PBS buffer (pH 7.4), protein sample from previous purification step was loaded, and eluted with 0.1 M Glycine (pH 3.0). Proteins were immediately buffer exchanged to 1× PBS buffer (pH 7.4) by using a HiPrep 26/10 desalting column prior to further characterization. The recombinant extracellular domain of EGFR protein (Met 1 – Gly 645), tagged with Fc fragment (EGFR-Fc), was also expressed in mammalian cells similarly as described by Timothy et al.<sup>3</sup> Briefly, pCDNA 3.1 (+) vector containing the sequence for EGFR-Fc was transfected into Expi293F™ HEK cells following the above transfection and culture condition. After 7 days of expression, proteins were purified from culture supernatant by using HiTrap Protein A column followed by buffer exchanged to PBS (pH 7.4).

***Building model structure and site selection for Anap incorporation:*** To design a sparse panel of fluorescent immunosensors, we used rational design principles to select sites in anti-EGFR scFv for incorporation of a fluorescent unnatural amino acid. As the anti-EGFR scFv is a V<sub>H</sub>-V<sub>L</sub> construct with identical variable domains to the anti-EGFR Fab panitumumab, we used the X-ray crystal structure of panitumumab in complex with EGFR domain III (PDB ID: 5SX4, chains H, L, N)<sup>4</sup> to select appropriate sites which could accommodate replacement by Anap. The following criteria were used to filter sites: (1) solvent accessibility of the sites are critical for either post-expression labelling or polarity difference upon target binding, therefore we focused on some CDR adjacent sites that may have variable exposure (highly, partial and less accessible) to solvents; (2) only the aromatic amino acids Phe, Tyr, and Trp were considered for mutation due to their structural similarity with Anap (Fig 1A), to minimise disruption to the residue's local environment; (3) only those residues

within 6 Å of a Trp were considered, because Trp-based quenching has previously been observed with related Prodan dyes, which might provide additional binding-induced spectral changes.<sup>5</sup> We used FoldX<sup>6</sup> to predict potential energetic penalties to protein folding using the scFv model. FoldX calculates an expected change to the Gibbs free energy of folding ( $\Delta\Delta G_f$ ) caused by a mutation, testing multiple conformations of the introduced residue, as well as alternate conformations of surrounding residues. As FoldX can only model the standard 20 amino acids, we assessed the effect of mutations to Anap by using Trp as a proxy for Anap. Since Anap is bulkier than a Trp sidechain, the calculated FoldX  $\Delta\Delta G_f$  were used conservatively, only to eliminate highly destabilising mutants (where FoldX predicted a  $\Delta\Delta G_f > 8$  kcal/mol). This set of criteria suggested a single suitable position for the mutation (H53Y). To expand our panel, we relaxed the selection criteria and included N- and C- termini, as well as additional sites at H91Y, L36Y, and H100AF.

***Intact mass analysis by ESI-MS:*** Protein samples were analysed by LC-MS using a quadrupole TOF mass spectrometer (MicroTOFq, Bruker Daltonics, Bremen, Germany) coupled online with a 1200 series capillary HPLC (Agilent Technologies, Santa Clara, CA, USA). Samples injected onto a MabPac SEC-1 5 µm 300 A 50×4 mm (ThermoScientific) column with 50% Acetonitrile 0.05% TFA, 0.05% FA at a flow rate of 50ul/minute. The proteins were eluted over a 20-minute run-time. The eluent was nebulised and ionised using the Bruker electrospray source with a capillary voltage of 4500 V dry gas at 180°C, flow rate of 4 L/minute and nebuliser gas pressure at 300 mbar. After 20 minutes the flow path was switched to infuse Low Concentration Tune Mix (Agilent Technologies, Santa Clara, CA, USA) to calibrate the spectrum post-acquisition. The spectra were extracted and deconvoluted using Data Explorer software version 3.4 build 192 (Bruker Daltonics, Bremen, Germany).

**HPLC-size exclusion chromatography:** For analytical purposes, 50  $\mu$ L of purified proteins with a concentration of 0.5 mg/mL were applied on a pre-packed TSKgel 3000SW<sub>XL</sub> column. The column was run with a constant flow rate of 0.8 mL/min with PBS + 200 mM NaCl (pH 7.3) as the mobile phase. A gel filtration standard (670/158/44/17/1.35 kDa) was used to calculate the apparent molecular weight of the eluting fractions.

**Thermal stability measurement:** Melting temperatures ( $T_m$ ) of the purified proteins were determined by nano-Differential Scanning Fluorimetry measuring Trp and Tyr fluorescence at 350 and 330 nm, respectively. Samples at 0.5–0.7 mg/mL in PBS (pH 7.4) were measured in triplicates using standard glass capillaries between 20°C and 95°C. The nano-DSF instrument was also equipped with a light-backscattering detector to assess the onset of protein aggregation. Data were analysed using Nanotemper software and plotted in GraphPad Prism 7.05.

**Dynamic Light Scattering (DLS) Measurement:** DLS measurement was performed in Zetasizer (Nano ZS, Malvern) using 100  $\mu$ L of each sample in clear cuvettes. For each Anap mutants and WT, we collected data based on 3 sets of 10 measurements from clean and unaggregated samples. All samples showed reproducible and high-quality correlation curves, and hence particle size was determined based on the number distribution, with data plotted in GraphPad Prism 7.05.

**Bio-Layer Interferometry (BLI):** BLI was performed in BLITZ (an octet family platform, ForteBio, Pall Inc.) as per manufacturer guidelines. In general, Anap mutants (10 nM) were loaded onto Ni-NTA biosensor and exposed to a flow of 2-fold serially diluted (200 nM to 0 nM) antigens in PBST buffer (0.01% Tween20), in accordance with manufacturer's instructions. Plotted data was fitted (Global) in BLITZ built-in software and dissociation constants were determined based on triplicate experiments.

**Fluorescence life time measurements:** Time-resolved fluorescence decays were measured by time-correlated single photon counting on a previously described home built set-up.<sup>7</sup> Briefly, excitation was provided by a 375 nm pulsed laser diode (PicoQuant, LDH-P-C-375) at 5 MHz. Emission was passed through a polariser set to the ‘magic angle’ (54.7°) and then a monochromator (CVI, dk480) before being detected by a microchannel plate photomultiplier tube (Hamamatsu, R3809U-50). Emission times were recorded and histogrammed in 8 ps bins using a photon counting device (PicoQuant, PicoHarp 300) with a trigger diode assembly (PicoQuant, TDA 200) to provide the start signal with the stop signal from the microchannel plate. Decay histograms were fitted by exponential decay components convolved with the instrument response function (IRF – typically ~90–100 ps, recorded using a scattering solution of dilute milk powder in water) using in-house software based on the Marquardt algorithm. Goodness-of-fit of the data by the fitting function was determined by the  $\chi^2$  fitting parameter ( $0.9 < \chi^2 < 1.2$ ) and the distribution of the residuals (data minus fit) which should be random around zero for a good fit. Fitting yielded two lifetimes ( $\tau$ ) with associated amplitudes ( $A$ ) from which average lifetimes  $\langle \tau \rangle$  were calculated using Eqn S1.

$$\langle \tau \rangle = \frac{\sum_i A_i \tau_i^2}{\sum_i A_i \tau_i} \quad \text{Eqn S1}$$

## Supplementary Data:

Table S1: Amino acid sequence of each mutant. While N- and C-term mutants were created by adding TAG codon at the start and end of the anti-EGFR original sequence, other mutants were created by mutating respective amino acids to Anap UAA such as H53Y, H91Y, L36Y, and H100aF.

Constructs	
N-term	<b>Anap</b> QLQLQESGPGLVKPSETLSLTCTVSGGSVSSGDYYWTWIRQSPGKGLEWIGHIYYSGNTNYPNPSLKSRLTISIDTSKTQFSLKLSSVTAADTAIYYCVRDRVTGAFDIWGQGTMTVTVSSGGGGSGGGGSGGGGSDIQMTQSPSSLSASVGDRVTITCQASQDISNYLNWYQQKPGKAPKLLIYDASNLETGVPSRFRSGSGSGTDFTFTISSLQPEDIATYFCQHFDHLPLAFGGGGTKVEIK
C-term	QLQLQESGPGLVKPSETLSLTCTVSGGSVSSGDYYWTWIRQSPGKGLEWIGHIYYSGNTNYPNPSLKSRLTISIDTSKTQFSLKLSSVTAADTAIYYCVRDRVTGAFDIWGQGTMTVTVSSGGGGSGGGGSGGGGSDIQMTQSPSSLSASVGDRVTITCQASQDISNYLNWYQQKPGKAPKLLIYDASNLETGVPSRFRSGSGSGTDFTFTISSLQPEDIATYFCQHFDHLPLAFGGGGTKVEIK <b>anap</b>
H53Y	QLQLQESGPGLVKPSETLSLTCTVSGGSVSSGDYYWTWIRQSPGKGLEWIGHIY <b>Anap</b> SGNTNYPNPSLKSRLTISIDTSKTQFSLKLSSVTAADTAIYYCVRDRVTGAFDIWGQGTMTVTVSSGGGGSGGGGSGGGGSDIQMTQSPSSLSASVGDRVTITCQASQDISNYLNWYQQKPGKAPKLLIYDASNLETGVPSRFRSGSGSGTDFTFTISSLQPEDIATYFCQHFDHLPLAFGGGGTKVEIK
H91Y	QLQLQESGPGLVKPSETLSLTCTVSGGSVSSGDYYWTWIRQSPGKGLEWIGHIYYSGNTNYPNPSLKSRLTISIDTSKTQFSLKLSSVTAADTAIY <b>Anap</b> CVRDRVTGAFDIWGQGTMTVTVSSGGGGSGGGGSGGGGSDIQMTQSPSSLSASVGDRVTITCQASQDISNYLNWYQQKPGKAPKLLIYDASNLETGVPSRFRSGSGSGTDFTFTISSLQPEDIATYFCQHFDHLPLAFGGGGTKVEIK
L36Y	QLQLQESGPGLVKPSETLSLTCTVSGGSVSSGDYYWTWIRQSPGKGLEWIGHIYYSGNTNYPNPSLKSRLTISIDTSKTQFSLKLSSVTAADTAIYYCVRDRVTGAFDIWGQGTMTVTVSSGGGGSGGGGSGGGGSDIQMTQSPSSLSASVGDRVTITCQASQDISNYLNW <b>Anap</b> QQKPGKAPKLLIYDASNLETGVPSRFRSGSGSGTDFTFTISSLQPEDIATYFCQHFDHLPLAFGGGGTKVEIK
H100aF	QLQLQESGPGLVKPSETLSLTCTVSGGSVSSGDYYWTWIRQSPGKGLEWIGHIYYSGNTNYPNPSLKSRLTISIDTSKTQFSLKLSSVTAADTAIYYCVRDRVTGA <b>Anap</b> DIWGQGTMTVTVSSGGGGSGGGGSGGGGSDIQMTQSPSSLSASVGDRVTITCQASQDISNYLNWYQQKPGKAPKLLIYDASNLETGVPSRFRSGSGSGTDFTFTISSLQPEDIATYFCQHFDHLPLAFGGGGTKVEIK

Table S2: Summary of steady-state and time-resolved emission properties of Anap in a range of polar solvents, incorporated in the H53Y mutant and in H53Y bound with EGFR.

Sample	$\epsilon_s^a$	$\lambda_{em-max}$ (nm)	$\Phi_{flu}$	$\tau_1$ (ns) (%) <sup>b</sup>	$\tau_2$ (ns) (%) <sup>b</sup>	$\langle\tau\rangle^c$ (ns)
Acetone	20.7	433	0.15	1.36 (33)	2.89 (67)	2.60
Acetonitrile	37.5	438	0.42	1.73 (41)	3.34 (59)	2.91
DMSO	46.7	455	0.64	1.91 (29)	3.47 (71)	3.18
Ethanol	24.5	472	0.90	1.74 (11)	3.41 (89)	3.31
Methanol	32.7	474	0.83	1.94 (30)	3.45 (70)	3.15
PBS	80.0	495	0.43	1.64 (68)	3.65 (32)	2.67
H53Y <sup>d</sup>	-	475	0.52 <sup>e</sup>	1.98 (53)	3.65 (47)	3.01
H53Y+EGFR <sup>c</sup>	-	459	0.58 <sup>e</sup>	2.18 (48)	3.93 (52)	3.34

<sup>a</sup>  $\epsilon_s$  dielectric constant

<sup>b</sup> % is the contribution of that component to the total initial amplitude.

<sup>c</sup>  $\langle\tau\rangle$  is average lifetime calculated from Eqn S1.

<sup>d</sup> measured in PBS

<sup>e</sup> estimated from an increase in area under fluorescence decay profile with respect to Anap in PBS buffer.

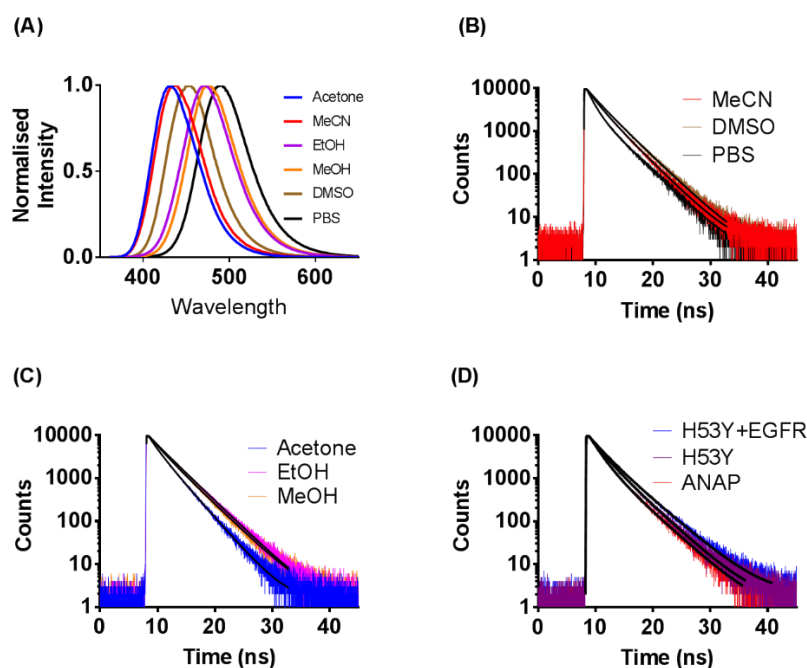


Figure S1: Steady state and time-resolved fluorescence analysis of Anap in a solvent series or incorporated into H53Y. (A) Steady state spectra of free Anap in a solvent series; (B/C) Time-resolved fluorescence decays and fitted functions (black lines) of free Anap in the same series of solvents; (D) Time-resolved fluorescence decays and fitted functions (black lines) of H53Y with and without EGFR or Anap in PBS. Note – MeCN = acetonitrile, DMSO = dimethylsulfoxide, EtOH = ethanol, MeOH = methanol, PBS = phosphate-buffered saline.

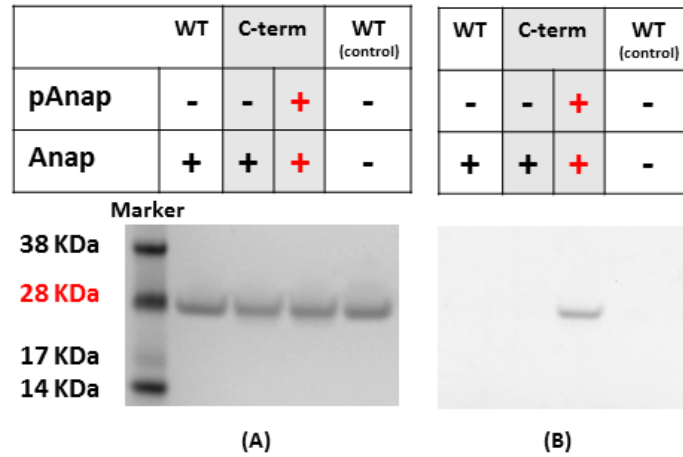


Figure S2: Confirmation of Anap incorporation selectively in response to TAG codon in the presence of Anap and pAnap plasmid. (A) Image of coomassie staining under white light; Anap UAA was supplied in the absence of pAnap during the expression of WT and C-term mutant. While WT does not contain TAG codon, C-term mutant contains TAG codon at the C-terminus sites. WT was also used as control (WT<sub>control</sub>) where neither Anap nor pAnap was supplied. (B) Image of Anap fluorescence under UV excitation shows fluorescence band only in the presence of TAG codon and Anap/pAnap pair (C-term). This clearly demonstrates the selectivity of Anap incorporation into the scFv mutant.

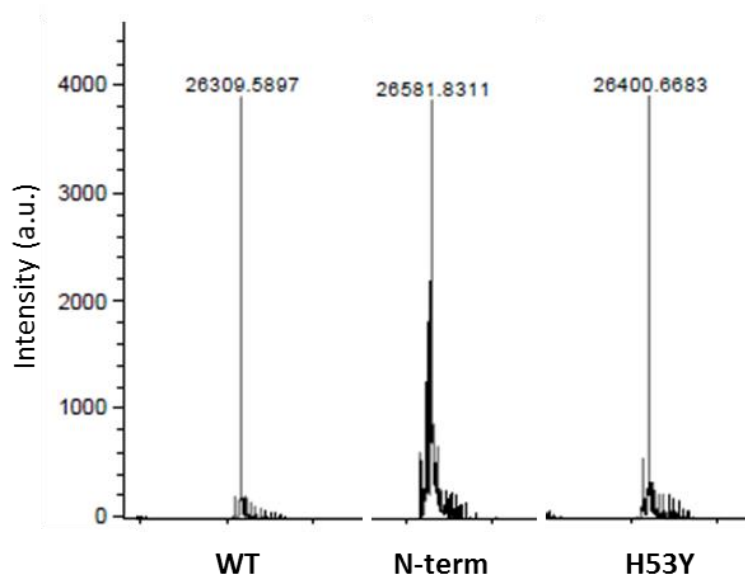


Figure S3: ESI-MS analysis. Spectrum shows observed mass of WT (26308 Da), N-term (26580 Da) and H53Y (26400 Da) mutant. A 272 da mass difference between N-term mutant and WT as well as 91 Da difference between H53Y and WT confirms selective incorporation of Anap (MW-272 Da).

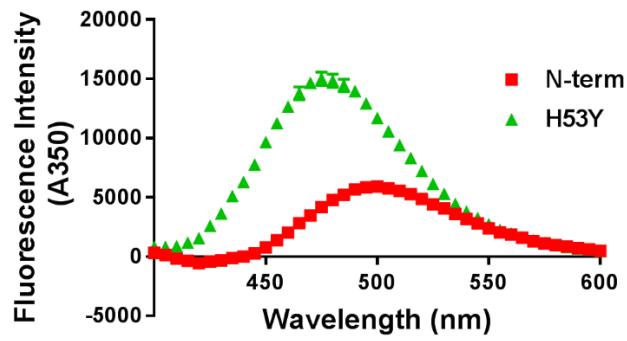


Figure S4: Fluorescence measurement of N-term and H53Y mutants from 50 nM concentrations. Each mutant exhibited unique emission peak and significant difference in fluorescence intensity. C-term mutant was not included here due to inefficient Anap labelling.

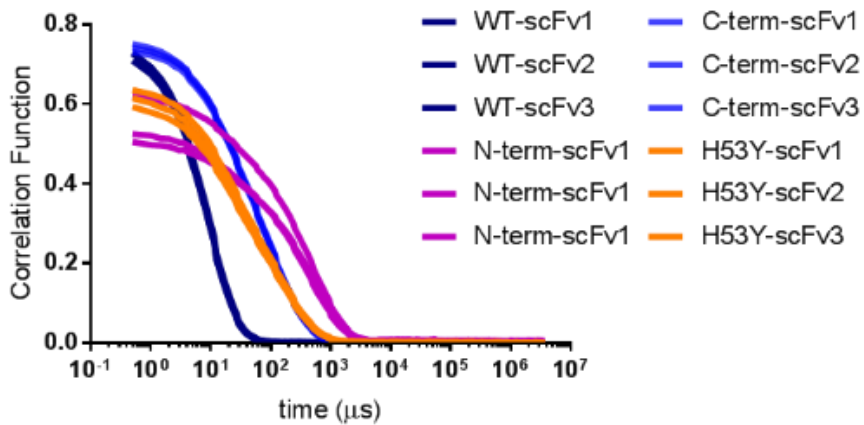


Figure S5: Correlation functions of Anap mutants carried out in Malvern ZetaSizer; 3 separate analyses were collected for each sample and plotted individually.

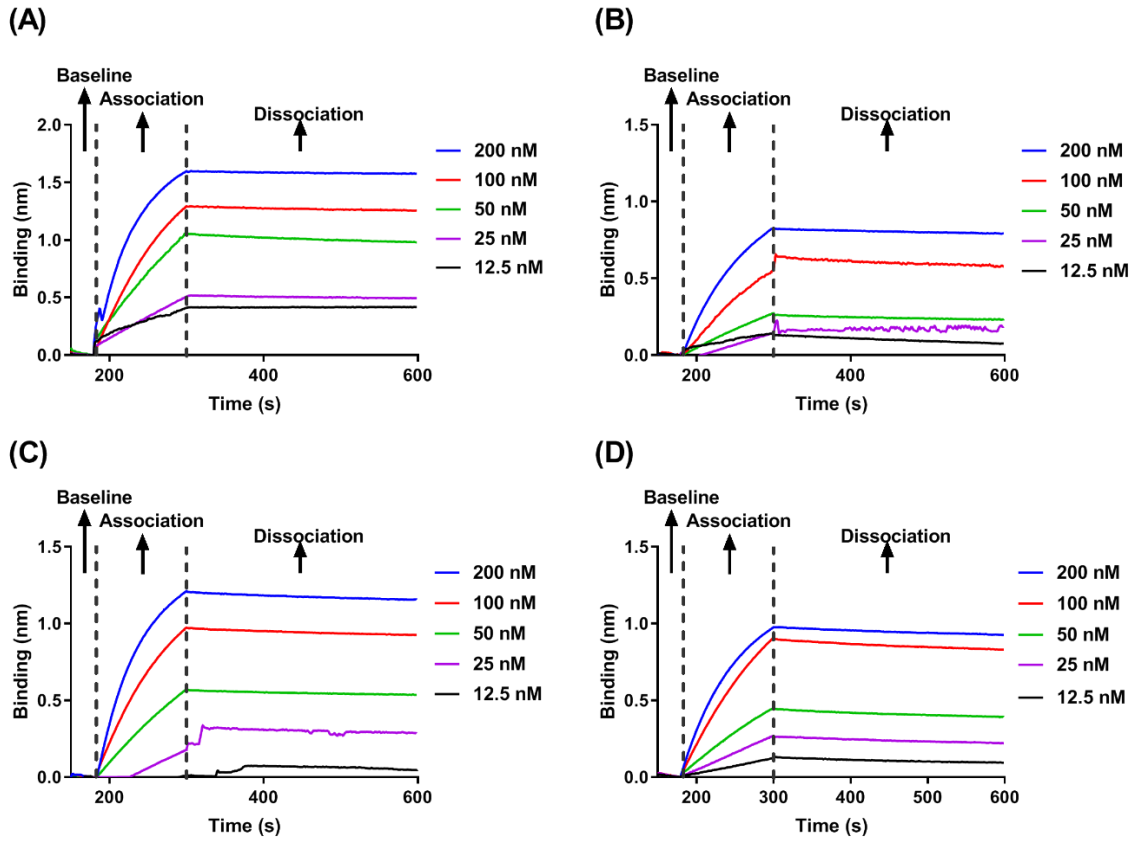


Figure S6: Binding kinetics of Anap mutants (A) WT, (B) C-term, (C) N-term and (D) H53Y mutant. Graphs are representing association and dissociation steps of EGFR antigens where mutants were captured on Ni-NTA biosensors followed by association and dissociation with various concentrations of EGFR target. Data was fitted (global) in Blitz built-in software by subtracting the reference background and step correction (at start of association).

## References:

1. Howard, C. B.; Fletcher, N.; Houston, Z. H.; Fuchs, A. V.; Boase, N. R. B.; Simpson, J. D.; Raftery, L. J.; Ruder, T.; Jones, M. L.; de Bakker, C. J.; Mahler, S. M.; Thurecht, K. J., Overcoming Instability of Antibody-Nanomaterial Conjugates: Next Generation Targeted Nanomedicines Using Bispecific Antibodies. *Adv. Healthcare Mater.* **2016**, 5 (16), 2055-2068.
2. Chatterjee, A.; Guo, J. T.; Lee, H. S.; Schultz, P. G., A Genetically Encoded Fluorescent Probe in Mammalian Cells. *J. Am. Chem. Soc.* **2013**, 135 (34), 12540-12543.
3. Adams, T. E.; Koziolok, E. J.; Hoyne, P. H.; Bentley, J. D.; Lu, L.; Lovrecz, G.; Ward, C. W.; Lee, F. T.; Scott, A. M.; Nash, A. D.; Rothacker, J.; Nice, E. C.; Burgess, A. W.; Johns, T. G., A truncated soluble epidermal growth factor receptor-Fc fusion ligand trap displays anti-tumour activity in vivo. *Growth Factors* **2009**, 27 (3), 141-154.
4. Sickmier, E. A.; Kurzeja, R. J. M.; Michelsen, K.; Vazir, M.; Yang, E.; Tasker, A. S., The Panitumumab EGFR Complex Reveals a Binding Mechanism That Overcomes Cetuximab Induced Resistance. *PLoS One* **2016**, 11 (9): e0163366.
5. Pospisil, P.; Luxem, K. E.; Ener, M.; Sykora, J.; Kocabova, J.; Gray, H. B.; Vlcek, A.; Hof, M., Fluorescence Quenching of (Dimethylamino)naphthalene Dyes Badan and Prodan by Tryptophan in Cytochromes P450 and Micelles. *J. Phys. Chem. B* **2014**, 118 (34), 10085-10091.
6. Schymkowitz, J.; Borg, J.; Stricher, F.; Nys, R.; Rousseau, F.; Serrano, L., The FoldX web server: an online force field. *Nucleic Acids Res.* **2005**, 33, W382-W388.
7. Cox, R. P.; Higginbotham, H. F.; Graystone, B. A.; Sandanayake, S.; Langford, S. J.; Bell, T. D. M., A new fluorescent H<sup>+</sup> sensor based on core-substituted naphthalene diimide. *Chem. Phys. Lett.* **2012**, 521, 59-63.

Though most of the aspects related to H53Y biosensor development have been described in the above manuscript, there are a few minor aspects that can be further discussed. Despite the fact that UAA technology generates highly efficient fluorescently labelled scFv antibodies, the technique also has some drawbacks. One of the disadvantages is the reduction of protein yield compared to the wild type construct. The decrease in yield is essentially due to the generation of truncated products. Furthermore, efficient labelling is dependent on the efficient tRNA-aaRS expression and the functionality of this pair. It was found that the protein yield was consistently reduced when the position of Anap incorporation sites moved from the terminal to internal sites of anti-EGFR scFv mutants. While WT scFv antibody expressed in remarkably high quantities, a gradual decrease of protein expression was evident in the sequence of C-term to N-term followed by H53Y mutant.

The site selection for UAA in an scFv antibody is also critical. It was found that only sites that are not critical for protein folding can be selected. For examples, some of the anti-EGFR scFv mutants (*e.g.* H91Y, L36Y and H100aF) did not bind to Protein L column. This issue can be elucidated by the possibility of incorrect folding resulted in possible conformational change or alteration in the functionality of the mutants due to the mutation at those sites. Thus, it is essential that only permissible sites can be selected for mutation. A careful selection can be made by the PyMOL based mutation prediction tool (Mutagenesis Wizard).

### 4.3 Chapter 4 summary

Following the optimisation of methods for unnatural amino acid incorporation into the terminus of scFv antibody in chapter 3, this chapter intended to vary the UAA incorporation sites into an internal site of an anti-EGFR scFv antibody. Due to the unavailability of the crystal structure of this scFv antibody, a rational design approach was deployed to identify possible internal Anap incorporation sites. Previously reported knowledge was utilised in the selection of sites by considering the distance from the active sites, the possibility of solvent accessibility into that sites, and mutations of amino acids that are structurally similar and deemed to be insignificant for protein folding. The sites were mutated to TAG codon to enable Anap incorporation. Exposure of these mutants to the cognate antigen revealed that only H53Y is the optically active mutant showing a blue shift of 20 nm in emission spectra in the presence of EGFR protein. The functionality of H53Y mutant was also explored in human plasma, a complex biological environment. The mutant showed similar fluorescence properties upon binding to the target molecule. These key attributes of this mutant make it a promising concept for next-generation *in vitro* biosensing tool. The outcome of this chapter was published in *Analytical Chemistry*, a Q1 journal published by American Chemical Society.

The proof-of-concept has the potential for minimising the number of steps used in traditional immunoassays, however, needs further validation by targeting different biomarkers. Instead of using multiple reagents and reliance on absorbance spectra of the secondary reagents, this one-step biosensor relies on unique properties of the fluorophore and single assay component. In the next chapter, the concept is employed for the detection of a cardiac biomarker.

## **Chapter Five**

### **5. Detection of Human Cardiac Troponin-I by Fluorescently Labelled Engineered Antibodies**

---

## 5.1 Introduction

Following success in developing a one-step reagentless fluorescent biosensor for EGFR detection in the previous chapter, the next step was to explore the suitability of the system in a different scFv-antigen combination. Herein, anti-cTnI scFv was chosen for the development of a biosensor to detect human cardiac Troponin I (cTnI) protein, a critical biomarker for heart disease. Cardiovascular disease is a leading cause of morbidity and mortality due to complications associated with the heart muscle. According to the World Health Organisation (WHO, 2017), cardiovascular disease accounts for 31% of global deaths or ~17 million deaths every year.[\[224\]](#) Acute myocardial infarction (AMI), commonly known as heart attack, is a common cardiovascular disease which requires early detection for successful treatment. The cTnI protein is a gold standard molecular biomarker for the diagnosis of AMI. Past research has indicated a strong correlation of elevated cTnI level with AMI due to its presence in blood circulation following damage to cardiomyocytes.[\[225, 226\]](#) Typically, the cTnI protein is found in the blood within 3-4 hrs after cardiac muscle damage and cTnI level remains high for up to 14 days.[\[226, 227\]](#) Previously, diagnosis of AMI was primarily based on electrocardiography (ECG) in hospital settings, but nearly half of these diagnoses were inaccurate, and the method was only indicative of AMI.[\[228, 229\]](#) Therefore, a combination of ECG with cTnI detection has been used for appropriate diagnosis. Due to the nature of the disease, an accurate and fast detection technique is desirable; however, current laboratory assays vary among the platforms in terms of detection time, detection limit, and reference ranges.[\[230\]](#)

One of the significant challenges in cTnI detection is to achieve a lower detection limit (*e.g.* 50-100 pM) in blood; however, discrepancies between detection platforms precluded absolute quantitation. Instead, the clinical cut-off

of cTnI is often described as the 99th percentile of the upper reference limit (URL) for healthy people, for each particular assay or instrument. The 99th percentile cut-off for common troponin detection methodologies is between 0.01-0.08 ng/mL. After a typical episode of AMI, the level of cTnI can rise from 0.04 ng/mL to as high as 50 ng/mL.[231] Despite the highly sensitive assays routinely performed in clinical settings, they are several limitations associated with these approaches. For example, the sample needs to be processed prior to detection including addition of EDTA or heparin followed by separation of blood cells. Additionally, the assays are affected by biological (*e.g.* cTnI avidity) or instrument variability (*e.g.* inconsistent results upon repetition).[230] Furthermore, the assays require highly trained professionals, and data interpretation is unique to each platform. Though these technologies are routinely used in the hospitals, there is still a definite room for improvement when it comes to cost, time and the need for laboratory infrastructure and highly trained healthcare professionals.[229]

The cTnI biomarker can be detected with many well-known techniques including electrochemical, optical and acoustic sensing methods. Apple *et al.* summarised recent advancement in cTnI detection strategies as outlined in *Table 6*. [231] All of the current commercially available cTnI detection strategies are based on some form of immunoassays (such as ELISA) combined with a microfluidic chip, lateral flow or traditional micro-well formats. Recent reviews demonstrated the need for commercially available one-step cTnI detection systems where secondary reagents or additional steps (*e.g.* washing, blocking, and incubation) are not necessary.[232] Despite several fluorescence-based strategies being reported, none of them have used recombinant antibody fragments for one-step biosensing.

Table 6: Performance and detection methods of different cTnI immunoassays reported for commercial use (adapted from Apple et al.[231])

Company/platform	Detection tag	99 <sup>th</sup> , µg/L	Detection limit (µg/L)
<b>Traditional assays</b>			
Abbott ARCHITECT	Acridinium	0.03	0.01
Beckman Access 2	ALP	0.02	0.01
Beckman Coulter DxI	ALP	0.03	0.01
Ortho-Clinical Diagnostics Vitros	HRP	0.03	0.01
Siemens Centaur Ultra	Acridinium	0.04	0.01
Siemens Dimension RxL	ALP	0.07	0.04
Siemens VISTA	Chemiluminescent	0.05	0.02
Tosoh AIA	ALP	0.01	0.06
<b>High-sensitivity assays</b>			
Abbott ARCHITECT hs-cTnI	Acridinium	0.02/0.03 <sup>b</sup>	0.001
Beckman Coulter Access hs-cTnI	ALP	0.02/0.05 <sup>b</sup>	0.003
Ortho-Clinical Diagnostics hs-cTnI	HRP	0.02/0.02 <sup>b</sup>	0.001
Siemens Vista hs-cTnI	luminescence	0.03/0.06 <sup>b</sup>	0.0005
Singulex Errena hs-cTnI	Fluorescence	0.03/0.04 <sup>b</sup>	0.00009

Point-of-care (POC) diagnostics are an emerging alternative to high-sensitivity lab-based assays; however, they are analytically less sensitive. The currently available POC devices cannot detect Troponin I during the early stages of AMI (<6 hrs from the onset of cardiac damage) due to their relatively poorer detection limits in comparison to gold standard laboratory assays.[233] Some of the POC devices and their LOD are presented in Table 7.[234] O’Kennedy *et al.* also demonstrated the potential use of recombinant antibodies for myeloperoxidase detection for applications in point-of-care diagnostics to study heart diseases.[235] With the advent of POC technologies, one particular advantage could be the detection of critical biomarkers outside of clinical settings

---

<sup>b</sup> Female/male

such as in an ambulance by paramedics. This technology will reduce not only the significant detection time but also treatment can be initiated earlier which may significantly reduce the pressure on hospital emergency department. Apple *et al.* reviewed the commercially available POC technologies by different companies as presented in *Table 7*. Han *et al.* also evaluated the potential of POC diagnostics development for cTnI detection based on the existing commercial and research-based immunoassays.[232] Though some of the reported POC assays have found clinical applications, they are still not as sensitive as lab-based assays. Future POC will need to feature ultra-sensitive detection capability, low cost and portable devices to diagnose AMI in out-of-hospital settings.

*Table 7: Lists of POC devices developed by different companies.[234] [231]*

<b>Manufacturer</b>	<b>Device name</b>	<b>Time (min)</b>	<b>LOD (µg/L)</b>	<b>99<sup>th</sup> percentile URL</b>	<b>Volume (µL)</b>
Alere	Triage Cardiac Panel Troponin I	20	0.05	<0.05	250
Radiometer	AQT90 FLEX cTnI	10–20	0.0095	0.023	2000
Radiometer	AQT90 FLEX cTnT	12	0.01	0.017	2000
Abott	i-STAT cardiac troponin I	7	0.02	0.08	17
Trinity	Meritas Troponin I	15	0.019	0.036	200
LSI Medicine corporation	PATHFAST	17	0.019	0.029	100
Response Biomedical	RAMP troponin I	20	0.03	<0.10	250
Siemens	Stratus CS	14	0.03	0.07	90
bioMerieux	VIDAS	20	0.01	0.01	200
Roche	CARDIAC T Quantitative	14	0.05	Not reported	150

In this chapter, avian scFv antibodies were investigated for detection of cTnI. Previously, the crystal structure of anti-cTnI avian scFv antibody was reported.[236] The reported scFv (ScFv 180) has been chosen here due to several reasons. Firstly, this scFv is well characterised, and the structural information is available for both the antigen bound complex and the unbound scFv. Secondly, the scFv 180 was selected using phage display biopanning against cTnI peptide

which was tailored for a biosensing purpose. Specifically, the antibody showed a high affinity towards antigen (~18 pM) to ensure rapid association that could be utilised for rapid detection of the ligand. Also, the reaction kinetics of this avian scFv is suited to room temperature operation which could be beneficial for POC device fabrication. Both the unbound structure of anti-cTnI scFv and the peptide-bound structure (supplied by Dr Paul Conroy, Dept. of Biochemistry and Molecular Biology, Monash University) were utilised in this study for selection of fluorophore incorporation sites.

Avian antibodies have some unique features that have been exploited to target different antigens for a wide range of applications in therapeutics and diagnostics.[\[237\]](#) One potential benefit of avian antibodies is the evolutionary distance that leads to a superior, unique and highly specific antibody generation. The simple v-gene arrangement and the extended CDRH3 offers superior biophysical attributes (*e.g.* specificity, stability and affinity).[\[236\]](#) The specific avidity of cTnI antibodies plays a critical role in detection strategies. For example, the mammalian-derived cTnI antibody has been found to interact with other nonspecific targets (*e.g.* auto-antibodies or sample processing substances such as heparin) present in blood samples.[\[238, 239\]](#) An important advantage of avian antibodies is that they do not cross-react with the mammalian rheumatoid factor or Fc region of mammalian antibodies that may be present in the blood; furthermore, they do not activate the human complement system (perhaps an excellent feature for *in vivo* diagnostics). Additionally, these antibodies can be rapidly generated in chickens and screened in phage-display technology, thus reducing the cost, time and use of the laboratory animals.[\[240, 241\]](#) The use of avian antibodies in immunoassays has been widely reported, dating back to the early 2000s.[\[242\]](#)

The biophysical characteristics of human cTnI presented difficulties in generating precise antibodies as it is present in different forms in human blood (*e.g.* unbound, complexed with troponin C, or complexed with troponin C and troponin T). Apart from the heart muscle, several other isoforms of cTnI are present in skeletal muscles (skTnI). The different forms of cTnI have increased the complexity in the selection of mAbs that specifically target correct epitopes of cardiac originated troponin I protein. Avian-originated anti-cTnI scFv has shown superior specificity that has the potential to combat these issues. Conroy *et al.* carried out a systematic case study for the development of a highly specific avian anti-cTnI antibody by targeting the amino-terminal epitope.[\[239\]](#) This knowledge-driven approach was applied for the detection of cTnI in a sandwich ELISA method.

Surface immobilisations can improve the sensitivity of solution-phase biosensors.[\[165, 243\]](#) One particular example is the immobilisation of biorecognition components onto the nanoparticle surfaces.[\[168\]](#) The emergence of “nanomedicine” has led to the possibility of combining nanoparticles and proteins for applications in drug delivery, imaging and biosensing.[\[244\]](#) Richard *et al.* and Arruebo *et al.* have systematically reviewed the immobilisation of antibodies onto nanoparticle surfaces for detection of target proteins.[\[168, 245\]](#) However, no studies to our knowledge have demonstrated one-step fluorescence immunosensing using nanoparticle-bound antibodies or related fragments. Surface attachment of the scFv-based fluorescent biosensor on nanoparticles could be used for diverse applications, including detection in a flow channel, or separation of bound antigen from the blood samples to minimise background signal to improve sensitivity. The overall objective of the surface attachment of fluorescently labelled scFv biosensors is to explore the potential benefits of solid-phase detection. Moreover, the proposed research also aims to gain a

fundamental understanding of the properties of H53Y and L27c-Y biosensors on the solid surfaces. There are a variety of solid phase surfaces which could be used; in an initial exploratory investigation, carbon nanotube, silica nanoparticles and agarose-beads were tested.

An alternative to traditional cTnI detection approaches is investigated in this chapter. In the previous chapter (Chapter 4), a fluorescence-based one-step detection method was developed by exploiting an antibody fragment as a bio-recognition agent that exhibited fluorescence changes upon binding specifically to the target antigen. Herein, the same principle was applied for the development of a one-step cTnI immunosensor, but a crystal structure-guided selection approach was employed for the determination of fluorophore incorporation sites. The sites of Anap incorporation were selected based on the conformational difference between the unbound scFv and scFv-peptide complex structures. The mutants were expressed in mammalian cells, purified and extensively characterised. These fluorescently labelled scFv mutants were screened to find the most optically active mutant. The resultant fluorescent biosensor was tested for quantification of cTnI peptide or full-length cTnI protein in buffered solutions with and without human plasma. Apart from the homogeneous solution-phase detection of target proteins, the reported biosensors (H53-Y and L27c-Y) were immobilised onto different surfaces for testing the suitability of solid-phase detection assays, with a view to future applications beyond homogenous assay formats.

## 5.2 Materials and Methods

### 5.2.1 Expression, purification and characterisation of anti-cTnI scFv antibodies

Selection of Anap mutation sites was determined based on the crystal structure of the anti-cTnI scFv antibody. Antigen bound (unpublished), and the unbound structure (4P48) were aligned in PyMOL molecular visualisation tool to determine the sites that exhibited some conformational changes from the native structure upon binding to the target molecule. In most cases, the differences between the bound and unbound structure were marginal and suggested that fine movements associated with single-chain were only required to differentiate the antigen bound from the antigen-free structure. Amino acids that were not critical for structural stability and antigen binding were selected as sites for incorporation of Anap. Solvent accessibility to these sites was also considered.

GenScript Biotech Corporation chemically synthesised a set of codon optimised genes with an amber suppression codon (TAG) introduced into the selected positions for the Anap incorporation, and these genes were cloned directly into pcDNA 3.1 (+) between NdeI and EcoRI restriction sites. The sequence of anti-cTnI WT scFv sequence is presented in *Figure 25*. The plasmid containing the sequence for tRNA/tRNA synthetase, herein referred as “pAnap” was purchased from Addgene (Catalogue number 48696). The plasmids were co-transfected in a ratio of 3:1 or 3:2 (scFv plasmid: pAnap) into Expi293F HEK cells. Briefly, cell cultures were adjusted to a concentration of  $\sim 3 \times 10^6$  cells/mL before transfection and 3  $\mu\text{g/mL}$  of anti-cTnI wild-type or variant plasmid were co-transfected with 1  $\mu\text{g/mL}$  of the pAnap harbouring plasmid. The transfected medium was supplemented with 30-50  $\mu\text{M}$  of Anap after 4-6 hrs of transfection. For efficient protein expression, cells were maintained in 5% (v/v) humidified incubator at 37°C, shaking at 100 rpm with the supplementation of 2mM

GlutaMAX and 33 mM of glucose. After 7 days, cells were harvested by centrifugation. Supernatants were filtered through 0.22 µm filter followed by purification with HisTrap Ni-NTA affinity chromatography. Elution fractions were pooled and concentrated to 1-4 mL before loading onto Sephacryl® S-100 HR size exclusion column (GE Healthcare). Proteins were eluted in PBS buffer, and the fractions were analysed by gel electrophoresis.

*Figure 25: Optimised anti-cTnI scFv WT sequence for expression in mammalian cells. Restriction sites are outlined in light blue colour.*

CATATG

CTGACCCAGCCGAGCAGCGTGAGCGCGAATCCGGGCGAAACCGTGAAAATTACCTGCAGCGGTGGTGGCCGTTAC  
TATGATGGCAGCTACTATTACGGTTGGTATCAACAAAAGAGCCCGGGTAGCGCGCCGGTGACCGTTATCTACGAG  
AACACCAAGCGTCCGAGCAACATTCCGAGCCGTTTCAGCGGTAGCAAAAGCGGTAGCACCGCGACCCGTGACCATC  
ACCGGTGTGCGTGCGGAGGACGAAGCGGTTTATTACTGCGGCAGCGCGGACGATAACATGAACCCGACCATTTTT  
GGTGCGGGTACCACCCTGACCGTGCTGGGTGAGAGCAGCCGTAGCAGCAGCGGTGGCGGTAGCAGCGCGGTGGC  
GGTAGCGCGGTGACCCTGGATGAGAGCGCGGTGGCCTGCAAAACCCGGGTGGCGCGCTGAGCCTGGTTTGAAG  
CGGAGCGGTTTACCTTTAGCAGCTATGGCATGCAGTGGGTGCGTCAAGCGCCGGTAAAGGCCTGGAATGGGTT  
GCGGGTATCCAGAACGACGATACCGGTACCTATTATGGTGCGGCGGTGAAGGGTCGTGCGACCATTAGCCGTGAC  
AACGGCCAGAGCACCCTTCGTCTGCAACTGAACAACCTCGGTGCGGAGGATACCGGTACCTATTACTGCGCGAAA  
GACGCGAGCAGCGATGGTGGCTACGGTGGCGACAGCATCGATGCGTGGGGTCACGGCACCGAAGTGATTGTTAGC  
AGCACCAGCGGCCAAGCGGGTCAGCACCACCACCACCACCGGCGGTACCCGTATGATGTTCCGGACTATGCG  
AGCTGA

GAATTC

**Western Blotting:** Proteins were detected on a Western blot by following a standard protocol. Generally, 2 µL of purified anti-cTnI scFv mutants and WT were run on SDS-PAGE for 60 min at 100 V. Mutants were transferred to a PVDF membrane by setting up a standard transfer apparatus (Bio-Rad). The apparatus was set up in a cold room (4°C) to maintain a low chamber temperature, and the transfer process was carried out for 60 min at a constant current of 345 mA. The membrane was blocked in 5% (w/v) skim milk at room temperature for 1 hr or 4°C overnight. After washing the membrane with PBST (0.1% v/v), HRP-labelled anti-His antibody was added and incubated for 1 hr at

room temperature followed by washing three times with PBST (0.1% v/v). Freshly made electrochemiluminescence (ECL) solution was added to the membrane as per manufacturer instructions. Signals were detected immediately in UVP-imaging systems.

***Indirect Enzyme-Linked Immunosorbent Assay (ELISA):*** Human Cardiac Troponin I peptide (15 µg/ml) in PBS buffer was coated in replicates in a 96 well plate (Nunc flat bottom, Maxisorp) overnight at 4°C. Fibrinogen, a nonspecific target, was coated at 10 µg/ml as a control. The coating solution was decanted followed by the addition of blocker solution containing 200 µL of 2% (w/v) skim milk diluent (0.05% PBST) to each well and incubated for one hr at room temperature for blocking nonspecific proteins. Purified WT and Anap-incorporated variants were added to each well at a concentration of 10 µg/mL. After 2 hrs incubation at room temperature, the wells were vigorously washed six times with PBST (PBS, 0.05% v/v Tween 20). The HRP-labelled anti-His antibody was diluted into blocker solution (1:5000) and added 100 µL to each well. After 30-60 min of incubation at room temperature, the anti-His antibody was decanted and washed six times with PBST manually. 100 µL of 3,3',5,5'-tetramethylbenzidine (TMB, ThermoFisher Scientific) was added to each well followed by a 10 min incubation for adequate colour development and the reaction was stopped by adding 2 M hydrochloric acid. The colorimetric reaction was analysed by recording absorbance at 450 nm in a Multiskan Microplate Spectrophotometer (ThermoFisher Scientific). Data were analysed by plotting in Excel or GraphPad software.

### **5.2.2 Fluorescence measurement**

A 96 well black plate (Costar) was blocked with 2% (w/v) skim milk in PBS overnight before measuring the fluorescence of Anap mutants. The plate was washed with PBS buffer, and 200 µL of 100 nM of each Anap mutant was added

to wells in triplicate. Mutants were excited at 350 nm, and the emission spectra were recorded between 400-500 nm. Background spectra were subtracted, and the data plotted in the GraphPad Prism software.

***Detection of cTnI peptide and protein in PBS:*** Using a similar approach as mentioned in chapter 4 ([Section 4.1](#)), titration assays were set up for investigating the response of scFv mutants to the target antigen. As a primary test, all the mutants were tested for cTnI peptide detection. In general, 150  $\mu$ L of anti-cTnI scFv (15 nM) mutant was added to each well. Fluorescence spectra were measured by exciting the protein at 350 nm and recording emission between 400-550 nm. Subsequently, 100  $\mu$ L of the cTnI peptide with 2-fold serial dilution was added (0 to 100 nM). Triplicates of each concentration were assayed for statistical relevance. The mixture was incubated for 60 min, and fluorescence spectra were recorded as above. Background emission spectra were subtracted in Excel. Graphs and statistical analysis were carried out in GraphPad Prism software. The same approach was conducted for the detection of full-length cTnI protein (Life Diagnostics, Cat#1210). The only exception is that 2-fold serial dilutions of cTnI protein (diluted in PBS) from 0 to 40 nM were used. Only L27c-Y mutant was selected for testing cTnI protein due to its significant fluorescence response against the peptide. Simultaneously a high concentration of nonspecific target (e.g. fibrinogen 5  $\mu$ M) was added to L27c-Y scFv as a control to investigate the specificity of target binding. Triplicates of each concentration were added (~100  $\mu$ L) to 150  $\mu$ L of 15 nM of L27c-Y mutant. After 1-hr of incubation at room temperature, fluorescence was measured in Tecan (Infinite 200Pro) fluorescence spectrometer as described above.

***Detection of cTnI protein in human plasma:*** Detection of cTnI protein in human plasma: Detection of cTnI protein was executed in human plasma by a similar approach used for detection in PBS buffer. Human plasma (5%) was

prepared by diluting into PBS buffer which was spiked with different concentrations of cTnI protein. First, 150  $\mu$ L anti-cTnI-Anap scFv (15 nM) mutant was added to each well. Equal distribution of mutant was ensured by measuring fluorescence on each well. About 100  $\mu$ L of cTnI spiked 5% (v/v) human plasma was added to each well. Antigens were used in triplicate for each concentration for statistical analysis. The mixture was incubated at room temperature for 60 min, and the fluorescence measured. The spectral readings were collected and analysed in MS Excel software. Statistical analysis, LOD determination, and graphs were plotted in the GraphPad Prism software. Lorentzian distributions (*Equation 1*) were used to apply curve-fitting algorithms to each fluorescence spectrum.

$$Y = \frac{\text{amplitude}}{\left(1 + \frac{(X - \text{center})^2}{\text{width}}\right)^2} \quad \text{Equation 1}$$

where amplitude corresponds to the height of the centre of the distribution in Y units, the centre is the X value at the centre of the distribution and width is a measure of the width of the distribution in the same units as X. Additionally, the standard error was also calculated in the fit that shows statistical variance in the wavelength shift. The goodness of the fit was evaluated from the calculated R<sup>2</sup> (always found >0.95). The centre wavelength generated from the Lorentzian distribution fit for the 0 nM data was subtracted from the wavelengths shifted in different samples. The wavelength shift was plotted against the corresponding concentration of the antigen. Nonlinear regression was employed to investigate statistical variability (agonist vs response-variable slope, four parameters, *Equation 2*). EC50 values were also determined from this analysis.[\[246\]](#)

$$Y = \text{bottom} + (X^{\text{Hillslope}}) * \frac{\text{top} - \text{bottom}}{X^{\text{Hillslope}} + \text{EC50}^{\text{Hillslope}}} \quad \text{Equation 2}$$

***Time-resolved fluorescence measurement:*** In this study, the life-time solvatochromism of Anap incorporated L27c-Y was investigated in the presence of different concentrations of cTnI peptide and protein using time-correlated single photon counting (TCSPC). About 300 nM of L27c-Y mutant was prepared to test various concentrations of peptide and protein. First, 200  $\mu$ L of L27c-Y was aliquoted into 1.5 mL centrifuge tubes. 100  $\mu$ L of respective concentrations of cTnI peptide and protein were added to L27c-Y scFv. After 45 min of incubation, TCSPC was performed. Data were fitted to the Marquardt algorithm. Details of measurements and curve fitting were also outlined in [Section 4.2](#). The principle of fluorescence lifetime analysis has been briefly outlined in [Section 7.11.1](#).

### **5.2.3 Affinity and stability testing**

***Bio-layer Interferometry (BLI):*** BLI is an indispensable tool for the determination of affinity of an antibody for the target antigen (the principle of BLI can be found in [Section 7.11.2](#)). Binding kinetics of anti-cTnI scFv mutants was examined using Biolayer Interferometry by immobilising biotinylated cTnI peptide on Streptavidin (SA) biosensors followed by capturing the scFv mutants in PBST (0.05% T20) buffer. The cTnI peptide was biotinylated using a commercially available biotinylation kit (Lightning-Link® Type B; Novus Biologics) as per the manufacturer protocol. 15  $\mu$ L of the biotinylated peptide was added to 300  $\mu$ L of PBST to adjust the final concentration to 500 nM. SA biosensors were equilibrated in PBST buffer for about 10 min before connecting to the Blitz equipment (ForteBio). Then, the biotinylated peptide was loaded onto SA biosensors for 30 s followed by washing in PBST buffer for 30 s to establish a baseline. The scFv antibody was captured for about 120 s (association) followed by washing in PBST buffer for 120 s to allow dissociation of the weakly bound scFv antibody. A reference sample was run to estimate the background signal and was subsequently subtracted from the other sample data. This was done by

loading the biotinylated peptide to SA biosensors followed by performing an association and dissociation step in the buffer without using the anti-cTnI mutant and WT scFv. These experimental parameters and steps were used for each of mutants across the concentrations evaluated. Additionally, the specificity of SA biosensors for mutants was also inspected by capturing mutants in the absence of biotinylated peptide. While the  $K_D$  value was calculated using the Blitz Pro1.1 software, the error was calculated by the standard error propagation formula as presented in *Equation 3*, where C is the dissociation constant ( $K_D$ ), A is the association rate ( $k_a$ ),  $\alpha$  is the error found in  $k_a$ , B is the dissociation rate ( $k_d$ ), and  $\beta$  is the error observed in  $k_d$ .

$$\delta = C \times \sqrt{\left(\frac{\alpha}{A}\right)^2 + \left(\frac{\beta}{B}\right)^2} \dots \dots \dots \quad \text{Equation 3}$$

**Dynamic light scattering (DLS):** Purified WT and L27c-Y samples were investigated by size distribution analysis in DLS. The samples were filtered through a 0.22  $\mu\text{m}$  filter. The concentration of the mutants was adjusted to about 1 mg/mL. About 100  $\mu\text{L}$  of these samples were pipetted into micro-cuvettes. For each of the mutants, three sets of 10 measurements were collected from the fresh samples by following a standard DLS size measurement protocol. Malvern Zetasizer software was used to determine particle size based on the number distribution. The graph was plotted in the GraphPad Prism software. A brief principle of DLS method is described in [Section 7.11.3](#).

#### 5.2.4 Surface attachment of H53Y and L27c-Y biosensors

**Surface attachment of H53Y onto carbon nanotubes:** 0.2 mg of single-stranded-DNA (ssDNA, Integrated DNA Technologies) modified with NTA functional group was suspended into 1 mL of PBS buffer (pH 7.4).

Simultaneously, 0.5 mg of single-walled carbon nanotube (SWCNT, HiPCO™

Unidym Inc.) was measured and directly added to the PBS buffer containing ss-DNA-NTA. The SWCNT was solubilised by sonication (probe sonicator) for about 30 min. The solubilised SWCNT was separated by centrifugation at high speed (50,000 rpm) using an ultracentrifuge (Sorvall Discovery 90SE). The sonicated sample was filtered through Amicon concentrator (100 kDa) by centrifuging at 15,000 rpm. The filtered SWCNT-ssDNA-NTA was resuspended into PBS buffer. Nickel (Ni) was attached to the complex by adding 50× molar excess of NiCl<sub>2</sub> to the SWCNT. Excess NiCl<sub>2</sub> was removed by dialysis against PBS buffer. The concentration of nanotube in solution was determined using a Jasco spectrophotometer (NIR, V-700 series).

Surface attachment of H53Y was obtained by directly adding 5-10× molar excess of H53Y to SWCNT-ssDNA-NiNTA-H53Y. Loading of H53Y onto SWCNT was confirmed by measuring size distribution on DLS. 100 µL of SWCNT-ssDNA-NiNTA-H53Y and a control sample was added to transparent cuvettes and the size distribution measured by DLS following a standard protocol. About 200 µL of 50 nM of ssDNA-NiNTA-SWCNT-H53Y was added in triplicates in a Costar black plate to measure the fluorescence of surface-bound H53Y mutant. Additionally, triplicates of the same molecule were used as controls. About 100 µL of EGFR (200 nM) was added to each well whereas 100 µL of PBS was added into the control wells. Following incubation for 45 min, fluorescence was measured by exciting the samples at 350 nm, and emission was recorded between 400-550 nm. The background signal was subtracted, and data were plotted in the GraphPad Prism software.

***Surface attachment of L27c-Y onto silica nanoparticles:*** Similarly, H53Y mutant was attached to commercial silica nanoparticles (DiagNano™ Ni-NTA Silica Particles, Creative Diagnostics). The silica nanoparticles were mixed with H53Y mutant in 50× molar excess in PBS buffer and incubated at room

temperature for about 1 hr. The excess unreacted H53Y mutant was removed by buffer exchange for 4× by centrifugation at 5000 rpm. The absorbance of flow-through from this step was measured to monitor the presence of H53Y mutant. Attachment of H53Y was further confirmed by visualising the Si-H53Y in the UVP gel imager.

**Surface attachment of L27c-Y onto agarose beads:** 500 µL (0.5 mg/mL) of commercially purchased agarose beads (Qiagen, Ni-NTA Agarose, # 30210) was aliquoted into a microcentrifuge tube. Storage solution was removed by centrifugation in a benchtop centrifuge for 1 min at 5000 g speed. The beads were washed 3-times with the PBS buffer (pH 7.4). About 200 µL of L27c-Y scFv (15 µM) was added to the beads followed by addition of 200 µL of PBS buffer to submerge the beads. After 1-2 hrs of incubation at room temperature, the beads were centrifuged and visualised in UVP Gel imager (Biospectrum). Fluorescence of Anap was visualised mostly at the bottom of the tube confirming the successful attachment of most of the scFv. The solution was removed, and OD was recorded at 280 to check the concentrations of the unbound scFv mutant in the solution. Beads were washed 3-times to remove unreacted scFv mutant. About 3 µL of L27c-Y-agarose (~50 nM) was added into each well of a black Costar plate. Fluorescence was measured by exciting the surface-bound L27c-Y at 350 nm, and emission was recorded between 400-600 nm. Following the background check, 100 µL of cTnI protein was added in a concentration range of 0-300 nM to L27c-Y (~50 nM). Background fluorescence of agarose beads was subtracted, and emission spectra were plotted.

## 5.3 Results and Discussions

### 5.3.1 Detection of cTnI protein

The crystal structure of a novel, high-affinity avian anti-cTnI-antibody was recently reported by Conroy and colleagues. [236] Following on from these studies, a variant of the anti-cTnI antibody (scFv 2B12) was demonstrated to be more amenable to peptide-complex crystallisation than the parental clones (scFv 180). The crystal structure of the anti-cTnI scFv bound to its cognate peptide (KISASRKLQLKT) was used here to select the Anap incorporation sites. This peptide-bound anti-cTnI scFv structured overlaid well with the structure of the cTnI reported in PDB (4P48). The aligned structure revealed a small shift of the conformation upon peptide binding within the CDRL3 binding region (*Figure 26*). It was found that L92D, L93D, L94N, L95M, and L95a-N amino acids of LCDR3 diverged from the unbound structure to accommodate the peptide.

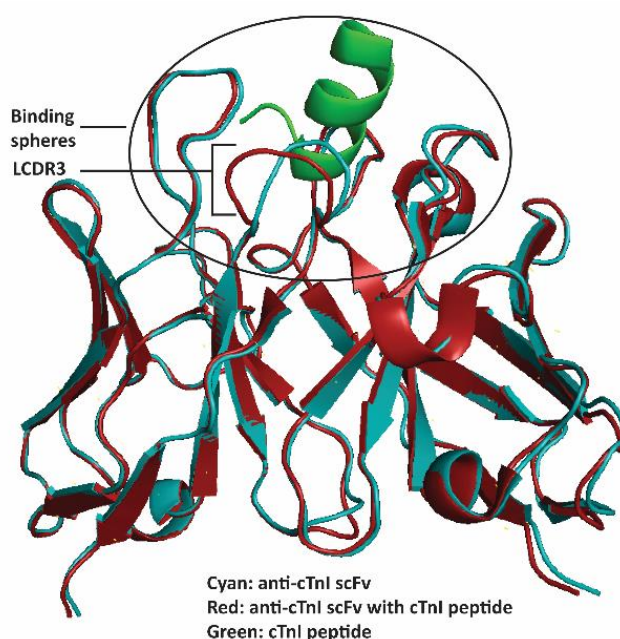


*Figure 26: Peptide-bound (firebrick red) and unbound (deep-teal cyan) crystal structure of anti-cTnI scFv antibody. A circle highlights the selection spheres. CDR3 in the light chain showed a significant conformational change in the peptide-bound structure when compared to the noncomplexed scFv structure alone.*

From the crystal structure, several key residues were identified for the incorporation of Anap into a suitable position within or near the complementary determining regions (CDR) of anti-cTnI scFv antibody. It is believed that any of these sites could be affected by antigen-induced conformational change resulting in polarity difference of the Anap due to changes in the local microenvironment. Solvent accessibility to these sites was considered to be a crucial aspect for polarity change. Furthermore, the distance of these mutation sites from the binding interface was also considered. Ten possible mutation sites (L3-A, L27a-R, L27c-Y, L92-D, L95a-N, L98-F, H54-D, H57-T, H58-Y, H98-S) represented in Kabat numbering scheme where “L” stands for the light chain, “H” stands for the heavy chain and the last letter is a symbol of respective amino acids; *Table 8*) were selected based on the conformation differences between the peptide-bound and unbound structure (*Figure 27*).

*Table 8: Sequence of anti-cTnI scFv (scFv 180). Potential sites of mutations are highlighted in red colour. Kabat numbering scheme was used to number the sequence. The CDR loops were also previously identified by North et al. [247]*

<b>VA</b>	<b>A</b> L T Q P S S V S A N P G G T V E I T C S G G G <b>R</b> Y Y D G S Y Y Y G W Y Q Q K S P G S A P V T V I Y E N T K R P S
Kabat	L1 L2 L3 L4 L5 L6 L7 L8 L9 L10 L11 L12 L13 L14 L15 L16 L17 L18 L19 L20 L21 L22 L23 L24 L25 L26 L27 L27A L27B L27C L28 L29 L30 L31 L32 L33 L34 L35 L36 L37 L38 L39 L39A L40 L41 L42 L43 L44 L45 L46 L47 L48 L49 L50 L51 L52 L53 L54 L55 L56
KABAT	LFR1 CDR-L1 LFR2 CDR-L2
NORTH et al.	LFR1 CDR-L1 LFR2 CDR-L2
<b>VA</b>	N I P S R F S G S K S G S T A T L T I T G V R A E D E A V Y Y C G S A <b>S</b> D N M N P T I <b>F</b> G A G T T L T V L
Kabat	L57 L58 L59 L60 L61 L62 L63 L64 L65 L66 L67 L68 L69 L70 L71 L72 L73 L74 L75 L76 L77 L78 L79 L80 L81 L82 L83 L84 L85 L86 L87 L88 L89 L90 L91 L92 L93 L94 L95 L95A L96 L97 L98 L99 L100 L101 L102 L103 L104 L105 L106 L106A
KABAT	LFR3 CDR-L3 LFR4
NORTH et al.	LFR3 CDR-L3 LFR4
<b>VH</b>	A L T L D E S G G G L Q T P G G A L S L V C K A S G F T F S S Y G M Q W V R Q A P G K G L E W V A
Kabat	H1 H2 H3 H4 H5 H6 H7 H8 H9 H10 H11 H12 H13 H14 H15 H16 H17 H18 H19 H20 H21 H22 H23 H24 H25 H26 H27 H28 H29 H30 H31 H32 H33 H34 H35 H36 H37 H38 H39 H40 H41 H42 H43 H44 H45 H46 H47 H48 H49
KABAT	HFR1 CDR-H1 HFR2
NORTH et al.	HFR1 CDR-H1 HFR2
<b>VH</b>	G I Q N <b>D</b> D T G <b>T</b> Y Y G A A V K G R A T I S R D N G Q S T V R L Q L N L R A E D T G T Y Y C A K D A S <b>S</b> D G G Y G G D S I <b>S</b> D A W G H G T E V I V S S
Kabat	H50 H51 H52 H52A H52B H53 H54 H55 H56 H57 H58 H59 H60 H61 H62 H63 H64 H65 H66 H67 H68 H69 H70 H71 H72 H73 H74 H75 H76 H77 H78 H79 H80 H81 H82 H83 H84 H85 H86 H87 H88 H89 H90 H91 H92 H93 H94 H95 H96 H97 H98 H99 H100 H100A H100B H100C H100D H100E H100F H100G H100H H100I H100J H101 H102 H103 H104 H105 H106 H107 H108 H109 H110 H111 H112 H113
KABAT	CDR-H2 HFR3 CDR-H3 HFR4
NORTH et al.	CDR-H2 HFR3 CDR-H3 HFR4

The selected sites were modified in the DNA sequence by mutating codons for the selected amino acids to an amber stop (TAG) codon. These mutated sequences were then cloned into a mammalian expression vector. The scFv was constructed in VL-VH orientation. For purification and further characterisation, a His-tag and an anti-HA tag were incorporated into the C-term site. The genes were synthesised and cloned by GenScript cloning service. Previously, the WT anti-cTnI scFv antibody was expressed in *E. coli*.[\[236\]](#) Here, the aim was to express in mammalian cells; hence, the gene sequences of all mutants were codon-optimised for mammalian expression. Cloning of the sequences was validated by DNA sequencing confirming the presence of the sequences in the plasmid. The sequencing result matched the sequence denoted in the certification of analysis provided by GenScript. Sequence analysis showed 100% identical sequence as expected and confirmed the presence of TAG codon in the respective positions ([Section 7.7](#)).

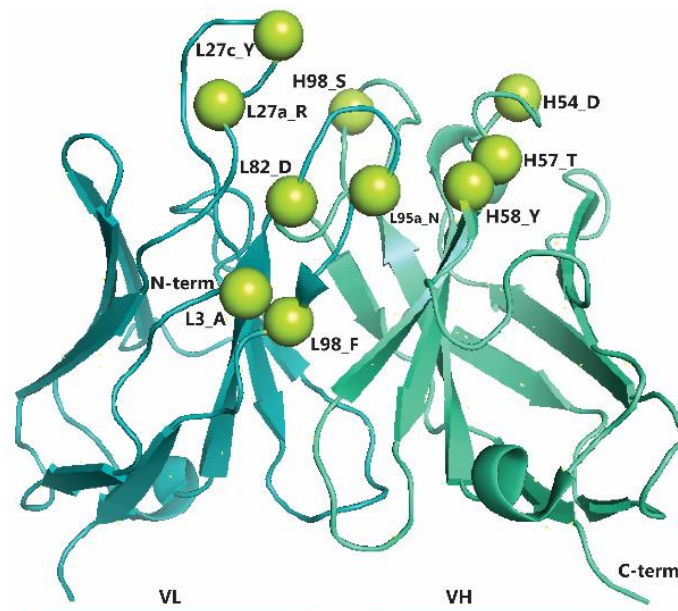


*Figure 27: Mutation sites for fluorophore incorporation. Residues mutated individually to incorporate an amber stop codon for the integration of fluorophore are highlighted in lime spheres.*

All the mutants were expressed in mammalian cells followed by purification and thorough characterisation with different bioanalytical methods. Mutants were purified by Ni-NTA affinity chromatography followed by size exclusion chromatography (SEC) to remove impurities carried over from the Ni-NTA affinity purification step. SDS-PAGE method was used to analyse the purified samples. Coomassie staining of the gel confirmed the presence of scFv mutants with relatively high purity. SDS-PAGE showed a band for each of the mutants in the expected region (~29 kDa) with minor variations of expression level among the mutants (*Figure 28A*). The gel also displayed minor impurities present in the purified protein samples, but this was not deemed significant for the purposes of the project because the proportion of contaminants was low when compared to the mutant and should not significantly affect fluorescence-based detection of the target. Even though all of the anti-cTnI scFv constructs were purified using SEC chromatography after IMAC purification, some impurities could not be removed by the SEC column. The purity can be improved by switching to a high-resolution column (*e.g.* Superdex75), which may be useful to remove low MW contaminating proteins. Alternatively, anti-HA agarose affinity beads can be used to remove impurities as the scFv mutants contain anti-HA tag along with the His-tag in the carboxyl-terminal site. Fluorescence scanning of the same gel displayed corresponding fluorescence bands, confirming the success of Anap incorporation into each mutant in comparison to WT (*Figure 28B*). A great feature of Anap-labelled scFv is that they can be readily detectable under the UV light in Gel doc imager, such as in a microcentrifuge tube or gel (*Figure 40A-B*).

Before proceeding to investigate the fluorescence properties, mutants were further characterised to confirm the expression and functionality of scFv mutants. The mutants were tested by Western blotting and enzyme

immunoassay. Distinct bands were detected using HRP-labelled anti-His antibody by Western blot experiment (*Figure 28C*). Though all the mutants had shown highly distinct bands by Coomassie staining, L3-A mutant showed a slightly less intense band in the Western Blotting analysis. In the same experiment, the sample containing the L98-F mutant also showed a second distinguishable band just below the 28 kDa mark. The anti-His antibody possibly detected this band due to nonspecific binding. There was no equivalent fluorescence band detected during the fluorescence scanning of the SDS-PAGE gel, confirming the absence of any possible Anap incorporated truncated product (*Figure 28B*).

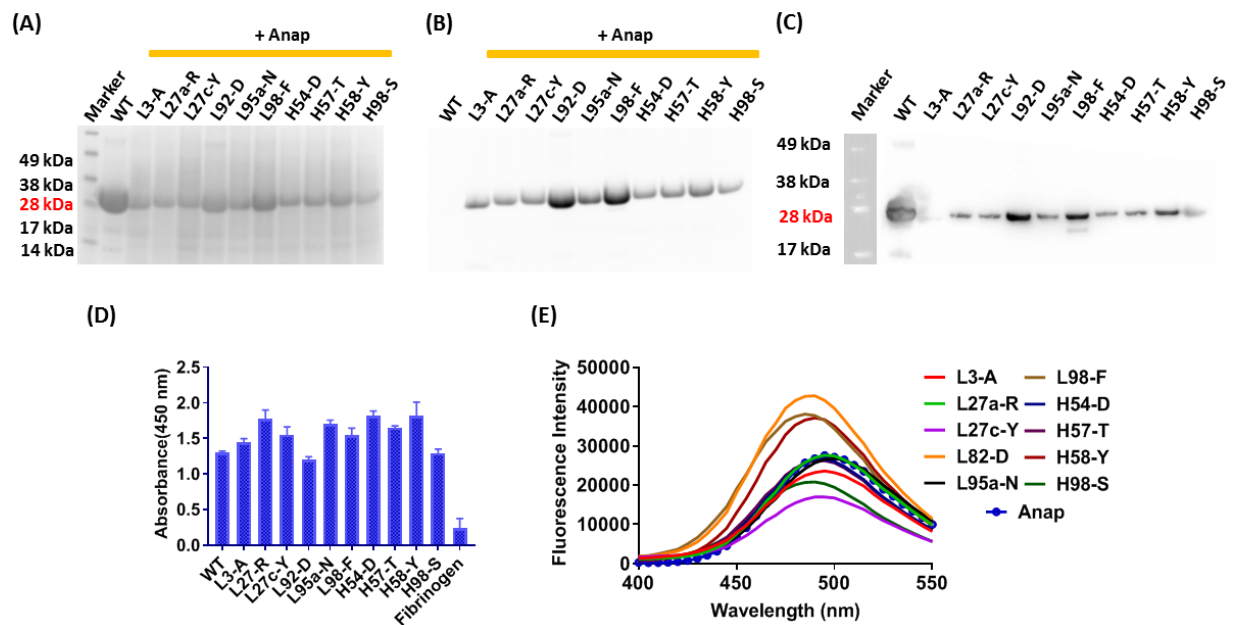


*Figure 28: Characterisation of Anap labelled anti-cTnI scFv mutants. (A) SDS-PAGE Coomassie staining confirms protein expression. Protein bands just above an apparent MW of 28 kDa corresponds well with the theoretical molecular weight of anti cTnI scFv (29 kDa). (B) Efficient incorporation of Anap is confirmed by fluorescence scanning of the same gel, which shows the corresponding fluorescence band. (C) The Western blotting analysis also confirms the expression of each mutant by detection of the His-tag and (D) ELISA confirms that each mutant is functional in its ability to bind to the cognate cTnI peptide. The negative control (fibrinogen) with the WT scFv does not show significant binding to fibrinogen. Error bars are calculated as  $\pm$ SD,  $n=3$  in figure D. (E) Fluorescence spectra of anti-cTnI scFv mutants at a normalised concentration of 100 nM. The mutants show unique emission spectra compared to free Anap in PBS buffer (dotted blue line).*

The performance of the expressed scFv mutants was further validated by indirect enzyme-linked immunoassay (*e.g.* ELISA). Exposure of each of the mutants towards surface coated cTnI peptides revealed some variations in the binding signal in comparison to the WT scFv constructs. The binding variability was attributed to variation in mutant concentrations since they contain some level of contaminating protein as mentioned. The detected absorbance at 450 nm, as illustrated in *Figure 28D*, confirmed substantial binding activity towards cTnI peptide when detected with HRP-labelled anti-His antibody. The result suggested that each scFv mutant was able to bind to the cTn1 target, but differences in their binding affinity needed to be analysed using kinetic assays. The findings also suggested that even though most mutation sites occurred within the CDR regions, incorporation of Anap into these sites did not affect protein expression or alter their binding specificity to a substantial degree. This was also consistent with the previous finding where Tyr was mutated to Anap at H53Y position of H-CDR2 in the anti-EGFR scFv antibody for fluorescence labelling ([Section 4.1](#)). These findings suggested that incorporation of a UAA within the binding sites had a negligible effect on antigen binding; however, a site that is critical for folding or associated to functionality (hence described as non-permissible) must be avoided.

Fluorescence properties of mutants were characterised by fluorescence spectroscopy. The fluorescence of each mutant was evaluated by measuring the emission spectra from a normalised concentration of 100 nM anti-cTnI scFv mutant. Upon excitation of the mutants, each of the mutants demonstrated a unique emission spectrum with a variable peak emission wavelength between 485-500 nm. The observed emission spectra were position specific representing the local polarity of Anap in each mutant. Additionally, significant fluorescence intensity differences were also observed between the scFv constructs.

Presumably, the intensity differences were attributed due to the incorporation of Anap in different positions within the structure (*Figure 28E*) leading to either variation in the local environment of Anap or degree of exposure to the excitation source. Despite the normalisation of scFv concentrations, there might be an inequivalent distribution of mutants due to the presence of impurities which might also contribute to some extent in the variation of fluorescence intensities.

Following characterization of the individual mutants, next, each mutant was then titrated with cTnI antigen to search for binding-induced spectral changes. Fluorescence spectra of each of the Anap-incorporated variants were assayed in the presence of the cTnI peptide (*e.g.* 0-50 nM). Results revealed that most of these mutants (L3-A, L27a-R, L92D, L95a-N, H54-D, H57-T207, and H98-S) did not show any significant fluorescence spectral shift (*Figure 29A-D, F, G, I*). The H58-Y mutant showed minor fluorescence intensity variation and a 1-2 nm wavelength blue-shift (*Figure 29H*). Surprisingly, a decreasing trend of fluorescence intensity with approximately 5-10 nm blue wavelength shift was observed for L98-F mutant (*Figure 29E*). It was assumed that binding of the target peptide might cause shielding of Anap fluorescence, whereas the wavelength shift was due to the decreasing polarity of the local environment.

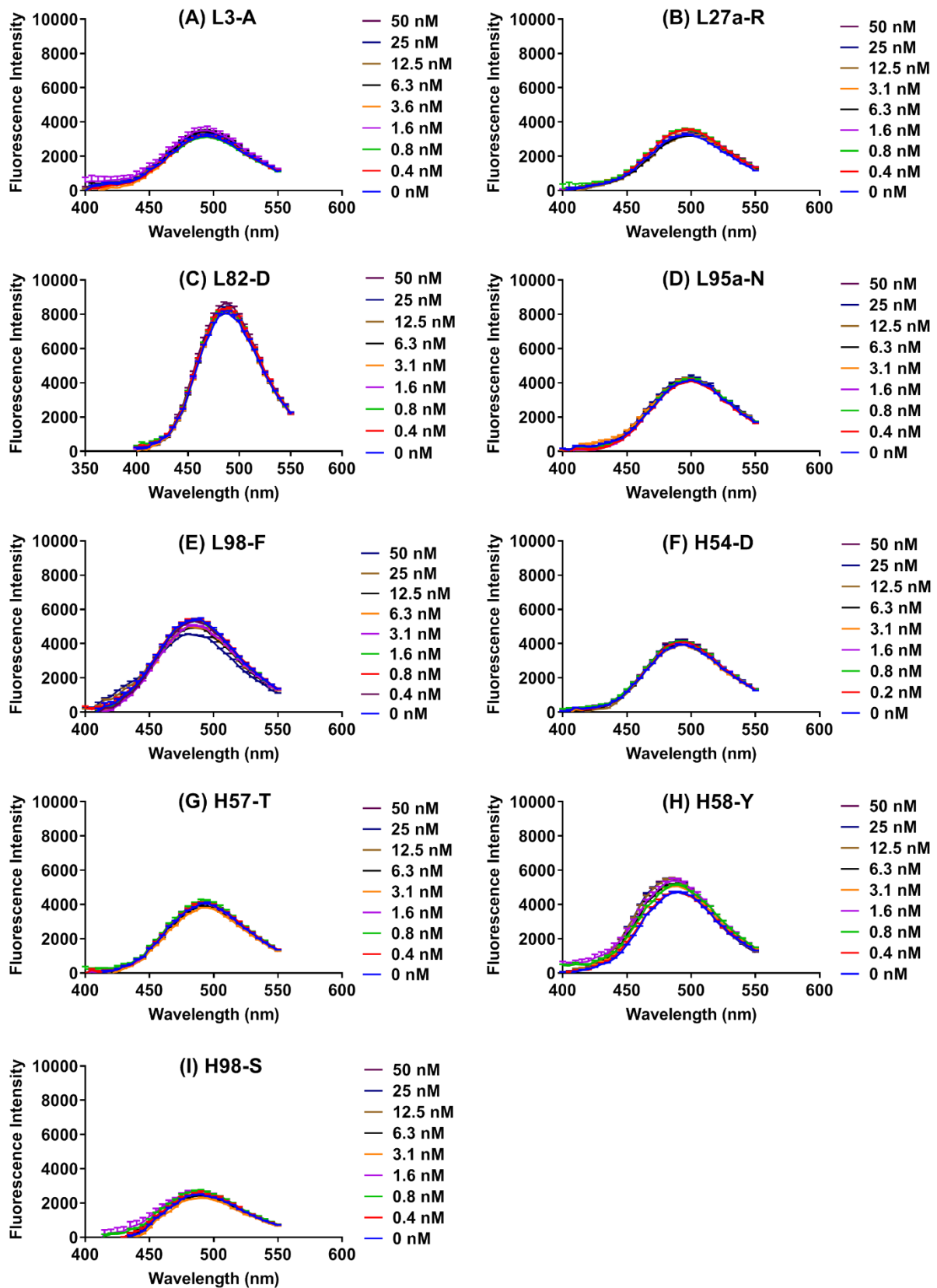


Figure 29: Response of anti-cTnI-Anap scFv mutants to the cTnI peptide. No significant fluorescence changes were detected for L3-A, L27a-R, L82-D, L95a-N, L98-F, H54-D, H57-T, H58-Y and H98-S (A-G). Error bars are represented in  $\pm$  SED,  $n=3$ .

In contrast, the L27c-Y mutant exhibited significant antigen-dependent spectral changes of up to 20 nm blue-shift and fluorescence intensity enhancement, similar to EGFR detection by H53Y biosensor. *Figure 30A* shows L27c-Y mutant was almost saturated in the presence of 50 nM cTnI peptide. Subsequently, the binding affinity of L27c-Y to the target peptide was calculated. The binding curve was generated to quantify the limit of detection (LOD) based on wavelength shift caused by the antigen concentrations. The curve was fitted by calculating a centre wavelength based on fitting a Lorentzian peak for each spectrum (*Equation 1*) followed by performing nonlinear regression to investigate statistical variability.[\[248\]](#) The LOD was calculated by describing the lowest concentration of cTnI generating signal higher than 1.65 standard deviations above the baseline as mentioned in chapter 4. The LOD was determined as ~1.8 nM in the PBS buffer for cTnI peptide detection (*Figure 30B*). The EC<sub>50</sub> value (defined as half maximal response to an antigen) of L27c-Y was determined as 4.7 nM for a cTnI peptide. L27c-Y was the most fluorescently active construct among the mutants despite minor fluorescence modulation (~5 nm blue-shift) also observed for L98-F and H58 mutants. Hence, L27c-Y was selected for further characterisation in the following sections.

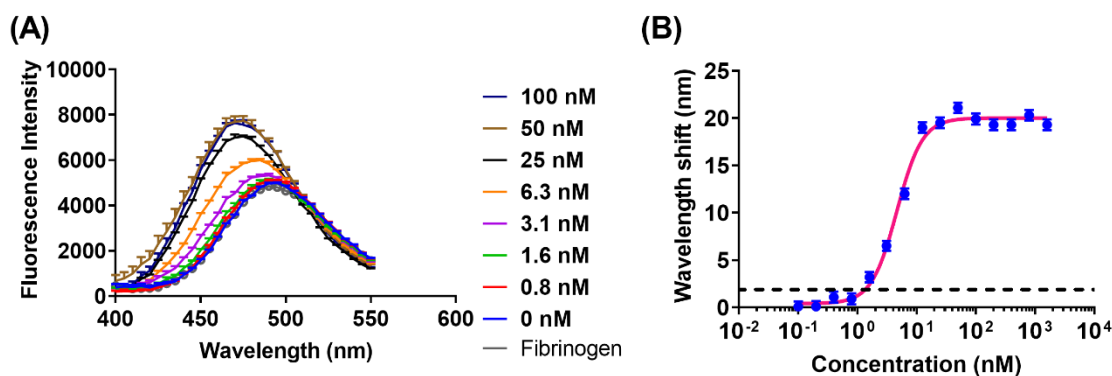


Figure 30: Detection of the cTnI peptide in PBS buffer. (A) The L27c-Y mutant showed an excellent dose-dependent response with an increase in fluorescence intensity and a wavelength shift. Error bars are represented as  $\pm$  SEM,  $n=3$ . Fibrinogen used as a non-specific reference which showed an identical overlap with 0 nM L27c-Y mutant. (B) Titration curve shows a wavelength shift ( $\sim 20$  nm) dependent on the cTnI peptide concentration. Error bars are represented as  $\pm$  SD,  $n=3$ .

Following the success of troponin peptide detection, the experiments were repeated using full-length human cTnI protein to investigate if there is a systematic effect on fluorescence spectral changes based on antigen size. The cTnI protein used in these experiments was obtained (Life Diagnostics, Cat#1210) as a complex with the rabbit skeletal muscle troponin-C (TnC), which is also found as cTnI-TnC complex in blood.[\[231\]](#) TnC conveys solubility to cTnI and protects it from protease activity while it does not interfere with the antibody binding.[\[249, 250\]](#) The effect of cTnI protein binding on the fluorescence of L27c-Y variant was assessed by applying a similar titration experiment design as described previously, where different concentrations of cTnI protein (0-40 nM) were exposed to this mutant. Notably, the results showed a more significant blue wavelength shift of up to 37 nm but did not display a significant fluorescence intensity variation (*Figure 31A*). In contrast, the pattern of fluorescence change occurred during the 20 nm blue-shift caused by peptide exposure was quite different to the 37 nm shift caused by exposure to full-length cTnI protein.

Presumably, interaction of sticky hydrophobic cTnI protein with the L27c-Y mutant affected Anap polarity to even a greater extent (448 nm).

Next, the activity of the L27c-Y biosensor was tested in diluted human plasma. A similar wavelength shift (~37 nm) was also observed when detecting cTnI in spiked human plasma (5% v/v), presented in *Figure 31C-D*. Following the formula and method described for cTnI peptide detection ([Section 5.2.2](#)) the EC<sub>50</sub> value for cTnI protein was determined as 6.1 nM and 9.3 nM in the PBS buffer and 5% human plasma respectively. The LOD was calculated as 0.6 nM (0.02 µg/mL) and 1.8 nM (0.06 µg/mL) in PBS buffer and human plasma respectively. The resultant detection limit falls within the nanomolar range which is within the range of many blood-borne biomarkers;[\[251\]](#) however, the calculated LOD is less sensitive compared to LOD of currently available complex cTnI detection assays and POC devices (*Table 7*). Further research is required to either incorporate a signal amplification process to detect the bound complexes at low concentrations or to identify different sets of biomarkers that have physiological ranges within the detection limit of the technique.

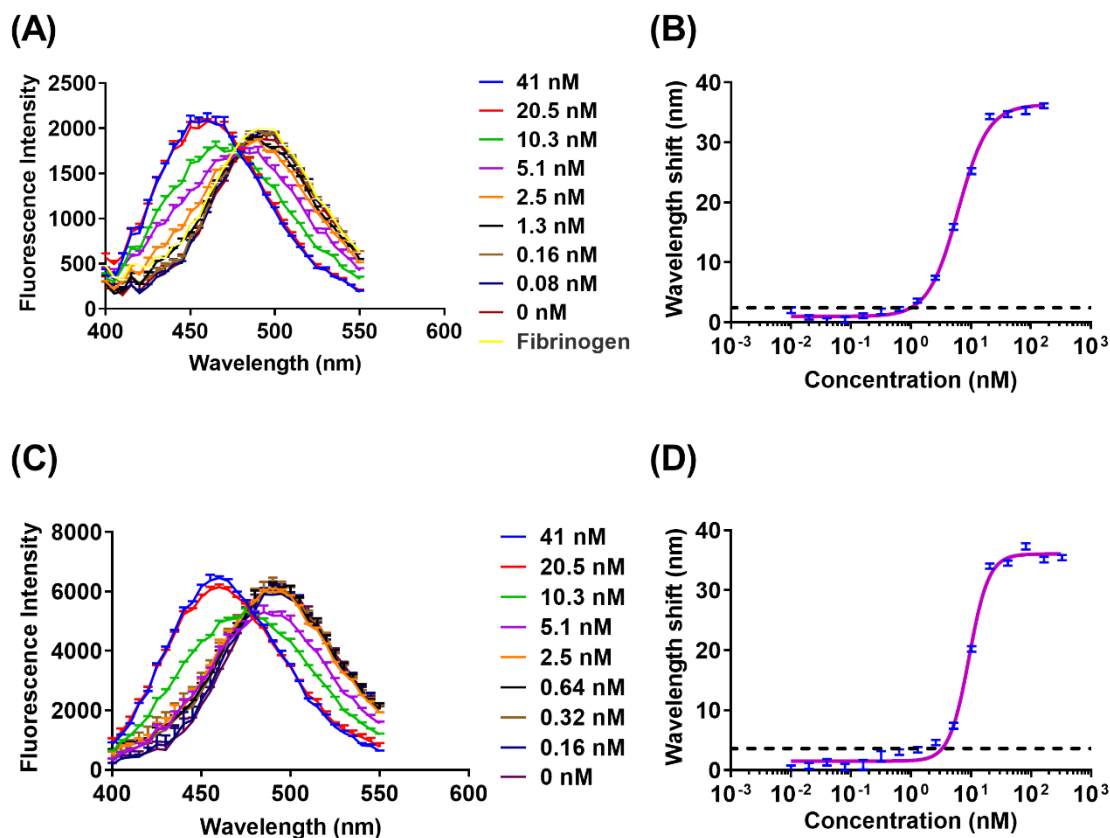
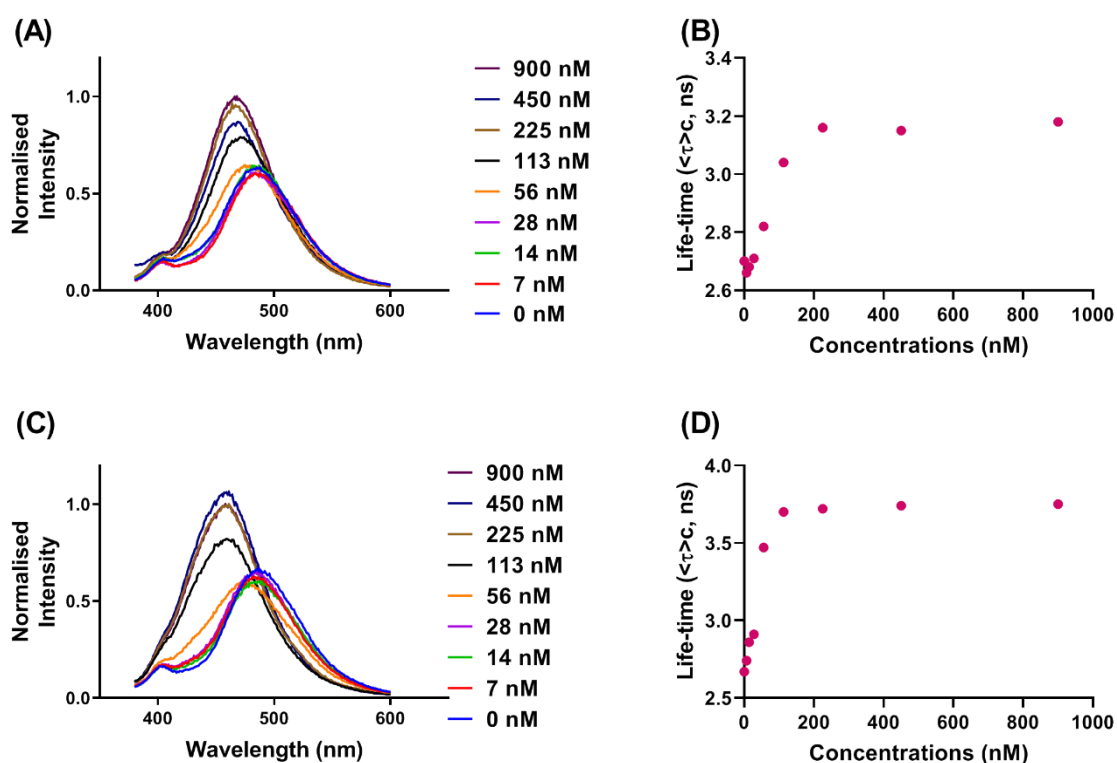


Figure 31: Detection of full-length cTnI protein in PBS buffer and human plasma. About 0 nM to 40 nM of purified cTnI protein was titrated with 15 nM of L27c-Y mutant. (A) Exposure of L27c-Y mutant to different concentrations of cTnI protein shows dramatic wavelength shift from 485 nm to 445 nm. Addition of fibrinogen instead of cTnI protein to L27c-Y mutant did not show any shift in emission spectra. Panel (B) shows the antigen-dependent wavelength shift in PBS buffer. (C) Testing the response of L27c-Y in 5% human plasma and (D) dose-dependent response of L27c-Y. Error bars are represented as  $\pm$  SEM in figure (A) and (C);  $\pm$ SD in (B) and (D);  $n=3$ .

The fluorescence lifetime of Anap (incorporated in the L27c-Y) in the presence of ligand was extensively examined to gain further insight on the mechanism of the polarity-dependent wavelength shift. Anap incorporated in the L27c-Y mutant displayed bi-exponential lifetime ( $\tau$ ) which was consistent with the previous findings (Chapter 4 manuscript supporting table S2, [Section 4.2](#)). While steady-state measurements showed a blue-shift of up to 20 nm (*Figure 32A*; consistent with *Figure 30*), the time-correlated fluorescence analysis

showed a concomitant increase in the average lifetime in response to the consistent wavelength shift as presented in *Figure 32B*.



*Figure 32: Time-correlated single photon counting (TCSPC) measurement to determine the fluorescence lifetime of Anap labelled L27c-Y mutant. Steady-state fluorescence detection of L27c-Y mutant in the presence of cTnI peptide (A) and protein (C). An average fluorescence lifetime in the presence of different concentrations of peptide and protein  $t$  is represented in (B) and (D) respectively.*

Similarly, the lifetime of the L27c-Y scFv mutant was investigated in the presence of several concentrations of human cTnI protein (0-900 nM). The protein-bound mutant showed a dose-dependent increase in lifetime concomitant with the increasing wavelength shift (*Figure 32C-D*). The lifetime analysis of L27c-Y in the presence of the peptide or protein showed increased lifetime while consistently showing blue-shift of emission which strongly correlates with the decreasing polarity of Anap microenvironment. These findings suggest that the blue-shift of emission wavelength was due to the local polarity change in the vicinity of the Anap dye during the bound and unbound state. The wavelength

shift by cTnI protein showed an initial decrease of fluorescence intensity which was possibly related to the interconversion between the protein-bound and unbound L27c-Y molecule (*Figure 32C*); however, the lifetime of complex consistently increased (*Figure 32D*) which is independent of fluorescence intensity.<sup>[252-254]</sup> The calculated average fluorescence lifetime of L27c-Y in the presence of peptide and protein is presented in *Table 9*.

*Table 9: Lifetime measurement in the absence and presence of cTnI peptide and protein. Anap incorporated in L27c-Y showed bi-exponential lifetime represented as  $\tau_1$  and  $\tau_2$ . Quantum yield ( $\Phi_{flu}$ ) was also calculated in the presence and absence of ligand. The average lifetime was calculated based on equation 2 mentioned in the manuscript presented in chapter 4. Statistical significance was analysed by the chi-squared test ( $\chi^2$ ).*

	$\tau_1$ (ns) (%)	$\tau_2$ (ns) (%)	$\Phi_{flu}$	$\langle\tau\rangle_c$ (ns)	$\chi^2$
L27c-Y	1.60 (75)	3.98 (25)	0.43	2.67	1.16
L27c-Y +PEPTIDE	2.10 (66)	4.22 (34)	0.53	3.18	1.10
L27c-Y +PROTEIN	3.33 (89)	5.69 (11)	0.67	3.75	1.11

Despite the evidence linking polarity dependence of Anap emission based on antigen binding, it is unclear whether the polarity difference was induced due to the conformational change in the scFv near the mutation site. The peptide-bound crystal structure of anti-cTnI scFv antibody showed a slight deviation in the region of L92D-L95a-N in CDR3 of the light chain (*Figure 26*) in comparison to the un-bound scFv structure. However, within the region of L27c-Y, no such deviation was observed between the structures, suggesting that binding of antigen surface was the critical event, removing solvent molecules from nearby the L27c-Y site, reducing the local polarity and causing spectral blue-shift and lifetime increase. Apart from the change in emission spectra, it would be useful to investigate any excitation wavelength shifts which might occur due to the change in the local environment. However, no such evidence was observed when measuring Anap in different solvents for quantification of quantum yield (*Table*

9 and *supplementary figure 2* in chapter 4). It may be noted that excitation of Anap across a range of wavelengths (e.g. 350-375 nm) did not show any difference in the emission spectra.

Emission wavelength shift is a preferred method of detection over fluorescence intensity change. Fluorescence intensity is an arbitrary number that can be affected by various factors (e.g. instruments and samples); however, emission wavelength remains distinctive regardless of instruments or influences from the external factors.<sup>[255]</sup> A compromised position is to monitor fluorescence intensity changes for two different species in the same molecule (ratiometric sensing); however, this usually requires the inclusion of two separate dyes, one of which is insensitive to antigen binding. The reproducibility of the polarity-induced Anap blue-shifts was tested in a different instrument by measuring the fluorescence spectra of L27c-Y in the presence of cTnI peptide (*Figure 32A*) and protein (*Figure 32C*) in an Agilent fluorescence spectrophotometer (Varian Cary Eclipse) instead of Tecan fluorescence spectrometer. Results showed that the maximum wavelength shift remained identical (*Figure 30A* and *Figure 31A-C*) in both types of instruments despite variations in fluorescence intensities. The variations of fluorescence intensities could be due to several factors such as measurement of fluorescence in different volumes (plate reader vs cuvette), instruments (Tecan vs Cary eclipse) and variations in concentrations (15 nM vs 300 nM). Nonetheless, the above finding signifies the universal use of wavelength shift as the basis of protein quantification in different instruments.

Apart from the detection of the fluorescence shift in a spectrophotometer, the emission shift can also be visualised by a fluorescence imager. When the L27c-Y mutant (5  $\mu\text{M}$ ) was incubated with different concentrations of the cTnI protein (0, 3, 4, 6, and 7  $\mu\text{M}$ ), it was observed that there was a consistent colour shift (towards blue) as presented in *Figure 33*. Higher concentrations of L27c-Y

and cTnI protein were chosen to get a brighter image as the image was captured in a UV gel imager. It may be noted that a high concentration of L27c-Y and full-length cTnI protein was used for this experiment to ensure detectable signals in UV gel imager. The finding demonstrates the potential applicability of the reported biosensors for *ex vivo* or *in vivo* imaging by using a fluorescence microscope and or camera.

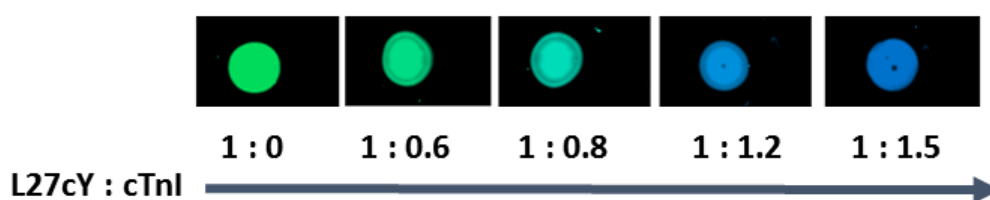


Figure 33: Emission wavelength shift imaging in UVP (BioSpectrum) gel imager. While L27c-Y alone (no antigen, 0  $\mu$ M) shows a greenish-yellow colour, the addition of cTnI antigen resulted in a colour change in response to increase of concentrations (0, 0.6, 0.8, 1.12 and 1.5 times).

As L27c-Y was identified as the most optically active mutant, the binding affinity of this molecule was compared to its WT counterpart. An important reason for a thorough analysis of binding kinetics was to investigate whether genetic incorporation of Anap into the binding site of anti-cTnI scFv mutant had any detrimental effect on binding to the target. Despite detecting the binding specificity of L27c-Y mutant towards cTnI peptide along with other constructs in ELISA (Figure 28C; appendices Figure 44), further analysis was required for precisely estimating the affinity of the mutants by BLI or SPR based (*e.g.* Biacore) methods.

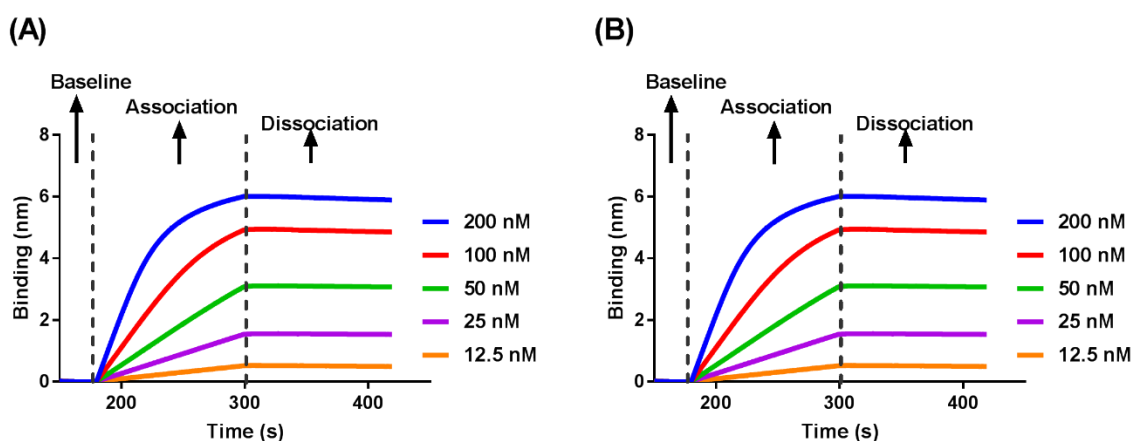


Figure 34: Binding kinetics analysis by biolayer interferometry. The affinity between WT (A) and L27c-Y (B) was compared by measuring their association and dissociation with cTnI peptide.

Binding kinetics analysis in BLI was initially conducted by immobilising the WT and L27c-Y mutant on Ni-NTA biosensors followed by detection of cTnI protein. However, evidence of nonspecific cTnI protein adsorption to Ni-NTA biosensors complicated the measurement of association and dissociation rate. The cTnI protein is known to be hydrophobic[256] (see the hydrophobicity determined by ProtScale in [Section 7.7](#)) and tends to interact non-specifically with both glass and plastic surfaces (information obtained through personal communication with Dr Chris Chadwick, President, Life Diagnostics). Therefore, an alternative approach was sought where cTnI peptide (instead of full-length cTnI proteins) was biotinylated for immobilisation on streptavidin biosensors followed by capturing the scFv mutants (*Figure 34*). The binding kinetics between the peptide and scFvs revealed a nanomolar affinity for both the WT (~1.05 nM) and L27c-Y (~2.94 nM) mutant (*Table 10*). The difference in  $K_D$  between WT and L27c-Y was less than three-fold and within a nanomolar range; hence, the affinity differences between these molecules were considered as minimal.[257]

Table 10: Affinity of constructs determined by binding kinetics analysis in BLI.

Sample ID	$K_D$ (nM)	$K_a(M^{-1}S^{-1}) \times 10^4$	$K_d(S^{-1}) \times 10^4$
WT anti-cTnI scFv	1.05±0.3	10.4±0.14	1.12±0.31
L27c-Y anti-cTnI scFv	2.94±0.2	4.32±0.13	1.27±0.32

The stability of both the L27c-Y and WT mutants was investigated by dynamic light scattering (DLS). Size distribution (by size or intensity) is widely known for ascertaining the presence of more than one species (*e.g.* aggregates) within the samples. The aggregation profile of L27c-Y and WT anti-cTnI scFv was interrogated by performing size distribution study in DLS (*Figure 35*). The data analysed in Zetasizer software denoted almost identical correlogram based on size distribution, confirming the presence of a single species in the L27c-Y scFv sample (*Figure 35A*). It may be noted that as the scFv mutants could not be entirely purified through SEC chromatography; hence, the presence of minor low molecular weight proteins was evident. The presence of impurities was reflected as a small shift in the correlation function in comparison to the WT scFv. The calculated hydrodynamic diameter for WT and L27c-Y (~6 nm; *Figure 35B*) was also consistent with the anti-EGFR WT and mutant scFvs (~4 nm; Chapter 4 manuscript figure 3, [Section 4.1](#)).

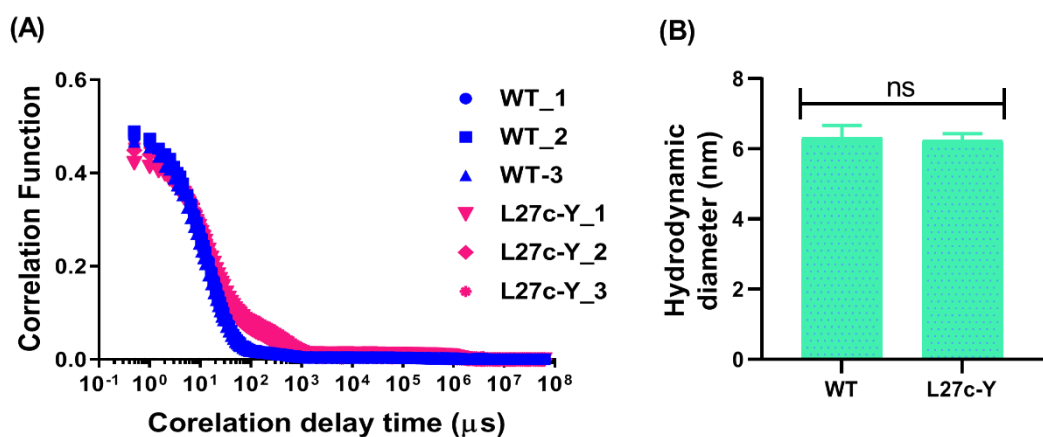


Figure 35: Size distribution study for WT and L27c-Y mutant in DLS. (A) The correlogram shows three sets of data acquired for determining the correlation function. (B) The average hydrodynamic diameter shows non-significant difference confirming the stability of the WT and L27c-Y mutant. Statistical significance was analysed by multiple *t*-tests. WT\_1-3 and L27c-Y\_1-3 are replicates of the respective samples ( $n=3$ ), and error bars are shown as  $\pm SEM$ .

Though Anap has excellent fluorescence properties for polarity-dependent biosensing, the excitation wavelength of this fluorophore falls within the UV region ( $<400$  nm). Human blood has a high degree of auto-fluorescence at this emission spectral range (400-500 nm) when excited at 350 nm.<sup>[258-260]</sup> Thus, the limitation of this fluorophore became apparent when samples were prepared that contained human plasma as a biologically and clinically relevant sample matrix. Due to this, the target antigen could only be detected in 5-10% human plasma by H53Y and L27c-Y biosensors, and low concentrations of antigen detection in  $>10\%$  human plasma was not possible. The difficulties were simply due to the inability to differentiate the fluorescence of Anap from the background auto-fluorescence of human plasma. This problem may be solved by replacing Anap with a near-infrared solvatochromic fluorophore.<sup>[162, 261]</sup> Past literature showed that the near-infrared fluorophores operate in a region with significantly less background auto-fluorescence compared to UV range fluorophores.<sup>[262]</sup> By reducing the background signal, it may be possible to improve the sensitivity of

the biosensors. Unfortunately, polarity sensitive near-infrared or infrared emitting fluorophores are less abundant both in the literature and commercially, and rarely display the same degree of blue-shifting in comparison to Anap (*i.e.* an 80 nm shift for Anap across a range of solvents).<sup>[263]</sup> There are a few possible dyes that may be used in future such as DY640 and DY641.<sup>[264]</sup> Preliminary characterisation of these dyes was conducted in different solvents and included in the appendices of this thesis ([Section 7.9](#)).

In order to replace Anap with a suitable near-infrared fluorophore via a clickable UAA, solvent accessibility to the site of fluorophore labelling is critical for efficient labelling. Solvent accessibility is an essential aspect of designing this type of fluorescent biosensor. Firstly, the solvent accessibility to the UAA incorporation site is vital for measurable changes in polarity. Secondly, the efficiency of *in vitro* fluorescence labelling via clickable UAA (*e.g.* pAzF or pAcF) is mostly dependent on the exposure of the UAA functional group to the complementary group in the fluorophore. Hence, the incorporation site needs to be exposed to some degree on the surface for efficient biosensor development. The solvent accessibility of a site in proteins can be measured by many bioinformatics tools such as GETAREA, NetSurfP, and PyMOL.<sup>[265-267]</sup> While visualising the structure with the PyMOL, the H53Y and L27c-Y mutant sites were found to be partially solvent accessible. The solvent accessibility of the mutants was validated further by running the PDB structure of anti-cTnI scFv in GETAREA 1.0 beta which predicted L27cY as a solvent-exposed residue ([Section 7.10](#)). Similarly, the H53Y site was also found to be solvent exposed using NetSurf (GETAREA 1.0 beta can only predict based on the PDB structure, so NetSurf was used for the anti-EGFR scFv homology model structure). The solvent accessibility was tested experimentally by labelling of L27cY scFv antibody with Cy5 fluorescent dye via pAzF UAA. The pAzF UAA was

incorporated to L27c-Y site of anti-cTnI scFv antibody by following a similar procedure described in [Section 3.3.2.2](#) except the utilisation of L27c-Y plasmid. Fluorescence scanning in SDS-PAGE analysis confirmed efficient labelling with DBCO-Cy5 fluorophore to the L27cY-pAzF scFv (*Figure 36*). This experiment was conducted by Dr Christian Fercher, Post-doctoral Researcher at The University of Queensland, Australia.

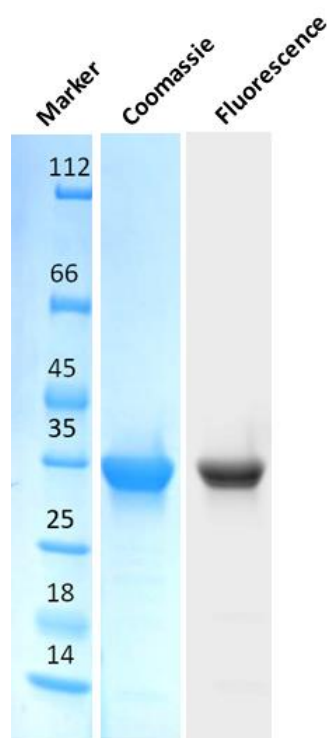


*Figure 36: Cy5 fluorescence labelling of the L27c-Y site via pAzF UAA. SDS-PAGE demonstrates the expression and purity of the mutant as a single dominant band is present between 25-35 kDa (expected MW is ~29 kDa). Lane 2 shows the Coomassie staining of L27c-Y pAzF labelled with DBCO functionalised Cy5 dye. Lane 3 shows the fluorescence scanning of the same gel suggesting efficient conjugation of Cy5 dye.*

Finding a general site for fluorophore incorporation in antibody fragments to develop a polarity-dependent biosensor is highly desirable to remove the laborious task of screening. The site screening process for both the anti-EGFR and anti-cTnI scFv included a range of mutation sites such as antigen binding sites, consensus and framework regions. It was found that only the second Tyr

residues in the HCDR2 of anti-EGFR (H53Y) and the LCDR1 of anti-cTnI scFv (L27c-Y) exhibited fluorescence change in response to antigen. Since these sites are part of the CDR region, they are not conserved entirely across the scFv antibodies. However, these two sites are located at the start of CDRS as can be seen when looking at the conformation of the two antibody fragments where antigen-antibody binding complex starts to form (*Figure 37*). Hence, the Tyr residues in these CDRs which are actively involved in complex formation could be a promising target for fluorophore incorporation. Simultaneously, further research needs to be conducted to validate the generic target site among other scFv antibodies for fluorophore incorporation.

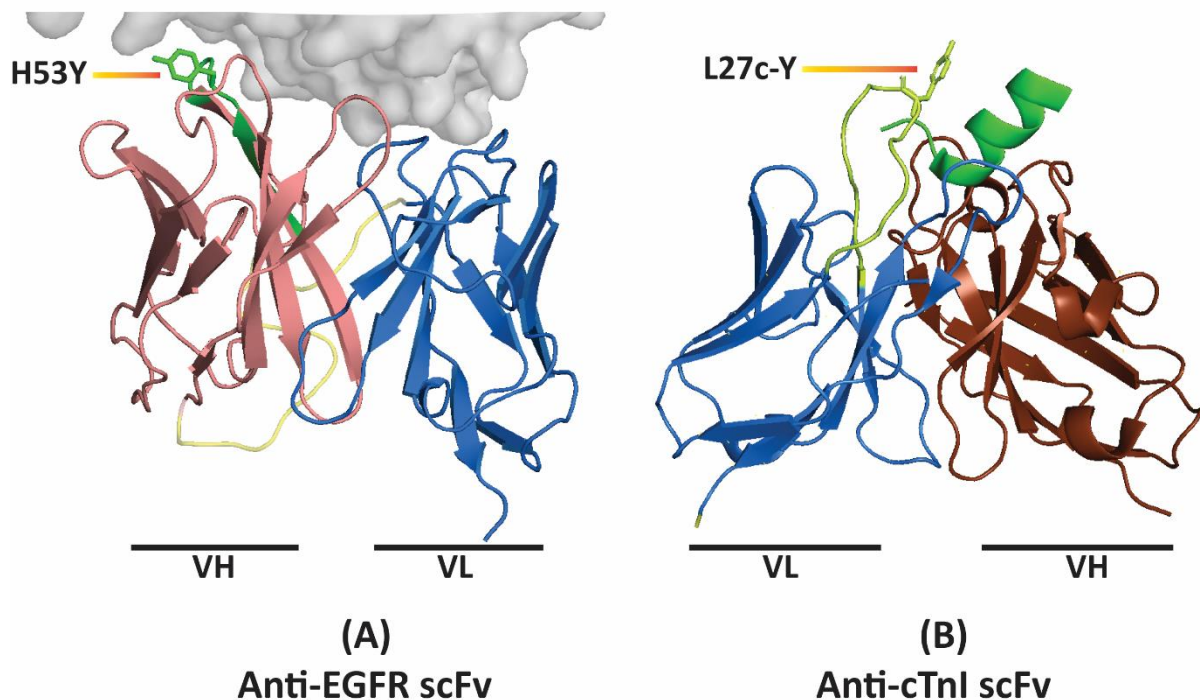


*Figure 37: Comparison of the most optically active mutants. (A) The H53Y mutation site is highlighted in the anti-EGFR scFv and (B) position of L27c-Y mutation site in the anti-cTnI scFv.*

### 5.3.2 Surface immobilisation of H53Y and L27c-Y biosensors

The functionality of H53Y and L27c-Y biosensors upon immobilisation onto the carbon nanotube, silica nanoparticles and agarose-beads surfaces were tested in this section. There are a variety of solid phase surfaces which could be used; however, due to the time restrictions only these surfaces were tested. Instead of using a traditional strategy of random surface immobilisation, an oriented immobilisation approach via His-tag (through Ni-NTA chemistry) was implemented.

#### 5.3.2.1 Immobilisation of H53Y on carbon nanotube and silica nanoparticles

Carbon nanotubes have been utilised widely in biomedical application due to their unique optical, mechanical, electrical and thermal properties. Single-walled carbon nanotubes (SWCNT) with different chiralities and size show different infrared emission spectra (900-1400 nm) depending on the excitation wavelength (600-900 nm). Carbon nanotubes were found to be exquisitely sensitive to the local microenvironment.<sup>[268]</sup> Williams *et al.* showed detection of biomarkers by immobilising antibodies on the surface of SWCNTs.<sup>[166]</sup> They reported that binding of target antigen onto the immobilised antibodies-SWCNT complexes resulted in a significant wavelength shift. The change in wavelength was due to the exclusion of water molecules from the SWCNT surface which was reflected in blue wavelength shift (*Figure 38*).

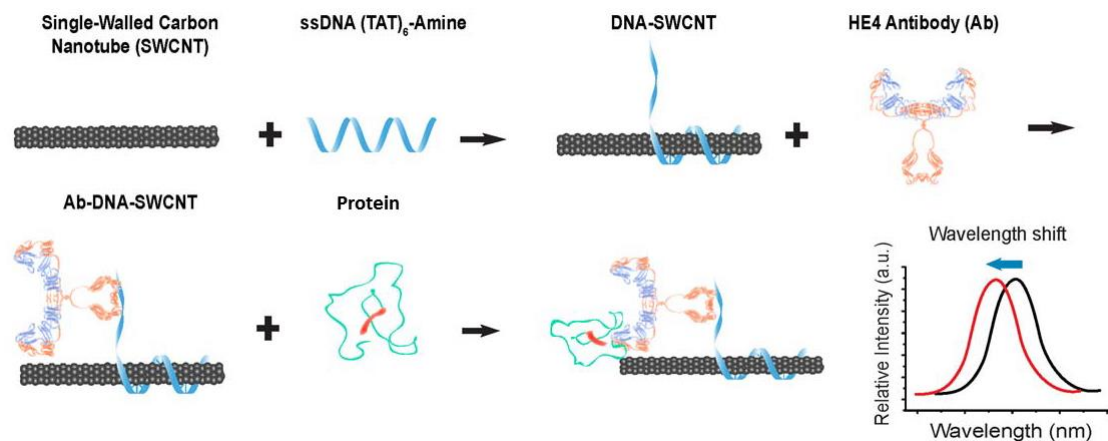


Figure 38: Scheme demonstrates surface immobilisation of antibody on SWCNT through functionalised short oligonucleotides. The interaction of antigen-antibody on the sensor surface resulted in a change of optical properties of SWCNT which was reflected in wavelength shift. Figure adapted from Williams et al.<sup>[166]</sup>

Immobilisation of H53Y mutant on SWCNT was performed to gain a fundamental understanding of the behaviour of this biosensor on the carbon nanotube surface. To test this aim, NTA conjugated single-stranded DNA oligonucleotides (TAT)<sub>6</sub> were attached to SWCNTs. Experimentally, these ssDNAs facilitated solubilisation of SWCNTs into solutions. The absorbance spectra of hybridised SWCNT-NiNTA-H53Y before and after conjugation with H53-Y showed similar absorbance spectra confirming the presence and stability of the complex (*Figure 39A*). A size distribution study with DLS showed an increase in the size of the SWCNT-NiNTA-H53Y complex (*Figure 39B*) compared to the control (unconjugated ssDNA-SWCNT). The presence of H53Y was also confirmed by fluorescence measurement of the SWCNT-NiNTA-H53Y complex in Tecan fluorescence spectrometer. Following a similar approach, as mentioned in the preceding chapters, excitation of the H53Y-ssDNA-SWCNT at 350 nm produced a characteristic Anap emission peak at 480 nm (*Figure 39C*). Upon addition of the EGFR target, a blue-shift of ~30 nm (~450 nm) was observed which was consistent with ~20 nm shift in solution phase detection of EGFR

(Figure 39D). These results suggest that immobilisation of H53Y on the SWCNTs itself did not change the local polarity of the Anap-labelled scFv, because the emission peak remained similar to that observed for protein in solution. The blue-shift occurred as expected with the addition of target analyte, suggesting that solid-phase assays based on similar approaches are possible. Potentially, these proteins might also be useful for exploring the local environment of candidate surfaces for biological applications.

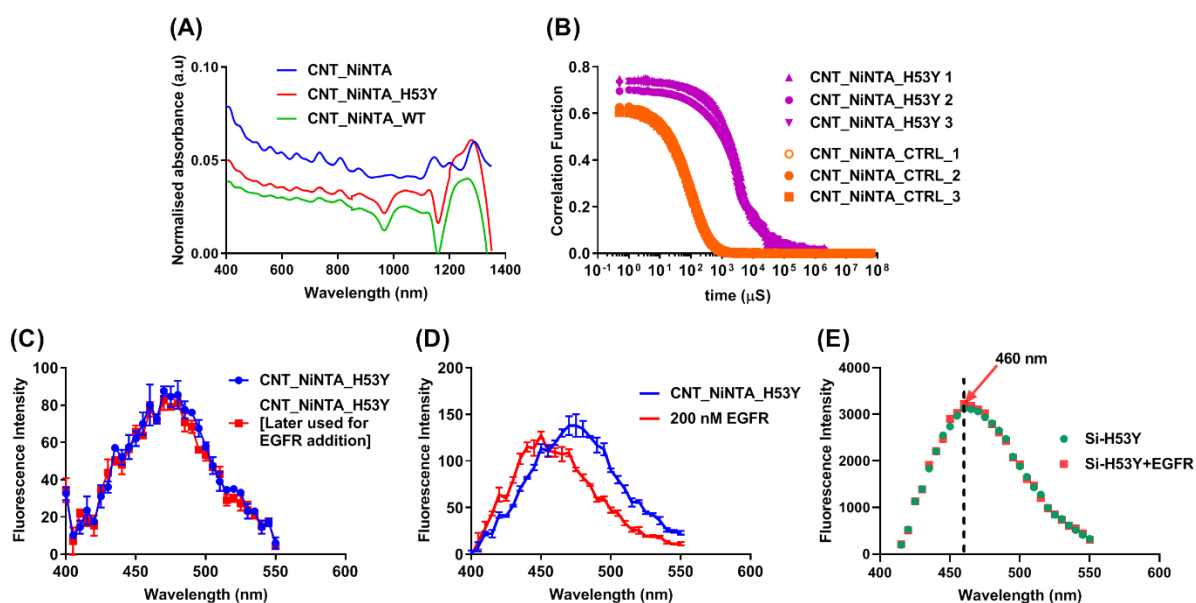


Figure 39: Immobilisation of H53Y biosensor onto carbon nanotube. (A) Absorbance spectra indicated different excitation peaks comparable between SWCNT-NiNTA-H53Y and SWCNT-NiNTA (control). (B) DLS size distribution study confirmed surface attachment of H53Y as represented by decreased correlation decay. (C) Fluorescence measurement of SWCNT-NiNTA-H53Y showed maximum emission at 480 nm, similar to free H53Y scFv in the PBS buffer. (D) Addition of 200 nM EGFR ligand showed about ~30 nm wavelength shift. (E) Immobilisation of H53Y on Ni-NTA functionalised silica particles showed an already shifted emission spectra of L53Y and addition of EGFR target did not have any further effect. Error bars were calculated as  $\pm$  SEM and  $n=3$ .

Apart from the immobilisation on SWCNT nanoparticles, immobilisation of H53Y mutant onto commercially available Ni-NTA functionalised 300 nm silica nanoparticles was also investigated. Fluorescence measurement was carried out in the presence and absence of EGFR ligand (Figure 39E). Interestingly, H53Y-

immobilised silica revealed a significantly shifted spectra (460 nm) before EGFR addition, and further addition of EGFR target did not cause any additional modulation. A possible explanation of this finding could be the loss of H53Y's structure on the silica surface, indicated by a change in Anap fluorescence, which in turn indicates a significant change in polarity in the CDRs. Literature suggests that protein stability on the nanoparticle surface could be improved by introducing a layer of poly(ethylene glycol) [PEG] molecule.[269] Future studies may improve the immobilisation of this biosensor with the generation of silica nanoparticles containing PEG layer on the outer surface.

#### **5.3.2.2 Immobilisation of L27c-Y on agarose beads**

The L27c-Y mutant was immobilised on Ni-NTA functionalised agarose beads and exposed to different concentrations of cTnI protein. This resulted in a blue-shift of emission spectra in a dose-dependent manner as presented in *Figure 40*. The highest spectral shift was observed in the highest concentrations (300 nM) which was similar to the observed blue-shift (~25 nm) in solution phase detection systems. This finding suggests that L27c-Y sensor did not lose its activity and remains functionally active on the surface.

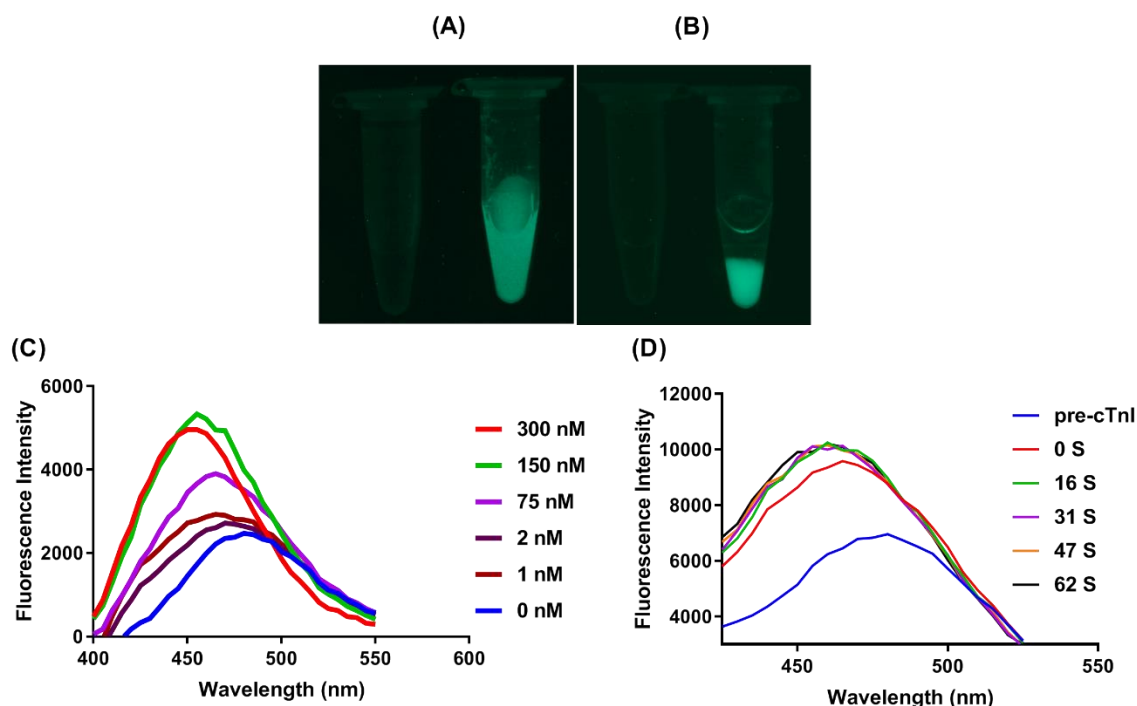


Figure 40: Immobilisation of L27c-Y sensor onto agarose beads. (A-B) Visualisation of L27c-Y attached agarose beads. Whereas image (A) shows bright fluorescence of agarose-L27c-Y complex in the PBS buffer (tube 2), centrifugation of the tube resulted in sedimentation of the complex depicted as a pellet (tube 2 in image B). Tube 1 used as a control containing PBS buffer only. Image captured under UV light (365 nm) in Biospectrum UVP imager. (C) The surface immobilised L27c-Y mutant shows maximum emission at 485 nm, similar to spectra of free L27c-Y in the PBS buffer. Addition of cTnI full-length protein (1-300 nM) leads to about ~25 nm of wavelength shift. (D) Kinetic analysis of L27c-Y immobilised on agarose beads in the presence of cTnI protein (300 nM). Fluorescence was continuously measured for 0-62 seconds as illustrated in the figure.

Following the detection of antigen from the surface-immobilised L27c-Y biosensor, an investigation was carried out to understand whether the surface attachment has altered the rate of antigen-antibody complex formation. It was found that in solution, the rate of antigen-antibody formation was too fast to allow kinetic analysis with available instruments. Fast reaction kinetics were also evident from the BLI measurement where saturation of L27c-Y scFv binding to its immobilised peptide occurred mostly within 45 sec. However, following the addition of cTnI protein to agarose-immobilised scFvs, the relevant emission peak shifted ~25 nm over a period of 1 minute (Figure 40 D).

## 5.4 Chapter 5 summary

The proof-of-concept developed in chapter 4, by using the anti-EGFR scFv as a model, was extended for the detection of cTnI biomarker in this chapter. While the selection of fluorophore incorporation site for anti-EGFR scFv was determined based on a homology model structure, a crystal structure-guided design was employed for cTnI. Based on the conformation difference in the ligand-bound and unbound crystal structure of anti-cTnI scFv, ten possible mutation sites were selected for Anap fluorophore incorporation. These mutants were expressed in mammalian cells using the optimised method in chapter 3 and 4. The mutants were purified using affinity and gel filtration chromatography followed by thorough characterisation of mutants with common bioanalytical methods to confirm the functionality and stability.

While measuring the fluorescence of the mutants in the presence of peptide ligand, only L27c-Y mutant was found to be suitably optically active showing a 20 nm blue-shift in a dose-dependent manner, strikingly similar to EGFR detection. The capability of this biosensor was validated further by successful detection of full-length human cTnI where the mutant showed a superior response towards full-length cTnI protein producing an even more significant wavelength shift (~37 nm) at the saturation peak. Time-resolved fluorescence studies provided further insight into the mechanism behind this polarity-based fluorescence sensing. The activity of the L27c-Y biosensor was tested in human serum and was able to replicate similar data.

Further characterisation was conducted to translate this solution-phase detection to solid-phase detection system by investigating the functionality of this mutant on agarose beads via oriented immobilisation with the use of Ni-NTA and His-tag affinity chemistry. It was evident that the surface attachment did not cause any significant damage to the L27c-Y biosensor. The immobilised

mutant was found to be fully functional which could be supported by the fact that the mutant was able to produce the expected wavelength shift in the presence of cTnI protein, quite similar to the solution-based measurement in PBS buffer. Carbon nanotubes and silica nanoparticles were also utilised as model surfaces. The H53Y biosensor remained functional on the carbon nanotube surface; however, when immobilised on the silica nanoparticles the sensor was optically inactive. Despite these preliminary studies, further systematic investigations are required in future to explore the full potential of these biosensors in solid-phase detection.

# Chapter six

## 6. Conclusions and Future Studies

---

The aim of this project was to develop a fluorescent biosensor by exploiting engineered antibodies as biorecognition elements that can detect target ligands in a single step without the need for further reagents. The literature survey revealed a significant research gap for polarity-based fluorescent biosensors that can produce ligand-dependent wavelength shifts. Instead of traditional fluorescence labelling strategies, UAA technology was employed for site-specific fluorophore incorporation into recombinant scFv proteins. A proof-of-concept was developed by incorporating a solvatochromic fluorescent UAA (Anap) near the epitope binding sites of anti-EGFR scFv. UAA incorporation sites were screened based on a homology model structure to identify the best position for polarity dependent response. The scFv mutants with various UAA incorporation sites were expressed mostly in mammalian cells followed by thorough characterisation to investigate their stability and performance. These mutants were tested for antigen-mediated changes in fluorescent properties. The concept was further applied into anti-cTnI scFv for detection of a human cardiac biomarker.

The results obtained show that the expressed anti-EGFR scFv mutants were similar to the wild-type protein in terms of structure and function. Though most of the mutants were purified using Protein L column, a few mutants could not be sufficiently purified. The purified mutants were tested broadly for identity, functionality, and conformity. The top three functional mutants were exposed to the EGFR target, and it was found that the H53Y mutant showed a significant blue-shift of approximately 20 nm upon EGFR binding. The fluorescence of the mutant was then further characterised to gain an understanding of the observed solvatochromic shift in response to ligand binding. Time-resolved fluorescence characterisation revealed a change of microenvironment of Anap dye from polar to a moderately non-polar state. The mutant was also tested in human plasma and found to be fully functional.

Moreover, the H53Y mutant was immobilised on a solid-phase surface (carbon nanotubes) and retained full functionality. These results together suggest the successful development of a novel polarity-dependent fluorescent biosensor by employing engineered antibodies.

Extended research was conducted to transform the developed concept for the detection of another clinically significant biomarker, cTnI. Several sites on an anti-cTnI scFv were chosen for Anap fluorophore incorporation based on a structure-guided design. Following expression, purification and characterisation of these mutants, they were exposed to the target ligand. Binding of a peptide fragment of cTnI to most of the mutants did not produce substantial spectral variations, except for the L27c-Y mutant which produced a 20 nm blue-shift. Exposure of this mutant to the full-length cTnI protein showed an even greater emission wavelength shift of about 37 nm. Extensive fluorescence characterisation of this mutant established the underlying mechanism of polarity dependent spectral modulation. The above findings of H53Y and L27c-Y biosensor development demonstrate the establishment of a promising polarity-based sensing principle that can be designed by incorporating a solvatochromic fluorophore near the antigen binding sites of engineered antibodies. Additionally, the sensor can be designed irrespective of the availability of scFv structures.

Despite two novel biosensors being reported in this PhD thesis, further studies are required to refine possible clinical applications. One possible application of H53Y biosensors could be *ex vivo* imaging for the detection of EGFR overexpression that could be useful for clinical diagnostics. Currently, various cancers (*e.g.* lung cancer) are detected based on EGFR mutation studies following the collection of cells from patients via biopsy.[\[270, 271\]](#) It may be possible to detect EGFR expression on the cell surface using the H53Y biosensor based on either qualitatively through fluorescence colour change (blue or red-

shift) or quantitatively by measuring simple fluorescence wavelength shift. As an example, Antczak *et al.* showed detection of EGFR activity in EGFR overexpressing cell lines in 384-well plate format based on fluorescence imaging.[272] Detection of EGFR on the cell surface under the microscope or simple imaging apparatus fitted with a proper excitation source could lead to an alternative detection strategy for an EGFR expression test. Hyper-spectral imaging can also be practically implemented to image antibody binding on the tumour surface based on the fluorescence of the H53Y biosensor.[166]

Improving the sensitivity of the reported L27c-Y biosensor will be necessary to meet the needs of a clinically-relevant cTnI assay. This may include developing a one-step cTnI biosensor which will reduce not only the time and cost associated with the assay but also could lead to a POC testing device. The sensitivity of this sensor could be improved by replacing Anap with a solvatochromic near-infrared fluorophore to reduce background signals.[273, 274] Apart from the replacement of fluorophore, sensitivity could also be improved by immobilising the L27c-Y biosensors on suitable surfaces. For instances, Krismastuti *et al.* demonstrated fluorescence intensity enhancement upon surface immobilisation to improve the sensitivity of a fluorescent biosensor.[275] In this study, the group functionalised a fluorescent peptide onto porous silicon resonant microcavity for the improved detection of matrix metalloproteinases where the photonic structure of this microcavity enhanced fluorescence intensity. Despite the possibility of signal improvement, the method developed here could potentially be better matched for the detection of nanomolar range (>1 nM) biomarkers (*e.g.* C-reactive protein)[251] because the LOD determination in this method is mostly dependent on the antigen-antibody complex formation. Hence, the higher the affinity of the scFv antibody, the lower the LOD could be achieved.

Future exploration may include miniaturisation of the cTnI detection system in order to develop a research or commercial prototype sensors. Such prototype sensors can be designed by using a small fluorimeter (instead of large fluorescence spectrometer used in a research laboratory, some examples of miniaturised fluorimeter are included in [Section 7.12](#)) that can measure the fluorescence of L27c-Y biosensors. Samples can be analysed in these miniaturised devices using a flow channel or micro/nano size cuvette. As an example, Tsujikawa *et al.* have demonstrated the potential use of fluorimeter where an ultra-Q-body biosensor was shown as a model (*Figure 41*).[\[276\]](#)

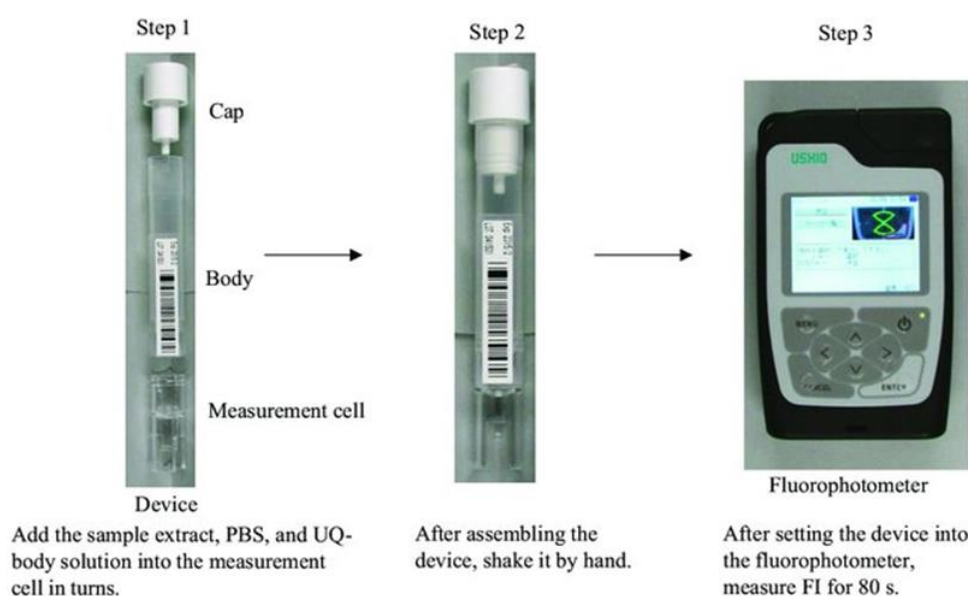


*Figure 41: Determination of fluorescence intensity (FI) change by the fluorimeter. The Ultra Q-body was shown as a model here for analysing samples. This figure was reproduced from Tsujikawa *et al.**

The conducted PhD study has discovered a one-step novel detection system that can be used as an alternative to conventional immunoassays. The concept can be explored further to target different diagnostic markers[\[251, 277\]](#) and can be integrated into a wide range of platforms such as paper-based test strips and multiplexed assays.[\[35, 278\]](#) Both the reported biosensors have the

potential for applications in many biosensing fields such as the creation of a solid-phase biosensor. Immobilisation of these sensors on a suitable surface could be useful for the detection of target ligand from sample flow (*e.g.* micro-fluidics devices for real-time detection), and development of POC technologies.[[44](#), [279](#), [280](#)] Despite the promising aspect of the developed technology, several issues need to be addressed in future. One of the current drawbacks of the development process is identifying a general site in scFv antibodies for fluorophore incorporation. Future studies may include finding a general conserved site among scFv antibodies to eliminate the mutant screening process. Even though Anap has shown promising results during concept development, the fluorescence properties of this dye, *i.e.* excitation in the UV region complicates measuring antigen concentrations in human blood due to the high fluorescence background signal.[[258](#), [259](#)] This is supported by the fact that the Anap signal was undetectable in a higher percentage of human plasma. The developed biosensors showed a reasonable level of detection (~ nanomolar range in plasma); however, some of the biomarkers are present in blood at low concentrations, and hence an improvement of LOD is required. Future studies that improve the signal-to-noise ratio by processes such as replacing Anap with a near-infrared solvatochromic dye may open opportunities for improved highly sensitive *in vitro* and *ex vivo* biosensors for the detection of target biomarkers.[[162](#), [281](#)]

In conclusion, a novel fluorescent biosensor was developed by exploiting engineered antibodies where detection of antigen relied on the emission wavelength shift instead of fluorescence intensity. The aims and hypotheses, identified in the literature review, have been well executed in each of the experimental chapters. Further research is required for developing a proto-type biosensor with an improved detection limit for possible applications in clinical diagnostics.

## **7. Appendices**

---

## 7.1 DNA sequence of anti-EGFR scFv

**GCCACC**ATGGGCTGGTCCTGCATCATCCTGTTTCTGGTGGCTACCGCCACCGGCGTGCACTCC  
**(TAG)**CAGCTCCAGCTGCAGGAATCCGGCCCTGGCCTGGTCAAGCCCTCCGAGACACTGTCCCTG  
ACCTGCACAGTGTCCGGCGGCTCTGTGTCTCCGGCGACTACTACTGGACCTGGATCAGA  
CAGTCCCCCGCAAGGGCCTGGAATGGATCGGCCACATCTACTACTCCGGCAACACCAAC  
TACAACCCAGCCTGAAGTCCCGGCTGACCATCTCCATCGACACCTCCAAGACCCAGTTC  
TCCCTGAAGCTGTCTCCGTGACCGCGCTGACACCGCTATCTACTACTGCGTGC GGAC  
AGAGTGACCGGCGCCTTCGACATCTGGGGCCAGGGCACCATGGTCACCGTGTCTCTGGC  
GGCGGAGGATCTGGCGGAGGTGGAAGCGGAGGCGGAGGCTCCGACATCCAGATGACCCAG  
TCCCCCTCCAGCCTGTCCGCCTCCGTGGGCGATAGAGTGACCATCACCTGTCAGGCCTCC  
CAGGACATCTCCAACCTGAACCTGGTATCAGCAGAAGCCCGGCAAGGCCCCCAAGCTG  
CTGATCTACGACGCCTCCAACCTGGAAACCGGCGTGCCCTCTCGGTTCTCCGGCTCTGGC  
TCTGGCACCGACTTTACCTTCACCATCTCCAGCCTCCAGCCCGAGGATATCGCCACCTAC  
TTTTGCCAGCACTTCGACCATCTGCCCTGGCCTTCGGCGGAGGCACCAAGGTGGAAATC  
AAG**CACCACCACCATCACCAC****(TAG)**TAA

**GCCACC** Kozak Sequence

**ATGGGCTGGTCCTGCATCATCCTGTTTCTGGTGGCTACCGCCACCGGCGTGCACTCC** Leader Sequence

**CACCACCACCATCACCAC** His Tag;

**TAG:** UAA Incorporation site; TAG codon was incorporated either N- or C-term for Anap incorporation.

**TAA-**Stop Codon

## 7.2 Commonly used tRNA-aaRS for UAA incorporation

Table 11: Commonly used UAA and their respective tRNA/tRNA synthetase sequence containing plasmid; some of the tRNA-aaRS are commercially available from *addgene.com*.

UAA	Plasmid name	Expression systems	Labelling/cr eating to...	Reason for UAA incorporation	Reference/Commercial availability
<b>pAcF</b>	pSup-pAcPhe	Bacterial	Alexa 488 (aminooxy)	pAcF incorporated to Fab, labelled with Alexa 488, then linked with biotin, used to attenuate Her2 for breast cancer	[282]
<b>pAcF</b>	pEVOLpAcPhe	Bacterial	Alexa 488	Dual labelling	[121]
<b>pAcF</b>	pEVOLpAcF	Bacterial	Bispecific Fab	Bispecific Fab through PEG linker	[122]
<b>pAcF</b>	pBKS-pAcPheRS	Bacterial	Alexa 488	Dual labelling single molecule FRET (smFRET)	[196]
<b>Alkynyll ysine &amp; pAcF</b>	<i>pACYCDuet-AIKRS-tRNAUCA</i> And <i>pRSFDuet-AcFRS-tRNACUA</i>	Bacterial	Cyanine 3 (Cy3) and cyanine 5 (Cy5)	Dual labelling smFRET	[283]
<b>pAcF</b>	Unknown	Mammalian	Alexa 488	Antibody drug conjugates; HER2 antibody, LXR	[124, 284]
<b>pAcF</b>		Mammalian	siRNA	Antibody polymer conjugates for siRNA delivery	[123]
<b>oMeY, eBK</b>	pShax-Pyl	Mammalian	Alexa 488	Anti-HER2 dual labelling with two different dyes	[285]
<b>BpF, oMeY</b>	pEYCUA-YRS	Mammalian	None	Mammalian expression protocol	[286]
<b>pMeF, pAcF, pBpF, pIpF, pAzF</b>	pCNA4- <i>EcTyrRS</i> <i>EcTyrRS</i> variants are Y37V/D182S/F183M (pMpaRS),	Mammalian		Mammalian expression protocol	[217]

<b>pPpF</b>	Y37I/D182G/F183M/L186 A  (pApaRS), Y37G/D182G/F183Y/L186M (pBpaRS), Y37I/D183S/F183M (pIpaRS),  Y37L/D182S/F183M/L186A (pAzpaRS), and Y37S/D182T/F183M/L186V (pPpaRS)				
<b>Dansylalanine</b>	pLeuRSB8T252A	Yeast	Fluorescent amino acids	Incorporated to hSOD protein to monitor unfolding	[139]
<b>BpF</b>	pEVOL-pBpF	Bacterial	Biotin	Biotinylation	[287] [288] Addgene.org
<b>pAzF</b>	pEVOL-pAzF	Bacterial	None	Bacterial expression protocol	[288] Addgene.org
<b>pCNPhe</b>	pULTRA-CNF	Bacterial	Infrared probe	Ligand binding	[289] Addgene.org
<b>Abk</b>	pDULE-ABK	Bacterial	crosslinking	Protein-protein interaction	[290] Addgene.org
<b>Anap</b>	pAnap	Mammalian / yeast	Fluorescent amino acids	Incorporated in EGFP for subcellular localization	[191] Addgene.org
<b>pBoF</b>	pMAH-POLY	Mammalian	Fluorescent amino acid	Detection of analytes	[291] Addgene.org

*UAA acronym: Abk: 3'-azibutyl-N-carbamoyl-lysine (AbK); eBK: e-tert-Boc-lysine; pBoF: boronophenylalanine; oMeY: o-Methyl-Tyrosine; pMeF: p-methoxy-phenylalanine; pBpF: p-benzophenylalanine; pAcF: p-aceto-phenylalanine; pIpF: p-Iodo-phenylalanine; pAzF: p-Azido-phenylalanine; pPpF: p-propargyloxy-phenylalanine.*

### 7.3 Extract of DNA sequence analysis for anti-EGFR scFv mutants

DNA sequencing of the anti-EGFR scFv sequence was performed at Australian Genome Research Facility (AGRF), University of Queensland. The obtained sequence was justified by multiple sequence alignment (Clustal Omega)

with the original sequence. The sequence of C-term and N-term are presented below:

**(A) C-term mutant**

```

AGRF_seq      -----GCCACCATGGGCTGGTCTCTGCATCATCCTGTTTCTGGTGGCTACCGCCACCGGC
Ori_seq      aagcttgccaccatgggctggtcctgcacatcctgtttctggtggctaccgccaccggc
                *****
AGRF_seq      GTGCACTCCGAGCTCCACCACCACCATCACCACCAGCTCCAGCTGCAGGAATCCGGCCCT
Ori_seq      gtgcaactccgagctccaccaccaccatcaccaccagctccagctgcaggaatccggccct
                *****
AGRF_seq      GGCTGGTCAAGCCCTCCGAGACACTGTCCCTGACCTGCACAGTGTCCGGCGGCTCTGTG
Ori_seq      ggcctggtcaagccctccgagacactgtccctgacctgcacagtgctccggcggtctgtg
                *****
AGRF_seq      TCCTCCGGCGACTACTACTGGACCTGGATCAGACAGTCCCCCGCAAGGGCCTGGAATGG
Ori_seq      tcctccggcgactactactggacctggatcagacagtcccccgcaagggcctggaatgg
                *****
AGRF_seq      ATCGCCACATCTACTACTCCGGCAACACCAACTACAACCCAGCCTGAAGTCCCGGCTG
Ori_seq      atcgccacatctactactccggcaacaccaactacaacccagcctgaagtcccggtg
                *****
AGRF_seq      ACCATCTCCATCGACACCTCCAAGACCCAGTTCTCCCTGAAGCTGTCTCCGTGACCGCC
Ori_seq      accatctccatcgacacctccaagaccagtctccctgaagctgtcctccgtgaccgcc
                *****
AGRF_seq      GCTGACACCGCTATCTACTACTGCGTGCGGGACAGAGTGACCGGCGCCTTCGACATCTGG
Ori_seq      gctgacaccgctatctactactgctgctgctgggacagagtgaccggcgcttcgacatctgg
                *****
AGRF_seq      GGCCAGGGCACCATGGTCACCGTGTCTCTGGCGGCGGAGGATCTGGCGGAGGTGGAAGC
Ori_seq      ggccagggcaccatggtcaccgtgtcctctgctggcgcgaggatctggcgagggtggaagc
                *****
AGRF_seq      GGAGGCGGAGGCTCCGACATCCAGATGACCCAGTCCCCCTCCAGCCTGTCCGCCTCCGTG
Ori_seq      ggaggcgaggctccgacatccagatgaccagtcctccctccagcctgtccgcctccgtg
                *****
AGRF_seq      GCGATAGAGTGACCATCACCTGTCAGGCCTCCAGGACATCTCCAACCTGAACTGG
Ori_seq      ggcgatagagtgaccatcacctgtcaggcctccaggacatctccaactacctgaactgg
                *****
AGRF_seq      TATCAGCAGAAGCCCGCAAGGCCCCCAAGCTGCTGATCTACGACGCTCCAACCTGGAA
Ori_seq      tatcagcagaagcccgcaaggccccaagctgctgatctacgacgctccaacctggaa
                *****
AGRF_seq      ACCGGCGTGCCCTCTCGGTTCTCCGGCTCTGGCTCTGGCACCGACTTTACCTTCACCATC
Ori_seq      accggcgtgccctctcggttctccggctctggctctggcacccgactttaccttcaccatc
                *****
AGRF_seq      TCCAGCTCCAGCCCGAGGATATCGCCACCTACTTTTGCCAGCACTTCGACCATCTGCC
Ori_seq      tccagctccagcccgaggatatcgccacctacttttgccagcaacttcgaccatctgcc

```

```

*****
AGRF_seq CTGGCCTTCGGCGGAGGCACCAAGGTGGAAATCAAGTAGTAA-----
Ori_seq ctggccttcggcgggagggaccaaggtggaatcaagtccggaggaggcgatccgaggtg
*****

```

**(B) N-term mutant**

```

AGRF_seq -----ACCGCCACCGGT
Ori_seq aagcttgccaccatgggtgtgctcctgcacatcctgtttctggtggctaccgccaccggc
*****
AGRF_seq GTCCA-----TTCCTAGCAGCTCCAGCTGCAGGAATCCGGCCCT
Ori_seq gtgcaactccgagctccaccaccaccatcaccaccagctccagctgcaggaatccggccct
** ** * * * *****
AGRF_seq GGCCCTGGTCAAGCCCTCCGAGACACTGTCCCTGACCTGCACAGTGTCCGGCGGCTCTGTG
Ori_seq ggcctggtcaagccctccgagacactgtccctgacctgcacagtgtccggcggtctgtg
*****
AGRF_seq TCCTCCGGCGACTACTACTGGACCTGGATCAGACAGTCCCCGGCAAGGCCTGGAATGG
Ori_seq tcctccggcgactactactggacctggatcagacagtcccccgcaagggcctggaatgg
*****
AGRF_seq ATCGGCCACATCTACTACTCCGGCAACACCAACTACAACCCAGCCTGAAGTCCCGGCTG
Ori_seq atcgccacatctactactccggcaacaccaactacaacccagcctgaagtccggcgtg
*****
AGRF_seq ACCATCTCCATCGACACCTCCAAGACCCAGTCTCCCTGAAGCTGTCTCCGTGACCGCC
Ori_seq accatctccatcgacacctccaagaccagtctcctgaagctgtcctccgtgaccgcc
*****
AGRF_seq GCTGACACCGCTATCTACTACTGCGTGCGGGACAGAGTGACCGGCGCCTTCGACATCTGG
Ori_seq gctgacaccgctatctactactgctgctgctgacagagtaccggcgcccttcgacatctgg
*****
AGRF_seq GGCCAGGCACCATGGTCACCGTGTCTCTGGCGGCGGAGGATCTGGCGGAGGTGGAAGC
Ori_seq ggccagggcaccatggtcaccgtgtcctctggcggcgaggatctggcggaggtggaagc
*****
AGRF_seq GGAGGCGGAGGCTCCGACATCCAGATGACCCAGTCCCCCTCCAGCCTGTCCGCTCCGTG
Ori_seq ggaggcggaggctccgacatccagatgaccagtccccctccagcctgtccgcctccgtg
*****
AGRF_seq GGCGATAGAGTGACCATCACCTGTGAGGCTCCAGGACATCTCCAACCTGAACCTGG
Ori_seq ggcgatagagtgaccatcacctgtcaggcctccagacatctccaactacctgaactgg
*****
AGRF_seq TATCAGCAGAAGCCCGCAAGGCCCCCAAGCTGCTGATCTACGACGCTCCAACCTGGAA
Ori_seq tatcagcagaagcccggcaaggcccccaagctgctgatctacgacgcctccaacctggaa
*****
AGRF_seq ACCGGCGTGCCCTCTCGGTCTCCGGCTCTGGCTCTGGCACCGACTTTACCTTCACCATC
Ori_seq accggcgtgccctctcggttctcggctctggctctggcacccgactttaccttcaccatc
*****

```

```

AGRF_seq      TCCAGCCTCCAGCCCAGGATATCGCCACCTACTTTTGCCAGCACTTCGACCATCTGCC
Ori_seq      tccagcctccagccccgaggatatacgccacctacttttgccagcacttcgaccatctgcc
*****
AGRF_seq      CTGGCCTTCGGCGGAGGCACCAAGGTGGAATCAAGCACCACCATC--A---TCATCATT
Ori_seq      ctggccttcggcggaggcaccaaggtggaatcaagtcggaggaggcgatccgaggtg
***** .* .. .: . *.: .*
AGRF_seq      AATCTAGA-----
Ori_seq      cagctggtcgaaagtggcggcgactggtcaaacctgggggcagcctgaagctgagctgc
.* **.*:

```

## 7.4 Cleavage of anti-EGFR scFv sequence by Trypsin

The cleavage sites of anti-EGFR scFv antibody sequence by Trypsin enzyme digestion was predicted by PeptideCutter bioinformatics tool. These theoretical fragments were used as a guide for the detection of sequence in peptide mass fingerprinting data analysis.



Figure 42: Prediction of Trypsin cleavage sites by ExPASy: PeptideCutter program.

## 7.5 Crystallisation experiments of anti-cTnI scFv

Crystallisation experiments were performed by Dr Paul Conroy, however for reference purpose a brief description is included below.

*Purification and crystallisation* - The anti-cTnI scFv was expressed and purified for crystallography as described previously (Conroy 2014). The scFv was

complexed with an excess of peptide (synthesised by GhL, China) for 2 hrs followed by separation of the antibody-peptide complex by size exclusion chromatography on an S75 16/60 column (GE) equilibrated in TBS (25 mM Tris pH7.4, 150 mM NaCl with protease inhibitors). The complex was concentrated to 10 mg.ml<sup>-1</sup> and crystallised by hanging-drop method. Diffraction quality crystals were obtained in Proplex™ (Molecular Dimensions) condition C12 (0.1 M MES pH 6.5, 0.2 M potassium iodide, 25% PEG 4000). The crystals were flash-cooled in liquid nitrogen using 25% (v/v) glycerol as the cryoprotectant.

*Structure and Refinement* - Data sets were collected at the Australian Synchrotron MX1 and MX2 beamlines at 100K. The data were merged and processed using XDS, POINTLESS and SCALA. Five percent of the data set was flagged as a validation set for calculation of the Rfree. Molecular replacement (MR) of was carried out using 4P48 and residues corresponding to the peptide from 1J1E (chain C) as search probes. One molecule was found per asymmetric unit cell and an initial model was generated using PHENIX. Model building was performed using COOT, and refinement was performed using PHENIX. Crystallographic and structural analysis was performed using the CCP4 suite.

## 7.6 Cloned sequence of anti-cTnT scFv antibody

*Table 12: The amino acid sequence of anti-cTnI scFv. Mutation sites are highlighted in red underlined, Ser-Gly linker is highlighted in green, the His-tag is highlighted in cyan and anti-HA tag is highlighted in grey colour.*

```

ALTQPSSVSANPGETVKITCSGGGRYYDGSYYYGWYQQKSPGSAPVTVIYE
NTRKPSNIPSRFSGSKSGSTATLTITGVRAEDEAVYYCGSADDDNMNPTIFGA
GTTTLTVLGQSSRSSSGGSSGGGSAVTLDESGGGLQTPGGALSLVCKASG
FTFSSYGMQWVRQAPGKGLEWVAGIQNDDTGTYYGA AVKGRATISRDNQQ
STVRLQLNNLRAEDTGTY YCAKDASSDGGYGGDSIDAWGHGTEVIVSSTSG
QAGQHHHHHHGAYPYDVPDYAS

```

## 7.7 Extract of DNA sequencing for anti-cTnI scFv mutants

The DNA sequence of all the anti-cTnI scFv WT and mutants were verified by Sanger DNA sequencing method. For a reference purpose only, sequence of L3-A and L27c-Y mutants are presented here. Multiple sequence alignment shows excellent match with the wild type anti-cTnI scFv sequence. TAG codon is highlighted in red (mutation site).

### A) L3-A

```

cTnI-scFv      GCTAGCCACCATGGAAACCGACACTCTGCTGCTATGGGTCTGCTGCTGTGGGTGCCTGG 60
L3-A          -----ACCGAGAACCGACACTCTGCTGCTATGGGTCTGCTGCTGTGGGTGCCTGG 51
                * *****
cTnI-scFv      CTCAACTGGAGACGCCCTGACTCAGCCCTCATCCGTGTCCGCCAACCCCGGCGAGACAGT 120
L3-A          CTCAACTGGAGACTAGCTGACTCAGCCCTCATCCGTGTCCGCCAACCCCGGCGAGACAGT 111
                *****
cTnI-scFv      GAAGATCACATGCAGCGGAGGCGCCGGTACTATGACGGCTCCTACTATTACGGCTGGTA 180
L3-A          GAAGATCACATGCAGCGGAGGCGCCGGTACTATGACGGCTCCTACTATTACGGCTGGTA 171
                *****
cTnI-scFv      TCAGCAGAAGTCTCCCGGCAGCGCCCTGTGACCGTGATCTATGAGAACACAAAGAGGCC 240
L3-A          TCAGCAGAAGTCTCCCGGCAGCGCCCTGTGACCGTGATCTATGAGAACACAAAGAGGCC 231
                *****
cTnI-scFv      ATCCAATATCCCCTCTCGCTTCTCCGGCTCTAAGAGCGGCTCCACCGCCACACTGACCAT 300
L3-A          ATCCAATATCCCCTCTCGCTTCTCCGGCTCTAAGAGCGGCTCCACCGCCACACTGACCAT 291
                *****
cTnI-scFv      CACAGGCGTGAGGGCAGAGGACGAGGCCGTCTATTACTGCGGCAGCGCCGACGATAACAT 360
L3-A          CACAGGCGTGAGGGCAGAGGACGAGGCCGTCTATTACTGCGGCAGCGCCGACGATAACAT 351
                *****
cTnI-scFv      GAATCCTACTATATTTGGCGCCGGCACCACACTGACAGTGCTAGGCCAGAGCTCTAGAAG 420
L3-A          GAATCCTACTATATTTGGCGCCGGCACCACACTGACAGTGCTAGGCCAGAGCTCTAGAAG 411
                *****
cTnI-scFv      CAGCAGCGGAGGAGGCAGCAGCGGAGGAGGCTCCGCCGTGACCCTGGATGAGTCTGG 480
L3-A          CAGCAGCGGAGGAGGCAGCAGCGGAGGAGGCTCCGCCGTGACCCTGGATGAGTCTGG 471
                *****
cTnI-scFv      AGGAGGCCTCCAGACACCTGGCGGCCCTGAGCCTGGTGTGCAAGGCCTCCGGCTTCAC 540
L3-A          AGGAGGCCTCCAGACACCTGGCGGCCCTGAGCCTGGTGTGCAAGGCCTCCGGCTTCAC 531
                *****
cTnI-scFv      CTTTTCTCTTATGGCATGCAGTGGGTGCGGCAGGCCCCAGGCAAGGGCCTGGAGTGGGT 600
L3-A          CTTTTCTCTTATGGCATGCAGTGGGTGCGGCAGGCCCCAGGCAAGGGCCTGGAGTGGGT 591
                *****
cTnI-scFv      GGCAGGCATCCAGAACGACGATAACCGGCACATACTACGGAGCCCGCTGAAGGGAAGGGC 660
L3-A          GGCAGGCATCCAGAACGACGATAACCGGCACATACTACGGAGCCCGCTGAAGGGAAGGGC 651

```

```

*****
cTnI-scFv      AACCATCAGCCGGGACAATGGCCAGAGCACAGTGC GGCTCCAGCTGAACAATCTGAGAGC 720
L3-A          AACCATCAGCCGGGACAATGGCCAGAGCACAGTGC GGCTCCAGCTGAACAATCTGAGAGC 711
*****
cTnI-scFv      CGAGGATACCGGCACCTACTACTGTGCCAAGGACGCTAGTAGTGATGGCGGATACGGCGG 780
L3-A          CGAGGATACCGGCACCTACTACTGTGCCAAGGACGCTAGTAGTGATGGCGGATACGGCGG 771
*****
cTnI-scFv      CGATAGTATCGATGCCTGGGGCCACGGCACCGAAGTGATCGTGAGCAGCACTAGTGGCCA 840
L3-A          CGATAGTATCGATGCCTGGGGCCACGGCACCGAAGTGATCGTGAGCAGCACTAGTGGCCA 831
*****
cTnI-scFv      GGCCGGACAGCATCACCACCACCACCACGGAGCCTATCCCTACGACGTGCCTGACTACGC 900
L3-A          GGCCGGACAGCATCACCACCACCACCACGGAGCCTATCCCTACGACGTGCCTGACTACGC 891
*****
cTnI-scFv      CAGCTGAAAGCTT----- 913
L3-A          CAGCTGAAAGCTTGGTACCGAGCTCGGATCCACTAGTCCAGTGTGGTGAATTCTGCAGA 951
*****
cTnI-scFv      ----- 913
L3-A          TATCCAGCACAGTGGCGGCCGCTCGAGTCTAGAGGGCCCGTTTAAACCCGCTGATCAGCC 1011
cTnI-scFv      ----- 913
L3-A          TCGACTGTGCCTTCTAGTGCAGCATCTGTGTTTGCCCTCCCCCGTGCTTCTGACCCTGG 1071
cTnI-scFv      ----- 913
L3-A          AAGGTGCCACTCCCCACTGTCCTTCCCTAATAAAATGA 1108

```

## B) L27c-Y

CLUSTAL O(1.2.4) multiple sequence alignment

```

cTnI-scFv      GCTAGCCACCATGGAAACCGACACTCTGCTGCTATGGGTCTGCTGCTGTGGGTGCCTGG 60
L27c-Y        -----CTCCTGGAACGACCTCTGCTGCTATGGGTCTGCTGCTGTGGGTGCCTGG 50
                *                               *****
cTnI-scFv      CTCAACTGGAGACGCCCTGACTCAGCCCTCATCCGTGTCCGCCAACCCCGGCGAGACAGT 120
L27c-Y        CTCAACTGGAGACGCCCTGACTCAGCCCTCATCCGTGTCCGCCAACCCCGGCGAGACAGT 110
                *****
cTnI-scFv      GAAGATCACATGCAGCGGAGGCGCCGGTACTATGACGGCTCCTACTATTACGGCTGGTA 180
L27c-Y        GAAGATCACATGCAGCGGAGGCGCCGGTACTAGGACGGCTCCTACTATTACGGCTGGTA 170
                *****
cTnI-scFv      TCAGCAGAAGTCTCCCGGCAGCGCCCTGTGACCGTGATCTATGAGAACACAAAGAGGCC 240
L27c-Y        TCAGCAGAAGTCTCCCGGCAGCGCCCTGTGACCGTGATCTATGAGAACACAAAGAGGCC 230
                *****
cTnI-scFv      ATCCAATATCCCTCTCGCTTCTCCGGCTCTAAGAGCGGCTCCACCGCCACACTGACCAT 300
L27c-Y        ATCCAATATCCCTCTCGCTTCTCCGGCTCTAAGAGCGGCTCCACCGCCACACTGACCAT 290
                *****
cTnI-scFv      CACAGGCGTGAGGGCAGAGGACGAGGCCGTCTATTACTGCGGCAGCGCCGACGATAACAT 360
L27c-Y        CACAGGCGTGAGGGCAGAGGACGAGGCCGTCTATTACTGCGGCAGCGCCGACGATAACAT 350
                *****

```

cTnI-scFv L27c-Y	GAATCCTACTATATTTGGCGCCGGCACCACACTGACAGTGCTAGGCCAGAGCTCTAGAAG GAATCCTACTATATTTGGCGCCGGCACCACACTGACAGTGCTAGGCCAGAGCTCTAGAAG *****	420 410
cTnI-scFv L27c-Y	CAGCAGCGGAGGAGGCAGCAGCGGAGGAGGCTCCGCCGTGACCCTGGATGAGTCTGG CAGCAGCGGAGGAGGCAGCAGCGGAGGAGGCTCCGCCGTGACCCTGGATGAGTCTGG *****	480 470
cTnI-scFv L27c-Y	AGGAGGCCTCCAGACACCTGGCGGCGCCCTGAGCCTGGTGTGCAAGGCCTCCGGCTTCAC AGGAGGCCTCCAGACACCTGGCGGCGCCCTGAGCCTGGTGTGCAAGGCCTCCGGCTTCAC *****	540 530
cTnI-scFv L27c-Y	CTTTTCTCTTATGGCATGCAGTGGGTGCGGCAGGCCCCAGGCAAGGCCTGGAGTGGGT CTTTTCTCTTATGGCATGCAGTGGGTGCGGCAGGCCCCAGGCAAGGCCTGGAGTGGGT *****	600 590
cTnI-scFv L27c-Y	GGCAGGCATCCAGAACGACGATAACCGGCACATACTACGGAGCCGCGTGAAGGGAAGGGC GGCAGGCATCCAGAACGACGATAACCGGCACATACTACGGAGCCGCGTGAAGGGAAGGGC *****	660 650
cTnI-scFv L27c-Y	AACCATCAGCCGGGACAATGGCCAGAGCACAGTGC GGCTCCAGCTGAACAATCTGAGAGC AACCATCAGCCGGGACAATGGCCAGAGCACAGTGC GGCTCCAGCTGAACAATCTGAGAGC *****	720 710
cTnI-scFv L27c-Y	CGAGGATAACCGGCACCTACTACTGTGCCAAGGACGCTAGTAGTGATGGCGGATACGGCGG CGAGGATAACCGGCACCTACTACTGTGCCAAGGACGCTAGTAGTGATGGCGGATACGGCGG *****	780 770
cTnI-scFv L27c-Y	CGATAGTATCGATGCCTGGGGCCACGGCACCGAAGTGATCGTGAGCAGCACTAGTGGCCA CGATAGTATCGATGCCTGGGGCCACGGCACCGAAGTGATCGTGAGCAGCACTAGTGGCCA *****	840 830
cTnI-scFv L27c-Y	GGCCGGACAGCATCACCACCACCACCGGAGCCTATCCCTACGACGTGCCTGACTACGC GGCCGGACAGCATCACCACCACCACCGGAGCCTATCCCTACGACGTGCCTGACTACGC *****	900 890
cTnI-scFv L27c-Y	CAGCTGAAAGCTT----- CAGCTGAAAGCTTGGTACCGAGCTCGGATCCACTAGTCCAGTGTGGTGAATTCTGCAGA *****	913 950
cTnI-scFv L27c-Y	----- TATCCAGCACAGTGGCGGCCGCTCGAGTCTAGAGGGCCCGTTTAAACCCGCTGATCAGCC	913 1010
cTnI-scFv L27c-Y	----- TCGACTGTGCTTCTAGTTGCCAGCCATCTGTTGTTTGCCCCTCCCGTGCCTTCCTTGAC	913 1070
cTnI-scFv L27c-Y	----- CCTGGAGGGTGCAA	913 1084

## 7.8 Parameters of cTnI protein

The amino acid of human cTnI protein and peptide sequence depicting the epitope of cTnI protein that was used in the crystallised structure is highlighted in the table below.

*Table 13: Recombinant cTnI amino acid sequence produced in E. coli. The peptide sequence used in crystallisation are highlighted in bold red. Sequence was sourced from Life Diagnostics.*

MADGSSDA AREPRPAPAP IRRRSSNYRA YATEPHA~~KKK~~ **SKISASRKLQ**  
**LKT**LLLQIAK QELEREAEER RGEKGRALST RCQPLELAGL  
GFAELQDLCR QLHARVDKVD EERYDIEAKV TKNITEIADL  
TQKIFDLRGKFKRPTLRRVR ISADAMMQAL LGARAKESLD  
LRAHLKQVKK EDTEKENREV GDWRKNIDAL SGMEGRKKKF ES

The hydrophathy of protein surface is an important parameter especially for selection of mutation sites. The hydrophobicity of protein surfaces can be determined by ExPASy: ProtScale tool originally based on hydrophathy index reported by Jack Kyte and Russell F. Doolittle.[\[292\]](#)

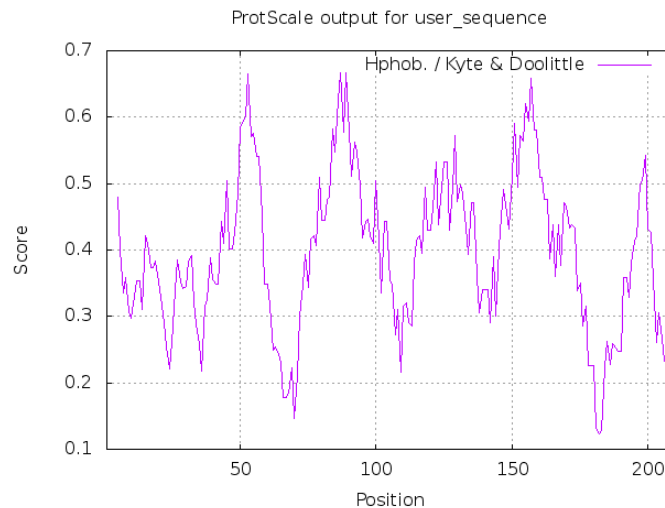


*Figure 43: Hydrophobicity of cTnI protein. The graph was generated by ProtScale programme (ExPASy bioinformatics tools). The score was generated based on Kyte & Doolittle hydrophobicity parameters. The scale is normalised between 0-1. The more the positive values, the more hydrophobic the region or amino acids are.*

## 7.9 Indirect ELISA to compare binding between L27c-Y and WT anti-cTnI scFv

Indirect ELISA was performed to compare the binding properties between the WT and L27c-Y anti-cTnI scFv. The experiment was performed by titrating 2-fold serial dilutions of L27c-Y and WT anti-cTnI scFv. The result showed an insignificant deviation in the absorbance as depicted in *Figure 44*.

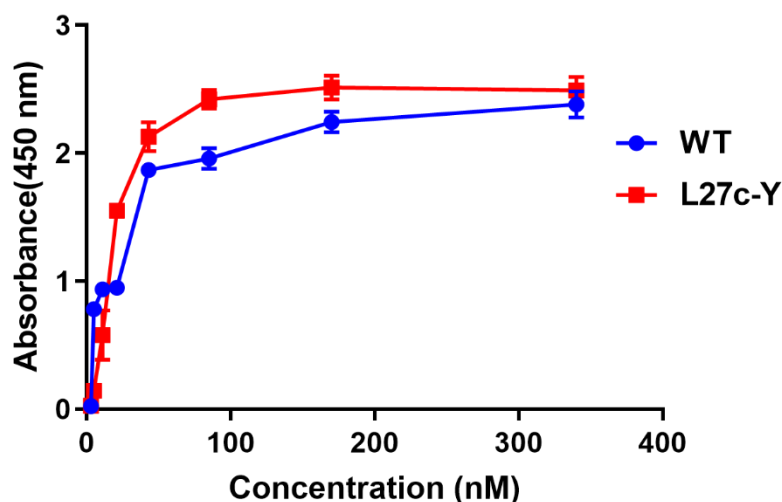


Figure 44: Comparison of binding specificity between WT and L27c-Y mutant. The recorded absorbance is identical confirming that incorporation of Anap did not alter binding specificity. Error bars are presented as  $\pm$  SD,  $n=4$ .

## 7.10 Fluorescence measurement of DY640 and DY641

The fluorescence of DY640 and DY641 (Innovative Optische Messtechnik GmbH, Germany) was measured in different solvents to investigate the solvatochromic effects in response to polarity. When excited at 640 nm (DY640) and 641 nm (DY641), the maximum emission spectra varied depending on the solvent polarity. While the maximum emission wavelength of DY640 in a polar environment (e.g. H<sub>2</sub>O) showed 675 nm, a blue shift of 15 nm was observed when measured in methanol (a less polar environment). In contrast, the DY641 showed maximum emission spectra at 680 nm, but a maximum of 15 nm blue shift was observed similar to DY641.

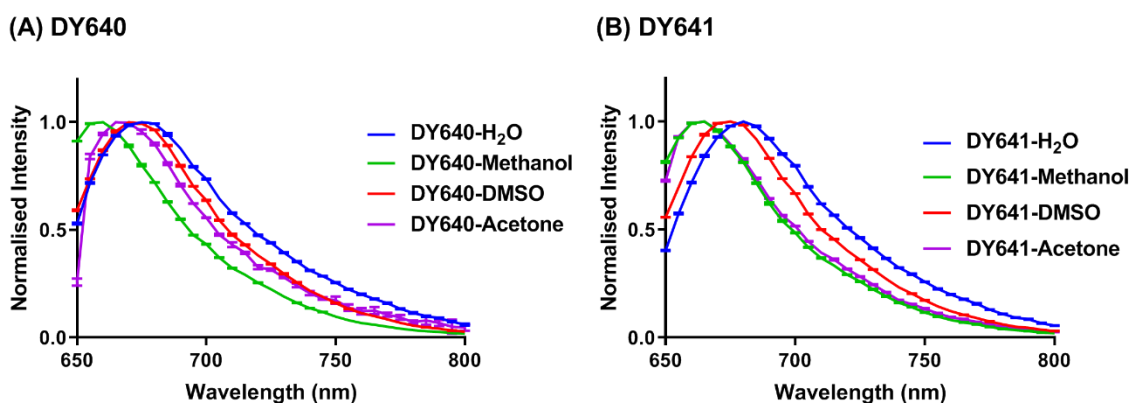


Figure 45: Fluorescence measurement of near-infrared fluorophore in different solvents, (A) DY640 and (B) DY641 fluorophore. Error bars are shown as  $\pm$  SEM,  $n=3$ .

## 7.11 Solvent accessibility determination by bioinformatics tools

The solvent accessibility of L27c-Y and other mutation sites was determined by residues determined by GETAREA 1.0 beta program available in <http://curie.utmb.edu/getarea.html>. The crystal structure available in PDB (4P48) was used in this program. The extract of analysis is presented in *Table 14* where Column 7 shows the average random coil value of amino acid residues. Residues are considered to be solvent exposed if the ratio value exceeds 50% and to be buried if the ratio is less than 20%. In the next column, the output is represented as "o" and "i" meaning exposed and buried respectively.

Table 14: GETAREA 1.0 beta generated solvent accessibility prediction of anti-cTnI scFv sequence.

Probe radius: 1.400

1	2	3	4	5	6	7	8
Residue	Total	Apolar	Backbone	Sidechain	Ratio(%)	In/Out	
ALA L3	109.83	67.40	43.20	66.63	100.0	o	
ARG L27a	151.22	63.05	26.39	124.83	63.8	o	
<u>TYR L27c</u>	<u>212.61</u>	<u>146.17</u>	<u>46.62</u>	<u>165.99</u>	<u>86.0</u>	<u>o</u>	
ASP L82	52.72	0.36	8.81	43.91	38.9		
ASN L95a	33.45	5.81	0.00	33.45	29.3		
PHE L98	16.23	0.87	15.36	0.87	0.5	i	
ASP H54	83.09	42.92	19.57	63.51	56.2	o	

THR	H57	46.63	9.02	12.82	33.82	31.8	
TYR	H58	68.17	35.76	1.57	66.61	34.5	
SER	H98	119.45	60.32	35.61	83.84	100.0	o

Similarly, solvent accessibility into the H53Y site and other mutation sites were determined by NetSurf program where the anti-EGFR scFv model structure was used as the structure template. The extract of the analysis is presented below (*Table 15*). The result showed in ten columns where the first column shows residues as buried (B) or exposed (E). The program can be accessed via <http://www.cbs.dtu.dk/services/NetSurfP/>.

*Table 15: NetSurfP analysis of solvent accessibility prediction for the anti-EFR scFv sequence*

```
# Column 1: Class assignment - B for buried or E for Exposed - Threshold: 25%
exposure, but not based on RSA
# Column 2: Amino acid
# Column 3: Sequence name
# Column 4: Amino acid number
# Column 5: Relative Surface Accessibility - RSA
# Column 6: Absolute Surface Accessibility
# Column 7: Z-fit score for RSA prediction
# Column 8: Probability for Alpha-Helix
# Column 9: Probability for Beta-strand
# Column 10: Probability for Coil
```

1	2	3	4	5	6	7	8	9	10
<b>E</b>	Y	Sequence	55	0.372	79.454	-0.798	0.004	0.197	0.799
B	Y	Sequence	96	0.055	11.689	0.756	0.087	0.683	0.230
B	Y	Sequence	170	0.040	8.484	0.142	0.018	0.846	0.136
B	F	Sequence	232	0.072	14.470	-0.273	0.005	0.336	0.660

## 7.12 Principles of some methods used in this thesis

### 7.12.1 Fluorescence lifetime

Fluorescence lifetime has been used for diverse applications in the biological fields including quantifying analytes with high sensitivity, and biological imaging. It is an inherent characteristic of a fluorescent molecule. According to Jablonski illustration, when a fluorophore is excited (absorbs energy) by a light, series of photo-physical events occur within the molecule that may include internal conversion of energy, loss of energy through radiation-less decay, fluorescence, vibrational relaxation, intersystem crossing, and phosphorescence as described by (Figure 46). The time a molecule spends in the excited state is determined by the sum of the kinetic constants of all the de-excitation processes. Fluorescence is observed if  $k_f$  is greater or equal to the sum of internal conversion ( $k_i$ ) and intersystem crossing ( $k_x$ ) i.e.  $k_f \gtrsim k_i + k_x$  where  $k$  is the rate constant for all these decay processes.

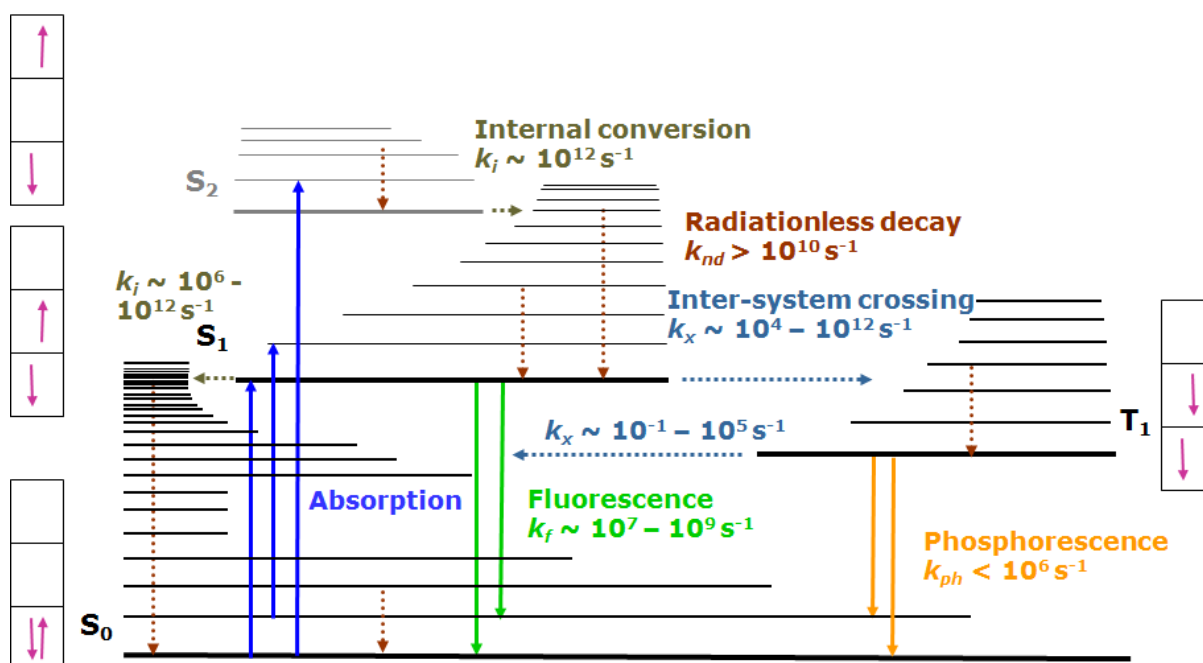


Figure 46: The Jablonski diagram depicts the life history of an excited state electron in a luminescent probe. The figure is adapted from Martin Hof, Radek Macháň, Czech Technical University, Prague.

Fluorescence lifetime ( $\tau$ ) is the time that the fluorescent dye takes to convert from one state to another, typically from the excited state to ground state by emitting photons. Lifetime is inversely proportional to decay rate ( $\tau=1/k$ ) and typically varies from femtoseconds to nanoseconds depending on the properties of the fluorophore. Fluorescence lifetime is not affected by the concentrations of a fluorophore, and absorbance by sample, rather it is affected by surrounding environments of the dye such as temperature, viscosity, and the polarity. It is also dependent on the internal structure of fluorophore.[\[252\]](#) The fluorescence lifetime of a polarity sensitive fluorophore is greatly influenced by the polarity of the solvent. As a rule of thumb, lifetime has been found to be shorter in the more polar environment as faster efficient energy transfer results due to the larger dipole moments of surrounding molecules. As an example of fluorescence lifetime influenced by solvent polarity, the lifetime of rhodamine fluorophore increased after binding to albumin in the blood due to the solvatochromism effect.[\[13\]](#)

Fluorescence lifetime can be measured based on the time or frequency domain. Among the available lifetime measurements, time-correlated single photon counting (TCSPC) is the mostly practising time domain methods due to the simplified data attainment and superior quantitative photon counting. Lifetime is measured from the decay slope as per the following equation:

$$F(t) = F_0 e^{-t/\tau} \qquad \text{Equation 4}$$

where  $F_0$  is the intensity at time  $t = 0$ ,  $t$  is the time after the absorption, and  $\tau$  is the fluorescence lifetime. Data are fitted with using curve fitting algorithms. Based on the goodness of fitting parameters, the lifetime could be mono-exponential if a single lifetime is detected whereas multi-exponential life-time resulted from the large deviation in the  $\chi^2$  due to the presence of at least two or lifetimes. Quantum yield (QY) is another parameter often used in fluorescence characterisation of dyes. Theoretically, QY is proportional to lifetime. Nevertheless, QY is determined based on the fluorescence intensity; hence, lifetime is preferred over QY as this is dependent on the excitation wavelength rather than the concentrations of fluorophores.

### 7.12.2 Bio-layer Interferometry

The affinity of antibodies plays a critical role in antibody-based biomolecular interaction studies. The binding of an antibody to its antigen is a reversible process, and the rate of the binding reaction is proportional to the concentrations of the reactants. In short, the rate of antibody-antigen complex formation is equal to the rate of dissociation into its components  $[Ab] + [Ag]$  in equilibrium. Binding kinetics of antibody to its cognate antigen is often represented by a dissociation constant ( $K_D$ ) calculated by a ratio of  $k_{dissociation}/k_{association}$  ( $k_{off}/k_{on}$ ). Theoretically,  $K_D$  is inversely proportional ( $1/K_D$ ) to the affinity, *i.e.* the lower  $K_D$  results. In other words, the smaller the  $K_D$  value is, the higher the affinity of the antibody for its binder. Measuring the affinity of mutants are commonly used to understand the effect of a mutation that may contribute to significant affinity disruption of the mutants compared to a parental antibody.

BLI is a powerful optical analytical tool used for biomolecular interaction based on the label-free detection systems, quite similar to the principle of SPR technique. BLI evaluates the interference pattern between the waves of white light. Usually, light is directed in fibre optic sensors containing two layers, composed of the reference layer and biocompatible layer on the surface (*Figure 47A*). Binding molecules to the biocompatible layer lead to the change of surface thickness causing a wavelength shift in the interference pattern. BLI is generally composed of five steps. First, the biosensor is dipped into the buffer to set up the baseline followed by loading the binder onto the biosensors by suitable linker chemistry, and the baseline is established by washing in the buffer. Then, the binder is allowed to capture the target molecule to record the associations over the time followed by subsequent dissociation in the buffer (*Figure 47B*).[\[293\]](#)

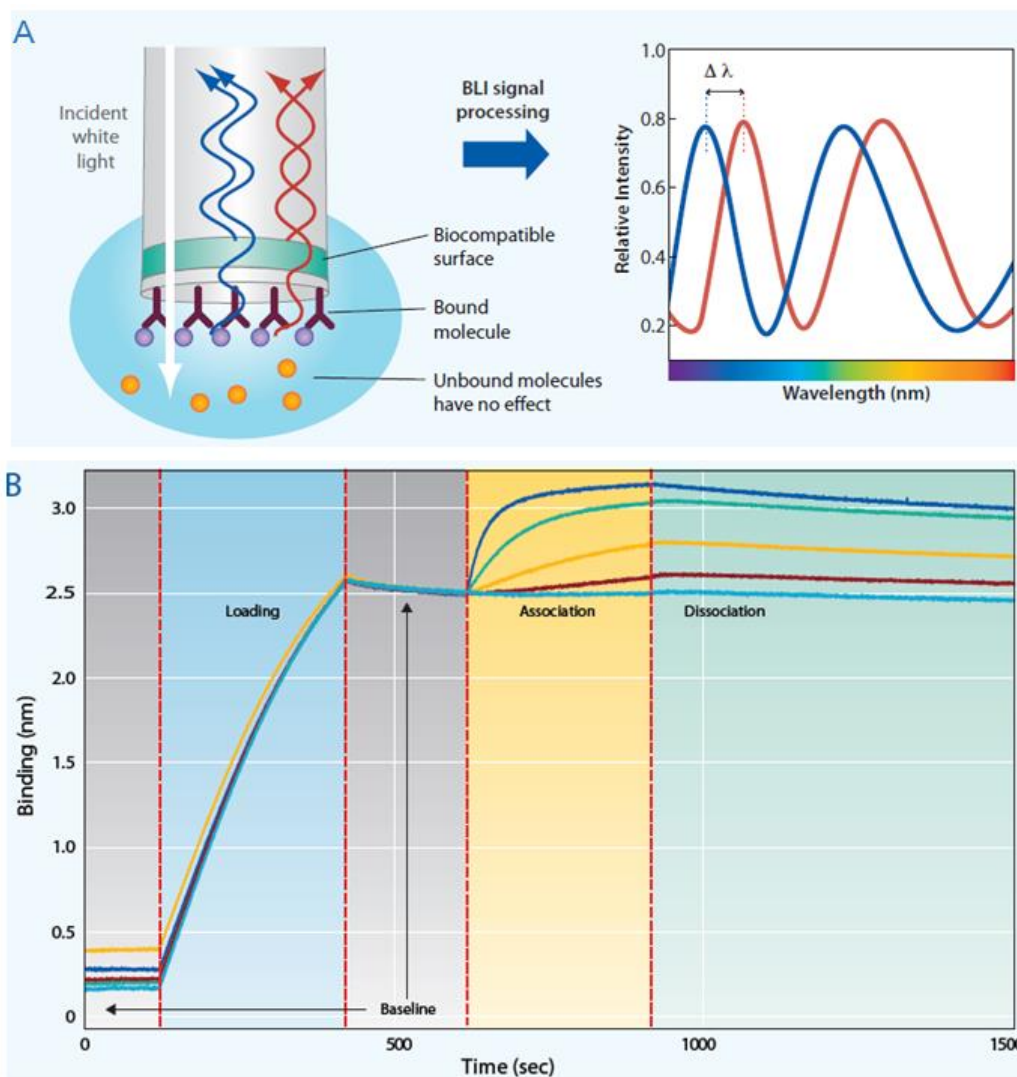


Figure 47: Schematically showing the (A) principles of BLI and (B) steps involved in a representative binding kinetics analysis in BLI. The figure is taken from the manufacturer's application note (ForteBio).

### 7.12.3 Dynamic light scattering

Dynamic light scattering (DLS), also known as photon correlation spectroscopy, has been widely used for various applications in the field of biomedical science. One of the applications is the study of homogeneity of proteins in the sample. Presence of aggregates is an obstacle in studying the biomolecular interactions. Usually, only purified protein samples are used in DLS for analysis, and a purified sample does not contain aggregates unless the presence of precipitants. The rate of precipitation between samples is an important parameter to identify the difference in the degree of stability. An

example may include measuring the aggregation of WT protein and its mutated version in solutions. DLS measures the size of particles based on the Brownian motion. Theoretically, the Brownian motion of molecules in the solvent varies depending on the size of molecules. The smaller the molecules are, the faster the molecule moves, and conversely larger molecules move slower. Viscosity and temperature are important parameters that affect the movement. The velocity of motion is represented as a translational diffusion coefficient. The hydrodynamic diameter of molecules can be calculated based on this coefficient by using the Stokes-Einstein formula. (*Equation 5*).

$$d(H) = \frac{kT}{3\pi\eta D} \quad \text{Equation 5}$$

### 7.13 Fluorescence detection by miniaturised fluorimeter

Several companies produced commercially available miniaturised fluorimeters. Some of the examples are presented here.

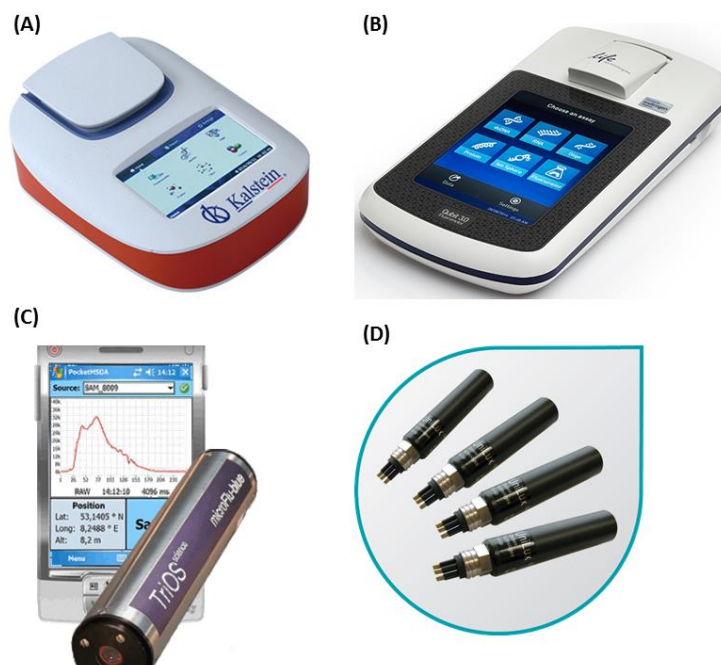


*Figure 48: Examples of fluorimeters. (A) Kalstein (Cat# YR412-A); (B) Invitrogen™ Qubit 3 Fluorometer by Thermo Fisher Scientific (Model# Q33216); (C) microFlu (TriOS) fluorimeter developed by ThermoFisher Scientific; and (D) UniLux Dye Tracing Sensor (Rhodamine or Fluorescein/Uranine) developed by Chelsea Technologies Group.*

## 8 References

---

1. Limited, P.S.P.S.I.P. *Biosensors Market (2012-2022)*. [Website] June 2016; Available from: <https://www.psmarketresearch.com/market-analysis/biosensors-market>.
2. Mehrotra, P., *Biosensors and their applications - A review*. Journal of Oral Biology and Craniofacial Research, 2016. 6(2): p. 153-159.
3. Bhalla, N., et al., *Introduction to biosensors*. Biosensor Technologies for Detection of Biomolecules, 2016. 60(1): p. 1-8.
4. Borisov, S.M. and O.S. Wolfbeis, *Optical biosensors*. Chemical Reviews, 2008. 108(2): p. 423-461.
5. Rong, G.X., S.R. Corrie, and H.A. Clark, *In Vivo Biosensing: Progress and Perspectives*. Acs Sensors, 2017. 2(3): p. 327-338.
6. Rong, G.X., et al., *Recent Developments in Nanosensors for Imaging Applications in Biological Systems*, in *Annual Review of Analytical Chemistry, Vol 12*, P.W. Bohn and J.E. Pemberton, Editors. 2019, Annual Reviews: Palo Alto. p. 109-128.
7. GS, S., A. CV, and B.B. Mathew, *Biosensors: A Modern Day Achievement*. Journal of Instrumentation Technology, 2014. 2(1): p. 26-39.
8. Clark, L.C. and C. Lyons, *electrode systems for continuous monitoring in cardiovascular surgery*. Annals of the New York Academy of Sciences, 1962. 102(1): p. 29-45.
9. Cammann, K., *Bio-Sensors Based on Ion-Selective Electrodes*. Fresenius Zeitschrift für Analytische Chemie, 1977. 287: p. 1-9.
10. Turner, A.P.F., *Biosensors: sense and sensibility*. Chemical Society Reviews, 2013. 42(8): p. 3184-3196.
11. Arugula, M.A. and A. Simonian, *Novel trends in affinity biosensors: current challenges and perspectives*. Measurement Science and Technology, 2014. 25(3), 032001.
12. Grieshaber, D., et al., *Electrochemical biosensors - Sensor principles and architectures*. Sensors, 2008. 8(3): p. 1400-1458.
13. Abugo, O.O., R. Nair, and J.R. Lakowicz, *Fluorescence properties of rhodamine 800 in whole blood and plasma*. Analytical Biochemistry, 2000. 279(2): p. 142-50.
14. Chen, C., et al., *Recent advances in electrochemical glucose biosensors: a review*. RSC Advances, 2013. 3(14): p. 4473-4491.
15. Rogers, K.R., *Principles of affinity-based biosensors*. Molecular Biotechnology, 2000. 14(2): p. 109-129.
16. Barfidokht, A. and J.J. Gooding, *Approaches Toward Allowing Electroanalytical Devices to be Used in Biological Fluids*. Electroanalysis, 2014. 26(6): p. 1182-1196.
17. Huang, Y., et al., *Disease-Related Detection with Electrochemical Biosensors: A Review*. Sensors, 2017. 17(10).
18. Mungroo, N.A. and S. Neethirajan, *Biosensors for the Detection of Antibiotics in Poultry Industry-A Review*. Biosensors-Basel, 2014. 4(4): p. 472-493.
19. Najeeb, M.A., et al., *A novel classification of prostate specific antigen (PSA) biosensors based on transducing elements*. Talanta, 2017. 168: p. 52-61.
20. Morales, M.A. and J.M. Halpern, *Guide to Selecting a Biorecognition Element for Biosensors*. Bioconjugate Chemistry, 2018. 29(10): p. 3231-3239.
21. Yalow, R.S. and S.A. Berson, *immunoassay of endogenous plasma insulin in man*. Journal of Clinical Investigation, 1960. 39(7): p. 1157-1175.
22. Saerens, D., et al., *Antibody fragments as probe in biosensor development*. Sensors, 2008. 8(8): p. 4669-4686.

23. Holliger, P. and P.J. Hudson, *Engineered antibody fragments and the rise of single domains*. Nature Biotechnology, 2005. 23(9): p. 1126-1136.
24. Bizzotto, D., et al., *Beyond Simple Cartoons: Challenges in Characterizing Electrochemical Biosensor Interfaces*. ACS Sensors, 2018. 3(1): p. 5-12.
25. Stulik, K., *Challenges and promises of electrochemical detection and sensing*. Electroanalysis, 1999. 11(14): p. 1001-1004.
26. Long, F., A.N. Zhu, and H.C. Shi, *Recent Advances in Optical Biosensors for Environmental Monitoring and Early Warning*. Sensors, 2013. 13(10): p. 13928-13948.
27. Damborský, P., Švitel, J., & Katrlík, J., *Optical biosensors*. Essays in biochemistry, 2016. 60(1), 91–100.
28. Daniels, J.S. and N. Pourmand, *Label-Free Impedance Biosensors: Opportunities and Challenges*. Electroanalysis, 2007. 19(12): p. 1239-1257.
29. Zhong, W.W., *Nanomaterials in fluorescence-based biosensing*. Analytical and Bioanalytical Chemistry, 2009. 394(1): p. 47-59.
30. Peltomaa, R., et al., *Optical Biosensors for Label-Free Detection of Small Molecules*. Sensors, 2018. 18(12): 4126.
31. Li, B.M., Q.L. Yu, and Y.X. Duan, *Fluorescent labels in biosensors for pathogen detection*. Critical Reviews in Biotechnology, 2015. 35(1): p. 82-93.
32. Dey, D. and T. Goswami, *Optical Biosensors: A Revolution Towards Quantum Nanoscale Electronics Device Fabrication*. Journal of Biomedicine and Biotechnology, 2011: 348218.
33. Schrittwieser, S., et al., *Homogeneous Biosensing Based on Magnetic Particle Labels*. Sensors, 2016. 16(6), 828.
34. Schrittwieser, S., et al., *Homogeneous biosensor based on optical detection of the rotational dynamics of anisotropic nanoparticles*. Procedia Engineering, 2010. 5: p. 1107-1110.
35. Zeng, X.Q., Z.H. Shen, and R. Mernaugh, *Recombinant antibodies and their use in biosensors*. Analytical and Bioanalytical Chemistry, 2012. 402(10): p. 3027-3038.
36. Liu, H.Q., et al., *A Wash-Free Homogeneous Colorimetric Immunoassay Method*. Theranostics, 2016. 6(1): p. 54-64.
37. Li, N., X.D. Su, and Y. Lu, *Nanomaterial-based biosensors using dual transducing elements for solution phase detection*. Analyst, 2015. 140(9): p. 2916-2943.
38. Rodionov, P.V., I.A. Veselova, and T.N. Shekhovtsova, *A solid-phase fluorescent biosensor for the determination of phenolic compounds and peroxides in samples with complex matrices*. Analytical and Bioanalytical Chemistry, 2014. 406(5): p. 1531-1540.
39. Faccio, G., *From Protein Features to Sensing Surfaces*. Sensors, 2018. 18(4): 1204.
40. Cicerone, M.T., M.J. Pikal, and K.K. Qian, *Stabilization of proteins in solid form*. Advanced Drug Delivery Reviews, 2015. 93: p. 14-24.
41. Barbosa, A.I. and N.M. Reis, *A critical insight into the development pipeline of microfluidic immunoassay devices for the sensitive quantitation of protein biomarkers at the point of care*. Analyst, 2017. 142(6): p. 858-882.
42. Merkoci, A., *Nanobiosensors in diagnostics applications*. Febs Open Bio, 2018. 8: p. 50-50.
43. Miranda, F.F., et al., *Reagentless fluorescent biosensors from artificial families of antigen binding proteins*. Biosensors & Bioelectronics, 2011. 26(10): p. 4184-4190.
44. Nawrot, W., et al., *A Fluorescent Biosensors for Detection Vital Body Fluids' Agents*. Sensors, 2018. 18(8).

45. Ueda, H. and J. Dong, *From fluorescence polarization to Quencherbody: Recent progress in fluorescent reagentless biosensors based on antibody and other binding proteins*. *Biochimica et Biophysica Acta-Proteins and Proteomics*, 2014. 1844(11): p. 1951-1959.
46. Bonham, A.J., *Utilizing Design Principles of Electrochemical DNA Aptamer Biosensors in Multiple Optical Assay Methodologies*. *Faseb Journal*, 2018. 32(1): p. 657-15.
47. Abe, R., et al., "*Quencherbodies*": *Quencher-Based Antibody Probes That Show Antigen-Dependent Fluorescence*. *Journal of the American Chemical Society*, 2011. 133(43): p. 17386-17394.
48. Galban, J., et al., *Reagentless fluorescent biosensors based on proteins for continuous monitoring systems*. *Analytical and Bioanalytical Chemistry*, 2012. 402(10): p. 3039-3054.
49. Toseland, C.P., *Fluorescent labeling and modification of proteins*. *Journal of chemical biology*, 2013. 6(3): p. 85-95.
50. Jakob, L., A. Gust, and D. Grohmann, *Evaluation and optimisation of unnatural amino acid incorporation and bioorthogonal bioconjugation for site-specific fluorescent labelling of proteins expressed in mammalian cells*. *Biochemistry and Biophysics Reports*, 2019. 17: p. 1-9.
51. Freise, A.C. and A.M. Wu, *In vivo imaging with antibodies and engineered fragments*. *Molecular Immunology*, 2015. 67(2): p. 142-152.
52. Knutson, S., et al., *Development and evaluation of a fluorescent antibody-drug conjugate for molecular imaging and targeted therapy of pancreatic cancer*. *Cancer Research*, 2015. 75.
53. Crivianu-Gaita, V. and M. Thompson, *Aptamers, antibody scFv, and antibody Fab' fragments: An overview and comparison of three of the most versatile biosensor biorecognition elements*. *Biosensors & Bioelectronics*, 2016. 85: p. 32-45.
54. Kierny, M.R., T.D. Cunningham, and B.K. Kay, *Detection of biomarkers using recombinant antibodies coupled to nanostructured platforms*. *Nano Reviews & Experiments*, 2012. 3(1): 17240.
55. Ducancel, F. and B.H. Muller, *Molecular engineering of antibodies for therapeutic and diagnostic purposes*. *Mabs*, 2012. 4(4): p. 445-457.
56. Skerra, A. and A. Pluckthun, *Assembly of a functional immunoglobulin-fv fragment in escherichia-coli*. *Science*, 1988. 240(4855): p. 1038-1041.
57. Gupta, S.K. and P. Shukla, *Microbial platform technology for recombinant antibody fragment production: A review*. *Critical Reviews in Microbiology*, 2017. 43(1): p. 31-42.
58. Orzáez, D., A. Granell, and M.A. Blázquez, *Manufacturing antibodies in the plant cell*. *Biotechnology Journal*, 2009. 4(12): p. 1712-1724.
59. Strohl, W.R., *Current progress in innovative engineered antibodies*. *Protein & Cell*, 2018. 9(1): p. 86-120.
60. Kaplon, H. and J.M. Reichert, *Antibodies to watch in 2019*. *Mabs*, 2019. 11(2): p. 219-238.
61. Sharma, S., H. Byrne, and R.J. O'Kennedy, *Antibodies and antibody-derived analytical biosensors*. *Biosensor Technologies for Detection of Biomolecules*, 2016. 60(1): p. 9-18.
62. Park, M., et al., *Carbon nanotubes-based chemiresistive immunosensor for small molecules: Detection of nitroaromatic explosives*. *Biosensors & Bioelectronics*, 2010. 26(4): p. 1297-1301.
63. Chebil, S., et al., *Electrochemical detection of D-dimer as deep vein thrombosis marker using single-chain D-dimer antibody immobilized on functionalized polypyrrole*. *Biosensors & Bioelectronics*, 2010. 26(2): p. 736-742.

64. Encarnacao, J.M., et al., *Piezoelectric biosensors for biorecognition analysis: Application to the kinetic study of HIV-1 Vif protein binding to recombinant antibodies*. Journal of Biotechnology, 2007. 132(2): p. 142-148.
65. Dunne, L., et al., *Surface plasmon resonance-based immunoassay for the detection of aflatoxin B-1 using single-chain antibody fragments*. Spectroscopy Letters, 2005. 38(3): p. 229-245.
66. Yan, H.P., et al., *Single Chain Fragment Variable Recombinant Antibody as a Template for Fc Sensors*. Analytical Chemistry, 2011. 83(2): p. 625-630.
67. Benhar, I., et al., *Recombinant single chain antibodies in bioelectrochemical sensors*. Talanta, 2001. 55(5): p. 899-907.
68. Grennan, K., et al., *Atrazine analysis using an amperometric immunosensor based on single-chain antibody fragments and regeneration-free multi-calibrant measurement*. Analytica Chimica Acta, 2003. 500(1-2): p. 287-298.
69. Love, T.E., C. Redmond, and C.N. Mayers, *Real time detection of anthrax spores using highly specific anti-EA1 recombinant antibodies produced by competitive panning*. Journal of Immunological Methods, 2008. 334(1-2): p. 1-10.
70. Grewal, Y.S., et al., *Label-free electrochemical detection of an Entamoeba histolytica antigen using cell-free yeast-scFv probes*. Chemical Communications, 2013. 49(15): p. 1551-1553.
71. Kausaite-Minkstimiene, A., et al., *A surface plasmon resonance immunosensor for human growth hormone based on fragmented antibodies*. Analytical Methods, 2013. 5(18): p. 4757-4763.
72. Al-Halabi, L., et al., *Recombinant antibody fragments allow repeated measurements of C-reactive protein with a quartz crystal microbalance immunosensor*. Mabs, 2013. 5(1): p. 140-149.
73. Backmann, N., et al., *A label-free immunosensor array using single-chain antibody fragments*. Proceedings of the National Academy of Sciences of the United States of America, 2005. 102(41): p. 14587-14592.
74. Abe, R., et al., *Ultra Q-bodies: quench-based antibody probes that utilize dye-dye interactions with enhanced antigen-dependent fluorescence*. Scientific Reports, 2014. 4.
75. Liu, Y., R.L. Mernaugh, and X.Q. Zeng, *Single chain fragment variable recombinant antibody functionalized gold nanoparticles for a highly sensitive colorimetric immunoassay*. Biosensors & Bioelectronics, 2009. 24(9): p. 2853-2857.
76. Mechaly, A., E. Zahavy, and A. Fisher, *Development and implementation of a single-chain Fv antibody for specific detection of Bacillus anthracis spores*. Applied and Environmental Microbiology, 2008. 74(3): p. 818-822.
77. Zdobnova, T.A., et al., *Fluorescent immunolabeling of cancer cells by quantum dots and antibody scFv fragment*. Journal of Biomedical Optics, 2009. 14(2): 021004.
78. Lu, R.M., et al., *Single chain anti-c-Met antibody conjugated nanoparticles for in vivo tumor-targeted imaging and drug delivery*. Biomaterials, 2011. 32(12): p. 3265-3274.
79. mackenzie, c.r., et al., *bifunctional fusion proteins consisting of a single-chain antibody and an engineered lanthanide-binding*. Immunotechnology, 1995. 1(2): p. 139-150.
80. Singh, R., et al., *Target-specific cytotoxic activity of recombinant immunotoxin scFv(MUC1)-ETA on breast carcinoma cells and primary breast tumors*. Molecular Cancer Therapeutics, 2007. 6(2): p. 562-569.
81. Zhang, W.Y., T.C. Yip, and C.S. Kwok, *Rapid purification of a new humanized single-chain Fv antibody/human interleukin-2 fusion protein reactive against HER2 receptor*. Acta Biochimica et Biophysica Sinica, 2004. 36(10): p. 707-712.

82. Wang, J.Q., et al., *Genetically fused single-chain anti-Salmonella antibody with aequorin: a bioluminescence immunoassay for a Salmonella antigen*. *Analytica Chimica Acta*, 2001. 435(2): p. 255-263.
83. Hu, W.G., et al., *Development of immunofiltration assay by light addressable potentiometric sensor with genetically biotinylated recombinant antibody for rapid identification of Venezuelan equine encephalitis virus*. *Journal of Immunological Methods*, 2004. 289(1-2): p. 27-35.
84. Le, H.Q.A., H. Sauriat-Dorizon, and H. Korri-Youssoufi, *Investigation of SPR and electrochemical detection of antigen with polypyrrole functionalized by biotinylated single-chain antibody: A review*. *Analytica Chimica Acta*, 2010. 674(1): p. 1-8.
85. Shen, Z.H., et al., *Recombinant antibody piezoelectrochemical sensors for the detection of cytochrome P4501B1*. *Analytical Chemistry*, 2007. 79(4): p. 1283-1289.
86. Horacek, J., et al., *Characterization of the interactions between immobilized parathion and the corresponding recombinant scFv antibody using a piezoelectric biosensor*. *Food and Agricultural Immunology*, 1998. 10(4): p. 363-374.
87. Ferreira, G.N.M., et al., *Recombinant single-chain variable fragment and single domain antibody piezoelectrochemical sensors for detection of HIV1 virion infectivity factor*. *Biosensors & Bioelectronics*, 2007. 23(3): p. 384-392.
88. Liu, X.J., et al., *Characterization of a Human Antibody Fragment Fab and Its Calcium Phosphate Nanoparticles that Inhibit Rabies Virus Infection with Vaccine*. *Plos One*, 2011. 6(5): e19848.
89. Romanazzo, D., et al., *Development of a recombinant Fab-fragment based electrochemical immunosensor for deoxynivalenol detection in food samples*. *Biosensors & Bioelectronics*, 2010. 25(12): p. 2615-2621.
90. Ionescu, R.E., et al., *Label-free impedimetric immunosensor for sensitive detection of atrazine*. *Electrochimica Acta*, 2010. 55(21): p. 6228-6232.
91. Lu, H.H., et al., *A recombinant Fab fragment-based electrochemical immunosensor for the determination of testosterone in bovine urine*. *Biosensors & Bioelectronics*, 2007. 22(8): p. 1756-1763.
92. Helali, S., et al., *A disposable immunomagnetic electrochemical sensor based on functionalised magnetic beads on gold surface for the detection of atrazine*. *Electrochimica Acta*, 2006. 51(24): p. 5182-5186.
93. Spain, E., et al., *Detection of prostate specific antigen based on electrocatalytic platinum nanoparticles conjugated to a recombinant scFv antibody*. *Biosensors & Bioelectronics*, 2016. 77: p. 759-766.
94. Singh, A., et al., *Single-domain antibody based thermally stable electrochemical immunosensor*. *Biosensors & Bioelectronics*, 2016. 83: p. 162-168.
95. Charles, P.T., et al., *Multi-channeled single chain variable fragment (scFv) based microfluidic device for explosives detection*. *Talanta*, 2015. 144: p. 439-444.
96. Krall, N., et al., *Site-selective protein-modification chemistry for basic biology and drug development*. *Nature Chemistry*, 2016. 8(2): p. 102-112.
97. Hsieh, T.Y., et al., *Monitoring Protein Misfolding by Site-Specific Labeling of Proteins In Vivo*. *Plos One*, 2014. 9(6): e99395.
98. Hink, M.A., et al., *Structural dynamics of green fluorescent protein alone and fused with a single chain Fv protein*. *Journal of Biological Chemistry*, 2000. 275(23): p. 17556-60.
99. Ferrara, F., et al., *Fluorescent Labeling of Antibody Fragments Using Split GFP*. *Plos One*, 2011. 6(10): e25727.

100. Kampmeier, F., et al., *Site-specific, covalent labeling of recombinant antibody fragments via fusion to an engineered version of 6-O-alkylguanine DNA alkyltransferase*. *Bioconjugate Chemistry*, 2009. 20(5): p. 1010-5.
101. Wingren, C., et al., *Microarrays based on affinity-tagged single-chain Fv antibodies: sensitive detection of analyte in complex proteomes*. *Proteomics*, 2005. 5(5): p. 1281-91.
102. Saunders, M.J., et al., *A bifunctional converter: fluorescein quenching scFv/fluorogen activating protein for photostability and improved signal to noise in fluorescence experiments*. *Bioconjugate Chemistry*, 2014. 25(8): p. 1556-64.
103. Siepert, E.M., et al., *Short-chain fluorescent tryptophan tags for on-line detection of functional recombinant proteins*. *BMC Biotechnology*, 2012. 12: p. 65.
104. Ramakrishnan, B., et al., *Multiple site-specific in vitro labeling of single-chain antibody*. *Bioconjugate Chemistry*, 2009. 20(7): p. 1383-9.
105. Eriksson, S., et al., *Dual-label time-resolved immunofluorometric assay of free and total prostate-specific antigen based on recombinant Fab fragments*. *Clinical Chemistry*, 2000. 46(5): p. 658-66.
106. Madej, M.P., et al., *Engineering of an anti-epidermal growth factor receptor antibody to single chain format and labeling by Sortase A-mediated protein ligation*. *Biotechnology and Bioengineering*, 2012. 109(6): p. 1461-70.
107. Ismail, N.F. and T.S. Lim, *Site-specific scFv labelling with invertase via Sortase A mechanism as a platform for antibody-antigen detection using the personal glucose meter*. *Scientific Reports*, 2016. 6: 19338.
108. Li, Z.Y., et al., *Fluorophore-Conjugated Holliday Junctions for Generating Super-Bright Antibodies and Antibody Fragments*. *Angewandte Chemie-International Edition*, 2015. 54(40): p. 11706-11710.
109. Sydor, J.R., et al., *Establishment of intein-mediated protein ligation under denaturing conditions: C-terminal labeling of a single-chain antibody for biochip screening*. *Bioconjugate Chemistry*, 2002. 13(4): p. 707-712.
110. Stech, M., et al., *Cell-free eukaryotic systems for the production, engineering, and modification of scFv antibody fragments*. *Engineering in Life Sciences*, 2014. 14(4): p. 387-398.
111. Lyons, A., et al., *Site-specific attachment to recombinant antibodies via introduced surface cysteine residues*. *Protein Engineering*, 1990. 3(8): p. 703-708.
112. Renard, M., et al., *Knowledge-based design of reagentless fluorescent biosensors from recombinant antibodies*. *Journal of Molecular Biology*, 2002. 318(2): p. 429-442.
113. Renard, M., L. Belkadi, and H. Bedouelle, *Deriving topological constraints from functional data for the design of reagentless fluorescent immunosensors*. *Journal of Molecular Biology*, 2003. 326(1): p. 167-175.
114. Sirk, S.J., et al., *Site-Specific, Thiol-Mediated Conjugation of Fluorescent Probes to Cysteine-Modified Diabodies Targeting CD20 or HER2*. *Bioconjugate Chemistry*, 2008. 19(12): p. 2527-2534.
115. Jeong, H.J., et al., *Q-Bodies from Recombinant Single-Chain Fv Fragment with Better Yield and Expanded Palette of Fluorophores*. *ACS Sensors*, 2016. 1(1): p. 88-94.
116. Kim, Y.G., et al., *Efficient site-specific Labeling of proteins via cysteines*. *Bioconjugate Chemistry*, 2008. 19(3): p. 786-791.
117. Wang, L., et al., *Expanding the genetic code of Escherichia coli*. *Science*, 2001. 292(5516): p. 498-500.
118. Wals, K. and H. Ovaa, *Unnatural amino acid incorporation in E. coli: current and future applications in the design of therapeutic proteins*. *Frontiers in Chemistry*, 2014. 2: 15.

119. Kim, C.H., J.Y. Axup, and P.G. Schultz, *Protein conjugation with genetically encoded unnatural amino acids*. *Current Opinion in Chemical Biology*, 2013. 17(3): p. 412-419.
120. Schmied, W.H., et al., *Efficient Multisite Unnatural Amino Acid Incorporation in Mammalian Cells via Optimized Pyrrolysyl tRNA Synthetase/tRNA Expression and Engineered eRF1*. *Journal of the American Chemical Society*, 2014. 136(44): p. 15577-15583.
121. Lemke, E.A., *Site-Specific Labeling of Proteins for Single-Molecule FRET Measurements Using Genetically Encoded Ketone Functionalities*. *Methods Molecular Biology*, 2011. 751: p. 3-15.
122. Kim, C.H., et al., *Synthesis of Bispecific Antibodies using Genetically Encoded Unnatural Amino Acids*. *Journal of the American Chemical Society*, 2012. 134(24): p. 9918-9921.
123. Lu, H., et al., *Site-specific antibody-polymer conjugates for siRNA delivery*. *Journal of the American Chemical Society*, 2013. 135(37): p. 13885-91.
124. Axup, J.Y., et al., *Synthesis of site-specific antibody-drug conjugates using unnatural amino acids*. *Proceedings of the National Academy of Sciences of the United States of America*, 2012. 109(40): p. 16101-16106.
125. Xie, J.M. and P.G. Schultz, *Innovation: A chemical toolkit for proteins - an expanded genetic code*. *Nature Reviews Molecular Cell Biology*, 2006. 7(10): p. 775-782.
126. Chin, J.W., *Expanding and Reprogramming the Genetic Code of Cells and Animals*, in *Annual Review of Biochemistry*, Annual Reviews of Biochemistry, 2014. 83: p. 379-408.
127. Ryu Y, Schultz PG, *Efficient incorporation of unnatural amino acids into proteins in Escherichia coli*. *Nature Methods*, 2006. 3(4):263-5.
128. Xie, J.M. and P.G. Schultz, *An expanding genetic code*. *Methods*, 2005. 36(3): p. 227-238.
129. Takimoto, J.K., et al., *Improving orthogonal tRNA-synthetase recognition for efficient unnatural amino acid incorporation and application in mammalian cells*. *Molecular Biosystems*, 2009. 5(9): p. 931-934.
130. Serfling, R., et al., *Designer tRNAs for efficient incorporation of non-canonical amino acids by the pyrrolysine system in mammalian cells*. *Nucleic Acids Research*, 2018. 46(1): p. 1-10.
131. Chatterjee, A., et al., *A Genetically Encoded Fluorescent Probe in Mammalian Cells*. *Journal of the American Chemical Society*, 2013. 135(34): p. 12540-12543.
132. Lee, H.S., et al., *Genetic Incorporation of a Small, Environmentally Sensitive, Fluorescent Probe into Proteins in Saccharomyces cerevisiae*. *Journal of the American Chemical Society*, 2009. 131(36): p. 12921-3.
133. Mitchell, A.L., et al., *A Unique Genetically Encoded FRET Pair in Mammalian Cells*. *ChemBioChem*, 2017. 18(6): p. 511-514.
134. Zagotta, W.N., et al., *Measuring distances between TRPV1 and the plasma membrane using a noncanonical amino acid and transition metal ion FRET*. *Journal of General Physiology*, 2016. 147(2): p. 201-216.
135. Soh, M.S., et al., *Probing the Structural Mechanism of Partial Agonism in Glycine Receptors Using the Fluorescent Artificial Amino Acid, ANAP*. *ACS Chemical Biology*, 2017. 12(3): p. 805-813.
136. Kalstrup, T. and R. Blunck, *Dynamics of internal pore opening in K-V channels probed by a fluorescent unnatural amino acid*. *Proceedings of the National Academy of Sciences of the United States of America*, 2013. 110(20): p. 8272-8277.
137. Sakata, S., et al., *Voltage-dependent motion of the catalytic region of voltage-sensing phosphatase monitored by a fluorescent amino acid*. *Proceedings of the National Academy of Sciences of the United States of America*, 2016. 113(27): p. 7521-7526.

138. Wen, M., et al., *Site-specific fluorescence spectrum detection and characterization of hASIC1a channels upon toxin mambalgin-1 binding in live mammalian cells*. Chemical Communications, 2015. 51(38): p. 8153-8156.
139. Summerer, D., et al., *A genetically encoded fluorescent amino acid*. Proceedings of the National Academy of Sciences of the United States of America, 2006. 103(26): p. 9785-9789.
140. Wang, W., et al., *Genetically encoding unnatural amino acids for cellular and neuronal studies*. Nature Neuroscience, 2007. 10(8): p. 1063-1072.
141. Shen, B., et al., *Genetically Encoding Unnatural Amino Acids in Neural Stem Cells and Optically Reporting Voltage-Sensitive Domain Changes in Differentiated Neurons*. Stem Cells, 2011. 29(8): p. 1231-1240.
142. Wang, J., J. Xie, and P.G. Schultz, *A genetically encoded fluorescent amino acid*. Journal of the American Chemical Society, 2006. 128(27): p. 8738-8739.
143. Villa, J.K., et al., *Fluorescence Modulation of Green Fluorescent Protein Using Fluorinated Unnatural Amino Acids*. Molecules, 2017. 22(7): E1194.
144. Lampkowski, J.S., D.M. Uthappa, and D.D. Young, *Site-specific incorporation of a fluorescent terphenyl unnatural amino acid*. Bioorganic & Medicinal Chemistry Letters, 2015. 25(22): p. 5277-5280.
145. Kang, D., et al., *New Architecture for Reagentless, Protein-Based Electrochemical Biosensors*. Journal of the American Chemical Society, 2017. 139(35): p. 12113-12116.
146. Vancaenenbroeck, R., S. Kunzelmann, and M.R. Webb, *Development of a range of fluorescent reagentless biosensors for ATP, based on malonyl-coenzyme A synthetase*. Plos One, 2017. 12(6): e0179547.
147. Solscheid, C., et al., *Development of a Reagent less Biosensor for Inorganic Phosphate, Applicable over a Wide Concentration Range*. Biochemistry, 2015. 54(32): p. 5054-5062.
148. Kunzelmann, S., C. Solscheid, and M.R. Webb, *Fluorescent biosensors: design and application to motor proteins*. Experientia Supplementum (2012), 2014. 105: p. 25-47.
149. Altschuh, D., S. Oncul, and A.P. Demchenko, *Fluorescence sensing of intermolecular interactions and development of direct molecular biosensors*. Journal of Molecular Recognition, 2006. 19(6): p. 459-477.
150. Brient-Litzler, E., A. Pluckthun, and H. Bedouelle, *Knowledge-based design of reagentless fluorescent biosensors from a designed ankyrin repeat protein*. Protein Engineering Design & Selection, 2010. 23(4): p. 229-241.
151. de Picciotto, S., et al., *Equilibrium and dynamic design principles for binding molecules engineered for reagentless biosensors*. Analytical Biochemistry, 2014. 460: p. 9-15.
152. Panigrahi, S.K. and A.K. Mishra, *Study on the dependence of fluorescence intensity on optical density of solutions: the use of fluorescence observation field for inner filter effect corrections*. Photochemical & Photobiological Sciences, 2019. 18(2): p. 583-591.
153. Zhou, J. and H.M. Ma, *Design principles of spectroscopic probes for biological applications*. Chemical Science, 2016. 7(10): p. 6309-6315.
154. Dong, J., H.-J. Jeong, and H. Ueda, *Preparation of Quenchbodies by protein transamination reaction*. Journal of Bioscience and Bioengineering, 2016. 122(1): p. 125-130.
155. Jeong, H.-J., et al., *Construction of dye-stapled Quenchbodies by photochemical crosslinking to antibody nucleotide-binding sites*. Chemical Communications, 2017. 53(73): p. 10200-10203.

156. Ohashi, H., et al., *Insight into the Working Mechanism of Quenchbody: Transition of the Dye around Antibody Variable Region That Fluoresces upon Antigen Binding*. *Bioconjugate Chemistry*, 2016. 27(10): p. 2248-2253.
157. Jeong, H.J., et al., *Development of a Quenchbody for the Detection and Imaging of the Cancer-Related Tight-Junction-Associated Membrane Protein Claudin*. *Analytical Chemistry*, 2017. 89(20): p. 10783-10789.
158. Nhat, K.P.H., et al., *Antibody-based fluorescent and fluorescent ratiometric indicators for detection of phosphotyrosine*. *Journal of Bioscience and Bioengineering*, 2016. 122(2): p. 146-154.
159. Jeong, H.-J., J. Dong, and H. Ueda, *Single-Step Detection of the Influenza Virus Hemagglutinin Using Bacterially-Produced Quenchbodies*. *Sensors*, 2019. 19(1): 52.
160. Kurumida, Y. and N. Hayashi, *Development of a Novel Q-body Using an In Vivo Site-Specific Unnatural Amino Acid Incorporation System*. *Sensors*, 2018. 18(8): E2519.
161. Jeong, H.J., et al., *Detection of vimentin serine phosphorylation by multicolor Quenchbodies*. *Biosensors & Bioelectronics*, 2013. 40(1): p. 17-23.
162. Klymchenko, A.S., *Solvatochromic and Fluorogenic Dyes as Environment-Sensitive Probes: Design and Biological Applications*. *Accounts of Chemical Research*, 2017. 50(2): p. 366-375.
163. De Lorimier, R.M., et al., *Construction of a fluorescent biosensor family*. *Protein Science*, 2002. 11(11): p. 2655-2675.
164. Singh, R.P., *Prospects of Nanobiomaterials for Biosensing*. *International Journal of Electrochemistry*, 2011. 125487: p. 30.
165. Holzinger, M., A. Le Goff, and S. Cosnier, *Nanomaterials for biosensing applications: a review*. *Frontiers in Chemistry*, 2014. 2: 63.
166. Williams, R.M., et al., *Noninvasive ovarian cancer biomarker detection via an optical nanosensor implant*. *Science Advances*, 2018. 4(4): eaaq1090.
167. Neely, A., et al., *Ultrasensitive and Highly Selective Detection of Alzheimer's Disease Biomarker Using Two-Photon Rayleigh Scattering Properties of Gold Nanoparticle*. *ACS Nano*, 2009. 3(9): p. 2834-2840.
168. Richards, D.A., A. Maruani, and V. Chudasama, *Antibody fragments as nanoparticle targeting ligands: a step in the right direction*. *Chemical Science*, 2017. 8(1): p. 63-77.
169. Anderson, G.P., et al., *Single domain antibody-quantum dot conjugates for ricin detection by both fluoroimmunoassay and surface plasmon resonance*. *Analytica Chimica Acta*, 2013. 786: p. 132-138.
170. Byun, J.Y., et al., *The use of an engineered single chain variable fragment in a localized surface plasmon resonance method for analysis of the C-reactive protein*. *Chemical Communications*, 2013. 49(82): p. 9497-9499.
171. Seo, M.H., et al., *Controlled and Oriented Immobilization of Protein by Site-Specific Incorporation of Unnatural Amino Acid*. *Analytical Chemistry*, 2011. 83(8): p. 2841-2845.
172. Raliski, B.K., C.A. Howard, and D.D. Young, *Site-Specific Protein Immobilization Using Unnatural Amino Acids*. *Bioconjugate Chemistry*, 2014. 25(11): p. 1916-1920.
173. Torrance, L., et al., *Oriented immobilisation of engineered single-chain antibodies to develop biosensors for virus detection*. *Journal of Virological Methods*, 2006. 134(1-2): p. 164-170.
174. Vikholm, I., *Self-assembly of antibody fragments and polymers onto gold for immunosensing*. *Sensors and Actuators B-Chemical*, 2005. 106(1): p. 311-316.

175. Maly, J., et al., *Immobilisation of engineered molecules on electrodes and optical surfaces*. Materials Science & Engineering C-Biomimetic and Supramolecular Systems, 2002. 22(2): p. 257-261.
176. Heo, N.S., et al., *Label-Free Electrochemical Diagnosis of Viral Antigens with Genetically Engineered Fusion Protein*. Sensors, 2012. 12(8): p. 10097-10108.
177. Zheng, S., et al., *Label-free optical diagnosis of hepatitis B virus with genetically engineered fusion proteins*. Talanta, 2010. 82(2): p. 803-809.
178. Ros, R., et al., *Antigen binding forces of individually addressed single-chain Fv antibody molecules*. Proceedings of the National Academy of Sciences of the United States of America, 1998. 95(13): p. 7402-7405.
179. Piervincenzi, R.T., W.M. Reichert, and H.W. Hellinga, *Genetic engineering of a single-chain antibody fragment for surface immobilization in an optical biosensor*. Biosensors & Bioelectronics, 1998. 13(3-4): p. 305-312.
180. Seurnynck-Servoss, S.L., et al., *Immobilization strategies for single-chain antibody microarrays*. Proteomics, 2008. 8(11): p. 2199-2210.
181. Howell, S., et al., *High-density immobilization of an antibody fragment to a carboxymethylated dextran-linked biosensor surface*. Journal of Molecular Recognition, 1998. 11(1-6): p. 200-203.
182. Park, T.J., et al., *Polyhydroxyalkanoate chip for the specific immobilization of recombinant proteins and its applications in immunodiagnosics*. Biotechnology and Bioprocess Engineering, 2006. 11(2): p. 173-177.
183. Hu, X.J., et al., *Covalent and Oriented Immobilization of scFv Antibody Fragments via an Engineered Glycan Moiety*. Biomacromolecules, 2013. 14(1): p. 153-159.
184. Kumada, Y., et al., *Novel solid-phase refolding method for preparation of scFv-immobilized polystyrene plates with high-antigen-binding activity*. Analytical and Bioanalytical Chemistry, 2010. 398(3): p. 1295-1303.
185. Li, Y.J., et al., *Reversible immobilization of proteins with streptavidin affinity tags on a surface plasmon resonance biosensor chip*. Analytical and Bioanalytical Chemistry, 2006. 386(5): p. 1321-1326.
186. Sugimura, Y., et al., *Novel site-specific immobilization of a functional protein using a preferred substrate sequence for transglutaminase 2*. Journal of Biotechnology, 2007. 131(2): p. 121-127.
187. Lo, Y.S., et al., *Oriented Immobilization of Antibody Fragments on Ni-Decorated Single-Walled Carbon Nanotube Devices*. ACS Nano, 2009. 3(11): p. 3649-3655.
188. Shen, Z.H., et al., *Engineering peptide linkers for scFv immunosensors*. Analytical Chemistry, 2008. 80(6): p. 1910-1917.
189. Shen, Z., et al., *Single-chain fragment variable antibody piezoelectrochemical sensors*. Analytical Chemistry, 2005. 77(3): p. 797-805.
190. Sahoo, H., *Fluorescent labeling techniques in biomolecules: a flashback*. Rsc Advances, 2012. 2(18): p. 7017-7029.
191. Chatterjee, A., et al., *A genetically encoded fluorescent probe in mammalian cells*. J Am Chem Soc, 2013. 135(34): p. 12540-3.
192. Jakob, L., A. Gust, and D. Grohmann, *Evaluation and optimisation of unnatural amino acid incorporation and bioorthogonal bioconjugation for site-specific fluorescent labelling of proteins expressed in mammalian cells*. Biochemistry and Biophysics Reports, 2018. 17: p. 1-9.
193. Niu, W. and J.T. Guo, *Novel Fluorescence-Based Biosensors Incorporating Unnatural Amino Acids*. Enzymes as Sensors, 2017. 589: p. 191-219.

194. Hallam, T.J. and V.V. Smider, *Unnatural amino acids in novel antibody conjugates*. *Future Medicinal Chemistry*, 2014. 6(11): p. 1309-1324.
195. Evans, E.G.B. and G.L. Millhauser, *Genetic Incorporation of the Unnatural Amino Acid p-Acetyl Phenylalanine into Proteins for Site-Directed Spin Labeling*. *Methods in Enzymology*, 2015. 563: p. 503-527.
196. Brustad, E.M., et al., *A General and Efficient Method for the Site-Specific Dual-Labeling of Proteins for Single Molecule Fluorescence Resonance Energy Transfer*. *Journal of the American Chemical Society*, 2008. 130(52): p. 17664-5.
197. Chin, J.W., et al., *Addition of p-azido-L-phenylalanine to the genetic code of Escherichia coli*. *Journal of the American Chemical Society*, 2002. 124(31): p. 9026-9027.
198. Wang, L., et al., *Addition of the keto functional group to the genetic code of Escherichia coli*. *Proceedings of the National Academy of Sciences of the United States of America*, 2003. 100(1): p. 56-61.
199. Yang, S.T., et al., *Site-specific fluorescent labeling to visualize membrane translocation of a myristoyl switch protein*. *Scientific Reports*, 2016. 6.
200. Gibson, T.B., A. Ranganathan, and A. Grothey, *Randomized phase III trial results of panitumumab, a fully human anti-epidermal growth factor receptor monoclonal antibody, in metastatic colorectal cancer*. *Clinical Colorectal Cancer*, 2006. 6(1): p. 29-31.
201. Watanabe, Y., et al., *In vitro and in vivo antitumor effects of recombinant bispecific antibodies based on humanized anti-EGFR antibody*. *Oncology Reports*, 2011. 26(4): p. 949-955.
202. Yang, L.L., et al., *Single Chain Epidermal Growth Factor Receptor Antibody Conjugated Nanoparticles for in vivo Tumor Targeting and Imaging*. *Small*, 2009. 5(2): p. 235-243.
203. Taylor, K., et al., *Nanocell targeting using engineered bispecific antibodies*. *Mabs*, 2015. 7(1): p. 53-65.
204. Wee, P. and Z.X. Wang, *Epidermal Growth Factor Receptor Cell Proliferation Signaling Pathways*. *Cancers*, 2017. 9(5): E52.
205. Ferguson, K.M., *Structure-based view of epidermal growth factor receptor regulation*. *Annual Review of Biophysics*, 2008. 37: p. 353-373.
206. Czajkowsky, D.M., et al., *Fc-fusion proteins: new developments and future perspectives*. *Embo Molecular Medicine*, 2012. 4(10): p. 1015-1028.
207. Howard, C.B., et al., *Overcoming Instability of Antibody-Nanomaterial Conjugates: Next Generation Targeted Nanomedicines Using Bispecific Antibodies*. *Advanced Healthcare Materials*, 2016. 5(16): p. 2055-2068.
208. Alvarez-Cienfuegos, A., et al., *Intramolecular trimerization, a novel strategy for making multispecific antibodies with controlled orientation of the antigen binding domains*. *Scientific Reports*, 2016. 6: 28643.
209. A. Cathrine Kettleborough, M.M.B., Keith, H. Ansell, Detlef Gussow, Jaume Adan, Francesc Mitjans, Elisabet Rosell, Francesc Blasco, Jaume Piulats *Anti-EGFR single-chain Fvs and anti-EGFR antibodies*, FDA, Editor. 1998: USA.
210. Wu, t.t. and e.a. kabat, *an analysis of sequences of variable regions of bence jones proteins and myeloma light chains and their implications for antibody complementarity*. *journal of experimental medicine*, 1970. 132(2): p. 211-50.
211. Lefranc, M.P., et al., *IMGT (R), the international ImMunoGeneTics information system (R) 25 years on*. *Nucleic Acids Research*, 2015. 43(D1): p. D413-D422.
212. Ehrenmann, F., et al., *IMGT/Collier de Perles: IMGT standardized representation of domains (IG, TR, and IgSF variable and constant domains, MH and MhSF groove domains)*. *Cold Spring Harb Protoc*, 2011. 2011(6): p. 726-36.

213. Sickmier, E.A., et al., *The Panitumumab EGFR Complex Reveals a Binding Mechanism That Overcomes Cetuximab Induced Resistance*. Plos One, 2016. 11(9): e0163366.
214. Zuberbuhler, K., et al., *A general method for the selection of high-level scFv and IgG antibody expression by stably transfected mammalian cells*. Protein Engineering Design & Selection, 2009. 22(3): p. 169-174.
215. Taki, S., et al., *A Novel Bispecific Antibody against Human CD3 and Ephrin Receptor A10 for Breast Cancer Therapy*. Plos One, 2015. 10(12): e0144712.
216. Hainfeld, J.F., et al., *Ni-NTA-gold clusters target his-tagged proteins*. Journal of Structural Biology, 1999. 127(2): p. 185-198.
217. Liu, W.S., et al., *Genetic incorporation of unnatural amino acids into proteins in mammalian cells*. Nature Methods, 2007. 4(3): p. 239-244.
218. Brinkmann, U., et al., *Phage display of disulfide-stabilized fv fragments*. Journal of Immunological Methods, 1995. 182(1): p. 41-50.
219. Moatsou, D., et al., *Self-Assembly of Temperature-Responsive Protein-Polymer Bioconjugates*. Bioconjugate Chemistry, 2015. 26(9): p. 1890-1899.
220. Wendeler, M., et al., *Enhanced Catalysis of Oxime-Based Bioconjugations by Substituted Anilines*. Bioconjugate Chemistry, 2014. 25(1): p. 93-101.
221. Larsen, D., et al., *New Organocatalyst Scaffolds with High Activity in Promoting Hydrazone and Oxime Formation at Neutral pH*. Organic Letters, 2015. 17(2): p. 274-277.
222. Memisoglu, G., et al., *Theoretical Modeling of Viscosity Monitoring with Vibrating Resonance Energy Transfer for Point-of-Care and Environmental Monitoring Applications*. Micromachines, 2019. 10(1).
223. Islam, J., et al., *Wavelength-Dependent Fluorescent Immunosensors via Incorporation of Polarity Indicators near the Binding Interface of Antibody Fragments*. Analytical Chemistry, 2019. 91(12): p. 7631-7638.
224. World Health Organisations, May 2017; "*Cardiovascular diseases (CVDs)*". Accessed 19 December 2019, Available from: [https://www.who.int/en/news-room/fact-sheets/detail/cardiovascular-diseases-\(cvds\)](https://www.who.int/en/news-room/fact-sheets/detail/cardiovascular-diseases-(cvds)).
225. Matetzky, S., et al., *Elevated troponin I level on admission is associated with adverse outcome of primary angioplasty in acute myocardial infarction*. Circulation, 2000. 102(14): p. 1611-1616.
226. Daubert, M.A. and A. Jeremias, *The utility of troponin measurement to detect myocardial infarction: review of the current findings*. Vascular Health and Risk Management, 2010. 6: p. 691-699.
227. Michos ED, B.Z., Yeh HC, et al. *Cardiac Troponins Used as Diagnostic and Prognostic Tests in Patients With Kidney Disease* [Internet]. Rockville (MD): Agency for Healthcare Research and Quality (US); 2014 Aug. (Comparative Effectiveness Review, No. 135.) Executive Summary. Available from: <https://www.ncbi.nlm.nih.gov/books/NBK241518/>.
228. Yahalom, M., et al., *Clinical Significance of Conditions Presenting with ECG Changes Mimicking Acute Myocardial Infarction*. International Journal of Angiology, 2013. 22(2): p. 115-122.
229. Upasham S, P.S., *Cardiac troponin biosensors: where are we now?* Advanced Health Care Technologies, 2018. 2018:4: p. 1-13.
230. Herman, D.S., P.A. Kavsak, and D.N. Greene, *Variability and Error in Cardiac Troponin Testing An ACLPS Critical Review*. American Journal of Clinical Pathology, 2017. 148(4): p. 281-295.

231. Apple, F.S., et al., *Cardiac Troponin Assays: Guide to Understanding Analytical Characteristics and Their Impact on Clinical Care*. Clinical Chemistry, 2017. 63(1): p. 73-81.
232. Han, X., et al., *Recent Development of Cardiac Troponin I Detection*. ACS Sensors, 2016. 1(2): p. 106-114.
233. (AACB), A.A.o.C.B. *Recommendations for Use of Point-of-Care (POC) Troponin Assays in Assessment of Acute Coronary Syndrome*. 2016; Available from: <https://www.aacb.asn.au/documents/item/4483>.
234. Amundson, B.E. and F.S. Apple, *Cardiac troponin assays: a review of quantitative point-of-care devices and their efficacy in the diagnosis of myocardial infarction*. Clinical Chemistry and Laboratory Medicine, 2015. 53(5): p. 665-676.
235. McDonnell, B., et al., *A high-affinity recombinant antibody permits rapid and sensitive direct detection of myeloperoxidase*. Analytical Biochemistry, 2011. 410(1): p. 1-6.
236. Conroy, P.J., et al., *Reconciling the Structural Attributes of Avian Antibodies*. Journal of Biological Chemistry, 2014. 289(22): p. 15384-15392.
237. Spillner, E., et al., *Avian IgY antibodies and their recombinant equivalents in research, diagnostics and therapy*. Biologicals, 2012. 40(5): p. 313-322.
238. Soetkamp, D., et al., *The continuing evolution of cardiac troponin I biomarker analysis: from protein to proteoform*. Expert Review of Proteomics, 2017. 14(11): p. 973-986.
239. Conroy, P.J., R.J. Okennedy, and S. Hearty, *Cardiac troponin I: a case study in rational antibody design for human diagnostics*. Protein Engineering Design & Selection, 2012. 25(6): p. 295-305.
240. Finlay, W.J.J., et al., *Generation of high-affinity chicken single-chain Fv antibody fragments for measurement of the Pseudonitzschia pungens toxin domoic acid*. Applied and Environmental Microbiology, 2006. 72(5): p. 3343-3349.
241. Narat, M., *Production of antibodies in chickens*. Food Technology and Biotechnology, 2003. 41(3): p. 259-267.
242. Cipolla, A., et al., *Campylobacter fetus diagnosis: Direct immunofluorescence comparing chicken IgY and rabbit IgG conjugates*. Altex-Alternativen Zu Tierexperimenten, 2001. 18(3): p. 165-170.
243. Njagi, J.I. and S.M. Kagwanja, *The Interface in Biosensing: Improving Selectivity and Sensitivity*. Interfaces and Interphases in Analytical Chemistry, 2011. 1062: p. 225-247.
244. Farka, Z., et al., *Nanoparticle-Based Immunochemical Biosensors and Assays: Recent Advances and Challenges*. Chemical Reviews, 2017. 117(15): p. 9973-10042.
245. Arruebo, M., M. Valladares, and A. Gonzalez-Fernandez, *Antibody-Conjugated Nanoparticles for Biomedical Applications*. Journal of Nanomaterials, 2009.
246. Harvey Motulsky, A.C., *Fitting Models to Biological Data Using Linear and Nonlinear Regression: A Practical Guide to Curve Fitting*. 2004: Oxford University Press.
247. North, B., A. Lehmann, and R.L. Dunbrack, *A New Clustering of Antibody CDR Loop Conformations*. Journal of Molecular Biology, 2011. 406(2): p. 228-256.
248. Weisstein, E.W. *Lorentzian Function*. 2019 [cited on 26 03 2019]; Available from: <http://mathworld.wolfram.com/LorentzianFunction.html>.
249. Guy, M.J., et al., *The impact of antibody selection on the detection of cardiac troponin I*. Clinica Chimica Acta, 2013. 420: p. 82-88.
250. Sheldahl, C., et al., *The calcium-saturated cTnI/cTnC complex: structure of the inhibitory region of cTnI*. Biophysical journal, 2003. 84(2 Pt 1): p. 1057-1064.

251. Anderson, N.L. and N.G. Anderson, *The human plasma proteome - History, character, and diagnostic prospects*. *Molecular & Cellular Proteomics*, 2002. 1(11): p. 845-867.
252. Berezin, M.Y. and S. Achilefu, *Fluorescence lifetime measurements and biological imaging*. *Chemical reviews*, 2010. 110(5): p. 2641-2684.
253. *Solvent and Environmental Effects*, in *Principles of Fluorescence Spectroscopy*, J.R. Lakowicz, Editor. 2006, Springer US: Boston, MA. p. 205-235.
254. Nagaraja, D., et al., *Solvent effect on the relative quantum yield and fluorescence quenching of a newly synthesized coumarin derivative*. *Luminescence*, 2015. 30(5): p. 495-502.
255. Gaigalas, A.K., et al., *The development of fluorescence intensity standards*. *Journal of Research of the National Institute of Standards and Technology*, 2001. 106(2): p. 381-389.
256. Wu, A.H.B. and Y.J. Feng, *Biochemical differences between cTnT and cTnI and their significance for diagnosis of acute coronary syndromes*. *European Heart Journal*, 1998. 19: p. N25-N29.
257. Goldbaum, F.A., et al., *Lack of significant differences in association rates and affinities of antibodies from short-term and long-term responses to hen egg lysozyme*. *Journal of Immunology*, 1999. 162(10): p. 6040-6045.
258. Lualdi, M., et al., *Natural fluorescence spectroscopy of human blood plasma in the diagnosis of colorectal cancer: Feasibility study and preliminary results*. *Tumori*, 2007. 93(6): p. 567-571.
259. Morgner, F., et al., *Terbium to Quantum Dot FRET Bioconjugates for Clinical Diagnostics: Influence of Human Plasma on Optical and Assembly Properties*. *Sensors*, 2011. 11(10): p. 9667-9684.
260. Shirshin, E., et al., *Native fluorescence spectroscopy of blood plasma of rats with experimental diabetes: identifying fingerprints of glucose-related metabolic pathways*. *Journal of Biomedical Optics*, 2015. 20(5): p. 1-6.
261. Berezin, M.Y., et al., *Near infrared dyes as lifetime solvatochromic probes for micropolarity measurements of biological systems*. *Biophysical Journal*, 2007. 93(8): p. 2892-9.
262. Adams, K.E., et al., *Comparison of visible and near-infrared wavelength-excitable fluorescent dyes for molecular imaging of cancer*. *Journal of Biomedical Optics*, 2007. 12(2): 024017 .
263. Berezin, M.Y., et al., *Near infrared dyes as lifetime solvatochromic probes for micropolarity measurements of biological systems*. *Biophysical Journal*, 2007. 93(8): p. 2892-2899.
264. Buschmann, V., K.D. Weston, and M. Sauer, *Spectroscopic study and evaluation of red-absorbing fluorescent dyes*. *Bioconjugate Chemistry*, 2003. 14(1): p. 195-204.
265. Klausen, M.S., et al., *NetSurfP-2.0: Improved prediction of protein structural features by integrated deep learning*. *Proteins-Structure Function and Bioinformatics*, 2019. 87(6): p. 520-527.
266. Surendra Negi, H.Z., Robert Fraczkiwicz, Werner Braun, *Solvent Accessible Surface Areas, Atomic Solvation Energies, and Their Gradients for Macromolecules*. 2015. cited as <http://curie.utmb.edu/getarea.html>.
267. The PyMOL Molecular Graphics System, V.S., LLC. 2019.
268. Heller, D.A., et al., *Multimodal optical sensing and analyte specificity using single-walled carbon nanotubes*. *Nature Nanotechnology*, 2008. 4: p. 114.
269. Michel, R., et al., *Influence of PEG architecture on protein adsorption and conformation*. *Langmuir*, 2005. 21(26): p. 12327-12332.

270. Bonomi, P.D., et al., *Predictive biomarkers for response to EGFR-directed monoclonal antibodies for advanced squamous cell lung cancer*. *Annals of Oncology*, 2018. 29(8): p. 1701-1709.
271. Shin, S., et al., *Assessment of real-time PCR method for detection of EGFR mutation using both supernatant and cell pellet of malignant pleural effusion samples from non-small-cell lung cancer patients*. *Clinical Chemistry and Laboratory Medicine*, 2017. 55(12): p. 1962-1969.
272. Antczak, C., et al., *Domain-Based Biosensor Assay to Screen for Epidermal Growth Factor Receptor Modulators in Live Cells*. *Assay and Drug Development Technologies*, 2012. 10(1): p. 24-36.
273. Chang, X.H., et al., *Research Progress of Near-Infrared Fluorescence Immunoassay*. *Micromachines*, 2019. 10(6): 422.
274. Zhang, X., et al., *A Near-Infrared Ratiometric Fluorescent Probe for Highly Selective Recognition and Bioimaging of Cysteine*. *Frontiers in Chemistry*, 2019. 7: 32.
275. Krismastuti, F.S.H., S. Pace, and N.H. Voelcker, *Porous Silicon Resonant Microcavity Biosensor for Matrix Metalloproteinase Detection*. *Advanced Functional Materials*, 2014. 24(23): p. 3639-3650.
276. Tsujikawa, K., et al., *Development of a novel immunoassay for herbal cannabis using a new fluorescent antibody probe, "Ultra Quenchbody"*. *Forensic Science International*, 2016. 266: p. 541-548.
277. Polanski, M. and N.L. Anderson, *A List of Candidate Cancer Biomarkers for Targeted Proteomics*. *Biomarker Insights*, 2006. 1: p. 1-48.
278. Shriver-Lake, L.C., et al., *Integrating scFv into xMAP Assays for the Detection of Marine Toxins*. *Toxins*, 2016. 8(11): E346.
279. Srinivasan, B. and S. Tung, *Development and Applications of Portable Biosensors*. *Journal of Laboratory Automation*, 2015. 20(4): p. 365-389.
280. Maguire, I., et al., *Novel Microfluidic Analytical Sensing Platform for the Simultaneous Detection of Three Algal Toxins in Water*. *ACS Omega*, 2018. 3(6): p. 6624-6634.
281. Ashoka, A.H., et al., *Solvatochromic Near-Infrared Probe for Polarity Mapping of Biomembranes and Lipid Droplets in Cells under Stress*. *Journal of Physical Chemistry Letters*, 2019. 10(10): p. 2414-2421.
282. Hutchins, B.M., et al., *Site-specific coupling and sterically controlled formation of multimeric antibody fab fragments with unnatural amino acids*. *Journal of Molecular Biology*, 2011. 406(4): p. 595-603.
283. Kim, J., et al., *Simple and efficient strategy for site-specific dual labeling of proteins for single-molecule fluorescence resonance energy transfer analysis*. *Analytical Chemistry*, 2013. 85(3): p. 1468-74.
284. Reyna K. V. Lim, S.Y., Bo Cheng, Sijia Li, Nam-Jung Kim, Yu Cao, Victor Chi, Ji Young Kim, Arnab K. Chatterjee, Peter G. Schultz, Matthew S. Tremblay and Stephanie A. Kazane, *Targeted Delivery of LXR Agonist Using a Site-Specific Antibody-Drug Conjugate*. *Bioconjugate Chemistry*, 2015: p. 2216-2222.
285. Xiao, H., et al., *Genetic Incorporation of Multiple Unnatural Amino Acids into Proteins in Mammalian Cells*. *Angewandte Chemie-International Edition*, 2013. 52(52): p. 14080-14083.
286. Wang, W.Y., et al., *Genetically encoding unnatural amino acids for cellular and neuronal studies*. *Nature Neuroscience*, 2007. 10(8): p. 1063-1072.
287. Kanje, S. and S. Hober, *In vivo biotinylation and incorporation of a photo-inducible unnatural amino acid to an antibody-binding domain improve site-specific labeling of antibodies*. *Biotechnology Journal*, 2015. 10(4): p. 564-74.

288. Chin, J.W., et al., *Addition of a photocrosslinking amino acid to the genetic code of Escherichia coli*. Proceedings of the National Academy of Sciences of the United States of America, 2002. 99(17): p. 11020-11024.
289. Schultz, K.C., et al., *A genetically encoded infrared probe*. Journal of the American Chemical Society, 2006. 128(43): p. 13984-13985.
290. Ai, H.W., et al., *Probing protein-protein interactions with a genetically encoded photocrosslinking amino acid*. ChemBioChem, 2011. 12(12): p. 1854-7.
291. Chen, Z.J., et al., *Genetically encoded fluorescent probe for the selective detection of peroxy nitrite*. Journal of the American Chemical Society, 2013. 135(40): p. 14940-3.
292. Kyte, J. and R.F. Doolittle, *A simple method for displaying the hydropathic character of a protein*. Journal of Molecular Biology, 1982. 157(1): p. 105-32.
293. Margreitter, C., et al., *Antibody humanization by molecular dynamics simulations-in-silico guided selection of critical backmutations*. Journal of Molecular Recognition, 2016. 29(6): p. 266-275.

~ THE END ~